

Springer Remote Sensing/Photogrammetry

Diofantos G. Hadjimitsis · Kyriacos Themistocleous
Branka Cuca · Athos Agapiou
Vasiliki Lysandrou · Rosa Lasaponara
Nicola Masini · Gunter Schreier *Editors*

Remote Sensing for Archaeology and Cultural Landscapes

Best Practices and Perspectives Across
Europe and the Middle East



Springer

Springer Remote Sensing/Photogrammetry

More information about this series at <http://www.springer.com/series/10182>

Diofantos G. Hadjimitsis
Kyriacos Themistocleous • Branka Cuca
Athos Agapiou • Vasiliki Lysandrou
Rosa Lasaponara • Nicola Masini • Gunter Schreier
Editors

Remote Sensing for Archaeology and Cultural Landscapes

Best Practices and Perspectives Across
Europe and the Middle East

 Springer

المنارة للاستشارات

Editors

Diofantos G. Hadjimitsis 
Department of Civil Engineering
and Geomatics
Faculty of Engineering and Technology
Cyprus University of Technology
Limassol, Cyprus

Kyriacos Themistocleous
Department of Civil Engineering
and Geomatics
Faculty of Engineering and Technology
Cyprus University of Technology
Limassol, Cyprus

Branka Cuca
Department of Civil Engineering
and Geomatics
Faculty of Engineering and Technology
Cyprus University of Technology
Limassol, Cyprus

Athos Agapiou
Department of Civil Engineering
and Geomatics
Faculty of Engineering and Technology
Cyprus University of Technology
Limassol, Cyprus

Vasiliki Lysandrou
Department of Civil Engineering
and Geomatics
Faculty of Engineering and Technology
Cyprus University of Technology
Limassol, Cyprus

Rosa Lasaponara
Institute of Methodologies for
Environmental Analysis
CNR-IMAA (Italy)
Tito Scalo, Potenza, Italy

Nicola Masini
Institute of Archaeological and Monumental
Heritage
CNR-IBAM (Italy)
Tito Scalo, Potenza, Italy

Gunter Schreier
Earth Observation Center (EOC)
German Aerospace Center (DLR)
Wessling, Germany

ISSN 2198-0721

ISSN 2198-073X (electronic)

Springer Remote Sensing/Photogrammetry

ISBN 978-3-030-10978-3

ISBN 978-3-030-10979-0 (eBook)

<https://doi.org/10.1007/978-3-030-10979-0>

Library of Congress Control Number: 2019933914

© Springer Nature Switzerland AG 2020, Corrected Publication 2020

This work is subject to copyright. All rights are reserved by the Publisher, whether the whole or part of the material is concerned, specifically the rights of translation, reprinting, reuse of illustrations, recitation, broadcasting, reproduction on microfilms or in any other physical way, and transmission or information storage and retrieval, electronic adaptation, computer software, or by similar or dissimilar methodology now known or hereafter developed.

The use of general descriptive names, registered names, trademarks, service marks, etc. in this publication does not imply, even in the absence of a specific statement, that such names are exempt from the relevant protective laws and regulations and therefore free for general use.

The publisher, the authors, and the editors are safe to assume that the advice and information in this book are believed to be true and accurate at the date of publication. Neither the publisher nor the authors or the editors give a warranty, express or implied, with respect to the material contained herein or for any errors or omissions that may have been made. The publisher remains neutral with regard to jurisdictional claims in published maps and institutional affiliations.

This Springer imprint is published by the registered company Springer Nature Switzerland AG
The registered company address is: Gewerbestrasse 11, 6330 Cham, Switzerland

Preface

Description and Purpose of the Work

Thanks to powerful search engines and innovative geo-portals able to display satellite imagery to the general public upon a click, the way we perceive and experience space technologies and their products has irreversibly changed in the last few decades. The new generations of satellites orbiting around the Earth are now being designed considering not only technology-driven possibilities, but also realistic user-driven necessities by providing a complete and timely coverage of the planet for research and monitoring purposes, in case of natural hazards and other emergencies. The next questions are why and how could information from satellites have a greater impact on research and business and on society today? And more specifically, what could be the outcome of this impact on our cultural heritage, including archaeological findings and cultural landscapes?

This book aims to investigate the potential value that satellite technologies and remote sensing (RS) could provide for a more sustainable mapping, monitoring, and management of heritage sites, be it for purposes of regular maintenance or for risk mitigation in case of natural or man-caused hazards. The framework of the publication is enhanced by recent events during armed conflicts in the Middle East, and the renewed attention of public administration toward the importance of international collaboration when it comes to the protection and conservation of cultural heritage and common values.

The first goal of this book is to provide a clear overview on policy perspective, regarding both space policy and heritage policy, and to provide possible suggestions for common ground of these two fields, both globally and in Europe (chapter “[Opportunities by the Copernicus Program for Archaeological Research and World Heritage Site Conservation](#)”). The decision-making process related to conservation and protection of heritage, especially in cases of emergency, involves considerations of technical preparation, economic feasibility, geo-environmental sustainability and cultural and social values. For this reason, interdisciplinary collaborations and international efforts are required both in policy planning and in the research and innovation projects that focus on remote sensing for cultural heritage and landscapes.

The second goal of this book is to summarize and update information regarding the advancements in theory of remote sensing. Here, the focus is given to the advancements of technologies and improvements of algorithms that can provide new answers and innovative chain processes for problem-solving regarding heritage detection, geometric documentation, and protection (chapter “[Recent Destructions in Palmyra, Syria: Looting and Illegal Antiquities Trade](#)”).

Our third goal is to provide an overview of cutting-edge applications on the real-case scenarios across Europe and the Middle East region (chapter “[Advancements in Earth Observations for Archaeology](#)”). In addition to the illustration of interesting applications, the aim of this chapter is to provide professionals who are not necessarily experts in geomatics (such as archaeologists, landscape experts, and architects but also public administration) with a clear picture on the full potential of RS and geographic information science and on their concrete contribution when it comes to tackling the challenges that affect heritage maintenance and protection. This chapter will also look into social and educational impacts that such an integrated approach could have on our society in geographic areas and on generations to come.

Another aim is to shed light on the importance of the in situ techniques (chapter “[Automatic Change Detection from High-Resolution Satellite Imagery](#)”) and how these contribute to a better understanding of satellite image-based analysis, i.e., such techniques provide valuable inputs for calibration, assessment, and interpretation of the results. The focus will be given to ground-penetrating radar (GPR), spectroradiometry, and other techniques applied in the case studies across Europe and in the region.

We believe that by advocating an integrated approach, it will be possible to better understand and share interests of different stakeholders. Therefore, this book intends to raise awareness about the value of heritage as both a cultural and economic asset, to provide illustration of solutions that could avoid any further loss of such a precious resource, and to propose RS technologies as a standard in a common methodology for action in case such loss should occur, for either natural or man-induced hazards, including armed conflicts and war. Overall, our hope is that this book facilitates national and international policy directions and future research projects by providing a number of examples of already existing methods, applications, and services that can be translated into information that is useful in decision-making processes. We are confident that bringing together innovation technology, concrete applications and political judgment can lead to a more complete vision of cultural heritage as a resource for future development of our society as a whole.

Limassol, Cyprus

Limassol, Cyprus

Limassol, Cyprus

Limassol, Cyprus

Limassol, Cyprus

Tito Scalo, Potenza, Italy

Tito Scalo, Potenza, Italy

Wessling, Germany

Diofantos G. Hadjimitsis

Kyriacos Themistocleous

Branka Cuca

Athos Agapiou

Vasiliki Lysandrou

Rosa Lasaponara

Nicola Masini

Gunter Schreier

Preface 1: Policy Perspective and Future Challenges

The possibilities that novel RS technologies can bring to society and to the cultural heritage sector seem to be well perceived by European policies, including the Valletta Convention (1995), Florence Convention (2000), and INSPIRE Directive. A significant “shift of scale” and tendency to observe landscapes and archaeo-landscapes, as a whole, is occurring not only traditionally in research practice but also in terms of territorial management and site protection. The direct link between space technologies and World Heritage Sites began in 2003, when UNESCO and European Space Agency (ESA) launched an “Open Initiative on the Use of Space Technologies to Support the World Heritage Convention.” Fifteen years later, in its most recent communication regarding culture “Towards an EU strategy for international cultural relations,” European Commission states its strong commitment for international collaboration when it comes to protection of cultural heritage, identifying Copernicus Emergency Management Service as the service that should majorly support this commitment by providing satellite imagery of cultural heritage sites at risk. Such a reference could be considered as the first official example that connects an Earth observation program (and hence, potential services and products derived from satellite RS technologies) with the domain of systematic monitoring, protection, and risk assessment of heritage sites. Chapter “[Opportunities by the Copernicus Program for Archaeological Research and World Heritage Site Conservation](#)” examines this scenario, providing an insight on the European space policy, on the most recent tendencies regarding heritage protection, and on the future possibilities for these two worlds to coexist in a common geopolitical framework.

This chapter examines the importance of cultural heritage monitoring to be included as a Copernicus service. Satellite data can assist in monitoring destruction of historic sites through conflict and natural disasters. The destruction and looting

of cultural heritage and antiquities in Palmyra has resulted in the illegal sale of priceless antiquities. However, there are no policies currently in place on how to limit the illegal trade in cultural heritage and to educate the public so they will not purchase illegally exported antiquities.

Wessling, Germany
Vienna, Austria

Gunter Schreier
Andreas Schmidt-Colinet

Preface 2: Remote Sensing: Advancements in Theory

Data regarding changes on the Earth surface has been increasing in both quantity and quality over the past few decades. The latest generation of European satellites of the Copernicus program, for example, provide a continuous coverage of Earth's surface with instruments that include both radar and optical sensors. Also, techniques for image processing are in continuous evolution due to higher computing power and more robust algorithms. Advancements in remote sensing for cultural heritage and archaeology are driven by the necessity for a progressively better interpretation of information – scientists continue to have a desire to see “better” and “more,” including detecting the features buried under the ground. This chapter focuses on the achievements in terms of innovative methodologies and algorithm development that are useful for better mapping of cultural heritage, including archaeological findings above and below the ground, and for identification and monitoring of risks to heritage sites such as geo-hazards, lack of maintenance, and looting.

Chapter “[Recent Destructions in Palmyra, Syria: Looting and Illegal Antiquities Trade](#)” examines various advancements in remote sensing that can be used for cultural heritage documentation and multitemporal monitoring. The use of digital technology in archaeology is examined as a technique to enhance knowledge and document cultural heritage sites as well as to support management and monitoring. The advantage of digital techniques is their capability to provide a huge amount of information in noninvasive, nondestructive ways, while protecting and preserving cultural heritage. The use of automatic change detection from high-resolution satellite imagery is an advancement that has been used in several of the case studies in

chapter “[Advancements in Earth Observations for Archaeology](#)”. The use of synthetic aperture radar has become more common, especially in time-series data. Finally, deriving digital surface models from aerial and satellite imagery is described and illustrated with examples.

Tito Scalo, Potenza, Italy
Tito Scalo, Potenza, Italy
Weßling, Germany
Weßling, Germany
Frascati, Italy

Rosa Lasaponara
Nicola Masini
Thomas Krauß
Jiaojiao Tian
Christopher Stewart

Preface 3: Archaeology and Cultural Landscapes

This chapter provides several case studies from Europe and the Middle East regarding the use of remote sensing for archaeological monitoring. The case studies include the identification of damage, whether through natural disasters such as earthquakes or through anthropogenic disasters such as war. The methodology for identifying and quantifying the damage is presented. Change detection can be used to monitor the damage of cultural heritage sites, such as in Palmyra, Syria, or in detecting changes in built cultural heritage as a result of climate risk, through the use of multi-resolution, multitemporal data satellite technology in archaeology. The growing developments of synthetic aperture radar (SAR) in archaeological applications address object detection and target recognition. Digital elevation models were also used to identify Roman and Byzantine ruins in the archaeolandscape of Syria and Turkey. Additionally, different methods for monitoring the archaeolandscape in the Wieprz River floodplains are presented. Finally, the techniques using unmanned aerial vehicles (UAVs) and photogrammetry to monitor and document cultural heritage and archaeological sites throughout Cyprus are discussed.

Tito Scalo, Potenza, Italy
Tito Scalo, Potenza, Italy
Milan, Italy
Limassol, Cyprus
Oulu, Finland
Oulu, Finland
Espoo, Finland
Oulu, Finland
Oulu, Finland
Oulu, Finland
Thessaloniki, Greece
Thessaloniki, Greece
Thessaloniki, Greece

Rosa Lasaponara
Nicola Masini
Luigi Barazzetti
Branka Cuca
Minna Silver
Kenneth Silver
Markus Törmä
Milton Nuñez
Jari Okkonen
Tuula Okkonen
Petros Patias
Charalampos Georgiadis
Dimitrios Kaimaris

Poznań, Poland
Poznań, Poland
Weßling, Germany
Weßling, Germany
Limassol, Cyprus

Łukasz Banaszek
Włodzimierz Rączkowski
Daniele Cerra
Simon Plank
Kyriacos Themistocleous

Preface 4: The Added Value of In Situ Data Integrated with Satellite Remote Sensing for Archaeology

Historically, on-site observation has been the most common way of monitoring archaeological sites. However, this procedure, which includes field surveying, ground-based data collection, periodical observations for all archaeological sites, and multi-analysis risk assessment, is time-consuming and expensive, especially over large or remote areas. Therefore, in recent years, satellite imagery has been used for monitoring archaeological sites, especially in areas that are inaccessible or dangerous. Although satellite remote sensing methods are a vital tool in monitoring archaeological sites, the resolution of satellite images is not detailed enough to replace on-site observations. Indeed, current trends in monitoring archaeological sites with satellite remote sensing include the integration of in situ data from multiple sources with satellite imagery.

Field surveys are measurements of various parameters and properties of soil, subsurface materials, and buried objects which use in situ techniques such as ground-penetrating radar, surface magnetometer, resistivity survey, geomagnetic and electromagnetic induction, and technologically advanced ground sensors. Integrative technologies that use in situ measurements are geodetic networks, where surveying techniques, such as total station, leveling, and global navigation satellite systems (GNSS) receivers, are used to measure the positional changes of any point on the surface at millimeter-level accuracy. The points on the geodetic network are measured regularly using GNSS receivers and ground measurements via high-precision total stations and levels. Spectroradiometers are often used in archaeological research since soil marks and crop marks often indicate the presence of buried features. Spectroradiometers are used to measure the spectral signature of the vegetation in the area of interest, as the growth stage and health of vegetation can indicate underground objects.

This section focuses on case studies that integrate satellite remote sensing with in situ measurements. The case studies include monitoring cultural heritage sites in Palmyra, Syria; Petra, Jordan; and Choroikoitia, Cyprus. The case studies illustrate

the integrated monitoring systems developed to monitor and document such sites, so that the relevant authorities can take appropriate actions to mitigate further damage to the site, as well as establish policies for preservation and conservation of the site.

Vienna, Austria
Limassol, Cyprus
Limassol, Cyprus

Andreas Schmidt-Colinet
Kyriacos Themistocleous
Chris Danezis

Contents

Part I Policy Perspective

Opportunities by the Copernicus Program for Archaeological Research and World Heritage Site Conservation	3
Gunter Schreier	

Recent Destructions in Palmyra, Syria: Looting and Illegal Antiquities Trade	19
Andreas Schmidt-Colinet	

Part II Advancements in Theory

Big Earth Data for Cultural Heritage in the Copernicus Era	31
Rosa Lasaponara and Nicola Masini	

Automatic Change Detection from High-Resolution Satellite Imagery	47
Thomas Krauß and Jiaojiao Tian	

SAR for Archaeological Prospection in Europe and in the Middle East	59
Christopher Stewart	

Dense Surface Models from Airborne and Spaceborne (Multi-)Stereo Images	85
Thomas Krauß	

Part III Archaeology and Cultural Landscapes

Active Satellite Sensors in Cultural Heritage Research: The Use of SAR for Archaeological Prospection	107
Rosa Lasaponara and Nicola Masini	

Recent and Past Archaeological Looting by Satellite Remote Sensing: Approach and Application in Syria	123
Nicola Masini and Rosa Lasaponara	
Identification of Buildings Damaged by Natural Hazards Using Very High-Resolution Satellite Images: The Case of Earthquake in L'Aquila, Italy	139
Luigi Barazzetti and Branka Cuca	
Remote Sensing Roman and Byzantine Eastern Frontier Zone in Landscape: Case Studies from Syria and Turkey	153
Minna Silver, Kenneth Silver, Markus Törmä, Milton Nuñez, Jari Okkonen, and Tuula Okkonen	
Archaeological Landscapes and Built Heritage: Climate Risk and Contribution of Remote Sensing Technologies	177
Petros Patias, Charalampos Georgiadis, and Dimitrios Kaimaris	
Interpreting Archaeological Features on the Wieprza River Floodplain, West Pomerania, Poland	203
Lukasz Banaszek and Włodzimierz Rączkowski	
Towards Early Warning for Damages to Cultural Heritage Sites: The Case of Palmyra	221
Daniele Cerra and Simon Plank	
The Use of UAVs for Cultural Heritage and Archaeology	241
Kyriacos Themistocleous	
Part IV Added Value of In-Situ Data	
Remote Sensing Work in Palmyra/Syria	273
Andreas Schmidt-Colinet	
Monitoring Cultural Heritage Sites Affected by Geo-Hazards Using In Situ and SAR Data: The Choirokoitia Case Study	285
Kyriacos Themistocleous and Chris Danezis	
Correction to: Towards Early Warning for Damages to Cultural Heritage Sites: The Case of Palmyra	C1

Part I
Policy Perspective

Opportunities by the Copernicus Program for Archaeological Research and World Heritage Site Conservation



Gunter Schreier

Abstract In its aim to adapt Copernicus to user needs, the European Commission is currently in a phase in contemplating further areas and users to be served by Copernicus. One such area is the monitoring and preservation of Cultural Heritage. Several events in the recent years showed how observation techniques from space can help to monitor the destruction of historic sites through conflict and natural disasters. The process to potentially include Cultural Heritage Monitoring into Copernicus services may take a while and needs further programmatic and political decisions.

Keywords Copernicus program · Earth observation · Cultural heritage protection · European Commission · ESA

The Copernicus Program

European Member States and the European Space Agency (ESA) have been active in Earth observation since the early 1980s. National missions, such as the French Spot program with optical satellites, and international collaborations, such as the German/Italian cooperation with the US/NASA for radar imaging from the Space Shuttle cargo bay, have been international landmarks in technology and the provision of global data. They resulted in successful national follow-on missions (SPOT, Pleiades, TerraSAR-X, and Cosmo-Skymed) involving European companies and public private partnerships (PPP) to commercialize data and services. Next to pure science missions, ESA also started pan-European missions to generate global observation data. The “Earth Remote Sensing” Missions 1 and 2 (ERS-1/2; 1991, 1995) followed by the ENVISAT mission (2002) carried already sophisticated radar,

G. Schreier (✉)

Earth Observation Center (EOC), German Aerospace Center (DLR), Wessling, Germany
e-mail: Gunter.Schreier@dlr.de

© Springer Nature Switzerland AG 2020

D. G. Hadjimitsis et al. (eds.), *Remote Sensing for Archaeology and Cultural Landscapes*, Springer Remote Sensing/Photogrammetry,

https://doi.org/10.1007/978-3-030-10979-0_1

optical, and atmospheric payloads, targeted to generate a sustainable supply of critical environmental information. However, it became evident that ESA in its status of a research and development agency cannot master alone the operational duties, the political challenges in data policy, and the long-term financing of a series of Earth observation missions. In a similar situation – the operational management of geostationary weather satellites – EUMETSAT was created in 1986. Hence, discussions started in the early 1990s about putting the European Commission in charge to define and manage a long-term pan-European Earth observation strategy. After initial studies (Churchill et al. 1995), the idea of a program for “Global Monitoring of Environment and Security” (GMES) was first initiated in a European conference in Baveno, Italy, in 1998 (Brachet 2004; Aschbacher and Milagro-Pérez 2012). The legal framework for the European Commission to get involved in Space missions was set with the treaty of Lisbon in 2007, where a new space strategy was adopted by all Member States. Therein, the European Commission was put in charge for defining and maintaining the European strategy for space science research and major space projects. Two of these large-scale projects have meanwhile been initiated and are now in an early operational phase. Next to an independent European global satellite navigation system (Galileo), the European Commission has taken over the governance of GMES, later christened Copernicus.

Copernicus shall make Europe independent in the supply of basic spaceborne Earth observation data. It shall deliver to European governmental agencies, but also to science, companies, and the citizen, critical and timely information on the state of environment and security in Europe and – where necessary – elsewhere.

To achieve this goal, Copernicus consists of several components and elements (see also Fig. 1).



Fig. 1 The segments and elements of the Copernicus program

Space Component

The space component ensures the provision, launch, and operations of dedicated Copernicus Earth observation missions, the Sentinels. Its operations include all ground facilities for mission control, payload data reception, processing, archiving, and delivery. Besides the Sentinels, also data from other national and commercial Earth observation satellites (contributing missions) is used to fulfill the Copernicus objectives. ESA is mandated to manage and control the space component. This is done in work-share with EUMETSAT, being responsible for those parts of the space component using EUMETSAT satellite facilities and within the mandate of EUMETSAT (i.e., specifically Sentinel-4/Sentinel-5/Sentinel-6 missions).

As of mid-2018, seven Sentinels are in orbit and in operations, delivering more than 10 terabyte of data every day, with this rate of data growing at a fast pace. The management, processing, and distribution of this amount of data constitute a specific challenge within Copernicus.

Service Component

The service component shall use the space component data and create information and services currently in six domains: atmosphere monitoring, marine environment monitoring, land monitoring, climate change, emergency management, and security. The Commission is coordinating the service component while leaving the concrete implementation and provision of services to European entrusted entities. The six domains of the service component are explained in more detail in the following paragraph.

In Situ Component

Space data is complemented by data gathered through airborne, seaborne, and ground-based installations, in order to support the abovementioned geo-information services. The European Environmental Agency (EEA) is mandated to manage the in situ component. Cartographic and geographic digital information shall – in general – be treated according to the European INSPIRE (Infrastructure for Spatial Information in the European Community) directive.

These three components define the operational core of the Copernicus program. Additional measures have been implemented to guarantee the adaptation of Copernicus data and information to national user needs, to ensure the acceptance of Copernicus to European users, and to face the challenges in managing the enormous amount of data Copernicus is generating.

Collaborative Ground Segment

Copernicus participating states (i.e., members of the European Union and countries having signed a special agreement (currently Norway and Iceland)) may implement special measures to allow their citizens an improved access to all Copernicus Sentinel data and information. This may be done either by the direct reception of Sentinel-1 data with national data acquisition stations (possible over most of the continental and marine European territory) or the replication of Sentinel data holdings on the national Internet-based user portals. By early 2017 12 of these national portals mirror Sentinel data and partly offer enhanced cloud-based online computing (ESA 2017a, b; 2018).

User Segment and Big Data

The European Commission and ESA take several measures to spread the knowledge about Copernicus, to support the implementation of new space-based applications, and to increase the competitiveness of European industry in dealing with the massive amount of Copernicus Sentinel data. These supportive measures include the stimulation of science using Earth observation thru the European Horizon2020 research program contests for new ideas (Copernicus Masters (<https://www.copernicus-masters.com>), Hackathons, etc.) and contracts to the European Information Technology industry to implement a Copernicus Data and Information Access System (DIAS).

Four such DIAS have been implemented by European industrial consortia, primed by Serco Europe; Creotech, Poland; ATOS France; and Airbus Defence and Space, France.

In addition, EUMETSAT has launched its own DIAS Service primarily targeting its own user community.

A regulation of the European Parliament (European Commission 2014) defines the concrete roles and responsibilities of the Commission as the owner and main financing organization of Copernicus, as well as the role of its European partners, specifically the European Space Agency (ESA) and the European Meteorological Satellite Organization (EUMETSAT), for implementing Copernicus.

A particular breakthrough in the definition and implementation of Copernicus is the data policy, declaring all Sentinel mission data and all Copernicus Service information free and open. This decision is reflecting the experience made with similar programs in the United States (e.g., Landsat) and the new and easy access to digital data provided by the Internet. This Copernicus data policy is aimed to stimulate the use of Earth observation data, including the implementation of new commercial services and businesses (Schreier 2016). The Copernicus data policy is also driven by the European INSPIRE (Infrastructure for Spatial Information in the European Community) directive (INSPIRE 2007), which harmonizes the policy, electronic access, and formats to geographic information within Europe.

The free and open policy does not apply for data from the contributing missions. These data from often higher resolution and commercial missions are purchased by the Copernicus Data Warehouse mechanism from the mission operators. The supply of this contribution mission data is regulated by the demand of the Copernicus Core Services and other Commission- and Member States-related activities. These have free access to the Data Warehouse.

The entire costs of the Copernicus program starting on European Commission side in the initial investment in the Framework 6 and 7 Research Programs and with ESA on GMES service evolution and the Copernicus Space Component up to the end of the first operational phase in 2020 are estimated about 8,8 billion Euro. This amount is complemented by various national activities and R&D budgets in the Horizon 2020 research program of the European Union. The first financial framework (until 2020) financed the procurement of current series of Sentinel satellites up to the D-units (four satellites for most Sentinel series). The European Commission is regularly evaluating the benefit of Copernicus for its policy, for economy, and the European citizen (PWC 2017). Although by mid-2018 still ongoing discussions on the BREXIT cast a slight shadow on the budget of the European Commission, it is assumed that the Copernicus program will be further financed and even be enlarged in satellites and services within the next Multiannual Financial Framework (MFF; 2021–2027).

The Copernicus Space Segment

The Copernicus Space Segment provides Europe with an autonomous access to spaceborne Earth observation data. The characteristics of the dedicated Sentinels have been defined following a process of recognizing European observation needs and the continuity of past ESA missions on one side and avoiding any conflict of interest with other European national and commercial missions, on the other side. The Sentinel observation data therefore refrain from delivering a better geometric resolution than 10 m (pan channel of Sentinel-2). Any geometric resolution better than 10 m is left to the Copernicus contributing missions. Whereas Copernicus Sentinel data is available at no cost, the contributing missions are available only via individual license fee mechanisms. For the various Copernicus Services, using contributing mission data, these licenses are organized in the Copernicus Data Warehouse and paid from the Copernicus budget.

In order to increase the frequency of observations and to guarantee redundancy in case of failures, two Sentinels of each series shall always be in orbit. The first series of Sentinels will have four spacecraft (A-, B-, C-, and D-unit) of about at least 7 years orbital lifetime. This would give this series of Sentinels an operation lifetime until the early 2030s.

Currently, six series of Sentinels constitute the operational Copernicus constellation. They deliver global Earth observation data in the optical and microwave domain, as well as information about the atmosphere and the oceans. The characteristics of the current Sentinel mission series are depicted in Fig. 2.


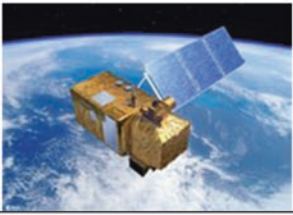

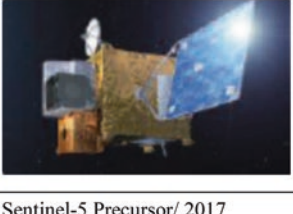

Sentinel/ first launch	main instruments	application examples
Sentinel-1/ 2014 	C-Band Synthetic Aperture Radar (SAR); 5m – 40 m resolution	Ocean and ice monitoring, maritime awareness; ship and oil detection; land surface moisture and topography, land/ soil motion (interferometry)
Sentinel-2/ 2015 	MSI (Multi Spectral Instrument) 13 spectral bands Spatial resolution: 10 m, 20 m and 60 m	European wide-swath high-resolution super-spectral imaging mission designed for data continuity for operational land and security services
Sentinel-3/ 2016 	OLCI (Ocean and Land Colour Instrument); Spatial sampling: 300 m @21 bands SLSTR (Sea and Land Surface Temperature Radiometer)	European global land and ocean monitoring mission. 2 day global coverage Earth observation data for sea and land applications
Sentinel-4/ 2022 	UVN instrument: high resolution spectrometer (305-400 nm) (400-500 nm) (750-775 nm) spatial sampling: 8 km	Covers the needs for continuous monitoring of the atmospheric chemistry from the geostationary orbit. The main data products will be O ₃ , NO ₂ , SO ₂ , HCHO and aerosol optical depth, generated with high temporal resolution (~ 1 hour).
Sentinel-5 Precursor/ 2017 	UV-VIS-NIR-SWIR push-broom grating: TROPOMI Spectral Range: 270-495 nm, 710-775 nm, 2305-2385 nm ground pixel 7x3,5 km ²	Dedicated to monitoring our atmosphere. The satellite carries the state-of-the-art Tropomi instrument to map a multitude of trace gases such as nitrogen dioxide, ozone, formaldehyde, sulphur dioxide, methane, carbon monoxide and aerosols – all of which affect the air we breathe and therefore our health, and our climate.

Fig. 2 The Copernicus Sentinel missions overview



Sentinel/ first launch	main instruments	application examples
Sentinel-5/ 2021 	high resolution spectrometer Spectral Range: 270-370 nm, 370-500, 685-773 nm, 1590-1675 & 2305-2385 nm ground pixel 7x3,5 km ²	Continuous monitoring of the atmospheric chemistry at high temporal and spatial resolution from a low-Earth orbit. The mission will provide coherent and long-term information on atmospheric variables in support of European policies
Sentinel-6/ 2020 	Poseidon-4 (SAR Radar Altimeter) AMR-C (Climate-quality microwave radiometer)	To provide continuity of the reference, high-precision ocean topography service after Jason-3

Fig. 2 (continued)

The early success and acceptance of the Sentinel data created a demand to consider even an extension of the current Sentinel observational capabilities. These resulted in considerations for the timely expansion of the Sentinel fleet (potentially from Sentinel 7 to 10). The following additional key observational requirements for the expansion missions are stated (as of end 2017):

Sentinel Exp.	Objective
Sentinel-7	Multi-satellite mission to measure the anthropogenic contribution to the CO ₂ cycle
Sentinel-8	Observations at high spatiotemporal resolution in the thermal infrared region of the optical spectrum in order to complement and expand the current Sentinel-2 measurements
Sentinel-9	New measurements on critical parameters of interest for the polar regions, such as sea ice/floating ice concentrations and surface elevation
Sentinel-10	Optical observations with hyper-spectral imaging capabilities to expand the current Sentinel-2 measurements

In parallel, analysis has started for a long-term scenario of Copernicus. Herein, the strategy of the next generation of Sentinels, operational beyond 2030, is defined. This strategy calls for an extension of the current Sentinel capabilities, e.g., potentially with an additional L-Band SAR and thermal components on the optical facilities.

Both Sentinel Expansion and Sentinel Extension mission are currently being discussed and will be turned into concrete plans and projects, pending on the appropriate budget from the European Commission and ESA.

The management of all Sentinel data from satellite data downlink to the distribution of Application Ready Products (ARD) to Copernicus Services and general

users is performed by the Copernicus Core Ground Segment. Likewise the Sentinels, it is managed by ESA and operated by European companies and aerospace entities, contracted by ESA.

The downlink of Sentinel data is performed via X-Band, received via four main core ground stations in Europe and in Northern Canada. An alternative downlink – only for Sentinel-1 and -2 series– is via a Laser Communication Terminal (LCT) mounted on board these Sentinels. Via a Laser beam, captured data is transmitted with up to 1.8 Gb/sec to currently one European Data Relay Satellite (EDRS-A). From there, the data is transmitted via Ka-Band to few European EDRS stations (Weilheim, DE, Redu, BE, Harwell, UK). EDRS increases the amount of data available especially with Sentinel-1 and therewith the global coverage. EDRS allows getting data faster from areas outside the reception of the core ground stations.

The X-Band and Ka-Band stations are connected via redundant high-capacity fiber links with the Processing and Archiving Centers (PACs). There, all the raw data is transformed into user products, all raw data and products are archived, and all products are disseminated to the Copernicus Core Services and dedicated Internet hubs. From these hubs, general users and European and international partners can grab the free and open Sentinel product data for their own use (Fig. 3).

As of mid-2018, the “open access hub” keeps all Sentinel product data from the beginning of operations (i.e., 2014). Meanwhile, the volume of data has reached several petabytes, and the science hub is overloaded with international data requests. From the beginning of operations to end of September 2018, about 89,52 PB of data have been downloaded by more than 170.000 users from the ESA Internet hubs (ESA 2018).

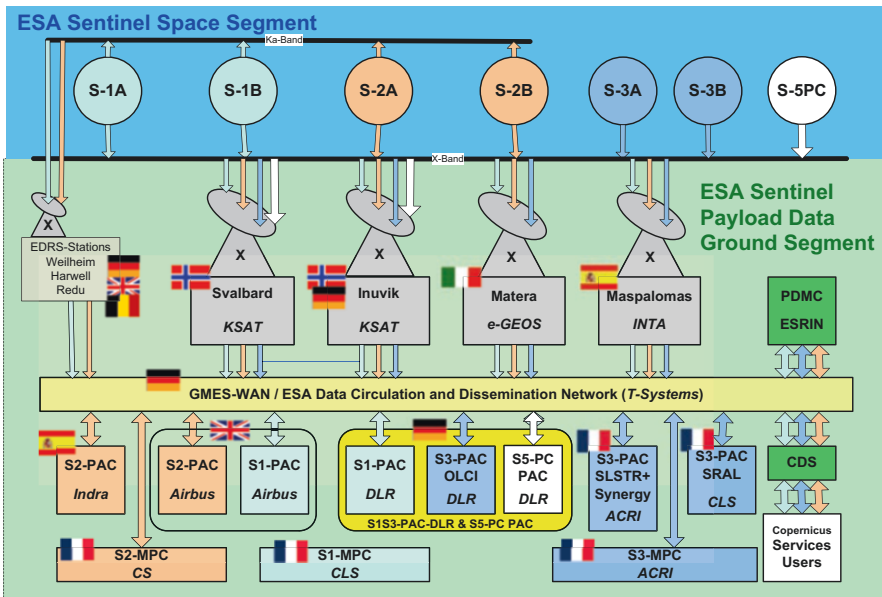


Fig. 3 Copernicus Sentinel Core Ground Segment in Europe and its functions. (Graphics: DLR)

The Copernicus Collaborative Ground Segment and Big Data

In order to satisfy all user requests for Sentinel data, ESA has opened alternative means to have access to data, among them, encouraging Member States to open their own national data distribution portals, eventually supported by further functions to make value out of the data. Next to the general “open access hub,” a dedicated hub serves the Copernicus Core Services. International partners, such as USGS, NASA, NOAA, and the Australian CSIRO, get Sentinel products via an “international hub.” European states are served via a “collaborative hub” (Fig. 4).

The purpose of the “international” and the “collaborative” hubs is to allow European and international partners to get most recent Sentinel data from this server and replicate these on Internet platforms for their national users. These Internet platforms offer regional or global data, and some offer additional capabilities such as processing of the Sentinel data directly with processors attached to the platform. By 2018 14 such national European platforms are in operations, all with slightly different data holdings and additional services (ESA, Serco, 2017a, b). For instance, the German national platform CODE-DE offers global Sentinel-1 and Sentinel-2 data, various preprocessed geo-information products, and a cloud space for user remote processing (Kiemle et al. 2016; Keuck et al. 2017).

Early in the operations of the Sentinel hubs, the Internet companies Amazon and Google uploaded the free and open data from Sentinel-1 and Sentinel-2 on their global data storage and processing systems. The Slovenian company Synergize was supported by Amazon to offer all Sentinel-2 data for download from Amazon servers (<http://www.sentinel-hub.com>). Google is offering this data on its Google Earth Engine (<https://earthengine.google.com>), offering free computing space for scientific and noncommercial purposes.

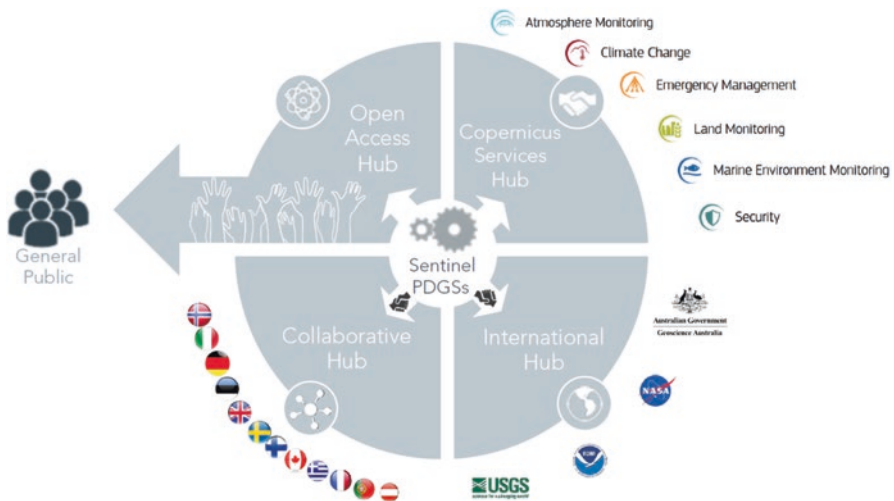


Fig. 4 The Sentinel Data Access System configuration by end Y2016. (ESA, Serco, 2017a, b)

The overwhelming demand for Sentinel satellite data and the pressure from the commercial Internet providers motivated the European Commission to take special actions in order to have all Sentinel data and information ready for online computing and therewith to support new scientific approaches and innovative Internet-based businesses. Together with ESA, the European Commission launched the creation of Copernicus Data and Information Access Systems (DIAS), to be implemented by European consortia. DIAS platforms shall have all Sentinel data (and more information) available online, shall enable remote cloud processing and moreover, and shall allow third-party users to establish their own – science, governmental, and commercial – offers based on these resources. End of 2017 contracts with four DIAS providers have been signed.

In any case, the avalanche of Earth observation data coming from Copernicus, national missions, and those operated by new commercial start-ups (New Space) is creating a new Big Data ecosystem. For Europe, it is estimated that Internet-based Earth observation online services will increase from about 10% today (2017) to about 25% in the next few years (EARSC 2017).

The online availability of global coverage long-term time series together with large-scale computing facilities also allows unprecedented advances in the understanding of global processes such as vegetation, global change, and urbanization (Hansen et al. 2013; Esch et al. 2016). Online availability of data is also a basis for new companies being created in the Earth observation value-added sector and big industrial players getting interested in adding Earth observation data in their business processes (Linz 2017).

The Copernicus Service Segment

Created as a program, where the data from satellites shall satisfy the needs of European policymakers, economy, and the citizen for geo-information, the Copernicus program has as a key element the Core Services. These services have been defined in comprehensive requirements process with many governmental and institutional stakeholders in Europe. Nearly all of them have been tested and prototyped during European Commission Framework 6 and 7 projects and have used the Earth observation data available before the Sentinels. The operational execution for most of the services has been entrusted by the European Commission to European agencies, involved by its mission statement in environmental, planning, and security topics. Further on, these entrusted entities implement the generation of the geo-information services through contracts to European consortia, selected in a competitive tendering process. With a few restrictions in the Emergency Management and Security Services, all products and information from these Core Services are – according to the general Copernicus data policy – free and openly available via Internet portals.

Currently, the following six Copernicus Core Services exists (adopted from the description on <http://copernicus.eu/main/services>):

The *Copernicus Atmosphere Monitoring Service* provides the capacity to continuously monitor the composition of the Earth's atmosphere at global and regional scales. This service capacity encompasses the description of the current situation (analysis), the prediction of the situation a few days ahead (forecast), and the provision of consistent retrospective data records for recent years (reanalysis). The service generates geophysical products which require further technical processing and various forms of high-level information to support decisionmakers. The main areas the Copernicus Atmosphere Monitoring Service focuses on are:

- Air quality and atmospheric composition
- Ozone layer and ultra-violet radiation
- Emissions and surface fluxes
- Solar radiation
- Climate forcing

The Copernicus Atmosphere Monitoring Service is entrusted to the European Centre for Medium-Range Weather Forecast (ECMWF), Reading, UK.

The *Copernicus Marine Environment Monitoring Service* provides regular and systematic information about the physical state and dynamics of the ocean and marine ecosystems for the global ocean and the European regional seas. This data covers analysis of the current situation, forecasts of the situation a few days in advance, and the provision of retrospective data records (reanalysis). The Copernicus Marine Environment Monitoring Service calculates and provides products describing currents, temperature, wind, salinity, sea level, sea ice, and biogeochemistry. These factors support marine and maritime applications and related EU policies, e.g., in the fields of:

- Marine safety
- Marine and coastal environment
- Marine resources
- Weather, seasonal forecasting, and climate

The Copernicus Marine Environment Monitoring Service is entrusted to Mercator Océan, Ramonville Saint-Agne, France.

The *Copernicus Land Monitoring Service* provides geographical information on land cover, land use, land cover-use changes over the years, vegetation state, or water cycle. Applications that are built upon and integrate the information supplied by the service can provide support in areas such as spatial planning, forest management, water management, agriculture and food security, and emergency management, among others. Service priorities and their relevance to users are defined and validated by the European Commission and the Member States. The three main components of the Copernicus Land Monitoring Service are currently:

- A Global component
- A pan-European component
- A local component

The Copernicus Land Monitoring Service is entrusted to the European Environmental Agency (EEA), Copenhagen, Denmark. The global component of the Land Service is coordinated by the European Commission DG Joint Research Centre (JRC), Ispra, Italy.

The *Copernicus Climate Change Service* is designed to respond to changes in the environment and society associated with climate change. The service will provide information for monitoring and predicting climate change and help to support adaptation and mitigation strategies. It will provide access to several climate indicators (e.g., temperature increase, sea level rise, ice sheet melting, ocean warming) and climate indices (e.g., based on records of temperature, precipitation, drought events) for both the identified climate drivers and the expected climate impacts. The Copernicus Climate Change Service will enter a pre-operational stage by the end of 2017. The operational phase will start before the end of 2018. This pre-operational phase is also supported by a series of projects funded by the EU research framework program related to climate modeling and observation analyses.

The Copernicus Climate Change Service is entrusted to the European Centre for Medium-Range Weather Forecast (ECMWF), Reading, UK.

The *Copernicus Emergency Management Service* delivers warnings and risk assessments of floods and forest fires and provides geospatial information derived from satellite images on the impact of natural and man-made disasters all over the world (before, during, or after a crisis). Through these, it supports crisis managers, civil protection, and hydrometeorological authorities, humanitarian aid actors dealing with natural disasters, man-made emergency situations, and humanitarian crises, as well as those involved in recovery, disaster risk reduction, and preparedness activities. As an EU service, the emergency management's first priority is responding to EU needs and interests, whether within the EU or abroad. The Emergency Management Service is provided free of charge to authorized users. The service has two main components:

- Early warning
- Mapping

The Copernicus Emergency Management Service is implemented by the European Commission DG Joint Research Centre (JRC), Ispra, Italy.

The *Copernicus Security Service* is one part of the Copernicus program. It aims to support related European Union policies by providing information in response to the security challenges Europe is facing, namely, improving crisis prevention, preparedness, and response capacities in the following key areas:

- Support to EU External Actions (implemented in partnership with the European Union Satellite Centre and the Emergency Management Service)
- Maritime surveillance (implemented in partnership with the European Maritime Safety Agency, EMSA)
- Border surveillance (implemented in partnership with FRONTEX) (Fig. 5)

Besides these Copernicus managed and funded Core Services, several European and national agencies and entities are already using Sentinel data for their services.

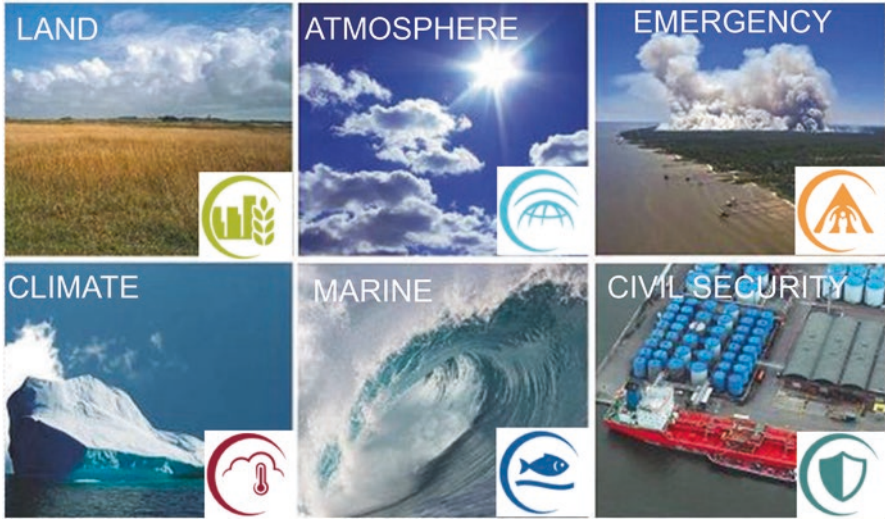


Fig. 5 The six Copernicus Core Services, delivering geo-information and decision support

For instance, the European Maritime Safety Agency (EMSA) in Lisbon, Portugal, is using, next to other spaceborne SAR data, also the data from Sentinel-1 for its trans-European oil-spill detection program CleanSeaNet (EMSA 2017). In the framework of the International Charter on Space and major Disasters (www.diasterscharter.org), the DLR Center for Satellite Based Crisis Information (ZKI) and several international partners are using Sentinel-1 and Sentinel-2 data for monitoring of global natural and humanitarian crisis situations (Voigt et al. 2016).

World Cultural Heritage and the Copernicus Program

Copernicus has to respond to emerging needs on critical geo-information for European interest. The Copernicus Core Services are therefore under regular review to consider new services and new user groups to be included in their free and open portfolio. After the first years of service operations, the European Commission has started a series of workshops to review needs in new services and listen to the demands of new user groups. Besides “polar applications,” “agriculture,” and “energy” (to name a few), a special workshop was also conducted on April 24, 2017, in Brussels (Copernicus Support Office 2017). The workshop covered the following aspects:

- Intermediate and end-users’ needs in the Cultural Heritage domain
- An overview of space-based applications in support of Cultural Heritage at EU and global level

- An outline of requirements for Copernicus-based products/services in support of Cultural Heritage
- Potential implementation scenarios for a structured Copernicus-based approach for Cultural Heritage support

About 100 participants of the workshop discussed these issues with the European Commission Copernicus Office. Stakeholders, such as the UNESCO, NEREUS, EARSEL, and national institutions, such as the German Archaeological Institute (DAI), presented their needs and capabilities in this area. Several European research framework and ESA projects on the matter have been presented.

The discussion and analysis yielded that Cultural Heritage applications range from long-term monitoring of various environmental conditions up to very fast crisis support in case of conflicts and natural disasters. For the latter, the need for fast access to very high-resolution optical and SAR data is evident. This need is shared with already existing Copernicus Core Services such as the emergency management and the civil security services.

The Copernicus civil security service already has a diverse spectrum of applications (e.g., border monitoring, maritime surveillance, external relations) and therewith is working with several European entities. The case of the destruction of the antiquities of Palmyra in Syria showed that conservation of Cultural Heritage and fast reaction in military conflicts seems to have similar needs. Therefore, some stakeholders would like to have the Copernicus security service have closer connections to European military, such as the European Defense Agency (EDA). It needs to be contemplated, however, whether such proximity of “culture” to “military intelligence” and therewith “classified information” would be appropriate. On the other site, organizations such as UNESCO have to rely on national police and military expertise on dealing with issues such as illegal trade of antiquities. For this purpose, UNESCO has signed an agreement with Italy to ask for support from a special task force of the Italian Carabinieri (UNESCO 2016).

National Space Agencies and aerospace research centers, such as DLR, support the use of Earth observation to preserve cultural heritage. DLR has supported the German Archaeological Institute (DAI) in various observations of its international sites. Likewise, DLR was active to monitor the destructions of the “Islamic State” in Palmyra (Cerra et al. 2016, 2017; Jung et al. 2016; and other chapters in this book).

Supporting the needs of European institutions and those of European citizens is the primary objective of the Copernicus program. Safeguarding the European Cultural Heritage by using spaceborne reconnaissance information from the Sentinels and very high-resolution contributing missions therefore would perfectly fit to launch a new service within the Core Services. More analysis and prototyping and improved dialogues with stakeholder and users are required to take place before defining cultural heritage preservation as an integral part of the Commission-financed services within Copernicus. Therefore, the European Commission has contracted Price Waterhouse Coopers of France with an analysis and developing options for such an implementation. At the time of writing (September 2018), this analysis was presented to the Copernicus boards, and further decisions are pending.

In any case, Earth observation satellite data – most of them available by Copernicus for free and open to all – is an unquestionable tool for the global societal goal to preserve cultural sites and monuments, in Europe and all over the globe.

References

- Aschbacher J, Milagro-Pérez M (2012) The European Earth monitoring (GMES) programme: status and perspectives. *Remote Sens Environ* 120:3–8
- Brachet G (2004) From initial ideas to a European plan: GMES as an exemplar of European space strategy. *Space Policy* 20(1):7–15
- Cerra D, Plank S, Lysandrou V, Tian J (2016) Cultural heritage sites in danger – Towards automatic damage detection from space. *Remote Sens* 8(9):1–15. <https://doi.org/10.3390/rs8090781>. ISSN 2072-4292
- Cerra D, Agapiou A, Plank S, Lysandrou V, Tian J, Schreier G (2017) From detection of underground archaeological relics to monitoring of world heritage sites in danger: ongoing research activities in the frame of the ATHENA twinning project. 37th international symposium on remote sensing of environment, ISRSE 2017, Tswane 8–12 May 2017
- Churchill P, Sharman M, Schreier G, Aschbacher J (1995) The Center for Earth Observation (CEO): an initiative of the European Commission to promote the use and availability of earth observation data. 16th Asian conference on remote sensing, Bangkok, Thailand, 20–24 Nov 1995
- Copernicus Support Office for European Commission - DG GROW (2017) Copernicus For Cultural Heritage Workshop. Report: <http://workshop.copernicus.eu/cultural-heritage>; 24. April 2017
- EARSC (European Association of Remote Sensing Companies) (2017) A Survey into the State & Health of the European EO Services Industry. www.earsc.org; Brussels, 2017
- ESA (2017a) Sentinel Data Access Annual Report (01/12/2015–30/11/2016); ESA document; COPE-SERCO-RP-17-0071; 05/04/2017
- ESA (2017b) SERCO Spa: COPE-SERCO-RP-17-0186: Sentinel data access annual report 2017-sentinels data access annual report 2017 Date 02-05-2018
- ESA (2018) Statistics of all Data Hub Services since start of operations, seen on: <https://scihub.copernicus.eu/reportsandstats/>
- Esch T et al (2016) Earth observation-based service platforms - a new instrument to provide geo-information for urban and regional planning. IEEE International Geoscience and Remote Sensing Symposium (IGARSS), Seiten 1774–1777. IEEE. IGARSS 2016, 10–15 July. Beijing, China. <https://doi.org/10.1109/IGARSS.2016.7729455>
- European Commission (2014) Regulation (EU) No 377/2014 of the European Parliament and of the Council of 3 April 2014 establishing the Copernicus Programme and repealing Regulation (EU) No 911/2010
- European Maritime Safety Agency, EMSA (2017) Information on the clean sea net program online under. <http://www.emsa.europa.eu/csn-menu.html>. Accessed 20 Sept 2017
- Hansen MC et al (2013) High-resolution global maps of 21st-century forest cover change. *Science* 342(6160):850–853. <https://doi.org/10.1126/science.1244693>
- INSPIRE (2007) Directive 2007/2/EC of the European Parliament and of the Council of 14 March 2007 establishing an Infrastructure for Spatial Information in the European Community (INSPIRE) <https://inspire.ec.europa.eu/inspire-legislation/26ESA>
- (2017) Copernicus Evolution - Draft Copernicus Space Component Long Term Scenario. September 2017. ESA/PB-EO (2017)31, Paris, 5th September 2017
- Jung B, Schreier G, Strunz G (2016) Legacies from the past – for the future: World heritage through the eyes of satellites, DLR magazine No 150; ISSN 2190–0108; June 2016
- Keuck V et al (2017) The German Copernicus data and exploitation platform “CODE-DE”. Proceedings, international astronomical conference, IAC-17, Adelaide, 2017

- Kiemle S, Molch K, Schropp S, Weiland N, Mikusch E (2016) Big data management in earth observation; IEEE Geoscience and remote sensing magazine; September 2016
- Linz C (2017) How Earth observation can empower digital leaders, SAP Presentation. In ESA workshop “Paradigm shifts and future prospects in Earth observation” 11 May 2017, http://esa-multimedia.esa.int/docs/EarthObservation/FutureEO/PM/5_Carsten_Linz/ParadigmShifts_CLINZ_2017-05-11.pdf. Accessed 20 Sept 2017
- Price Waterhouse Coopers (2017) Copernicus ex-ante benefits assessment, study for the European Commission, Final Report, Dec 2nd, 2017
- Schreier G (2016) Copernicus: Earth observation 4.0: DLR Magazine, No 148/149, ISSN 2190–0108; March 2016
- UNESCO (2016) Italy creates a UNESCO Emergency Task Force for Culture; Press Release, 16 February 2016 on-line: <http://whc.unesco.org/en/news/1436/>. Accessed 20 Sept 2017
- Voigt S et al (2016) Global trends in satellite-based emergency mapping. Science 353(6296):247–252. <https://doi.org/10.1126/science.aad8728>. ISSN 0036-8075

Recent Destructions in Palmyra, Syria: Looting and Illegal Antiquities Trade



Andreas Schmidt-Colinet

Abstract Since 2011, the best preserved monuments of the unique antique city of Palmyra, Syria, were damaged or destroyed, either by “collateral” damage of war activities or by wanton destructive vandalism, especially executed by the so-called Islamic State (Daesh). Some of these destructions become visible especially on satellite pictures. Furthermore, several underground tombs were broken and robbed; many funerary sculptures were destroyed, damaged or stolen. Such illegally exported sculptures are offered more and more in international art galleries, also in the Internet, with the provenance of “Syria” and ownership as “property of a gentleman”. During the last years, the illegal trade in plundered artefacts especially also from Palmyra did increase enormously. Several national and international projects have the aim to curb illegal trade in cultural heritage and to increase the consciousness that buying or dealing with illicitly exported antiquities is a crime and a theft of the historical heritage and memory of us all.

Keywords Palmyra · Syria · Destruction · Antiquities · Illegal trade · Cultural heritage · Satellite pictures

Introduction

The best preserved monuments of the unique antique city of Palmyra, Syria (Fig. 1), were damaged or destroyed during the war in Syria, either by “collateral” damage of war activities or by wanton destructive vandalism, especially executed by the so-called Islamic State (IS or Daesh). Many of these destructions can be recognized best on satellite pictures.

Already before the arrival of the IS to Palmyra, in 2014, part of the Sanctuary of Bel was damaged by tank grenades (Fig. 2).

A. Schmidt-Colinet (✉)

Institute of Classical Archaeology, University of Vienna, Vienna, Austria

e-mail: Andreas.Schmidt-Colinet@univie.ac.at

© Springer Nature Switzerland AG 2020

D. G. Hadjimitsis et al. (eds.), *Remote Sensing for Archaeology and Cultural Landscapes*, Springer Remote Sensing/Photogrammetry,

https://doi.org/10.1007/978-3-030-10979-0_2



Fig. 1 Palmyra, satellite picture. (DigitalGlobe, European Space Imaging, 2011)

Fig. 2 Palmyra, Temple of Bel, West wall, 2014. (DGAM)



Case Studies

Then, in 2015, members of the IS exploded first some Islamic monuments and the Temple of Baalshamin, then the Temple of Bel (Fig. 3), several tower tombs in the Valley of the Tombs (Figs. 4 and 5) and the Arch at the beginning of the great Colonnade Road.

Later, in 2017, the IS destroyed part of the theatre and of the tetrapylon in the centre of the antique town (Fig. 6). Several tombs were damaged in the South-East Necropolis, such as the so-called Aviation Tomb (Fig. 7).

The underground tomb called Tomb of the Three Brothers was used as military headquarter. Several military constructions were installed in the North Necropolis in 2015; in 2016 even a Russian military camp was constructed within this antiquities' zone (Fig. 8)

The Archaeological Museum of Palmyra also was severely damaged outside and inside. Many sculptures as well as small finds were damaged or destroyed (Fig. 9).

Furthermore, several underground tombs especially in the South-East Necropolis were broken and plundered. Already before the arrival of IS, these underground tombs were easily accessed by grave robbers. Funerary sculptures were broken out



Fig. 3 Palmyra, Sanctuary of Bel, before and after destruction. (DigitalGlobe ASOR)

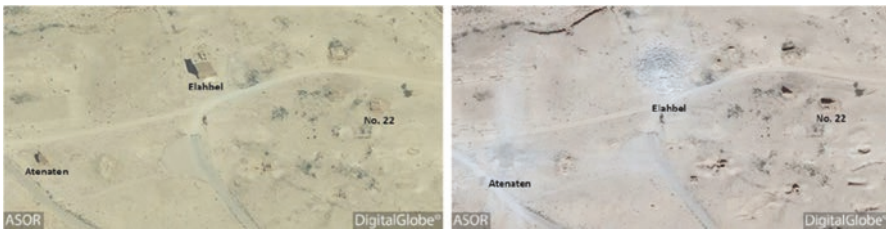


Fig. 4 Palmyra, Valley of the Tombs, Tombs of Atenatan and Elahbel, before and after destruction. (DigitalGlobe ASOR)

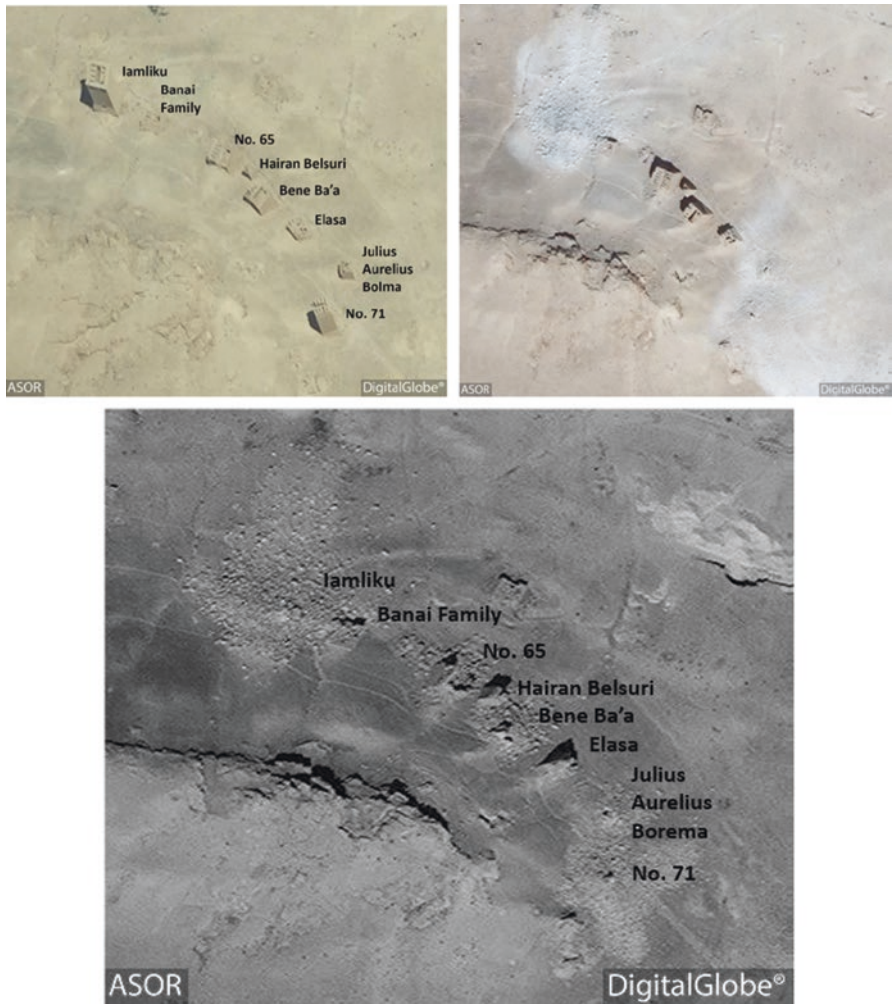


Fig. 5 Palmyra, Valley of the Tombs and Tombs of Yamblik and others, before and after destruction. (DigitalGlobe ASOR)



Fig. 6 Palmyra, theatre and tetrapylon, before and after destruction. (DigitalGlobe ASOR)



Fig. 7 Palmyra, South Necropolis, so-called Aviation Tomb, before and after destruction. (DigitalGlobe ASOR)



Fig. 8 Palmyra, North Necropolis, increasing military constructions, cf. Fig. 1. (DigitalGlobe ASOR)



Fig. 9 Palmyra, Museum, destructions. (DGAM)

of the walls, destroyed, damaged or stolen. We may refer to pictures taken by the customs officials of the Syrian and Lebanese antiquity authorities in 2014 already (Fig. 10).

The Tombs of Artaban and that of Tybel were violated (Figs. 11 and 12), complete panels were ripped from the walls, sculptures were effaced, and heads were broken off and stolen.

When, shortly after that, fragments of very similar reliefs appeared on the international art market (Figs. 13 and 14), doubts may be permitted about the provenance of these pieces and for questioning the legality of these sales.



Fig. 10 Stolen Palmyrene sculptures. (DGAM)



Fig. 11 Palmyra, Tomb of Tybel, before and after destructions. (DGAM)



Fig. 12 Palmyra, Tomb of Tybel, before and after destructions. (DGAM)



Fig. 13 Palmyrene sculpture in art galleries in London and the USA, 2014



Fig. 14 Left: Palmyra, stucco head of excavation in 2009. Right: Palmyrene stucco head. (Art gallery Munich 2014)

Between 2005 and 2010, the residence of a noble Palmyrene family was excavated with wall painting reliefs with Dionysian themes (theatre masks) and miniature stucco heads. Until that time, such decorations were unknown in Palmyra. The stucco heads were exhibited in the museum at Palmyra in 2010, and the final publication did appear in 2014. In 2014, astonishing similar such stucco heads were offered for sale by an art gallery with the provenance of “Palmyra” and the property “from an old Bavarian private collection”.

Conclusions

Political chaos and the absence of the rule of law have led to a steep rise in pirate excavations – the plundering and destruction of monuments and the illegal trade in stolen artefacts. No wonder that illegally exported sculptures are offered more and more for sale in international art galleries, also in online catalogues, with the provenance of “Syria” and ownership as “property of a gentleman”. During the last years, the illegal trade in plundered artefacts especially also from Palmyra did increase enormously. The international crime statistics now show that the illicit trade in cultural artefacts ranks with that of the illegal trade in arms, drugs and human beings. It has been established that different sides involved in the conflict in Syria are financing their weapons’ purchases partly with the illegal trade in artefacts.

There is now a broad international cooperation to document the plundering, systematic theft and irreparable destruction of the cultural heritage of Syria (Figs. 15 and 16) and to discuss carefully the possibilities for the future that means to be prepared for the time after the crisis.



Fig. 15 “Red list” of ICOM. (2017)



Fig. 16 Resolution 47 (2019) of UN Security Council

All these efforts and considerations are well-intentioned, even if there may be some repetitive and duplicated actions. At the same time, all these activities are “culturally minded acts of defiance” (Thomas Weber). But they may help once to restore and to save the cultural heritage of Syria and to increase the consciousness that buying or dealing with illicitly exported antiquities is a crime and a theft of the historical heritage and memory not only of the Syrian people but of us all.

References

- Abdulkarim M (2013). The Archaeological Heritage in Syria throughout the Crisis between 2011-2013 (Damascus 2013) <http://www.dgam.gov.sy/?d=314&id=1043> (18.08.2017)
- Abdulkarim M (2017) Warten auf die Stunde Null, Süddeutsche Zeitung 5, 7.–8. January 2017, p 2
- Dietrich R (2017) Antiken Recht und Markt. http://www.dnk.de/_uploads/beitrag-pdf/9921262238a40e606de3694019735439.pdf (18.08.2017)
- Gazzetta Ufficiale n. 105, (8 May 2003) Supplemento Ordinario n. 72, Ordinanza del Presidente del Consiglio dei Ministri n.3274, March 20th, 2003 “Primi elementi in materia di criteri generali per la classificazione sismica del territorio nazionale e di normative tecniche per le costruzioni in zona sismica”
- Gersch C (2014) Kulturgut in Gefahr. Raubgrabungen und illegaler Handel. Internationale Tagung Berlin 11.-12. Dezember 2014, pp 1–22. Berlin https://www.bundesregierung.de/Content/DE/_Anlagen/BKM/2014-12-11-tagungsbericht-illegaler-kulturguthandel.pdf?__blob=publicationFile&v=1 (18.08.2017)
- Graeppler D (2015) Italiens Kampf gegen Raubgrabungen und illegalen Antikenhandel, Art Value. Positionen zum Wert der Kunst 9/15, 2015, pp 54–58

- Jung B, Schreier G, Sturz G (2016) Sehen, was nicht verborgen bleiben darf, DLR Magazin 150, June 2016, pp 22–27
- Knöfel U (2017) Scherbenhaufen, Der Spiegel 7/2016, pp 124f. <http://www.spiegel.de/spiegel/print/d-142879056.html> (18.08.2017)
- Leon Ch (2015) Aber so was von stinkfalsch, Der Spiegel 6, 2015, pp 98–101; <http://www.spiegel.de/spiegel/print/d-131578967.html> (18.08.2017)
- Pacifici F, Chini M, Bignami C, Stramondo S, Emery WJ (2010) “Automatic damage detection using pulse-coupled neural networks for the 2009 Italian earthquake,” International Geoscience and Remote Sensing Symposium 2010, Honolulu, USA, July 25–30 (2010)
- Parzinger H (2015) Eine weltweite Seuche, Art Value. Positionen zum Wert der Kunst 9/15, 2015, pp 25–28
- Rezaeian M (2010) Assessment of earthquake damages by image-based techniques, Diss.. ETH Zurich N. 19178, 149 pages (2010)
- Schmidt-Colinet A (2016a) Palmyra geht uns alle an. Ein Krieg zerstört unser historisches Gedächtnis, AW 2016/1, pp 46–49
- Schmidt-Colinet A (2016b) Palmyra: Zerstörung und Rettung unseres kulturellen Erbes, Gymnasium 123, 2016, pp 491–495
- Schmidt-Colinet A (2016c) Krieg in Syrien. Die Zerstörung unseres kulturellen Erbes, Insights. Archive und Menschen im digitalen Zeitalter 1, 2016, pp 18f
- Schmidt-Colinet A (2017) Forschungsstand und Perspektiven, Gnomon 89, 2017 (forthcoming)
- Siehr K (2015) Geschichte des rechtlichen Schutzes archäologischer Kulturgüter, Art Value. Positionen zum Wert der Kunst 9/15, 2015, pp 8–24
- Solder R (2016) Geraubte Kultur, Südwind Magazin 3, März 2016, pp 36–38
- Tober B (2013) Stuck und Wandmalerei. In: Schmidt-Colinet A, al-As‘ad W (eds) Palmyras Reichtum durch weltweiten Handel. Archäologische Untersuchungen im Bereich der hellenistischen Stadt, vol 1, Vienna, pp 170–252. (with English and Arabic summaries) https://e-book.fwf.ac.at/detail_object/o:382 (18.08.2017)
- Wessel G (2015) Das schmutzige Geschäft mit der Antike. Der globale Handel mit illegalen Kulturgütern, preface by M. Hilgert, and conclusion by F. Fless (Berlin 2015) http://www.deutschlandfunkkultur.de/raubgrabungen-das-schmutzige-geschaeft-mit-der-antike.976.de.html?dram:article_id=330465 (18.08.2017)

Part II
Advancements in Theory

Big Earth Data for Cultural Heritage in the Copernicus Era



Rosa Lasaponara and Nicola Masini

Abstract Digital data is stepping in its golden age characterized by an increasing growth of both classical and emerging big earth data along with trans- and multidisciplinary methodological approaches and services addressed to the study, preservation and sustainable exploitation of cultural heritage (CH). The availability of new digital technologies has opened new possibilities, unthinkable only a few years ago for cultural heritage. The currently available digital data, tools and services with particular reference to Copernicus initiatives make possible to characterize and understand the state of conservation of CH for preventive restoration and opened up a frontier of possibilities for the discovery of archaeological sites from above and also for supporting their excavation, monitoring and preservation. The different areas of intervention require the availability and integration of rigorous information from different sources for improving knowledge and interpretation, risk assessment and management in order to make more successful all the actions oriented to the preservation of cultural properties. One of the biggest challenges is to fully involve the citizen also from an emotional point of view connecting “pixels with people” and “bridging” remote sensing and social sensing.

Keywords Big data · Digital archaeology · Remote sensing · Data integration · Cultural heritage management

R. Lasaponara (✉)

Institute of Methodologies for Environmental Analysis, CNR-IMAA (Italy),
Tito Scalo, Potenza, Italy
e-mail: rosa.lasaponara@imaa.cnr.it

N. Masini

Institute of Archaeological and Monumental Heritage, CNR-IBAM (Italy),
Tito Scalo, Potenza, Italy

© Springer Nature Switzerland AG 2020

D. G. Hadjimitsis et al. (eds.), *Remote Sensing for Archaeology and Cultural Landscapes*, Springer Remote Sensing/Photogrammetry,
https://doi.org/10.1007/978-3-030-10979-0_3

Introduction

In the last 20 years, remote sensing (RS) along with big data and information and communication technologies has radically changed the current cultural heritage (CH) scenery and future prospects (Lasaponara & Masini 2008; Opitz & Hermann 2018). The digital data and tools nowadays available for CH enable us to get rich and detailed information from heterogeneous data sources, for example, earth observation (EO), sensor networks, digital libraries, web data service, social networks and IoT (Internet of things) that replaced the simplest traditional ones to cope with big data challenges from the storing to the processing, mining, integration and interpretation.

Big data have emerged in the past few years providing opportunities to improve and/or enable research and decision support applications with unprecedented value for digital CH and archaeology. The possibility to fast analyse relatively large, varied and rapidly changing huge quantities of data has sped up the work during the diverse phases of application ranging from survey, mapping, documentation, exploitation and monitoring at diverse scales of interest, moving from small artefacts to architectural structures and landscape scale.

There is, therefore, no doubt that EO big data will significantly change the scientific approach, data analysis and methodologies as well as discoveries of unknown archaeological sites and the visualizations of the results to also engage citizens into the human past and its contemporary legacies.

Scientific big data have a number of characteristics, including complexity, comprehensiveness and global coverage, as well as high degree of integration with information and communication technology which will provide a great contribution to the study of the human past, as *processual archaeology* (Patterson 1989) modelled using scientific method, to find and make clear the (theoretical) general laws of cultural growth in the way that societies responded to their environments.

Big data will bring together perspectives coming not only from cultural heritage but also from the creative arts, design, software development and social science transforming the current approaches and moving from single discipline to multidisciplinary and interdisciplinary approaches.

The latest generation of satellite sensors opened up a frontier of possibilities providing ever-closer and more comprehensive look at the earth's surface, with the potentiality to inform us about present and past human activity.

Moreover, augmented and virtual reality makes possible to integrate virtual restoration with the current status of the historical buildings, ancient environment reconstruction also including anthropological aspects and mapping past flora and fauna (Gabellone et al. 2017; Pescarin 2015).

One of the most important points is that all of these technologies are available at different costs for different purposes and needs. Even with a small budget, it is possible to implement very effective solutions. For example, by satellite optical imagery available from Google Earth (Luo et al. 2018) or using a small "drone", equipped with GPS and digital camera remotely controlled (Campana 2017), it is possible to

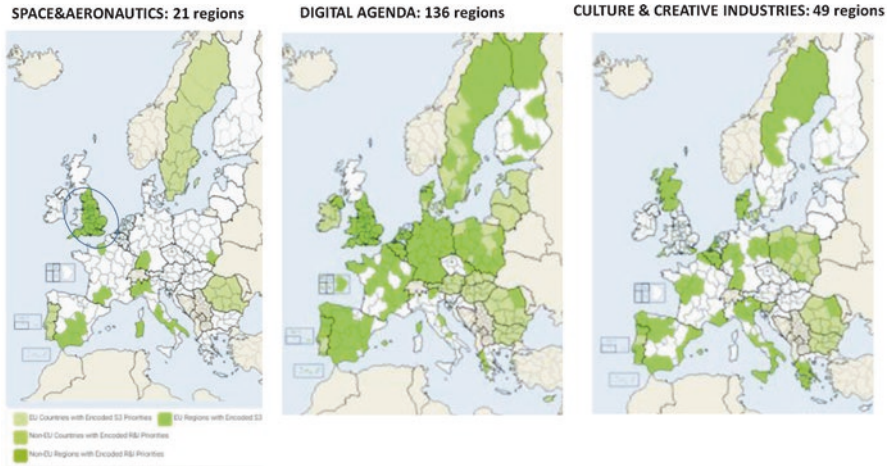


Fig. 1 Smart specialisation platform: regional priorities. (Image source: EYE@RIS3 tool, EC)

carry on detailed surveys, operational monitoring activities of complex structures and areas of archaeological interest (Masini et al. 2018a, b). Moreover, the growing availability of free data and open access software tools, with particular reference to Copernicus initiatives, enhances a powerful link between in situ investigations and EO data, research and operational services thus offering a new opportunity for the exploitation of big earth data also addressed to the social benefits and economic development of culture and creative industries (see Fig. 1).

Therefore, the new and emerging challenges are the dissemination of data, the interoperability, the costs, the simplicity in use and the speed of applications, to make them open and understandable to everybody and useful for operational monitoring and preservation of CH properties. Focussing on this strategic challenge, as also highlighted in the 2030 Agenda and relative Sustainable Development Goals (SDGs), it is important to remind that the factors that most of all threaten cultural heritage sites are among the others: social/cultural uses of heritage, use/modification of cultural properties, physical resource extraction, local conditions affecting physical fabric, transportation and utilities infrastructure, urban sprawl, pollution and biological resource. In other words, today cultural heritage is (according to UNESCO) “increasingly threatened with destruction not only by the traditional causes of decay, but also by changing social and economic conditions which aggravate the situation with even more formidable phenomena of damage or destruction” (from the general conference of the UNESCO in Paris from 17 October to 21 November 1972). To face these drawbacks, the increasing involvement of citizens and their awareness on the importance of preserving CH along with a continuous monitoring in terms of type and extent of adverse changes over time is essential for supporting planners and decision-makers as also highlighted in the framework of 2030 Agenda and SDGs, with particular reference the sustainable exploitation and preservation of CH (see Albert 2017).

The main issue of great importance for supporting the evolution processes in a “sustainable development” approach is the availability of information on past and current conditions to estimate potential future scenarios. In this context, big earth data (also available free of charge), with particular reference to Sentinel missions (http://www.esa.int/Our_Activities/Observing_the_Earth/Copernicus/Overview4) and services (<https://www.copernicus.eu/en>), can be fruitfully used for (i) improving knowledge and documentation of cultural heritage sites, (ii) monitoring and planning purposes, (iii) recording ongoing trends and (iv) estimating natural and anthropogenic risks at a detailed level (Agapiou et al. 2014). Moreover, the availability of free-of-charge satellite imagery and services represents a cost-effective mean for obtaining useful data and reliable information that can be easily and systematically updated for the whole globe and, therefore, can fruitfully be adopted for developing reliable and accurate SDG indicators for the monitoring of the achievements of the identified goals.

Copernicus

The Copernicus programme, financed by the European Community and managed by the European Space Agency (ESA), thanks to a wide range of technologies, from satellites to terrestrial, marine and aerial surveying systems, provides operational data and services information (for a wide range of application areas) in a complete, open and freeway. Copernicus has opened the season of big geospatial data (https://cordis.europa.eu/news/rcn/128882_it.html) that are strategic for the development of services for decision support in various application contexts with a view to sustainability.

There are four pillars, on which Copernicus is founded: (i) the spatial component (satellites and associated ground infrastructures), (ii) in situ measures (aerial and terrestrial measures), (iii) harmonization/standardization of data and (iv) services for users. The Copernicus services are based on information from a constellation of dedicated satellites, called “Sentinels”, and dozens of other satellites, the so-called participating missions. This information is supplemented with data obtained from in situ (i.e. local) sensors. In particular, the spatial component related to the constellation of dedicated satellites consists of various Sentinel missions with the following objectives.

- Sentinel-1 provides monitoring services for terrestrial and marine areas with radar images. The first Sentinel-1a satellite was launched on 3 April 2014.
- Sentinel-2 provides high-resolution optical images for terrestrial services (e.g. monitoring of vegetation, soil, inland waters and coastal areas). Sentinel-2 can provide useful information in cases of emergency.
- Sentinel-3 provides services for the global monitoring of terrestrial and oceanic areas.
- Sentinel-4 will provide data on atmospheric composition.

Table 1 Sentinel missions: satellites and applications

Sentinel missions	Number of satellite	Mission
Sentinel-1	4 satellites	Synthetic aperture radar (C band) mission designed to monitor sea ice zones, the Arctic environment and the risk of land-surface motion as well as generate forest, water and soil mapping
Sentinel-2	2 satellites	Optical mission with a multispectral instrument mainly for agricultural applications such as crop monitoring and management, vegetation and forest monitoring (e.g. leaf area index, chlorophyll concentration, carbon mass estimations), monitoring land cover change for environmental monitoring, observation of coastal zones (marine environmental monitoring, coastal zone mapping), inland water monitoring, glacier monitoring and ice extent and snow cover mapping. Burnt area mapping and fire severity estimation
Sentinel-3	3 satellites	Multipurpose mission with multiple instruments, mainly for sea-surface as well as sea and land ice topography, sea- and land-surface temperature, ocean- and land-surface colour, seawater and inland water quality and pollution monitoring, land use change monitoring, forest cover mapping, fire detection, marine and general weather forecasting, snow cover monitoring, measuring earth's thermal radiation for atmospheric applications and last but not least for overall environmental and climate monitoring and modelling.
Sentinel-4	<i>Sentinel-4</i> will be placed on geostationary Meteosat	Monitoring of the composition of the atmosphere for air quality, stratospheric ozone and solar radiation as well as climate monitoring
Sentinel-5	<i>Sentinel-5</i> plus Sentinel-5 precursor are carried on the polar-orbiting MetOp	Monitoring of the composition of the atmosphere for air quality, stratospheric ozone and solar radiation as well as climate monitoring

- Sentinel-5 provides Sentinel-4 in the provision of atmospheric composition data.
- Sentinel-6 will contribute to the precision altimetry missions (see Jason-2 satellite lens).

Table 1 summarizes the Sentinel missions and their main applications, but obviously it is expected that the integration and complementary use of diverse data source and services will provide improvements in cultural heritage monitoring and management.

Copernicus marked the beginning of a new era in earth observation. The first Sentinel satellites have been launched, and a huge amount of data (big earth data) is now available throughout the globe together with other information (such as weather forecasts at different space/time scales, pollution and air quality forecasts,

etc.). The amount of data that is now being created and stored globally is enormous and is constantly growing.

The constellation Copernicus has changed the paradigm with which the citizen is related to the spatial datum, because it is open access, available to all. Therefore, space is a huge opportunity for a society, today, that evolves very quickly and offers challenges and opportunities. In the light of recent sensor developments and data availability, innovative models and methodologies are needed for data analysis and the integration of different information, as well as new strategies for the exploitation.

However, despite the increasing availability of data, information and forecasts the increasing impact of natural and artificial disasters, the operational monitoring and documentation activities are still today limited.

Therefore, there are important challenges and opportunities related (i) to the extraction of information, (ii) to the integration of different data sources, (iii) to the efficient management and (iv) to technology transfer.

Copernicus is, therefore, an important element for scientific progress and the development of European industrial capacities and generates opportunities for innovation by allowing not only the improvement of existing monitoring and control systems but also and above all the development of new applications and services with high added value (known as “downstream” sector).

Copernicus portfolio services (<https://services-portfolios.copernicus.eu/>) provide around 1092 operational products (http://www.esa.int/Our_Activities/Observing_the_Earth/Copernicus/Services_overview) which are essential information for the 6 main Copernicus domains: ocean, land and atmosphere monitoring, emergency response, security and climate change that are another critical issues for both CH and SDGs.

All the Copernicus services are based on information from Sentinel satellites (shown in Table 1) and from the so-called “participating missions”, supplemented with data obtained from in situ (i.e. local) sensors and aerial/drone survey. In sections “[Copernicus Satellite Data and Cultural Heritage](#)” and “[Aerial Data for Cultural Heritage](#)” a brief overview on satellite, aerial data for CH is provided, in order to highlight that the capability to extract information from data is linked with the capability to integrate data and info available from diverse sources to transform data into knowledge.

Copernicus Satellite Data and Cultural Heritage

Even if still today the applications of RS data in operational disaster management and monitoring are still difficult tasks, the recent improvements in EO (including both active and passive sensors from satellite, aerial and in situ technologies) offer data which can enable new applications specifically for the documentation and assessment of heritage sites. To this aim, a dedicated workshop was organized by EU on 01 September 2017 (http://ec.europa.eu/growth/content/copernicus-cultural-heritage-workshop-0_en)

which focussed on the characterization and mapping of Copernicus capabilities and existing solutions over user needs and the identification of potential solutions to effectively support cultural heritage. The workshop aimed to (i) “identify the main user requirements for space-based applications associated with the preservation and management of cultural heritage assets” along with (ii) opportunities for standardization taking into account “what is already being done in some European countries, with risk assessments associated to each cultural asset also taking account of environmental risks”.

The use of satellite data for CH has more paid great attention worldwide, due to main factors, among them:

- (i) The improvement in spectral and spatial resolution reveals increasing detailed information for CH purposes.
- (ii) The synoptic view offered by satellite data helps us to understand the complexity of CH investigations at a variety of different scales.
- (iii) Satellite-based digital elevation models (DEMs) are widely used in CH for several purposes to considerably improve data analysis and interpretation.
- (iv) The availability of long satellite time series allows the monitoring of hazard and risk in CH sites.
- (v) Remotely sensed data enable us to carry out both inter- and intra-site prospection and data analysis.

Nowadays, in some fields, as urban sprawl (see Fig. 2), land degradation, fire, drought, flooding and extreme weather events disturbances, biological risks, etc., remote-sensing-based techniques are promptly ready for an operational use in natural heritage monitoring and risk assessment, whereas for other applications it is necessary to improve the capacity in the use of satellite data to monitor the state of conservation of cultural heritage. For example, Sentinel-1 is a SAR in C band and, therefore, provides useful data for monitoring and mapping urban deformation and land subsidence, as well as for detecting structural damage and/or underground construction thus improving risk estimation and safety and at the same time contribute to reduce economic loss.

SAR enables us to overcome some limitations of optical imaging providing (i) all weather acquisitions (ii) at any time of day or night and (iii) capable to “penetrate” (to some extends) vegetation and/or soil depending on the antenna wavelength, surface characteristics (ice, desert sand, close canopy, etc.) and conditions (moisture content). SAR has shown the great potential for site CH monitoring and as well as for landscape archaeology (Lasaponara & Masini 2014) and the detection of buried or emerging archaeological remains (Chen et al. 2015, 2016, 2018; Lasaponara & Masini 2012; Stewart 2017; Stewart et al. 2018). Although several achievements have been made in recent years, the SAR remote sensing is still today underexploited for CH.

The availability of Sentinel-1 free of charge for all can really make the difference in the next future, being that over the years, one strong limitation in the use of SAR satellite data has been the difficulty in accessing to the data and the complexity of processing. Moreover, new promising applications of data integration include the

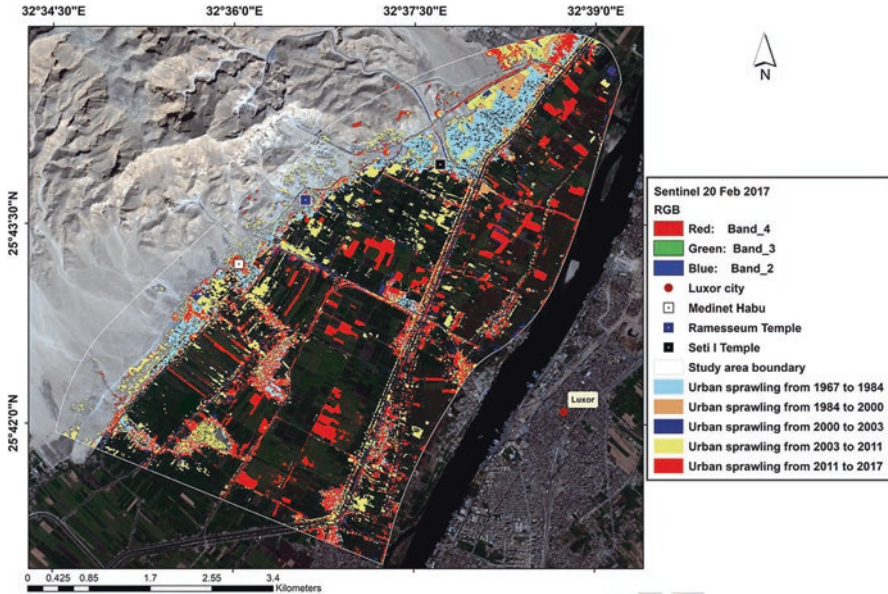


Fig. 2 Urban sprawl 1984–2017 automatic detection around the Luxor (Egypt) archaeological area (in Elfadaly et al. 2018)

use of SAR with other remote-sensing methods including optical data, in situ acquisition as well as aerial survey (Lasaponara et al. 2017).

The availability of high-resolution satellite data has been so rapidly growing that new problems have arisen mainly linked with methodological aspects of data analysis. In this context, the main concern is the lack of correspondence between the great amount of remote-sensing images and effective data processing methods capable to integrate data from diverse sources (EO and traditional data), to reliably enhance and to automatically process the data (Masini et al. 2008). Presently, the great amount of services including climatic ones along with multisensor data from Copernicus missions will suitably support new promising applications for the preservation of CH that is today one of the topics of great economic and social significance, so that, for the first time, culture was included in the 2030 Agenda for Sustainable Development. Therein culture was recognized as a “driver of economic, social and environmental development as at the heart of humanity, shaping human beliefs, hopes and interactions” (<https://www.iccrom.org/transforming-our-world-iccrom-and-2030-agenda-sustainable-development>). Among the 17 SDGs of the 2030 Agenda, 8 are relevant to culture heritage preservation, and the current and future challenge is to provide member states with particular reference to Middle East area “with the tools, knowledge, skills and enabling environments to preserve cultural heritage in all its forms, for the benefit of all people”. In this context, it is important to highlight that cultural heritage and historical landscape especially, where heavily influenced by human activities, have to be systematically monitored

and accordingly managed to be preserved. In the past decades, many countries across the world have been involved and are today experiencing an increasing frequency and impact of disasters, such as extreme hydrometeorological events, most probably related to climate change, floods, landslides, earthquakes, volcano eruptions, fires, uncontrolled urbanization and air pollution (Lasaponara and Masini 2017). In order to face with the increasing frequency and adverse impact of disasters, it is necessary to set up systematic monitoring activities and tools to identify issues and changes that can destroy or deteriorate heritage increasing its vulnerability. This may require the use of heterogeneous data essential to identify the major threats as well as to reconstruct the historical landscape and to compare it with the current one, in order to detect remains of the past, analyse the transformations and detect ongoing changes and potential threats.

Aerial Data for Cultural Heritage

A wide availability of digital technologies, acquired from passive and active aerial sensors, as multi-hyper-spectral sensors, SAR and laser scanning, historically had provided data and information useful to address manifold strategic challenges, thus opening a new horizon for many application fields including CH and archaeological investigations also addressed to virtual 4D modelling, augmented reality, etc.

Aerial Archaeology

Historically, aerial photography has been the first remote-sensing tool extensively used for digital archaeology for surveying emerging archaeological remains as well as for detecting underground archaeological structures through the reconnaissance of proxy indicators, generally known as “soil”, “crop” and “shadow” marks (Wilson 1982).

Crop marks are linked to the presence of buried walls and/or filled ditches in vegetated areas. They produce local variations in moisture and nutrient content and, consequently, in the growth of vegetation, which can be revealed by differences of height or colour in crops (Evans and Jones 1977; Masini and Lasaponara 2017). Using multispectral and hyperspectral images, crop marks can be detected by spectral variations in specific channels more sensitive to vegetation (as near-infrared) or spectral indices (i.e. mathematical combinations of different spectral channels) as NDVI (Doneus et al. 2014; Agapiou et al. 2016; Kalayci et al. 2019).

Damp marks occur in presence of buried walls, filled ditches and pits which induce local changes in the drainage capability of the soil. They can be revealed by changes in colour or texture exploiting spectral variations in specific channels more sensitive to moisture or spectral indices (i.e. mathematical combinations of different spectral channels) as NDVI, NDWI, etc.

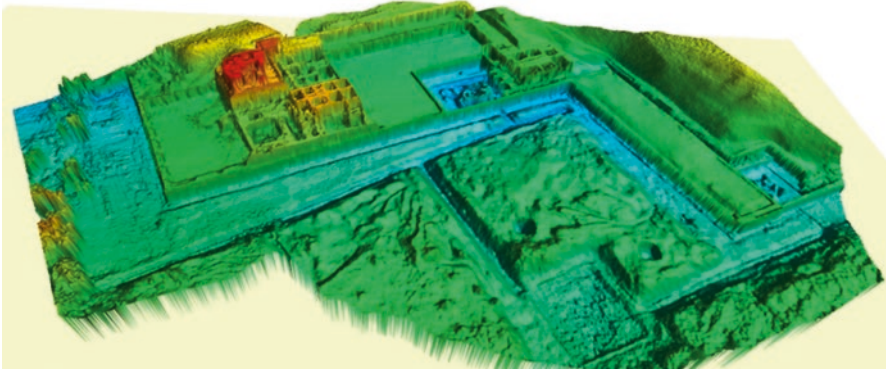


Fig. 3 3D model of Acclawasi palace in Pachacamac (Peru) obtained by structure from motion applied to images taken from a drone

Finally, shadow marks are micro/medium microtopographic relief linked to archaeological remains, as artworks, platforms, ditches and shallow remains, and they can be revealed by the presence of shadow.

The visibility of the traces of archaeological interest appearing as (in many cases subtle) crop/weed, soil and shadow marks has a great intra- and inter-year variability due to changes in crop types and phenology, soil moisture content and other surface parameters (Masini et al. 2018a). Additionally, the visibility of microrelief depends on many factors, such as off-nadir viewing angle of the collected imagery, time of image acquisition, view geometry, sun angle and surface characteristics; in particular, the presence of vegetation can completely cover the microrelief. These limitations can be overcome by (i) UASs (Fig. 3) and (ii) airborne laser scanner (ALS), also referred to as light detection and ranging (LiDAR).

Currently, a LiDAR survey could be carried out by using two different types of ALS sensor system: (i) conventional scanners or discrete echo scanners and (ii) full-waveform (FW) scanners (Doneus and Briese 2006). The first delivers only the first and last echo, thus losing many other reflections. The second is able to detect the entire echo waveform for each emitted laser beam, thus offering improved capabilities especially in areas with complex morphology and/or dense vegetation cover (Fig. 4).

ALS systems are generally made up of different components which contribute to the final accuracy of the range data. All the components should be accurately calibrated and integrated.

Nowadays, ALS is regarded as a well-established tool used for archaeology and cultural landscape studies. The majority of published studies are based on data collected by conventional ALS, for the management of archaeological monuments, landscape studies and archaeological investigations to depict microtopographic

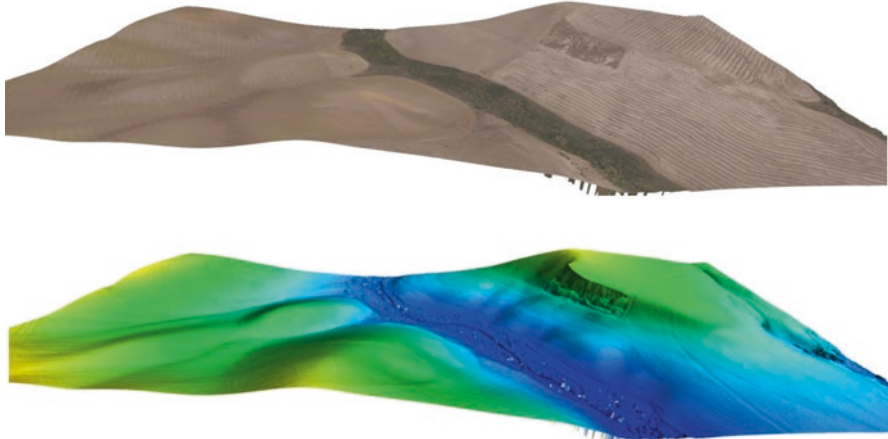


Fig. 4 Airborne laser scanning survey aerial photo (up) and DTM (bottom) obtained after the removal of vegetation cover along a river

earthworks in bare ground sites and in forested areas (Canuto et al. 2018; Chase et al. 2011, 2017; Doneus et al. 2008; Evans et al. 2013).

LiDAR sensors are also mainly powerful tool for investigating archaeological heritage in densely vegetated sites (as wooded areas, rain forests, etc.). ALS can penetrate vegetation canopies and model accurately underlying terrain elevation. The discoveries of Evans et al. (2013) in Angkor and of Chase in Belize (Chase et al. 2011) demonstrate the effectiveness of this technology for archaeological research.

LiDAR provides direct range measurements mapped into 3D point clouds between a laser scanner and earth's topography. The high detail of the digital terrain models allows us a precise characterization of geomorphological features and the identification of relief linked to human activity. The interpretation of LiDAR products aimed at identifying potential traces of cultural interest is based on the visual criteria and the degree to which the features appeared anthropogenic versus non-anthropogenic: shape, pattern, texture and shadow, as in the case of passive data (from the panchromatic to multispectral and hyperspectral imagery). To this aim, it is crucial (1) to process the point clouds and classify terrain and off-terrain objects by applying adequate filtering methods, in order to obtain very accurate DTM; (2) to “manipulate” the DTMs with appropriate techniques of visualization, such as Sky View Factor (Fig. 5), Openness, Local Relief Model (Hesse 2010; Zakšek et al. 2011; Doneus 2013), aimed at emphasizing changes of topography, discontinuities of the landscape, platforms and any kind of earthworks attributable to the human work. In some cases the post-processing based on visualization techniques is fundamental to understand the urban shape of settlements and to identify the main building phases (Lasaponara et al. 2010; Lasaponara & Masini 2009; Masini et al. 2018b, see Fig. 5).

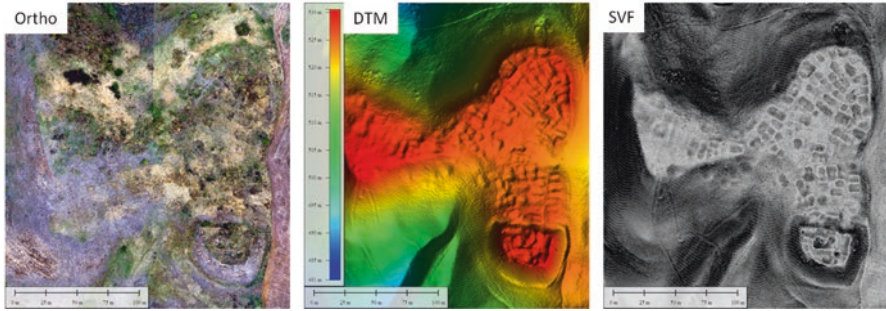


Fig. 5 LiDAR-based investigation of the mediaeval village of *Yrsum* near Matera (Southern Italy) founded in the eleventh century and abandoned in the fifteenth century. The archaeological proxy indicators observed from the DEM derived from LiDAR(middle), as microrelief, are more significant respect to the crop-marks visible from the optical image (left). The Sky View Factor map (right) allows to extract in an automatic way the urban shape of the village

UAV Systems

The increasing technical developments of aerial sensors in terms of miniaturization and data quality offer an invaluable opportunity and at the same time pose several challenges related to the acquisition, processing, integration, analysis and interpretation and above all standardization of the diverse data acquisition and processing steps in order to ensure full operational applicability. Undoubtedly, compared to traditional aerial survey, the unmanned aerial vehicles (UAVs) offer several advantages, particularly low cost and ability to cover large areas in a short time (Campana 2017) under a wide range of wind and weather conditions.

In particular, drone is also useful for aerial thermography (Casana et al. 2014), for which it is mandatory to capture imagery in a short window of time when the contrast in thermal inertia is highest between the target and the background, generally sunrise or sunset. In addition, to reduce the possible changing in thermal values due to difference in the superficial/environmental characteristics, the area under investigation should be surveyed in a time as short as possible.

Moreover, the low altitude of UAV operations along with the improved technical imaging systems enable very detailed surveys with spatial resolution significantly higher compared to those obtained from satellites or manned aircraft. For this reason, drone is especially useful in archaeology before (Kaimaris et al. 2018), during and after excavation. In particular, (i) before the excavations, detail achieved by drone photography and derived results including orthophoto and DEM allows us to identify potential archaeological proxy indicators and (ii) during and after the excavations provides fast and detailed surveys for documentation related both to the advancements in the excavation virtual reconstruction, etc.

Additionally, the rapid response of UAV imaging systems has received a lot of attention also for CH risk monitoring and post disaster damage assessment.

The recent continuous technological developments in UAV platforms, sensors and image processing techniques have resulted in a rapidly increasing use of these

platforms and sensors for remote-sensing applications with new potential in cultural heritage. UAV platforms equipped with sensors for RGB, multispectral, hyperspectral and thermal imaging, as well as with laser scanning, miniature RADAR and passive microwave radiometers, have demonstrated high capability in traditional CH research fields and significant research opportunities in novel UAV-based applications. This is opening up a vast new area of opportunities in remote sensing for cultural heritage for the survey, mapping, monitoring and management. Additionally, UAVs have been traditionally used to test new sensors or integration of instruments, and the continuous improvements in data processing techniques as well as the development of ad hoc processing workflows devised for the specific application issues will allow us to address novel research questions.

Final Remarks: Integrating EO and Social Science New Frontiers of Earth Observations

The currently available digital tools, with particular reference to Copernicus initiatives, make possible to characterize and early understand the state of preservation of cultural properties to identify ongoing changes and assess the effectiveness of conservation and management strategies also addressed to “preventive restoration”, namely, systematic strategic maintenance planned according to the real status of the cultural properties before its deterioration.

The different areas of intervention for CH require the availability of rigorous information for study and documentation, protection and conservation, monitoring, risk assessment and management. In particular, the structural, environmental and microclimatic monitoring is a crucial activity for preserving an important part of the CH to assure a proper conservation of buildings, statues, frescoes, paintings, artworks and also ancient books, tools and artefacts. It is important that management strategies will include the systematic monitoring of structural and environmental parameters as a crucial activity for preserving CH. The full exploitation of data provided by diverse sensors (from aerial, space and ground acquisition) and the usage of 3D models, acquired from airborne and terrestrial laser scans, impose the integration of all the available information (Masini & Soldovieri 2017).

Remote sensing is particularly useful in providing regular and repeated imagery (even for less accessible areas), of unparalleled importance for monitoring the effects of climate change, urban and rural development, degradation, damage from disasters or voluntary destruction, etc. For countries with fledgling sites and monument records, EO provides the only cost-effective means for CH monitoring and preservation as well as for locating and defining archaeological sites and landscapes.

Space technologies have multiple potentialities serving numerous applications in the cultural heritage ranging from the documentation and monitoring to the management and preservation. One of the most important steps for all the diverse applications is the information extraction and the interpretation. The final results are

generally useful information depicted as beautiful pictures that have also the potential to show complex phenomena as paintings or pieces of art. This suggests the possibility of wide dissemination showing to end users and citizens (in museums or schools and other public spaces) the results of the researches using a simple but very effective language as the images are.

Therefore, the main challenge is to (i) fully involve the citizen also from an emotional point of view in the process on monitoring and preservation of cultural properties and landscape and (ii) better exploit the EO and advanced data processing methods to assess and monitor both natural and man risks affecting CH at different scales of intervention, from landscape down at a single building view, with particular reference to Copernicus missions and services. Remote sensing is a key tool for the knowledge, management, monitoring and preservation of cultural and natural heritage, but at the same time the challenge is to fully involve the citizens also from an emotional point of view in the process on monitoring and preservation of cultural properties and landscape.

References

- Agapiou A, Alexakis D, Sarris A, Hadjimitsis DG (2014) Evaluating the potentials of Sentinel-2 for archaeological perspective. *Remote Sens* 6(3). <https://doi.org/10.3390/rs6032176>
- Agapiou A, Lysandrou V, Lasaponara R, Masini N, Hadjimitsis DG (2016) Study of the variations of archaeological marks at neolithic site of Lucera, Italy using high-resolution multispectral datasets. *Remote Sens* 8:723. <https://doi.org/10.3390/rs8090723>
- Albert M-T (2017) The potential of culture for sustainable development in heritage studies. In: Albert M-T, Bandarin F, Pereira Roders A (eds) *Going beyond. Perceptions of sustainability in heritage studies no. 2*. Springer, Cham, pp 33–43
- Campana S (2017) Drones in archaeology. *State-of-the-art and future perspectives*. *Archaeol Prospect* 24(4):275–296
- Canuto MA, Estrada-Belli F, Garrison TG et al (2018) Ancient lowland Maya complexity as revealed by airborne laser scanning of northern Guatemala. *Science* 361:1355
- Casana J, Kanter J, Wiesel A, Cothren J (2014) Archaeological aerial thermography: a case study at the Chaco-era Blue J community, New Mexico. *J Archaeol Sci* 45:207–219
- Chase AF, Chase DZ, Weishampel JF, Drake JB, Shrestha RL, Slatton KC, Awe J, Carter WE (2011) Airborne LiDAR, archaeology, and the ancient Maya landscape at Caracol, Belize. *J Archaeol Sci* 38:387–398
- Chase ASZ, Chase DZ, Chase AF (2017) LiDAR for archaeological research and the study of historical landscapes. In: Masini N, Soldovieri F (eds) *Sensing the past: from artifact to historical site*. Springer, New York, pp 89–100
- Chen F, Masini N, Yang R, Milillo P, Feng D, Lasaponara R (2015) A space view of radar archaeological Marks: first applications of COSMO-SkyMed X-band data. *Remote Sens* 7:24–50. <https://doi.org/10.3390/rs70100024>
- Chen F, Masini N, Liu J, You J, Lasaponara R (2016) Multi-frequency satellite radar imaging of cultural heritage: the case studies of the Yumen Frontier Pass and Niya ruins in the Western Regions of the Silk Road Corridor. *Int J Digit Earth* 9(12):1224–1241. <https://doi.org/10.1080/17538947.2016.1181213>
- Chen F, You J, Tanh P, Zhou W, Masini N, Lasaponara R (2018) Unique performance of spaceborne SAR remote sensing in cultural heritage applications: overviews and perspectives. *Archaeol Prospect* 25:71–79. <https://doi.org/10.1002/arp.1591>

- Doneus M, Briese C, Fera M, Janner M (2008) Archaeological prospection of forested areas using full-waveform airborne laser scanning. *Journal of Archaeological Science* 35(4): 882–893
- Doneus M (2013) Openness as visualization technique for interpretative mapping of airborne LiDAR derived digital terrain models. *Remote Sens* 5:6427–6442
- Doneus M, Briese C (2006) Full-waveform airborne laser scanning as a tool for archaeological reconnaissance. *BAR Int Ser* 1568:99
- Doneus M, Verhoeven G, Atzberger C, Wess M, Ruš M (2014) New ways to extract archaeological information from hyperspectral pixels. *J Archaeol Sci* 52:84–96. <https://doi.org/10.1016/j.jas.2014.08.023>
- Elfadaly A, Attia W, Qelichi MM, Murgante B, Lasaponara R (2018) Management of cultural heritage sites using remote sensing indices and spatial analysis techniques. *Surv Geophys* 39(6):1347–1377
- Evans R, Jones RJA (1977) Crop marks and soils at two archaeological sites in Britain. *J Archaeol Sci* 4(1):163–176
- Evans DH, Fletcher RJ, Pottier C, Chevance JB, Soutif D, Tan BS, Im S, Ea D et al (2013) Uncovering archaeological landscapes at Angkor using LiDAR. *Proc Natl Acad Sci U S A* 110:12595–12600
- Gabellone F, Lanorte A, Masini N, Lasaponara R (2017) From remote sensing to a serious game: digital reconstruction of an abandoned medieval village in Southern Italy. *J Cult Herit*. <https://doi.org/10.1016/j.culher.2016.01.012>
- Hesse R (2010) LiDAR-derived Local Relief Models a new tool for archaeological prospection. *Archaeol Prospect* 17:67–72
- Kaimaris D, Karadedos G, Georgiadis C, Patias P (2018) Locating and Mapping the Traces of the Covered Ancient Theater of Amphipolis (Eastern Macedonia, Greece). *Heritage* 1: 306–319
- Kalayci T, Lasaponara R, Wainwright J, Masini N (2019) Multispectral Contrast of Archaeological Features: A Quantitative Evaluation. *Remote Sens.*, 11, 913, <https://doi.org/10.3390/rs11080913>
- Lasaponara R, Masini N (2008) Advances in Remote Sensing for Archaeology and Cultural Heritage Management, Proc. of I International EARSeL Workshop “Advances in Remote Sensing for Archaeology and Cultural Heritage Management”, Rome 30 September–4 October, 2008, Aracne, Roma, 2008. ISBN: 978-88-548-2030-2
- Lasaponara R, Masini N (2009) Full-waveform Airborne Laser Scanning for the detection of medieval archaeological microtopographic relief. *J Cult Herit* 10S:78–82. <https://doi.org/10.1016/j.culher.2009.10.004>
- Lasaponara R, Masini N (2012) Image Enhancement, Feature Extraction and Geospatial Analysis in an Archaeological Perspective. In: Lasaponara R., Masini N (Eds), *Satellite Remote Sensing: a new tool for Archaeology*, Springer, Verlag Berlin Heidelberg, ISBN 978-90-481-8800-0, https://doi.org/10.1007/978-90-481-8801-7_2, pp. 17–64
- Lasaponara R, Masini N (2014) Beyond modern landscape features: New insights in the archaeological area of Tiwanaku in Bolivia from satellite data. *International Journal of Applied Earth Observation and Geoinformation* 26:464–471, <https://doi.org/10.1016/j.jag.2013.09.006>
- Lasaponara R, Masini N (2017) Preserving the past from space: an overview of risk estimation and monitoring tools. In: Masini N, Soldovieri F (eds) *Sensing the past. From artifact to historical site*. Springer International Publishing, pp 61–88. https://doi.org/10.1007/978-3-319-50518-3_3
- Lasaponara R, Coluzzi R, Gizzi FT, Masini N (2010) On the LiDAR contribution for the archaeological and geomorphological study of a deserted medieval village in Southern Italy. *J Geophys Eng* 7:155–163. <https://doi.org/10.1088/1742-2132/7/2/S01>
- Lasaponara R, Masini N, Pecci A, Perciante A, Pozzi Escot D, Rizzo E, Scavone M, Sileo M (2017) Qualitative evaluation of COSMO SkyMed in the detection of earthen archaeological remains: the case of Pachacamac (Peru). *J Cult Herit*. <https://doi.org/10.1016/j.culher.2015.12.010>
- Luo L, Wang X, Guo H, Lasaponara R, Shi P, Bachagha N, Li L, Yao Y, Masini N, Chen F, Ji W, Cao H, Li C, Hu N (2018) Google earth as a powerful tool for archaeological and cultural heritage applications: a review. *Remote Sens* 10:1558. <https://doi.org/10.3390/rs10101558>

- Masini N, Rizzo E, Lasaponara R, Orefici G (2008) Integrated remote sensing techniques for the detection of buried archaeological adobe structures: preliminary results in Cahuachi (Peru), *Advances in Geosciences* 19:75–82, <https://doi.org/10.5194/adgeo-19-75-2008>
- Masini N, Lasaponara R (2017) Sensing the past from space: approaches to site detection. In: Masini N, Soldovieri F (eds) *Sensing the past. From artifact to historical site*. Springer International Publishing, pp 23–60. https://doi.org/10.1007/978-3-319-50518-3_2
- Masini N, Soldovieri F (2017). *Sensing the Past. From artifact to historical site*. *Geotechnologies and the Environment*, Vol. 16. Springer International Publishing, <https://doi.org/10.1007/978-3-319-50518-3>, pp. 575
- Masini N, Marzo C, Manzari P, Belmonte A, Sabia C, Lasaponara R (2018a) On the characterization of temporal and spatial patterns of archaeological crop-marks. *J Cult Herit.* <https://doi.org/10.1016/j.culher.2017.12.009>
- Masini N, Gizzi FT, Biscione M, Fundone V, Sedile M, Sileo M, Pecci A, Lacovara B, Lasaponara R (2018b) Medieval archaeology under the canopy with LiDAR. The (re)discovery of a medieval fortified settlement in Southern Italy. *Remote Sens* 10:1598
- Opitz R, Herrmann J (2018) Recent trends and Long-standing Problems in Archaeological Remote Sensing. *Journal of Computer Applications in Archaeology* 1(1):19–41. <http://doi.org/10.5334/jcaa.1>
- Patterson TC (1989) History and the post-processual archaeologies. *Man* 24(4):555–566
- Pescarin S (2015) Virtual museums interacting and augmenting cultural heritage: a European perspective. *Lect Notes Comput Sci* 9254
- Stewart C (2017) Detection of Archaeological residues in vegetated areas using satellite synthetic aperture radar. *Remote Sens* 9(2):118. <https://doi.org/10.3390/rs9020118>
- Stewart C, Oren EO, Cohen-Sasson E (2018) Satellite remote sensing analysis of the Qasrawet archaeological site in North Sinai. *Remote Sens* 10(7):1090. <https://doi.org/10.3390/rs10071090>
- Wilson DR (1982) *Air photo interpretation for archaeologists*. St. Martin's Press, London. <https://doi.org/10.1080/00665983.1983.11077756>
- Zakšek K, Oštir K, Kokalj Ž (2011) Sky-view factor as a relief visualization technique. *Remote Sens* 3:398–415

Automatic Change Detection from High-Resolution Satellite Imagery



Thomas Krauß and Jiaojiao Tian

Abstract Change detection using remote sensing data is one of the most essential processing steps for monitoring urban and forest areas. And it provides an invaluable tool for archaeological sites in times of war or natural disasters. However, until now the visual interpretation is still the main technique in analyzing changes from these images. In this chapter, the state of the art of the change detection on archaeology applications and the latest change detection techniques in 2D and 3D are introduced.

Keywords Change detection · Stereo imagery · Culture heritage

Introduction

Following the 11th Europae Archaeologiae Consilium Heritage Management Symposium in 2010, in 2016 a technique session named cultural heritage data acquisition and processing has drawn special attention in the 23rd International Society for Photogrammetry and Remote Sensing (ISPRS) congress, which is one of the most influential international conferences in remote sensing. Remote sensing technology is helping and influencing the archaeology research since long time (van Genderen 1976; Osicki 2000). Change detection is an invaluable remote sensing technique for the archaeology site monitoring, especially during the war time and after natural disasters. Normally two kinds of changes are of interest in archaeology sites: one is the changes of the archaeology constructions, and the other is the changes of the environments, mainly the vegetation cover changes like crops. In 2016, experts of the German Aerospace Center (DLR) have processed and analyzed the remote sensing images from the Temple of Bel, Palmyra's Valley in Syria, and Nimrud archaeological site in Iraq to check the cultural heritage status (Cerra et al. 2016). Besides war,

T. Krauß (✉) · J. Tian

German Aerospace Center (DLR), Remote Sensing Technology Institute, Weßling, Germany
e-mail: thomas.krauss@dlr.de

© Springer Nature Switzerland AG 2020

D. G. Hadjimitsis et al. (eds.), *Remote Sensing for Archaeology and Cultural Landscapes*, Springer Remote Sensing/Photogrammetry,

https://doi.org/10.1007/978-3-030-10979-0_4

the natural disasters like earthquake and tsunami are also non-negligible threats to the cultural heritage. After the earthquake in Emilia-Romagna and Lombardy, Italy, a status survey of the important culture heritage constructions was performed using the remote sensing technologies (Adami et al. 2016). For the second kind of changes, the main goal is to detect the potential threats to the archaeology sites, thus to further protect the culture heritage. The regrowth and reforestation in the coastal area of north Norway were analyzed by comparing the Normalized Difference Vegetation Index (NDVI) applied to Landsat images (Barlindhaug et al. 2007). Nevertheless, in the archaeological operative practice, the use of remote sensing is still underexploited and in particular reduced to a mere visual interpretation exercise. Jahjah et al. (2007) analyzed the pre-postwar situation of Babylon archaeological site. Eighteen aerial photos were digitized and inserted to a GIS system to analyze the changes. In Fig. 1, the red circle has highlighted the location of some disappeared archaeological objects (segments, roads, and ruins).

In case of change monitoring of large heritage regions, visual interpretation is time-consuming, and the quality is difficult to control. Therefore, introducing the latest remote sensing change detection technologies to archaeological site monitoring is of great values. In this chapter, change detection approaches have been categorized into 2D change detection and 3D change detection. In Section “2D Change Detection,” an overview of the existing 2D change detection and their applications

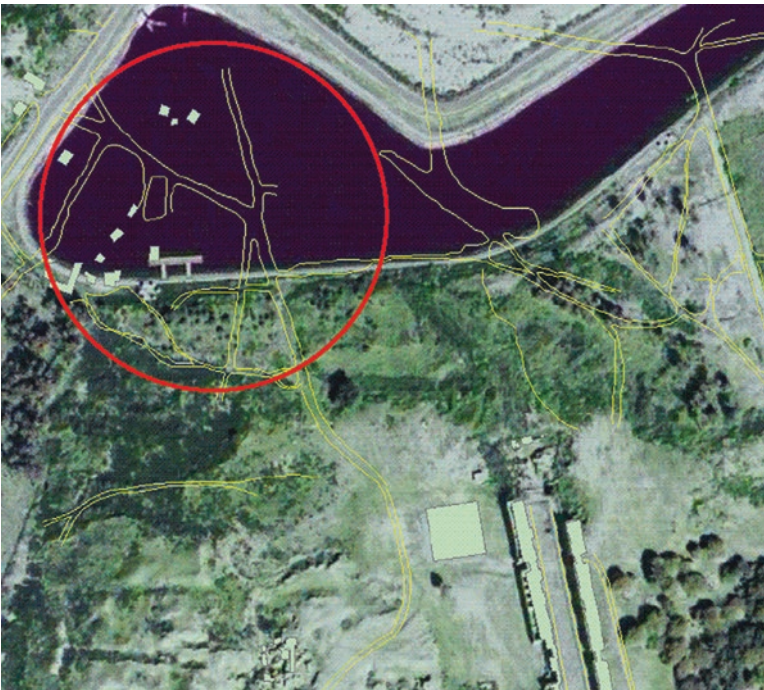


Fig. 1 Location of disappeared archaeological features using GIS technique. (Jahjah et al. 2007)

in archaeology applications is given. In Section “3D Change Detection,” the latest 3D change detection approaches are introduced. Section “Summary” concludes the chapter. Unlike fire or in some cases even flooding events (Alexakis et al. 2014), earthquakes cannot be prevented and cannot be controlled. For this reason the focus of emergency management strategies in these cases is on phases of preparedness and response, i.e., on measures aimed at (i) reducing the risk, (ii) enhancing earthquake resistance, (iii) improving earthquake detection and monitoring, and (iv) developing a response plan (Stovel 1998). In case of an earthquake in fact, the phase regarding damages evaluation is highly important for the first emergency response for securing of people, animals, and structures and during the recovery phase in order to support assistance and inspection teams. Furthermore, such evaluations can be valuable also to reconsider the phases preceding the event (such as prevention, mitigation, and preparedness) providing inputs to evaluation of economic damage and future urban planning and resilience strategies.

2D Change Detection

Recently, many advanced change detection algorithms and techniques have been presented and investigated in literature, most of which are based on satellite images, benefiting the large cover region and short revisit time. Change detection algorithms are built on features which can be extracted from multi-temporal images or digital surface models. They can also be generated with statistical methods by using information from multispectral or hyperspectral channels. Numerous approaches have been developed for change detection using only the 2D satellite images. Many articles reviewing the existing change detection methodologies can be found, such as Coppin and Bauer (1996), Lu et al. (2004), Macleod and Congalton (1998), Mas (1999), and Singh (1989). Recent developments in change detection can be divided into pixel-based and region-based methods. Both require that the multi-temporal remote sensing images are properly co-registered.

Pixel-Based 2D Change Detection

Pixel-based change detection methods are based on features extracted by combining images at pixel level, e.g., pixel-based subtraction, rationing, and image regression. When multispectral information is available, a feature vector can be obtained for each pixel. In addition to the pixel spectrum, more features, such as features after color transformation or texture features, can be extracted. To reduce data redundancy between bands and to emphasize the difference between objects and background, image transformations can be performed, such as color space transformation or principal component analysis (PCA) (Lillesand et al. 1987), Gram-Schmidt (Laben and Brower 2000), and chi-squared transformation. Paper (Fung 1990)

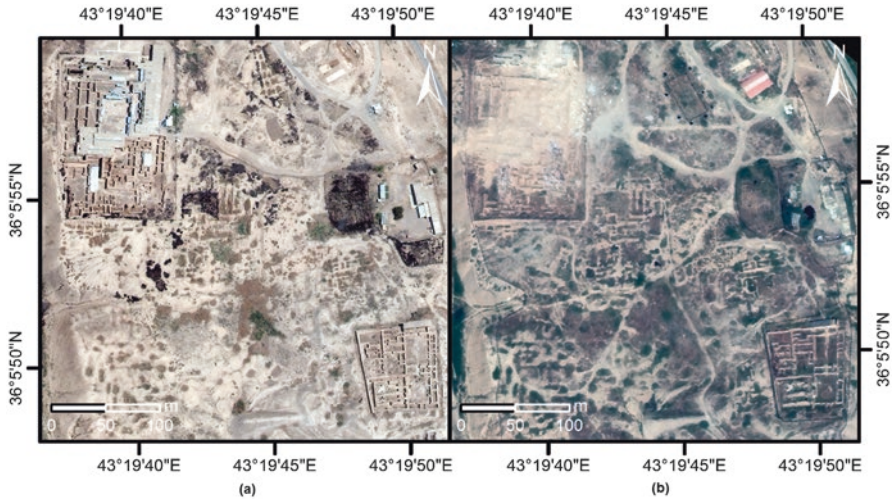


Fig. 2 (a) Nimrud pre- (GeoEye-1, 11th July 2011) and (b) post-event image (WorldView-2, 20th April 2015) (Cerra et al. 2016)

compared image differencing, principal component analysis, and tasseled-cap transformation based on Landsat TM data. These combinations can improve the mathematical combination result, and the original images can be filtered or transformed to achieve a better change map. For the research project applications of geomatics for long-term archaeological settlement pattern analysis, Jahjah et al. (2007) have analyzed the pre-postwar changes in Babylon archaeological site, Iraq. Both historic maps and satellite imagery have been collected for this research. Changes were analyzed with visual interpretation of the historic dataset. In Cerra et al. (2016), a change vector analysis is applied to the GeoEye-1 (Fig. 2a) and WorldView-2 images (Fig. 2b). The destroyed temples were well highlighted in the final result (Fig. 3).

Region-Based 2D Change Detection

The increasing high resolution of satellite images allows the extraction of more detailed changed objects with higher accuracy but also introduces some false alarm that are not related to the changes of interest. The main drawback of pixel-based change detection, called the salt-and-pepper effect, is a result of these false alarms. Therefore, region-based change detection methods have gained more interest in recent years (Blaschke 2005). Instead of analyzing pixels independently, region-based approaches take the pixels inside one meaningful homogeneous region. Some papers refer to this method as object-based change detection (OBCD) (Blaschke 2005; Hall and Hay 2003), as one feature of OBCD is to extract meaningful objects from images. Initially, these meaningful objects were obtained from Geographic

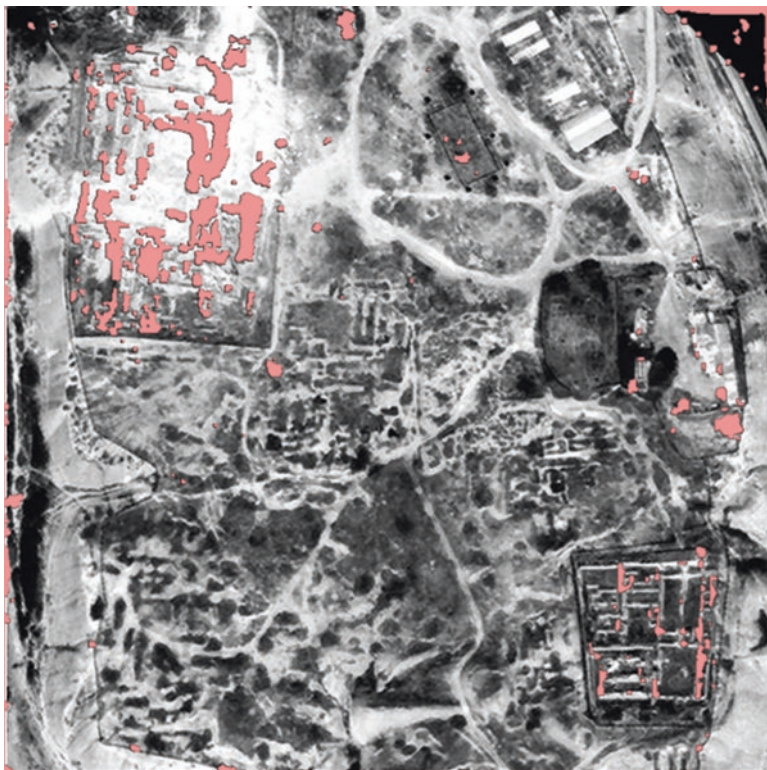


Fig. 3 3D change detection (Cerra et al. 2016)

Information System (GIS) databases (Coppin and Bauer 1996; Durieux et al. 2008; Walter 2004). However, in more recent work, these objects are often extracted using segmentation: thus, the obtained regions might not always be a whole object, such as a complete building or bridge, but very probably only one part of it. Therefore, referring to these methods as region-based is more suitable. Region-based change detection evolved from region-based image analysis, which combines spectral images with segmentation or GIS data for image understanding or land cover classification. The GIS database can also be used as training data, since it includes not only the boundary but also the attributes of each region (Walter 2004). As the use of GIS data is limited to the available data sources, object-based change detection using image data is usually preferred, along with the development of automatic segmentation techniques. After segmentation, the images can be divided into a number of homogeneous regions. The research in this direction is thus focused on obtaining an appropriate segmentation level for all land covers of interest. Bruzzone and Prieto (2000) stated that the original segments that can be used for change detection should be elementary homogeneous regions. However, it is difficult to provide an ideal definition of homogeneous when various objects are of interest: for example, the cars on the road, the cars in car parks, etc. Multilevel segments are preferred for detecting changes to various classes of objects (Bovolo 2009).

In Jahjah et al. (2007), a region-based classification on the very high-resolution satellite images was performed. The results could be used to update the Geographic Information System (GIS) database.

3D Change Detection

Even though 2D multi-temporal satellite images can already provide plenty of useful information, it is usually insufficient when dealing with changes in the vertical direction. Moreover, if only one class of changes, such as the buildings in archaeology site, is of interest, it is often difficult to distinguish between relevant and irrelevant changes. In such cases, the information provided by digital surface models (DSMs) is crucial, as it provides additional height information, which can be indispensable when analyzing changes.

DSMs can assist 3D change detection in a variety of approaches. Limited to the quality of the DSMs generated from stereo imagery, it is hard to reach precise change detection results using only the DSMs. Therefore, DSMs should be used in combination with the spectral information from the original stereo images. As the DSMs are generated using stereo images, spectral information of the same time and area is always available. After orthorectification of these images using the generated DSM, the orthophoto and DSM are well co-registered, and pixel-wise fusion is applicable. Many methods have been proposed to fuse data from two or more kinds of sources. The main difference of these methods is how and when the DSM content is fused with the original images. Three classes of data fusion techniques are summarized in Hall and Llinas (1997) and Pohl and Van Genderen (1998) and named as pixel/data level fusion, feature level fusion, and decision-level fusion approaches, as shown in Fig. 4. For our purpose, the selected fusion method should be able to resolve the quality restriction of DSMs by using the additional information available in the corresponding spectral images. Depending on the quality of the DSMs,

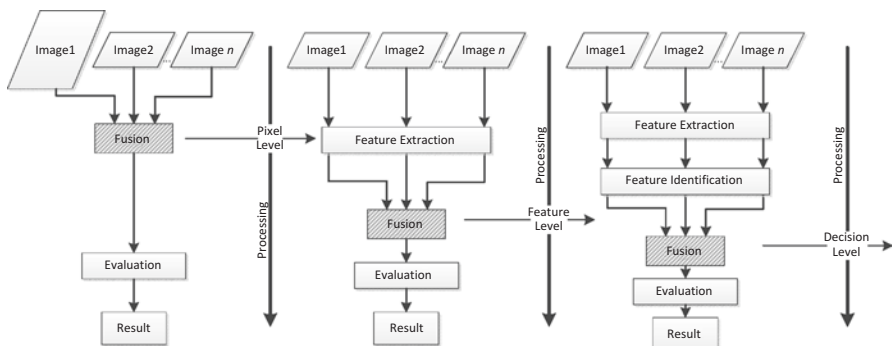


Fig. 4 Processing levels of image fusion

the availability of multispectral channels, and the requirements of the individual change detection task, proper 3D change detection methods have to be developed.

The recently published 3D change detection review paper (Qin et al. 2016a) has classified the 3D change detection approaches into geometric comparison and combined geometric and spectral analysis. The geometric comparison relies mainly on the height information. This kind of approaches performed better on DSMs with higher quality. However, directly subtracting two DSMs does not always result in an ideal change map due to multisensor and co-registration problems (Tian 2013). Shown in Fig. 5 are several newly constructed buildings located in the middle of Fig. 5b. Figure 5c features the direct subtraction results of the corresponding DSMs, showing only the positive values: all the negative values have been set to 0 for better display. As can be seen from this difference image, some unchanged buildings around them also show quite high positive change values. Moreover, some false height values exist in the middle of the rightmost building. However, after the robust difference measure, the noise in the background is successfully reduced, while the yellow and green areas as shown in Fig. 5d, which are more likely to be real changed areas, are not influenced significantly, especially in the building boundary area.

Advanced denoising and distance measurements enable improved change detection results (Akca 2007; Tian et al. 2010; Qin et al. 2016b). But the improvement is negligible in many cases. Under the framework of satellite stereo imagery, spectral information is always available and could lead to enhanced change detection results.

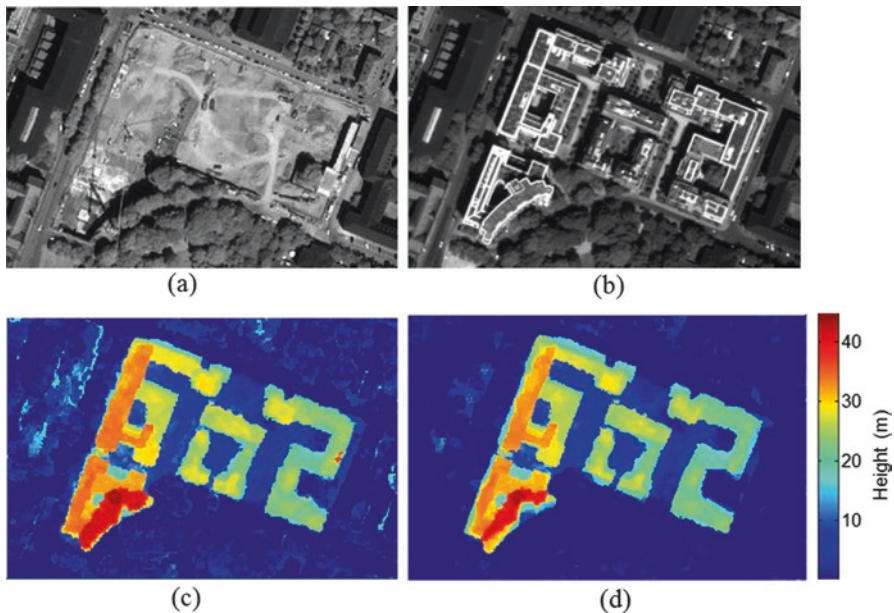


Fig. 5 DSM subtraction results of a building site: panchromatic images from Date1 (a) and from Date2 (b); DSMs subtraction result (c) and the robust height difference result with a window size of 15×15 (d) (Tian 2013)

When only one or some specific objects of changes are of interest, both of the height information and spectral information bring advantages and false alarms. Thus, the main challenge in fusing spectral and height information is to appropriately address the advantages of each information sources without bringing additional false alarms. In general, the available fusion approaches can be categorized into three groups: (1) post-refinement, (2) direct feature fusion, and (3) decision fusion.

Post-refinement

The post-refinement approach starts by extracting change candidates using the height information (Jung 2004). With DSM subtraction, it is computationally easy to obtain the initial change map, which can be improved to a more precise building change map using additional spectral information.

Many 3D change detection methods can be categorized into this approach. Hong et al. (1999) and Zhifang et al. (2003) detected house changes based on DSMs from airborne images. DSMs were computed on the digital photogrammetry workstation Virtuoso. These potential changed areas were generated based on DSM subtraction. The candidate regions obtained were classified into newly built, demolished, and rebuilt buildings using gradient direction histograms. These histograms were extracted from the original airborne images. In Jung (2004), DSMs generated from airborne stereo imagery were employed to obtain an initial change map. The change regions from subtracted DSMs are used as candidates. Subsequently, these candidate regions from four images (two stereo pairs) are classified into building and no-building areas based on graph features. Regions which have building within one dataset and no-building in the other dataset are considered changed buildings. This method will fail if one building is only partly changed or if buildings are rebuilt. Also in high-density building areas, several buildings might exist in one candidate region. A false alarm will be produced if only a part of these buildings have changed. Zhu et al. (2008) detected building changes based on ADS 40 airborne stereo imagery. In their change detection procedure, initial change candidates were derived from the height difference of the two DSMs. Height thresholding followed by low-pass morphological filtering was used to reduce the noise level. These change candidates were combined with the extracted building masks from two dates. The building masks were extracted separately for two DSMs by combining the building extraction result of two methods: local surface normal angle transform and marker-controlled watershed segmentation. Height change was analyzed only for the regions detected as buildings. Tian et al. (2010) tried to refine the building change map using a box-fitting algorithm. To remove the false alarms within the initial change candidate map, in the work of Chaabouni-Chouayakh et al. (2010), post-processing steps such as morphological operations and contextual knowledge introduction have been proposed. These methods help to remove virtual changes and to preserve the real ones. When only building changes are of interest, shape features can also be used to refine the change map (Tian et al. 2011). However the

post-refinement approaches have mainly employed to remove false alarms in the change candidate data. Therefore, the false negatives in the initial step can be hardly recovered with these refinement approaches.

Direct Feature Fusion

Under the category of direct feature fusion, various features were extracted from images and DSMs, respectively. Height difference from DSMs is normally used as change/no-change features or more detailed negative/positive/no-change features. This feature can be directly fused with change features from spectral images to enhance the change detection accuracy. They can be fused either at feature level or at decision level. In the feature fusion level, the 2D change detection approaches can be directly applied by taking height changes as one feature vector. For instance, Sasagawa et al. (2008) combined the pixel changes generated from least square fitting of two images and height changes detected by DSM subtraction, to generate the final change map containing three channels (green, pixel change; red, positive DSM change; blue, negative DSM change). This change map was provided together with spectral imagery for manual interpretation. As an automatic change detection approach, Tian et al. (2013) fused the height and spectral intensity changes of Cartosat-1 data based on change vector analysis (CVA). As a subsequent work, focusing on forest changes, the kernel minimum noise fraction (kMNF) was adopted to transform the change vector matrix that was composed with height change and radiometric changes. As well as feature fusion in pixel-level, the object-level change detection can be performed. In this approach the object map can be produced through image segmentation (Kranz et al. 2017; Tian et al. 2013) and classification (Vögtle and Steinle 2004). In addition, the available GIS database can also be used as object map (Champion 2007).

Tian et al. (2014) have introduced the belief function-based decision fusion to the 3D change detection. The belief function integrated changes that were extracted separately from images and DSM. Images were assumed to highlight all kinds of changes, while height changes were indicating only changes of high-level objects. The fusion model has been further revised in their later publications (Tian et al. 2015).

Post-classification

Land use and land cover classification is a task of great importance in remote sensing. Post-classification approach proposes to detect changes by comparing the classification results or object extraction results. A widely used building change extraction procedure is building detection+change detection (Champion et al. 2008; Olsen 2004; Matikainen et al. 2010). Thus the 3D change detection is actually a follow-up step of 3D building extraction. A main advantage of this approach is to use the

existing classification/object extraction method or the existing GIS data. In addition, a more detailed from-to change map can be delivered. However, in most cases, the change detection performance of this method highly depends on the classification accuracy and efficiency.

Summary

The chapter has presented an exhaustive review of the available literature in the field of change detection, especially 3D change detection. Many practical 2D change detection approaches have been presented, and several applications using these techniques have also been reported. These 2D change detection techniques have recently been adopted for 3D change detection purposes. Previous studies have demonstrated that 3D change detection that works by fusing DSM and spectral imagery is possible and relatively good results can be achieved. However, until now, most of the change detection methods have been carried out only for one or two representative test regions. The 2D/3D change detection approaches are so disparate; thus there is no universally best method/strategy that outperforms others. Further investigation of the existing change detection approaches on archaeology applications could be of interest.

References

- Adami A, Chiarini S, Cremonesi S, Fregonese L, Taffurelli L, Valente MV (2016) The survey of cultural heritage after an earthquake: the case of emilia-lombardia in 2012. *Int Arch Photogramm Remote Sens Spat Inf Sci* 41
- Akca D (2007) Matching of 3d surfaces and their intensities. *ISPRS J Photogramm Remote Sens* 62(2):112–121
- Alexakis DD, Grillakis MG, Koutroulis AG, Agapiou A, Themistocleous K, Tsanis IK, ... & Retalis A (2014). GIS and remote sensing techniques for the assessment of land use change impact on flood hydrology: the case study of Yialias basin in Cyprus. *Natural Hazards and Earth System Sciences* 14(2):413–426
- Barlindhaug S, Holm-Olsen IM, Tømmervik H (2007) Monitoring archaeological sites in a changing landscape—using multitemporal satellite remote sensing as an early warning method for detecting regrowth processes. *Archaeol Prospect* 14(4):231–244
- Blaschke T (2005) Towards a framework for change detection based on image objects. *Götinger Geographische Abhandlungen* 113:1–9
- Bovolenta F (2009) A multilevel parcel-based approach to change detection in very high resolution multitemporal images. *IEEE Geosci Remote Sens Lett* 6(1):33–37
- Bruzzone L, Prieto DF (2000) Automatic analysis of the difference image for unsupervised change detection. *IEEE Trans Geosci Remote Sens* 38(3):1171–1182
- Cerra D, Plank S, Lysandrou V, Tian J (2016) Cultural heritage sites in danger towards automatic damage detection from space. *Remote Sens* 8(9):781
- Chaabouni-Chouayakh H, Krauss T, d'Angelo P, Reinartz P (2010) 3d change detection inside urban areas using different digital surface models. *Int Arch Photogramm Remote Sens Spat Inf Sci* 38:86–91

- Champion N (2007) 2d building change detection from high resolution aerial images and correlation digital surface models. *Int Arch Photogramm Remote Sens Spat Inf Sci* 36(Part 3):W49A
- Champion N, Matikainen L, Rottensteiner F, Liang X, Hyypä J (2008) A test of 2d building change detection methods: Comparison, evaluation and perspectives. *Int Arch Photogramm Remote Sens Spat Inf Sci* 37:297–305
- Coppin PR, Bauer ME (1996) Digital change detection in forest ecosystems with remote sensing imagery. *Remote Sens Rev* 13(3–4):207–234
- Durieux L, Lagabrielle E, Nelson A (2008) A method for monitoring building construction in urban sprawl areas using object-based analysis of spot 5 images and existing gis data. *ISPRS J Photogramm Remote Sens* 63(4):399–408
- Hong F, Jianqing Z, Zuxun Z, Zhifang L (1999) House change detection based on dsm of aerial image in urban area. *Geospat Inf Sci* 2(1):68–72
- Fung T (1990) An assessment of tm imagery for land-cover change detection. *IEEE Trans Geosci Remote Sens* 28(4):681–684
- Hall DL, Llinas J (1997) An introduction to multisensor data fusion. *Proc IEEE* 85(1):6–23
- Hall O, Hay GJ (2003) A multiscale object-specific approach to digital change detection. *Int J Appl Earth Obs Geoinf* 4(4):311–327
- Jahjah M, Olivieri C, Invernizzi A, Parapetti R (2007) Archaeological remote sensing application pre-post war situation of babylon archaeological site iraq. *Acta Astronaut* 61(1):121–130
- Jung F (2004) Detecting building changes from multitemporal aerial stereo pairs. *ISPRS J Photogramm Remote Sens* 58(3):187–201
- Kranz O, Lang S, Schoepfer E (2017) 2.5 d change detection from satellite imagery to monitor small-scale mining activities in the Democratic Re-public of the Congo. *Int J Appl Earth Obs Geoinf* 61:81–91
- Laben CA, Brower BV (2000) Process for enhancing the spatial resolution of multispectral imagery using pan-sharpening, U.S. Patent 6,011,875, issued January 4, 2000
- Lillesand TM, Kiefer RW, Chipman J (1987) *Remote sensing and image processing*. John Wiley & Sons, New York
- Zhifang L, Jianqing Z, Zuxun Z, Hong F (2003) Change detection based on dsm and image features in urban areas. *Geospat Inf Sci* 6(2):35–41
- Lu D, Mausel P, Brondizio E, Moran E (June 2004) Change detection techniques. *Int J Remote Sens* 25(12):2365–2407
- Macleod RD, Congalton RG (1998) A quantitative comparison of change-detection algorithms for monitoring eelgrass from remotely sensed data. *Photogramm Eng Remote Sens* 64(3):207–216
- Mas J-F (1999) Monitoring land-cover changes: a comparison of change detection techniques. *Int J Remote Sens* 20(1):139–152
- Matikainen L, Hyypä J, Ahokas E, Markelin L, Kaartinen H (2010) Automatic detection of buildings and changes in buildings for updating of maps. *Remote Sens* 2(5):1217–1248
- Olsen BP (2004) Automatic change detection for validation of digital map databases. *Int Arch Photogramm Remote Sens* 30:569–574
- Osicki A (2000) A review of remote sensing application in archaeological research. *Research report for Geography course*, pp. 1–22
- Pohl C, Van Genderen JL (1998) Review article multisensor image fusion in remote sensing: concepts, methods and applications. *Int J Remote Sens* 19(5):823–854
- Qin R, Tian J, Reinartz P (2016a) 3d change detection– approaches and applications. *ISPRS J Photogramm Remote Sens* 122:41–56
- Qin R, Tian J, Reinartz P (2016b) Spatiotemporal inferences for use in building detection using series of very-high-resolution space-borne stereo images. *Int J Remote Sens* 37(15):3455–3476
- Sasagawa A, Watanabe K, Nakajima S, Koido K, Ohno H, Fujimura H (2008) Automatic change detection based on pixel-change and dsm-change. *Int Arch Photogramm Remote Sens Spat Inf Sci* 37:1645–1650
- Singh A (1989) Digital change detection techniques using remotely-sensed data. *Int J Remote Sens* 10(6):989–1003

- Stovel H (1998). Risk preparedness: a management manual for world cultural heritage, Rome: ICCROM
- Tian J (2013) 3D change detection from high and very high resolution satellite stereo imagery. PhD thesis, Osnabrueck University
- Tian J, Chaabouni-Chouayakh H, Reinartz P, Krauß T, d'Angelo P (2010) Automatic 3D change detection based on optical satellite stereo imagery. ISPRS TC VII Symposium 100 Years ISPRS, volume XXXVIII - Part 7B, Vienna, pp 586–591
- Tian J, Chaabouni-Chouayakh H, Reinartz P (2011) 3d building change detection from high resolution spaceborne stereo imagery. In Multi- Platform/Multi-Sensor Remote Sensing and Mapping (M2RSM), 2011 International Workshop on, pp. 1–7. IEEE
- Tian J, Reinartz P, d'Angelo P, Ehlers M (2013) Region-based automatic building and forest change detection on Cartosat-1 stereo imagery. ISPRS J Photogramm Remote Sens 79:226–239
- Tian J, Cui S, Reinartz P (2014) Building change detection based on satellite stereo imagery and digital surface models. IEEE Trans Geosci Remote Sens 52(1):406–417
- Tian J, Reinartz P, Dezert J (2015) Building change detection in satellite stereo imagery based on belief functions. In Urban Remote Sensing Event (JURSE), 2015 Joint, pp. 1–4. IEEE
- van Genderen JL (1976) Remote sensing in archaeology. Archaeol J 133(1):1–8
- Vögtle T, Steinle E (2004) Detection and recognition of changes in building geometry derived from multitemporal laser scanning data. Int Arch Photogramm Remote Sens Spat Inf Sci 35(B2):428–433
- Walter V (2004) Object-based classification of remote sensing data for change detection. ISPRS J Photogramm Remote Sens 58(3):225–238
- Zhu L, Shimamura H, Tachibana K, Li Y, Gong P (2008) Building change detection based on object extraction in dense urban areas. Int Arch Photogramm Remote Sens Spat Inf Sci 37:905–908

SAR for Archaeological Prospection in Europe and in the Middle East



Christopher Stewart

Abstract This chapter describes recent studies on the use of synthetic aperture radar for archaeological prospection and anthropogenic feature extraction. Radar remote sensing can provide unique information about objects on the ground from its sensitivity to the relative permittivity of materials and to surface roughness, as a function of the microwave wavelength. Methods have been developed to detect residues of buried structures over land cover types typical to Europe and the Middle East. These include agriculture, grassland and sand-covered areas. The techniques attempt to exploit the full information content of radar data, contained in both the amplitude and phase of the signal. They also attempt to make efficient use of time series. Results show that surface residues of buried archaeological structures in temperate vegetated areas can be identified in variously processed radar images. Anthropogenic features in sand-covered areas can also be efficiently detected. Developments in Big Data analytics and Earth observation data accessibility have the potential to bring radar remote sensing closer to the cultural heritage community.

Keywords Synthetic Aperture Radar · Big Data · Cultural Heritage · Archaeological Prospection

Introduction

Microwave signals emitted by active sensors are uniquely sensitive to various properties of target materials. Synthetic aperture radar (SAR) imagery can reveal subtle variations in surface roughness, relative to the signal wavelength (Ulaby et al. 1982). SAR is also sensitive to the relative permittivity of materials (Massonnet and Souyris 2008), which, in the case of soils, is largely related to the presence of moisture (Dubois et al. 1995). Variations in surface roughness and moisture content may

C. Stewart (✉)

Earth Observation Programmes, Future Systems Department, European Space Agency (ESA), Frascati, Italy

© Springer Nature Switzerland AG 2020

D. G. Hadjimitsis et al. (eds.), *Remote Sensing for Archaeology and Cultural Landscapes*, Springer Remote Sensing/Photogrammetry,

https://doi.org/10.1007/978-3-030-10979-0_5

indicate the presence of archaeological objects (Wiseman and El-Baz 2007; Stewart 2017). Moreover, in dry sand, the low relative permittivity may permit some signal penetration, which can also be exploited for archaeological applications (Stewart et al. 2016).

Despite the utility of SAR for archaeological applications, microwave remote sensing has experienced a slower rate of uptake by the cultural heritage community than remote sensing in the optical region. This is perhaps due to the challenges associated with the processing and interpretation of radar data and, until recently, high costs and lack of data availability.

We are currently experiencing an unprecedented increase in the volume, variety and velocity of remote data acquisition, referred to as “Big Data” (Manyika et al. 2011). Moreover, we are seeing a positive trend in the availability, accessibility and openness of scientific data and results. These developments are revolutionising the way remote sensing is carried out and is opening up opportunities for users of existing and new application areas, including cultural heritage.

This chapter summarises recent studies that aim to take advantage of new opportunities brought by the Big Data revolution to exploit large time series of SAR data for archaeological prospection. Two studies are described here. Each focuses on very different geographical regions, land cover types and methods of prospection. The first involves the use of SAR to detect vegetation or soil residues of buried archaeological structures in areas surrounding the city of Rome, in Italy. The second demonstrates the use of SAR to efficiently detect buried or surface traces of human activity in sand-covered regions of North Sinai, Egypt.

SAR in Vegetated Areas

The aim of the study presented here is to assess the use of both the amplitude and phase of the SAR signal to detect surface residues of buried archaeological structures in a temperate vegetated region. These are likely to be indirect indicators of buried structures in the form of crop or soil marks. No significant penetration of the radar signal into the ground would take place in these areas given the high relative permittivity from the water in the soil and the overlying vegetation. The research summarised here is described in more detail in Stewart (2017).

Six areas of interest (AOIs) have been selected for the analysis. These all surround the area of Rome and comprise agricultural fields or pasture beneath which archaeological structures are known to exist from noninvasive archaeological survey (see Fig. 1). The geology of three of the AOIs (Appia, Prenestina and Veii) is characterised by volcanic deposits, mainly pyroclastic tuff, from the Albano and Sabatino volcano districts, with undulating eroded valleys. The remaining three AOIs of Ostia, Portus and Salaria are in the alluvial Tiber valley and delta, characterised by very flat topography.

The SAR data procured for the analysis includes a large time series of very-high-resolution imagery acquired by the Italian Constellation of Small Satellites for

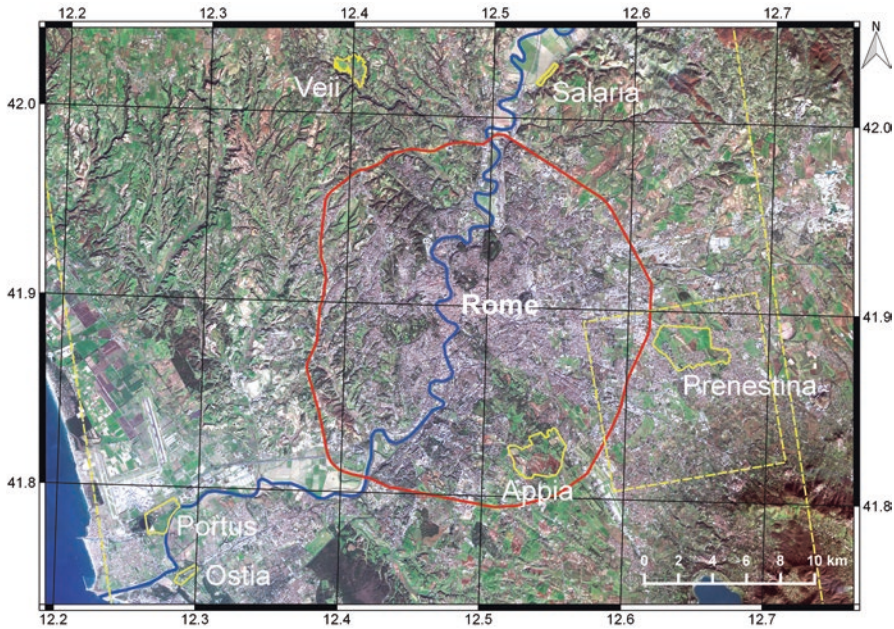


Fig. 1 Areas of interest (AOIs) shown in yellow polygons. Footprints of CSK stripmap and spotlight data shown as dashed yellow rectangles

Table 1 Details of CSK data acquired for the analysis

Sensor mode	Enhanced spotlight	Stripmap HIMAGE
Number of scenes	27	77
Acquisition date range (year/month)	2010/06 to 2012/08	2011/03 to 2015/07
Polarisation	24 × HH, 3 × VV	HH
Pass	Asc	Asc
Scene centre incidence angle	25.25	33.95
Spatial resolution	1 m	2.5 m
Wavelength	3.1 cm (X-band)	

Mediterranean basin Observation (COSMO-SkyMed) (see Table 1). This data was provided by the Italian Space Agency (ASI). It was obtained for the following reasons: (1) to have as large as possible a time series in order to cover a range of environmental and ground conditions; (2) to have data at the highest available spatial resolution, to resolve small-scale features corresponding to recognisable archaeological structures; and (3) to have the highest possible frequency of acquisition, to be able to perform coherence and interferometric SAR (InSAR) digital elevation model (DEM) calculation, without complete loss of coherence.

Processing was carried out to derive three types of information from the SAR data, including (1) multitemporal speckle filtered backscatter, which may be sensi-

tive to roughness and moisture anomalies at the surface caused by underlying archaeological structures; (2) interferometric coherence, which may be sensitive to small-scale random change between acquisitions, which in turn may provide an indicator of vegetation characteristics altered by the presence of buried structures; and (3) DEM, derived from interferometry, to detect subtle surface topographic traces of archaeological features beneath the ground.

Filtered Backscatter (Roughness and Moisture Anomalies)

As previously stated, SAR backscatter is sensitive to variations in both surface roughness and soil moisture content. Subtle changes in either may be due to the presence of buried structures, which may result from the same mechanisms which lead to the well-studied phenomena of crop and soil marks (Jones and Evans 1975; Evans and Jones 1977; Wilson 2000; Agapiou et al. 2013). These may be visible as differences in SAR backscatter. To better distinguish these from the image speckle, a method was adopted to remove as much of the image speckle as possible while retaining the spatial resolution and small differences which may appear in individual images. To achieve this, multitemporal De Grandi (1997), speckle filtering was carried out. The De Grandi filter averages in the temporal domain parts of images that are statistically homogenous, reducing the speckle, but retaining key statistical backscatter properties of each single image. If an area of the coregistered images contains a feature in only one or a few images, the areas to be averaged are divided to exclude this feature (De Grandi et al. 1997). The De Grandi filter preserves the spatial resolution of the input images. The De Grandi filter is thus suitable for identifying small anomaly features with only slight variations in backscatter from surrounding areas (De Grandi et al. 1997; Stewart et al. 2016).

Interferometric Coherence (Small-Scale Random Change Between Acquisitions as Indicator of Vegetation Characteristics)

Another type of information that was extracted from the SAR data for the analysis includes the interferometric coherence between consecutive CSK image acquisitions. The interferometric coherence can provide an indication of the extent of random and small-scale spatial change in surface materials between image acquisitions. Such change may include the position and orientation of plants as they are blown by the wind. This in turn may provide information on vegetation type and growth, as the extent of random wind-driven displacement differs by vegetation type and stage of growth. Subtle differences in vegetation type and height may be due to underlying archaeological structures.

DEM (Subtle Surface Relief Variations)

A third type of information includes heights calculated through SAR interferometry (InSAR). Given the right conditions, with InSAR it is possible to derive height information through the phase difference between SAR image acquisitions separated by a spatial baseline perpendicular to the satellite azimuth. To derive such information over mainly vegetated areas, it was necessary to apply a technique called SBAS (small baseline subsets) (Berardino et al. 2002). SBAS works through the generation of many interferograms, each with minimal spatial (for displacement velocities) and temporal baselines between acquisitions to avoid decorrelation effects (Berardino et al. 2002). SBAS is mainly used to calculate small-scale displacement, but it can also be used for DEM generation.

Analysis of Features

Surface residues of buried structures have been found in the filtered CSK backscatter, coherences and DEMs. In an attempt to understand the mechanisms and conditions responsible for the appearance of residues in each layer in which they were present, an analysis of results has been carried out with interferometric coherence (calculated from the SAR data) and potential soil moisture deficit (PSMD) (derived from rainfall and potential evapotranspiration measurements). The methodology is described in more detail in Stewart (2017).

Results

Archaeological residues were found in all three types of processed SAR data (backscatter, coherence and DEM). More residues were found in the area of the Tiber valley and delta, characterised by alluvial substrate and flat topography. Less residues were found in the volcanic districts on either side of the Tiber valley, characterised by a volcanic substrate and undulating topography. Residues were found in particular in three of the AOIs (Portus, Salaria and Prenestina). In these areas, features in the processed SAR data corresponded with archaeological finds documented in the archaeological surveys. These are discussed here according to the type of SAR processed data on which they appeared.

Filtered Backscatter

De Grandi speckle filtering made a huge difference in the ability to detect potential archaeological features. Figure 2 shows the difference that De Grandi filtering can make on the clarity of features.

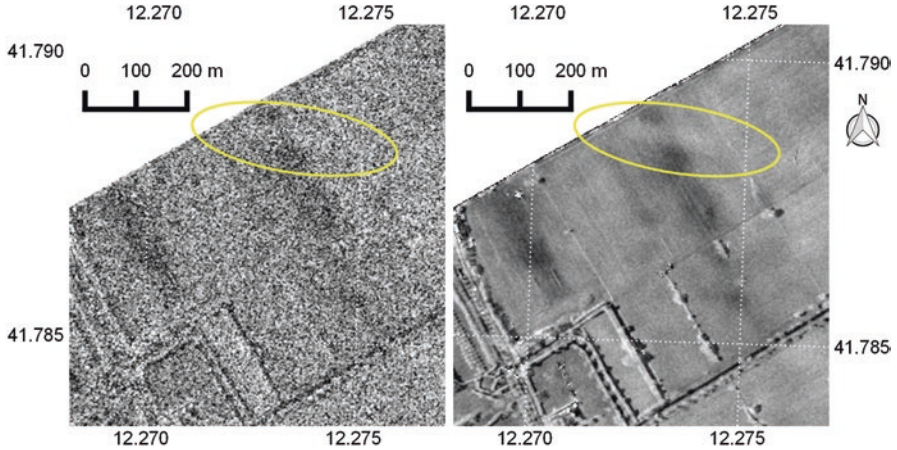


Fig. 2 Example of De Grandi multitemporal speckle filter. Left: Single image with surface residue of a buried Claudian canal (in yellow ellipse), barely evident in the Portus AOI. Right: The same image after having undergone De Grandi multitemporal speckle filtering using all 77 images in time series. The residue of the Claudian canal appears much clearer on the De Grandi filtered image

Several features of both high and low relative backscatter corresponded with buried archaeological structures in the Portus, Prenestina and Salaria AOIs.

In the Portus AOI, a feature of lower backscatter corresponds with built-up areas detected by a magnetometry survey carried out by Keay et al. (2005) (see Fig. 3). In the same AOI, a feature of higher backscatter corresponds with a Claudian canal, detected in the same survey (see Fig. 4). The two features are not correlated, in that they are not always visible in the same filtered imagery. Neither corresponds with PSMD.

The Claudian canal is more visible in times of high coherence (see Figs 4 and 6). At X-band wavelengths and 16-day temporal baselines, coherence is almost immediately lost (Zalite et al. 2016; Zalite et al. 2014). If coherence is high, it is likely therefore that the field is fallow or that it contains vegetation that does not move very much in the wind (such as beans tied to poles). In either case, it is likely that the feature is a soil mark.

The urban feature never appears clearly at times of high coherence (see Fig. 4). It is therefore possible that this is a crop mark, as vegetation tends to cause loss in coherence. The fact that the mark is distinguishable by lower backscatter would suggest the surface is less moist, or smoother; this would correspond with a negative crop mark, characterised by stunted growth caused by buried building material.

A feature of high backscatter was observed in some of the filtered backscatter imagery in the Prenestina AOI (see Figs 7 and 8). The feature corresponds with the suspected continuation of a buried road, documented by Quilici (1974). This may be a crop mark, given that the area is always characterised by low coherence.

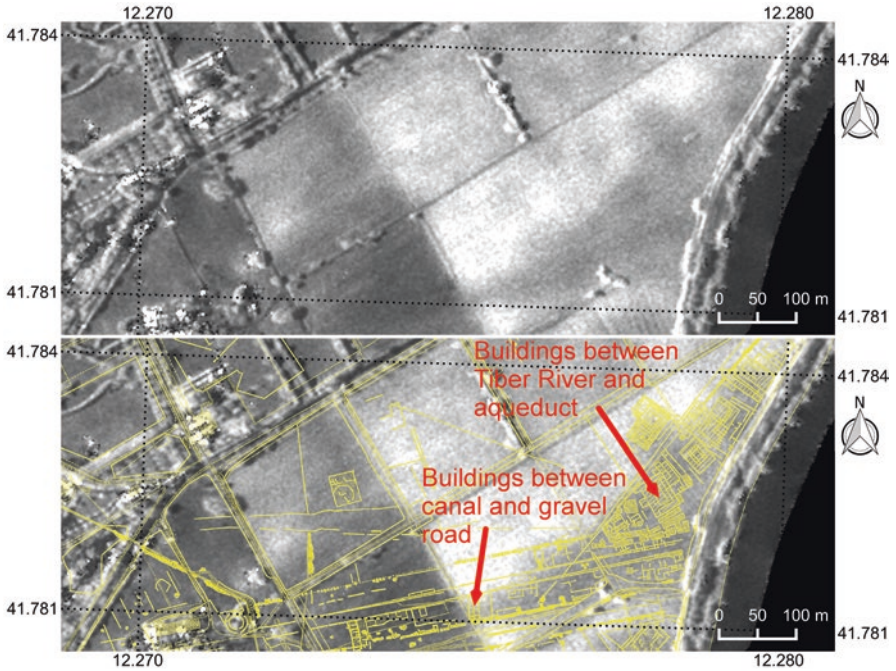


Fig. 3 Residue of buried buildings on image of De Grandi speckle filtered backscatter acquired on 9 July 2012. Overlain in yellow on the image below is the interpretation by Keay and his colleagues of the integrated archaeological survey (mainly magnetometry) published in Keay et al. (2005). COSMO-SkyMed data provided by the Italian Space Agency

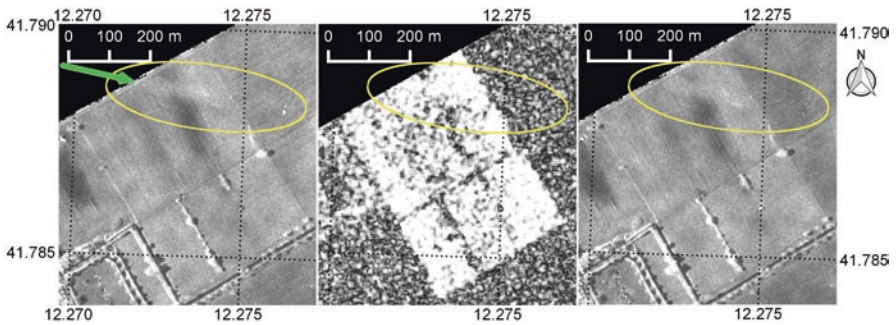


Fig. 4 Residue of Claudian canal (highlighted by yellow ellipse) on image of filtered backscatter acquired on 22 April 2011 (left) and 8 May 2011 (right). In the centre is the coherence image between these two acquisitions. Very-high coherence can be observed over the fields in which the residue is visible. The green arrow indicates the location and direction from which the photo in Fig. 5 was acquired. COSMO-SkyMed data provided by the Italian Space Agency



Fig. 5 Photo acquired of the location of the residue of the Claudian canal. Photo acquired on 24 May 2013 at 18:45. No trace of the Claudian canal is visible on the ground at the time of photo acquisition

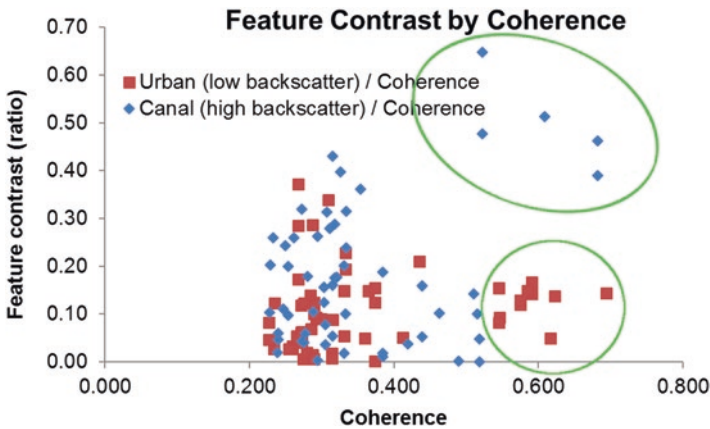


Fig. 6 Graph showing feature contrast (clarity) of the Claudian canal (in blue diamonds) and the urban area (in red squares), plotted against coherence. Where high coherence is observed, the contrast of the Claudian canal is often high, while the contrast of the urban area is consistently low. These patterns are shown in green ellipses

Moreover, it may be a positive crop mark, given that the feature is characterised by higher backscatter, due either to higher moisture or roughness, which may be a result of more abundant vegetation. The time of greatest feature visibility corresponds with highest PSMD. This would support the argument of a crop mark, which

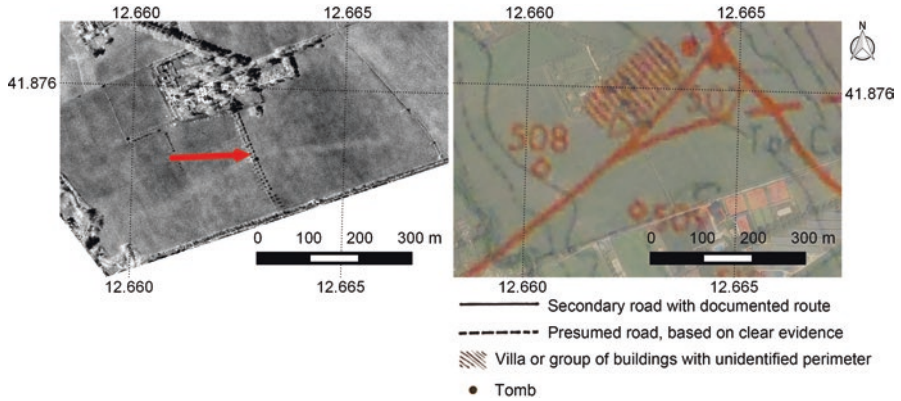


Fig. 7 Left: Residue of road visible on image of filtered backscatter, acquired on 25 July 2010. Right: Archaeological chart of Quilici (1974) of the same area overlain on true-colour Pleiades image acquired on 20 April 2014. Red arrow indicates location and direction from which photo in Fig. 8 was acquired. COSMO-SkyMed data provided by the Italian Space Agency. Pleiades data provided by the European Space Agency



Fig. 8 Photo of residue shown in Fig. 7, acquired on 19 September 2015 at 17:03. No evidence of residue was visible on the ground at that time

is more likely to appear at times of low moisture. No residues were found over the other features documented in this area. However, in most cases these have been interpreted from scant surface fragments which do not have a coherent form and are unlikely to leave a recognisable trace in the SAR data.

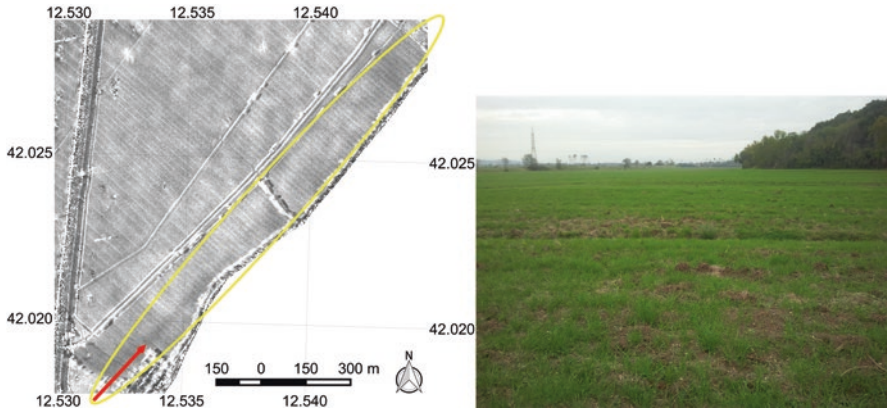


Fig. 9 Left: Image of filtered backscatter acquired on 7 April 2013 showing a trace of the ancient Via Salaria (highlighted by yellow ellipse). Red arrow indicates location and direction from which photo was acquired. Right: Photo acquired on 1 October 2016 at 17.14 of the location of the trace of the ancient Via Salaria. There was no visible evidence of the ancient Via Salaria on the ground at this time. COSMO-SkyMed data provided by the Italian Space Agency

In the Salaria AOI, a trace of the ancient Via Salaria is visible in some of the imagery (see Fig. 9). This appears as low backscatter. There is no clear correspondence between the feature clarity and PSMD, although the times of highest contrast coincide with a period of low PSMD, which is not a characteristic of crop marks. Throughout most of the time series, there is no clear feature contrast, and coherence is consistently low. At the time of feature contrast, the coherence is at the same low value as throughout most of the time period. Given that the feature is characterised by low backscatter, and given the low coherence in all images, it is likely that these residues are manifestations of negative crop marks. This would be possible if the paving stones of the ancient Via Salaria were buried beneath the ground.

Interferometric Coherence

In some cases, residues were present in the coherence images. These residues only occur over the Prenestina AOI and are always characterised by lower coherence. The residues correspond with the location of ancient roads documented by Quilici (1974). An inspection of these areas on the ground showed that most correspond with slight topographic valleys, although in one case no topography was visible on the ground. However, in this last case, a very-high-resolution DEM was produced from UAV photogrammetry in which a very slight topographic trace was notable. It may be therefore that the low coherence features are due to increased crop growth at the bottom of valleys where water would collect. The coherence residues generally appear at times of high soil moisture deficit and less with high soil moisture surplus. This also supports the argument that the coherence residues are crop marks.

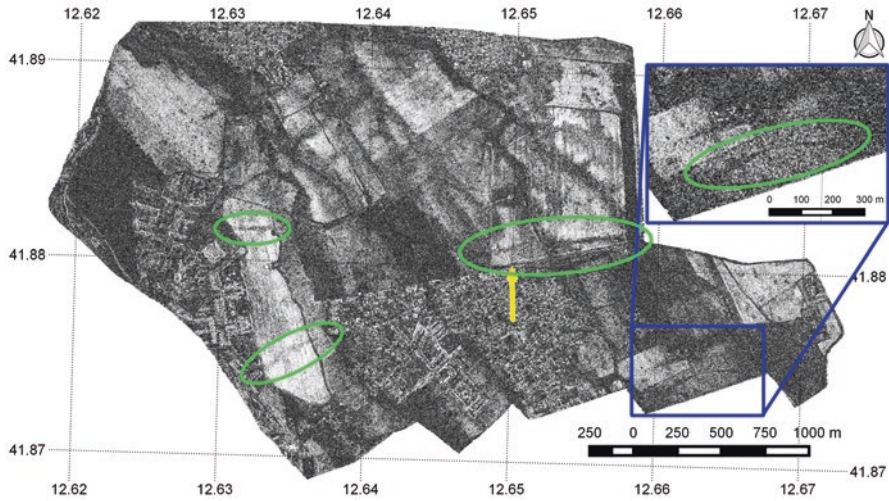


Fig. 10 Coherence image from CSK spotlight InSAR pair acquired on 9 and 25 July 2010 over the Prenestina AOI. Green ellipses show the locations of residues. The yellow arrow shows the location and direction from which the photo in Fig. 12 was acquired on the ground. COSMO-SkyMed data provided by the Italian Space Agency

Only some of the coherence residues correspond with faint backscatter traces, apart from one feature (see inset of Fig. 10), which clearly corresponds with a backscatter residue (see Figs. 7 and 8). Aside from this last feature, all correspond with clear topographic traces on the SBAS DEM (see Figs. 11 and 13).

DEM

An attempt at deriving heights using the SBAS technique only worked well for the Prenestina AOI. Over all other AOIs, the coherence was too low for most of the interferograms for the technique to work. The topographic features on the Prenestina AOI correspond with the location of ancient roads documented by Quilici (1974) (see Figs. 13 and 14). The scale of the topographic traces range from 50 m to 145 m in width and were all around 2 m in height.

Over the Prenestina AOI, while most of the interferograms had too low coherence, a very coarse DEM was possible from the image pair acquired on 10 and 26 August 2012 (see Fig. 15). The DEM is very noisy given the low coherence, but the ancient Via Salaria can be seen very clearly as a valley or ditch traversing the fields. This corresponds with the filtered backscatter residue (see Fig. 9), but interestingly, no obvious topographic trace is visible on the ground (see Fig. 9).

The image pair used for the DEM is not amongst those that reveal residues of the Via Salaria as backscatter anomalies. The presence of this slight valley may be the reason why the backscatter residue appears more clearly at a time of low PSMD,

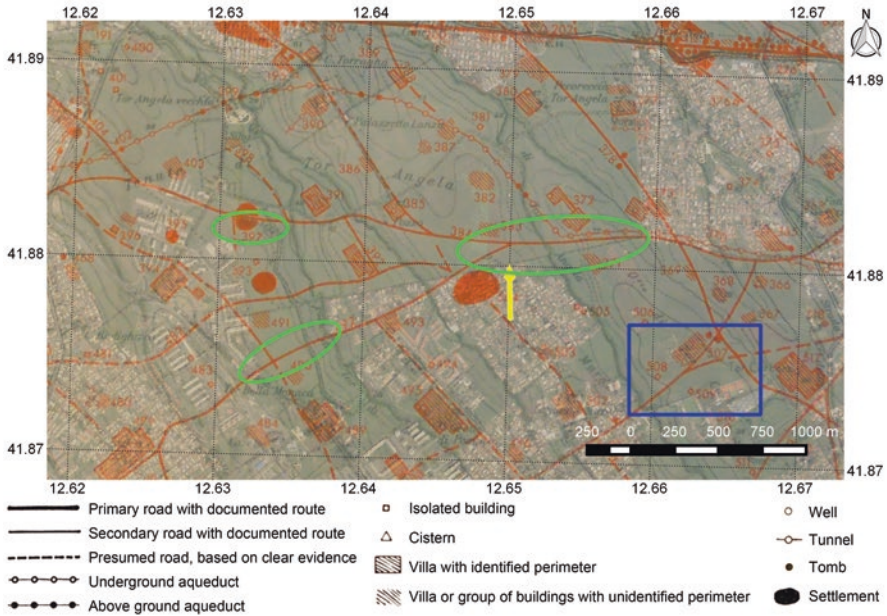


Fig. 11 Subset of archaeological chart over the Prenestina AOI published by Quilici (1974) as part of the Forma Italiae series. Red features show documented archaeological structures. Green ellipses and blue rectangle show the locations of residues visible in Fig. 10. The yellow arrow shows the location and direction from which the photo in Fig. 12 was acquired on the ground



Fig. 12 Photo acquired of one of the residues shown in Fig. 10. The photo shows that this residue is situated in the centre of a broad valley. The photo was acquired on 6 October 2015 at 12:36

as this would perhaps enhance the difference between abundant vegetation growth in the valley and stunted growth over the buried road.

The DEM image acquisitions coincide with high PSMD and high coherence. Perhaps shorter and dryer vegetation is less likely to contribute to temporal decorrelation than if the vegetation were healthy and abundant. Crop marks typically

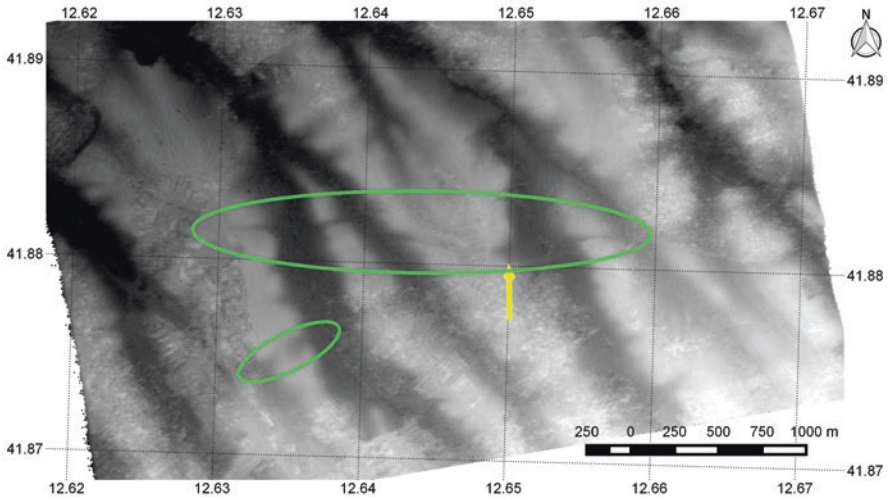


Fig. 13 SBAS DEM produced from CSK stripmap imagery over the Prenestina AOI. Green ellipses show the locations of archaeological features. Yellow arrow shows the location and direction from which the photo in Fig. 12 was acquired. COSMO-SkyMed data provided by the Italian Space Agency

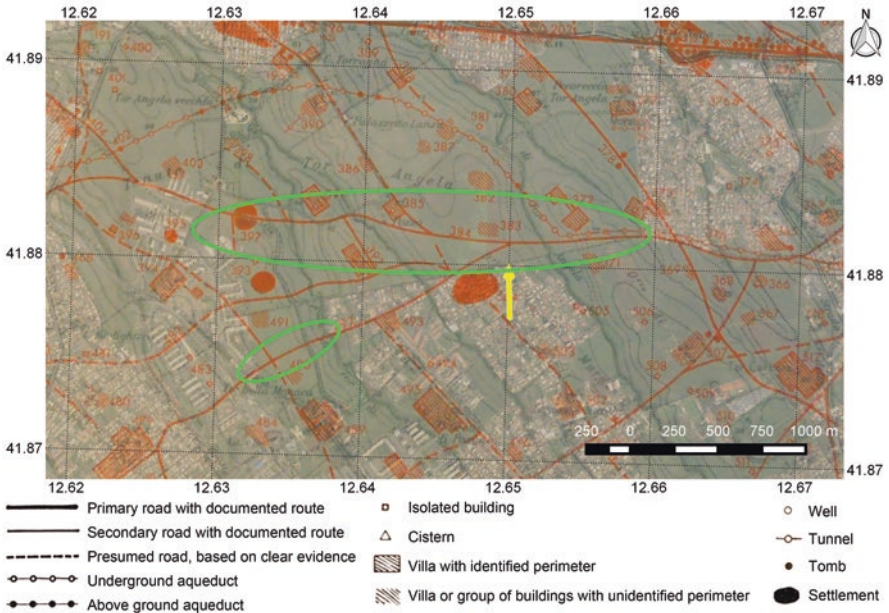


Fig. 14 Subset of archaeological chart over the Prenestina AOI published by Quilici (1974) as part of the Forma Italiae series. Annotations in red show documented archaeological structures. Green ellipses show the locations of residues. Yellow arrow shows the location and direction from which the photo in Fig. 12 was acquired

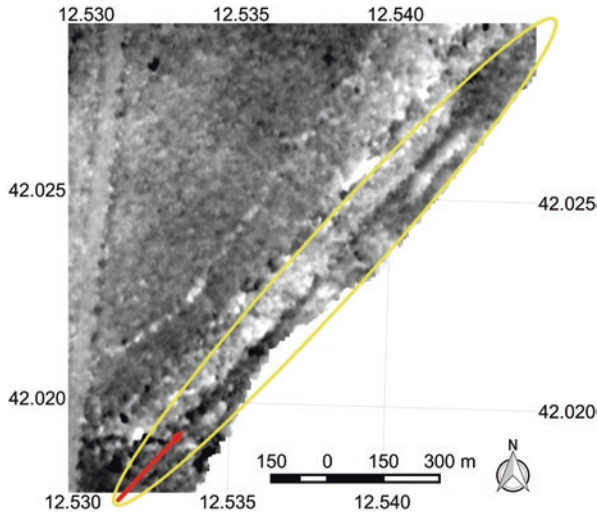


Fig. 15 DEM over the Salaria AOI derived from InSAR using the CSK stripmap image pair acquired on 10 and 26 August 2012. Yellow ellipse shows location of the residue of the ancient Via Salaria. The DEM is very noisy, but the residue of the ancient Via Salaria can clearly be seen. Red arrow shows the direction and location from which the photo in Fig. 9 was acquired

emerge in such conditions when plants are in need of moisture (Jones and Evans 1975; Evans and Jones 1977; Agapiou et al. 2013). It may be therefore that the topographic anomaly is due to differential crop growth, perhaps not as enhanced as at other times but possible to measure with InSAR due to the higher coherence.

Conclusions

This study demonstrates that surface residues of buried archaeological features in temperate vegetated areas can (in some cases) be detected in SAR data. It also shows that full use of all information contained in both the amplitude and phase of SAR data can greatly enhance the detection capability. The study reveals that some archaeological features are better visible as one of either coherence, topographic or backscatter residues. Analysing all three not only helps to detect features, but it also helps to interpret them as either soil marks or as positive or negative crop marks, which in turn provides more information on the structure buried beneath the ground.

The study also demonstrates how a large time series of data can greatly aid detection of features. The more data is available, the better the speckle can be removed through filtering in the temporal domain, to preserve spatial resolution. A large time series also improves the ability to produce a DEM in vegetated areas using the SBAS technique. Finally, with a coherence time series, additional information on the state of the vegetation cover can be derived, which can aid interpretation of features.

SAR in Desert Areas

The sensitivity of SAR to roughness and relative permittivity renders it very useful in desert environments. Under certain conditions, microwave radiation can penetrate into dry sand. The penetration depth, δ_p , is a function of the microwave wavelength, λ , and the relative permittivity, $\varepsilon = \varepsilon' - j\varepsilon''$, according to the expression

$$\delta_p \cong \frac{\lambda \sqrt{\varepsilon'}}{2\pi\varepsilon''} \quad (1)$$

This is valid when $\frac{\varepsilon''}{\varepsilon'} < 0.1$, which is the case for most natural land surfaces, including sand (Ulaby et al. 1982).

For dry sand, the imaginary component of the relative permittivity is very low, which explains why signal penetration occurs at microwave wavelengths. The expression also shows that the longer the wavelength, the greater the penetration.

The real interest in the use of SAR remote sensing for geoarchaeological applications followed the Shuttle Imaging Radar (SIR-A) discovery of buried palaeorivers in the Sahara in November 1981. The imagery acquired over the Selima Sand Sheet, and drift sand of the eastern Sahara, revealed previously unknown buried valleys and geologic features (McCauley et al. 1982). SIR-A operated at L-band wavelength (24 cm), but even shorter wavelengths can reveal features beneath a layer of sand due to signal penetration. Figure 16 shows a part of the area first imaged by SIR-A, revisited with Sentinel-1 and Sentinel-2. Even at the shorter frequency of C-band, the palaeorivers of the Bir Safsaf area of the Eastern Sahara are clearly visible in the Sentinel-1 data, while the Sentinel-2 data provides information on the surface characteristics.

A recent study is summarised here on the systematic extraction of anthropogenic features in the North Sinai desert, taking advantage of the unique characteristics of microwave interaction with dry sand. To fully exploit these characteristics, both the amplitude and phase of long-wavelength SAR data from the phased array type L-band SAR (PALSAR) sensor have been used. A full description of the research is described in Stewart et al. (2016).

The North Sinai desert was chosen as a test area due to its archaeological importance as a land bridge connecting Africa and Western Asia (e.g. Mumford (2015) and Oren (1989)). The area is composed mainly of Aeolian sand dune fields and interdune areas, referred to as the northern Sinai dune field, or the Sinai-Negev erg (Muhs et al. 2013). A significant problem in the region is caused by sand drift and dune migration, which can rapidly bury ancient sites that may have been excavated in the past (Di Iorio et al. 2010), and even modern structures (Misak and Draz 1997; Hermas et al. 2012). The large size of the region, combined with the inhospitable terrain and frequent political instability (Gold 2014), makes regular systematic survey of the area challenging. Efficient and cost-effective methods for regular, large-scale surveys of such areas are therefore very much required. This area was chosen as a test site to determine whether SAR remote sensing techniques could meet these requirements (see Fig. 17).

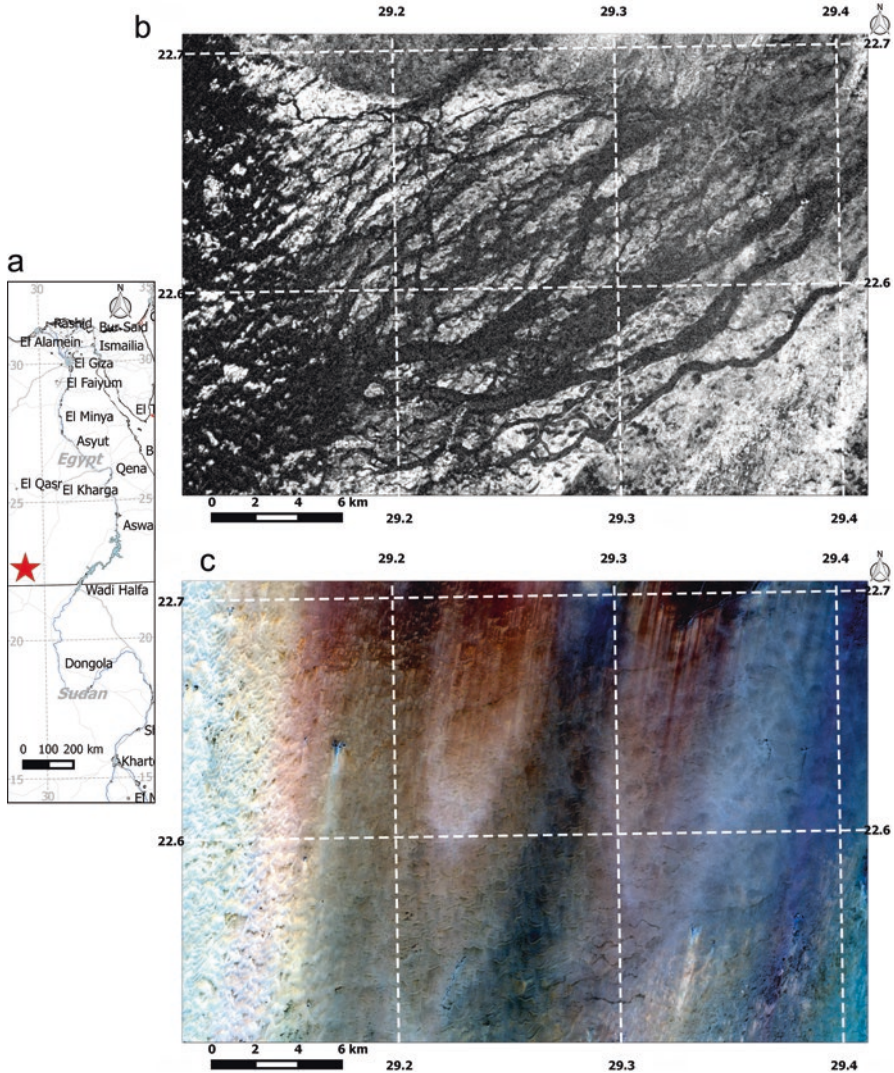


Fig. 16 (a) Map of the Bir Safsaf area where the images in (b) and (c) were acquired. (b) Sentinel-1A IW GRD VV σ^0 backscatter (in dB) image acquired on 11 February 2016. (c) Sentinel-2A L1C image acquired on 20 March 2016 corresponding to the same area as in (b). Displayed as a true-colour combination of band 4 (red), band 3 (green) and band 2 (blue). Contains modified Copernicus Sentinel data 2017

Table 2 shows the characteristics of the SAR data used for the analysis. Seventy-four PALSAR-1 images in fine beam single and fine beam dual polarisation modes were obtained from the European Space Agency (ESA). These were acquired over nine tracks and frames which together almost completely cover the North Sinai desert (see Fig. 17). For each track and frame, a time series of (on average seven) images was available with a date range from 2007 to 2010 or 2011. Over a small subset area,

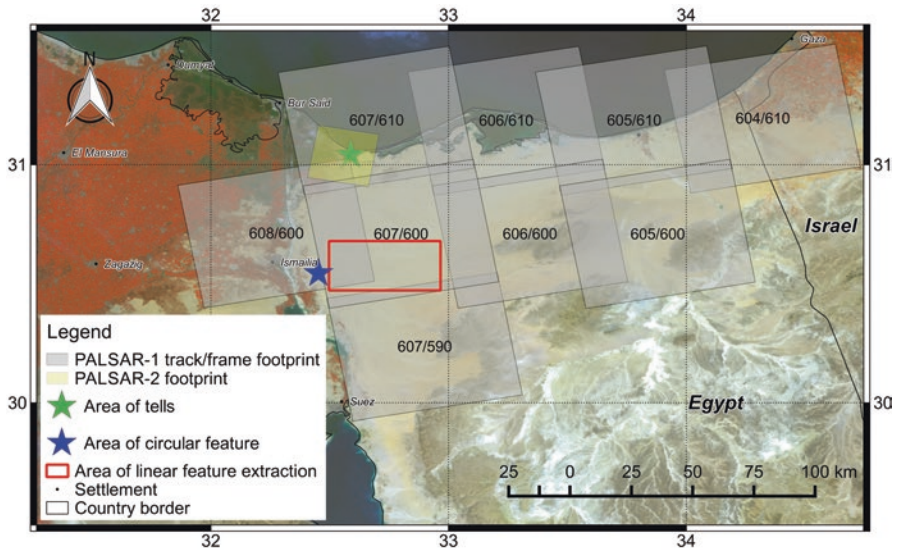


Fig. 17 Map showing North Sinai with the footprints of the PALSAR-1 and 2 imagery used for the analysis. The track/frame identification number of each PALSAR-1 stack is shown. The locations of features and areas of interest are shown by green and blue stars and red rectangle. The background image is a near-infrared and visible false-colour composite of an ENVISAT Medium-Resolution Imaging Spectrometer (MERIS) image at 300 m resolution with band 10 (754 nm) displayed as red, band 5 (560 nm) as green and band 2 (443 nm) as blue. Data provided by ESA

Table 2 Characteristics of PALSAR-1 and 2 imagery used for the analysis

Sensor	PALSAR-1	PALSAR-2
Number of scenes	74	7
Acquisition date range (year/month)	2007/06 to 2011/02	2015/08 to 2015/10
Polarisation	HH	HH
Pass	Asc	Des
Scene centre incidence angle	38.7	40–49
Final pixel spacing	10 m	2 m
Wavelength	23.6 cm (L-band)	22.9 cm (L-band)

new acquisitions of PALSAR-2 data in spotlight mode were requested to the Japanese Space Agency (JAXA), who provided seven new data acquisitions in 2015.

The objective of the analysis and the chosen dataset was to experiment with different techniques for anthropogenic feature detection over multiple areas and make full use of the information content of the time series. Techniques were applied on both the amplitude and the phase of the data in single-look complex (SLC) format. With the amplitude data, multitemporal De Grandi speckle filtering was applied to reduce the image speckle while preserving spatial resolution. Time series analysis was carried out to determine the utility of the mean, maximum, minimum, standard deviation and other parameters calculated from the time series. Processing of the

phase involved coherence calculation between consecutive image acquisitions and averaging all coherences.

An analysis of all imagery was carried out by a multidisciplinary team of Egyptologists, geologists and SAR experts. A comparison of the SAR-derived information was also made with other raster and vector information layers in a geographic information system (GIS). These layers included geological and archaeological charts, remotely sensed optical imagery and web map service (WMS) vector layers of infrastructure (roads, railways, canals, etc.). The objective of this analysis was to assess whether any potential anthropogenic features existed which were uniquely identified, or better highlighted, in the variously processed SAR data.

Results of this analysis revealed that many seemingly man-made features were distinguished by abnormally high backscatter compared to the surrounding sand. Many of these were in linear form. A much smaller number of potential anthropogenic structures were characterised by lower backscatter relative to surrounding areas. These were mainly confined to an area near the eastern Nile delta and Mediterranean coast, around the archaeological sites of Tell el-Farama, Tell el-Mahzan and Tell el-Kanais (see Fig. 17). It was decided to focus further research on two areas of interest (AOIs):

- AOI 1. The region east of Ismailia: An area of mobile sand dunes where many anomaly linear features of high relative backscatter were identified.
- AOI 2. The area of Tell el-Farama, Tell el-Mahzan and Tell el-Kanais: A coastal area with potential archaeological features of low relative backscatter.

Over AOI 1, many of the features of high backscatter that seemed likely to be anthropogenic were of a linear nature. A method was attempted to extract these and convert them to vector format to facilitate comparison and analysis with other layers in the GIS. A linear feature detection algorithm was thus developed. This was first attempted using the multitemporal De Grandi speckle filtered imagery as input. It worked by performing the following tests, for straight lines in all orientations, in a moving window of pixels:

$$\text{a. } \bar{x}_L > T_1 * \bar{x}_B \quad (2)$$

$$\text{b. } \sigma_L > T_2 * \sigma_B \quad (3)$$

$$\text{c. } \sigma^2(\theta_{\text{LOCAL}}) < T_3 \quad (4)$$

where, for a line of a particular orientation, \bar{x}_L is the mean value of pixels along the line, \bar{x}_B is the mean value of background pixels (outside the line, but within the moving window of pixels), σ_L is the standard deviation of line pixels, σ_B is the standard deviation of pixels outside the line, $\sigma^2(\theta_{\text{LOCAL}})$ is the variance of the local incidence angle (calculated from the SRTM 1 arc-second DEM) and T_1 , T_2 and T_3 are threshold values.

Test c was necessary to discard lines caused by high backscatter from sand dunes. At small incidence angles, peak backscatter usually occurs at the incidence angle equal to the angle of repose of sand dunes (Blom and Elachi 1987). Particularly for sand dunes oriented along the SAR azimuth direction, a line of bright pixels can be seen along the dunes.

It was noticed that the average coherence revealed the same pattern of high-backscatter features (but as areas of high coherence) but without the lines over the sand dunes. The linear feature extraction algorithm was therefore applied using the average coherence as input and discarding test c. This yielded much better results.

Over AOI 2, a time series of PALSAR-2 spotlight imagery was procured to complement the existing data. Processing included a range of multitemporal techniques to better extract the low-backscatter anomaly structures. These were then interpreted through comparison with other information layers and with the results of previous archaeological survey in the area.

Results

High-Backscatter Features

An example of a seemingly man-made feature of high backscatter is shown in Fig. 18. This is one of the many features identified by the team of geologists, archaeologists and remote sensing experts that do not appear in any of the available optical remote sensing imagery or WMS data. The concentric circles shown in Fig. 18 are present in all the seven De Grandi speckle filtered PALSAR-1 images in the time series acquired over this area from November 2007 to April 2010. As shown in the

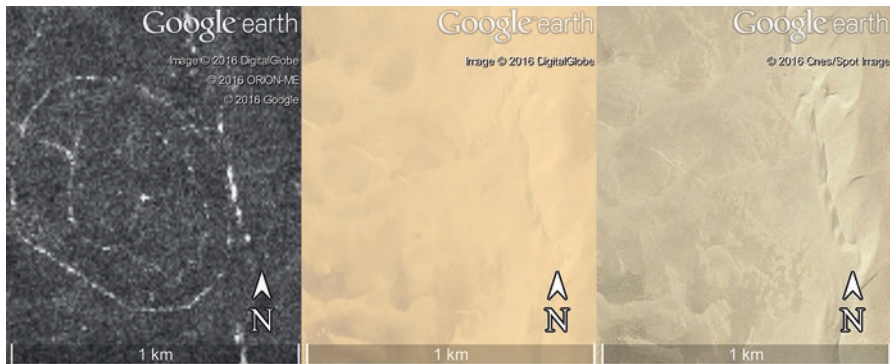


Fig. 18 Left: Feature identified in PALSAR-1 De Grandi filtered backscatter imagery. The feature is centred at 30.544° latitude and 32.452° longitude. Centre: Optical image of the same area, available on Google Earth, acquired on 5 May 2010. Right: Optical image of same area, available on Google Earth, acquired on 7 February 2007. PALSAR-1 data provided by ESA

figure, the same features are not evident in the two very-high-resolution (VHR) optical images available on Google Earth, reported, respectively, in February 2007 and May 2010. While the shape of this feature may resemble that of early Bronze Age sites, such as those illustrated in Arieh (1974), its scale does not. The feature in the SAR imagery is around one order of magnitude larger than the early Bronze Age sites in Arieh (1974). It is more likely that this particular feature is a buried relic of a military installation from one of the past wars that took place in this region, such as the Six Day War (Dunstan 2012).

Over AOI 1, results of the linear feature extraction algorithm applied to the average coherence image are shown in Fig. 19. Figure 19a shows a Sentinel-2 optical image of the AOI overlain with all available vectors of infrastructure which appear on at least one of the following WMS: Google Maps, Open Street Map, Bing Maps and Apple iPhoto map. Figure 19b shows the same Sentinel-2 image overlain with the vectors of anthropogenic linear features extracted automatically from the average

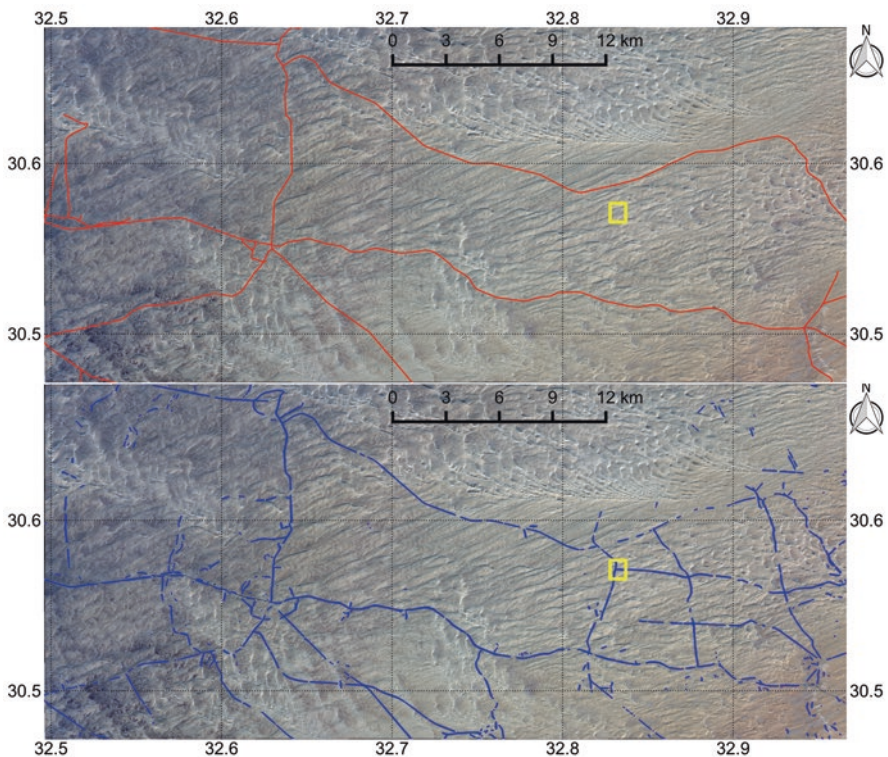


Fig. 19 Top: Sentinel-2 image over AOI 1 overlain with all WMS vectors of infrastructure (in red) from Google Maps, Open Street Map, Bing Maps and Apple iPhoto map. Image acquired on 19 February 2016. Full-resolution (10 m) true-colour composite. All vectors correspond to roads. Bottom: Lines extracted from average PALSAR-1 coherence (in blue) overlain on the same Sentinel-2 subset image as in top part of figure. Yellow rectangle shows location of detail in Fig. 20. Contains modified Copernicus Sentinel data 2016

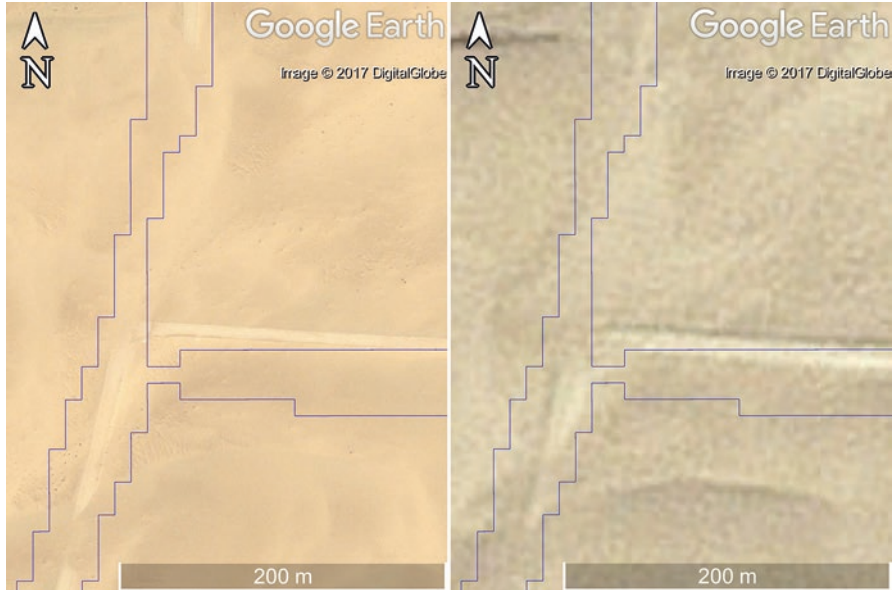


Fig. 20 Detail of partially buried road junction on optical remotely sensed images available on Google Earth acquired on 5 May 2010 (left) and 7 February 2007 (right). Lines extracted from average PALSAR-1 coherence overlain in blue. The road junction is an example of a feature not present on any of the available WSM vector layers. It appears unchanged from 2007 to 2010 and is visible in multitemporal speckle filtered PALSAR-1 imagery also from 2007 to 2010

coherence image. Many linear features extracted from the SAR data are not present in any of the considered WMS vectors. Figure 20 shows a close-up of an area containing such features overlain on VHR optical imagery available on Google Earth, purported to have been acquired on 7 February 2007 and 5 May 2010, respectively. In both images traces of partially buried tracks correspond with the SAR-derived vectors overlain. The pattern of sand dunes in both images seems the same and suggests that no significant sand dune movement took place between the two acquisition dates.

Low-Backscatter Features

Over AOI 2, the features of potential archaeological interest characterised by low backscatter are evident in Fig. 21. This shows the areas surrounding Tell el-Farama, Tell el-Mahzan and Tell el-Kanais in the average of De Grandi filtered PALSAR-1 images in Fig. 21a, and a close-up of the areas of Tell el-Mahzan and Tell el-Kanais in the coefficient of variation (CoV) of the De Grandi filtered PALSAR-2 spotlight images in Fig. 21b. Figure 22 shows the same area and close-up detail as in Fig. 21, on a VHR optical satellite image acquired by the Pleiades sensor.

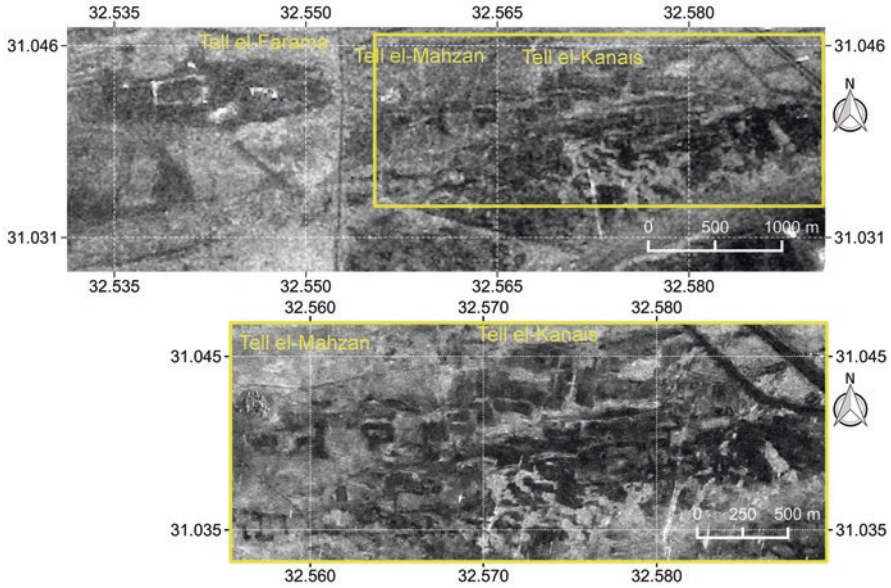


Fig. 21 Top: Average of De Grandi filtered PALSAR-1 images over the region of tells in AOI 1 (Tell el-Farama, Tell el-Mahzan and Tell el-Kanais). Yellow rectangle shows area of bottom part of figure. Data provided by ESA. Bottom: Coefficient of variation of seven PALSAR-2 spotlight multitemporal De Grandi speckle filtered images over the region surrounding Tell el-Mahzan and Tell el-Kanais. PALSAR-2 data provided by JAXA

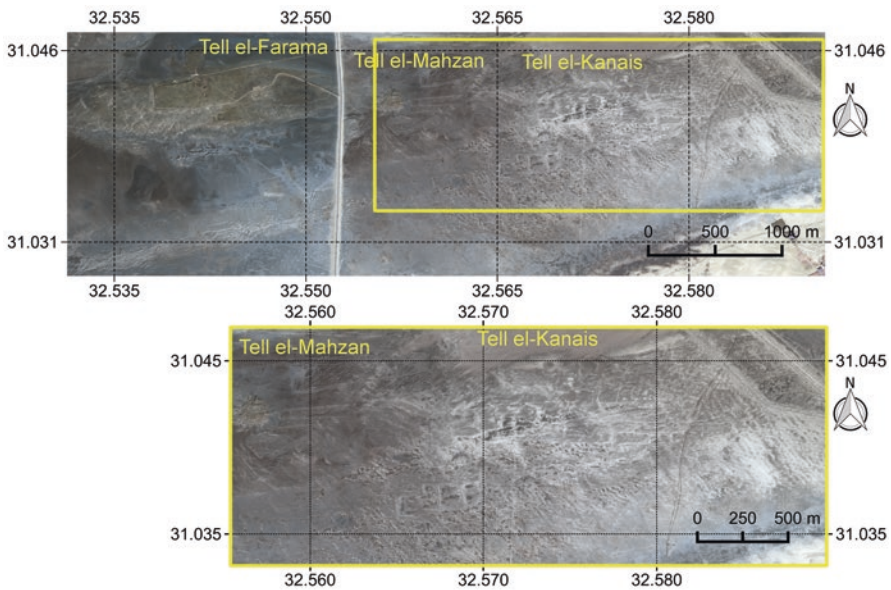


Fig. 22 Pleiades image acquired on 24 November 2015, covering the same area as in Fig. 21. Image has been pansharpended to 0.5 m pixel spacing and is displayed as enhanced true-colour composite. Pleiades data provided by ESA

The tells were thriving inhabited areas when the Pelusiac branch of the Nile was active and when the Mediterranean coastline was situated just to the north of the tells. Its importance declined when the coastline migrated north and the Pelusiac Branch silted up and was eventually abandoned by the time of the Crusades (Stanley et al. 2008). The area comprises silt and sand, covered in places with salt crusts (Jaritz et al. 1996).

For the areas of Tell el-Mahzan and Tell el-Kanais, Jaritz and his colleagues published a map showing the distribution of anthropogenic surface remains in four density classes. The map shows that surface remains seem to be clustered in a number of islands (Jaritz et al. 1996). It was suggested by the authors of this map that these islands may have been dry areas, more attractive for settlement, surrounded by wet and marshy land. Interestingly, the dark features on both the PALSAR-1 and 2 data show a similar pattern of island features, characterised by lower backscatter and lower CoV of backscatter. It is suggested by Stewart et al. (2016) that a possible reason why this pattern is also visible in the SAR data is that there may still be a higher concentration of moisture in the formerly inundated areas. This increased moisture presence would likely produce a higher SAR backscatter response given the increased relative permittivity (Ulaby et al. 1982).

Conclusions

The sensitivity of SAR to surface roughness and the relative permittivity of materials have long been recognised as useful for archaeological applications in desert regions. The recent study carried out by Stewart et al. (2016) demonstrates the added value that can be derived from using the phase in addition to the amplitude of SAR data for feature extraction in desert regions. It also shows the utility of having a time series.

Analyses of long-wave PALSAR-1 and 2 data over the North Sinai desert show that features of historical interest can be efficiently identified and extracted over large areas. These features may be characterised by high backscatter and high coherence relative to surrounding areas, or by low backscatter. An interpretation of such features can be challenging and is often not possible using the SAR data alone.

In the case of the high-backscatter features, an automatic extraction algorithm was devised to detect only linear anthropogenic structures. It was discovered that a distinction between backscatter due to natural sand dunes and anthropogenic features could be more efficiently carried out with images of average coherence rather than backscatter intensity. However, in either case, no distinction was made between ancient and modern features. Nonetheless, efficient techniques to detect human infrastructure (modern or ancient) abandoned or partially covered by sand could be of significant utility in North Sinai given the problems associated with sand drift and dune migration in the region, which can rapidly bury modern structures (Misak and Draz 1997; Hermas et al. 2012) or ancient sites that may have been excavated in the past (Di Iorio et al. 2010).

In a coastal region of the eastern Nile delta, a number of low-backscatter features were evident in the areas of Tell el-Farama, Tell el-Mahzan and Tell el-Kanais. A possible interpretation of these was suggested by Stewart et al. (2016) following the comparison of SAR-derived results with the outcome of previous research in the region. Identification of features in the SAR data was aided by the availability of not just one but a time series of SAR imagery. This enabled speckle reduction and the extraction of parameters such as the coefficient of variation, in which features of potential archaeological interest were more evident. Identification of features was also facilitated by the availability of higher resolution data in the form of a time series of PALSAR-2 spotlight imagery.

Discussion

Microwaves interact uniquely with surface materials. Recent studies present novel ways that this interaction can be exploited for archaeological applications over land cover types typical to Europe (such as areas of bare soil, crop and grassland) and the Middle East (such as desert sand and coastal mudflat). These attempt to exploit the full information content of SAR data, contained in both the amplitude and phase of the signal. They also attempt to make efficient use of time series.

These studies have been carried out at a time of unprecedented increase in the quantity and availability of data which is stimulating a complete transformation in scientific analysis and operational usage. Previous limitations on data volume, costs, analysis time and complexity are progressively being overcome, and we are seeing the potential for new applications and user communities to reap the benefits. The complexity of SAR data processing and interpretation has always been challenging and has hindered its uptake in many application areas, including cultural heritage. Demonstrations of the successful utility of SAR for cultural heritage managers could help to raise awareness of its benefits and accelerate its eventual adoption as an operational tool.

References

- Agapiou A, Hadjimitsis DG, Sarris A, Georgopoulos A, Alexakis DD (2013) Optimum temporal and spectral window for monitoring crop marks over archaeological remains in the Mediterranean region. *J Archaeol Sci* 40(3):1479–1492
- Arieh IB (1974) An early Bronze Age II site at Nabi Salah in southern Sinai. *Tel Aviv* 1(4): 144–156
- Berardino P, Fornaro G, Lanari R, Sansosti E (2002) A new algorithm for surface deformation monitoring based on small baseline differential SAR interferograms. *IEEE Trans Geosci Remote Sens* 40(11):2375–2383
- Blom R, Elachi C (1987) Multifrequency and multipolarization radar scatterometry of sand dunes and comparison with spaceborne and airborne radar images. *J Geophys Res* B 92(B8):7877–7889

- De Grandi GF, Leysen M, Lee JS, Schuler D (1997) Radar reflectivity estimation using multiple SAR scenes of the same target: technique and applications. In: Geoscience and remote sensing, 1997. IGARSS'97. Remote sensing-a scientific vision for sustainable development, 1997 IEEE International, vol 2. IEEE
- Di Iorio A, Straccia N, Carlucci R (2010) Advancement in automatic monitoring and detection of archaeological sites using a hybrid process of remote sensing, GIS techniques and a shape detection algorithm. In: Proceedings of the 30th EARSeL Symposium, Paris, vol 31, pp 53–63. Paris
- Dubois PC, Van Zyl J, Engman T (1995) Measuring soil moisture with imaging radars. *IEEE Trans Geosci Remote Sens* 33(4):915–926
- Dunstan S (2012) *The six day war 1967*. Bloomsbury Publishing, Sinai
- Evans R, Jones RJ (1977) Crop marks and soils at two archaeological sites in Britain. *J Archaeol Sci* 4(1):63–76
- Gold Z (2014) *Security in the Sinai: present and future*. ICCT Research Paper, March
- Hermas E, Leprince S, El-Magd IA (2012) Retrieving sand dune movements using sub-pixel correlation of multi-temporal optical remote sensing imagery, northwest Sinai Peninsula, Egypt. *Remote Sens Environ* 121:51–60
- Jaritz H, Favre S, Nogara G, Rodziewicz M, Carrez-Maratray J-Y (1996) Pelusium. prospection archéologique et topographique de la région de Tell el-Kana'is 1993 et 1994. *Beiträge zur ägyptischen Bauforschung und Altertumskunde* 12:29
- Jones RJ, Evans R (1975) Soil and crop marks in the recognition of archaeological sites by air photography. *Aerial Reconnaissance Archaeol*:1–11
- Keay S, Millett M, Paroli L, Strutt K (2005) *Portus: an archaeological survey of the port of Imperial Rome*, vol 15. British School at Rome, London
- Manyika J, Chui M, Brown B, Bughin J, Dobbs R, Roxburgh C, Byers AH (2011) *Big data: the next frontier for innovation, competition, and productivity*. McKinsey, Lexington
- Massonnet D, Souyris J-C (2008) *Imaging with synthetic aperture radar*. CRC Press, Boca Raton
- McCauley JF, Schaber GG, Breed CS, Grolier MJ, Haynes CV, Issawi B et al (1982) Subsurface valleys and geoarcheology of the eastern Sahara revealed by shuttle radar. *Science* 218(4576):1004–1020
- Misak R, Draz M (1997) Sand drift control of selected coastal and desert dunes in Egypt: case studies. *J Arid Environ* 35(1):17–28
- Muhs DR, Roskin J, Tsoar H, Skipp G, Budahn JR, Sneh A et al (2013) Origin of the Sinai–Negev erg, Egypt and Israel: mineralogical and geochemical evidence for the importance of the Nile and sea level history. *Quat Sci Rev* 69:28–48
- Mumford G (2015) The Sinai Peninsula and its environs: our changing perceptions of a pivotal land bridge between Egypt, the Levant, and Arabia. *J Anc Egypt Interconn* 7(1):1–24
- Oren ED (1989) Early Bronze Age settlement on northern Sinai: a model for Egypto-Canaanite interconnections. In: de Miroshedji P, L'urbanisation de la Palestine à l'âge du Bronze ancien. Bilan et perspectives des recherches actuelles. Actes du Colloque d'Emmaüs (20–24 octobre 1986), vol 527. Oxford: BAR IS, pp 389–405
- Quilici L (1974) *Collatia (Vol. Regio 1)*. De Luca Editore, Rome
- Stanley J-D, Bernasconi MP, Jorstad TF (2008) Pelusium, an ancient port fortress on Egypt's Nile Delta coast: its evolving environmental setting from foundation to demise. *J Coast Res*:451–462
- Stewart C (2017) Detection of archaeological residues in vegetated areas using satellite synthetic aperture radar. *Remote Sens* 9(2):45
- Stewart C, Montanaro R, Sala M, Riccardi P (2016) Feature extraction in the north Sinai desert using spaceborne synthetic aperture radar: potential archaeological applications. *Remote Sens* 8(10):27
- Ulaby T, Moore K, Fung K (1982) *Microwave remote sensing. Volume II: radar remote sensing and surface scattering and emission theory*. Addison Wesley, New York
- Wilson DR (2000) *Air photo interpretation for archaeologists*. Tempus Publishing, Stroud
- Wiseman J, El-Baz F (2007) *Remote sensing in archaeology. Interdisciplinary contributions to archaeology*. Springer, New York

- Zalite K, Voormansik K, Praks J, Antropov O, Noorma M (2014) Towards detecting mowing of agricultural grasslands from multi-temporal COSMO-SkyMed data. In: Proceedings of the 2014 IEEE geoscience and remote sensing symposium. Quebec City: IEEE, pp 5076–5079
- Zalite K, Antropov O, Praks J, Voormansik K, Noorma M (2016) Monitoring of agricultural grasslands with time series of X-band repeat-pass interferometric SAR. IEEE J Sel Top Appl Earth Observ Remote Sens:3687–3697

Dense Surface Models from Airborne and Spaceborne (Multi-)Stereo Images



Thomas Krauß

Abstract Digital surface models representing the heights of an area can be derived from two or more (multi-)stereo images of airborne or spaceborne sensors. A satellite stereo image of a current very-high-resolution satellite like WorldView or GeoEye with ground pixel sizes of about half a meter allows the derivation of surface models in the range of the same resolution. Such surface models are the basis of many applications like the three-dimensional representation of the area, 3D change detection, calculation of volumes, detection of sight lines, or water flow and flooding. Satellite imagery covers large areas of about 400 square kilometers with ground resolution of about 1 meter, while airborne images from planes or drones usually cover only small areas but with higher resolution. In this chapter the basics of digital surface models are shown, and the actually best method for deriving dense digital surface models from airborne and spaceborne images is described. Some examples finally show the possible results.

Keywords Digital surface models · Dense stereo matching · Satellite-borne stereo imagery · Airborne stereo imagery · Semi-global matching

What Are Dense Digital Surface Models?

Digital surface models represent heights of an area on Earth's surface. For this a digital surface model – subsequently referred to as DSM – is a georeferenced image containing a height value, e.g. above sea level, for each point of the area. The DSM represents the upper boundary of all objects on Earth as the heights of roofs or the top of trees or other vegetation areas. In contrast the digital terrain model (DTM) represents the height of the bare ground without any natural or man-made objects on it. The latter will be of interest, e.g. in the calculation of water runoff, and can be derived from a dense DSM.

T. Krauß (✉)

German Aerospace Center (DLR), Remote Sensing Technology Institute, Weßling, Germany
e-mail: thomas.krauss@dlr.de

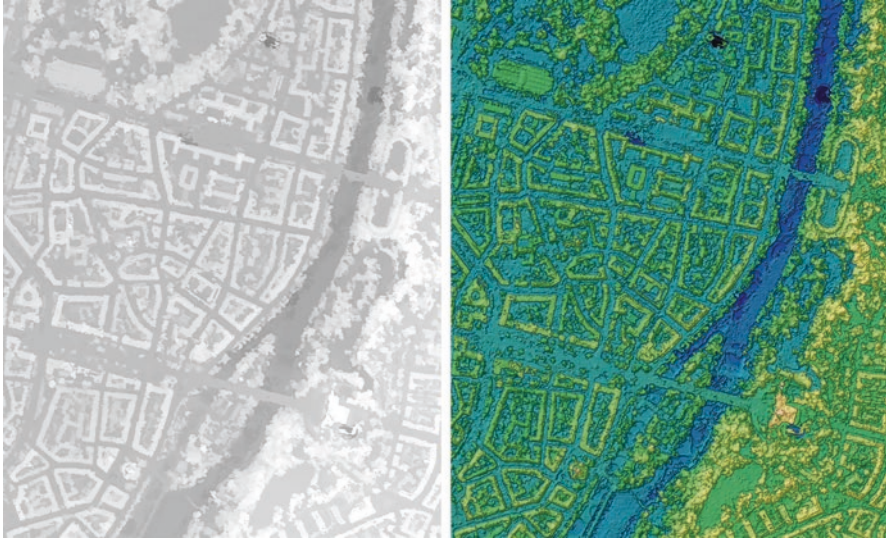


Fig. 1 Example of a dense DSM of the center of Munich (1.1×1.35 square km); left, DSM representation as gray values (black = 500 m, white = 600 m above WGS84 ellipsoid); right, shaded and color-coded DSM

A “dense” digital surface model is a DSM with individually calculated heights for each possible pixel of the input images in contrast to DSMs interpolated from only a few derived height values. Figure 1 shows a dense DSM derived from WorldView-2 satellite data acquired 10th of July 2012 over the center of Munich (Germany). The DSM is generated at a ground sampling distance (pixel size) of 0.5 m which is also the resolution of the satellite images. In Fig. 1, left, the representation of the DSM in gray values is shown. Lighter areas are higher than dark areas. The gray coding in this DSM runs from 500 m above WGS84 ellipsoid (black) to 600 m (white). Figure 1, right, shows the same DSM in a color-coded and shaded representation which is more intuitive for most people.

Digital surface models can be extracted from any kind of stereo imagery acquired from above the area in question. Having two images of the same area from different viewpoints allows the calculation of relative parallaxes (so-called disparities) between points in the images. By using the known acquisition position, viewing angles and internal parameters of the camera also the absolute height as shown in Fig. 2 can be derived.

The two acquired images – referred as “left” and “right” image in Fig. 2 – show objects of different heights at different relative positions. The relative difference or disparity allows the calculation of the absolute height if the position and camera parameters of the sensor are known.

Airborne images from planes or drones are mostly acquired as frame camera images – the whole image is acquired at once. To take stereo images, only an

Fig. 2 Principle of the derivation of heights from stereo imagery – higher points (nearer to the sensor) show larger disparities

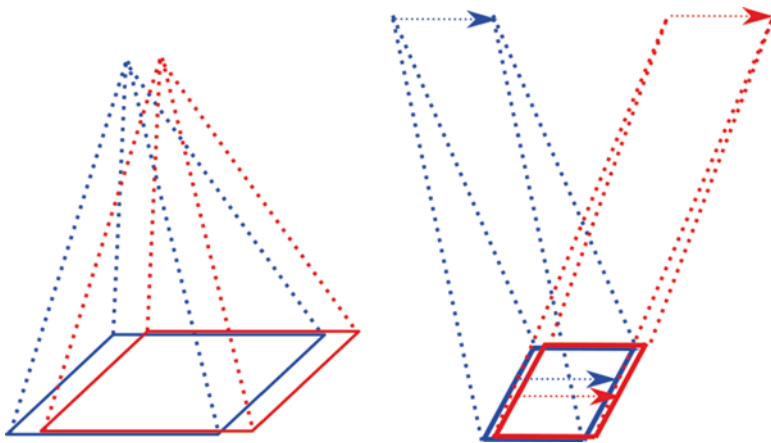
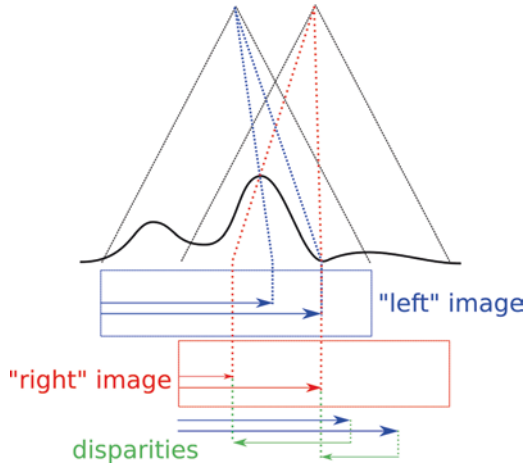


Fig. 3 Frame camera (left) vs. push broom sensor (right)

in-flight-direction acquisition of two or more images with high overlaps is required. In contrast satellite-borne images are mostly acquired by so-called push broom sensors. A push broom sensor has only one line of CCD pixels and builds up the image while scanning over an area line by line during the movement of the satellite in orbit. To fetch the second stereo image, the sensor has to be rotated, and the area under investigation has to be scanned a second time as shown in Fig. 3.

Image Correlation

To derive a DSM from two (or more) stereo images, it is therefore needed to find identical points in the images. Since the (automatic) generation of surface models has already a long history in image processing and Earth observation, there exists a broad amount of approaches. Here the classical approach will be presented together with a simple dense matching and the actually most advanced method – the semi-global matching (SGM).

The classical approach searches for corresponding corner points in the two stereo images using an image pyramid approach with a window-based cross-correlation matching and local least squares sub-pixel refinement.

In contrast the simple dense matching method utilizes the fact that two stereo images can be transformed to a so-called epipolar geometry in which the disparities are only horizontal shifts and no more general two-dimensional vectors in the images. But this simple method suffers from the missing linkage between subsequent lines, so the resulting dense DSMs show many stripes or streaking effects (Scharstein and Szeliski 2002).

A solution for this is the semi-global matching developed in 2005 at DLR (Hirschmüller 2005). This method interconnects the disparities of the epipolar lines using eight or sixteen scanning directions for calculation.

A benchmark initiated by Scharstein and Szeliski (2002) collected for long years all relevant approaches from computer vision for derivation of disparity maps from stereo imagery. For a long time, graph-based methods like “maximum flow minimum cut” competed with dynamic programming-based methods like described here. Nowadays the semi-global matching (Hirschmüller 2005) together with its improvements for satellite imagery (d’Angelo et al. 2008) is actually the fastest and qualitatively best possible operational approach.

Classical Approach

The classic approach (Lehner and Gill 1992; Otto and Chau 1989) is based on the detection of so-called interest points in one of the images and finds the corresponding points in the other stereo mate. These interest points are corner points with strong gradients in two perpendicular directions.

First the stereo images are scaled down in an image pyramid by $1/2, 1/4, \dots, 1/2^n$ (e.g., $1/64$). In the smallest image, interest points are searched. These points are correlated to the corresponding points in the stereo partner image by using a window-based cross-correlation matching followed by a sub-pixel local least squares matching. The found correlations are propagated to the next higher level of the pyramid as first estimations of the correlating window positions for the matching, and the steps “search interest points,” “window based cross correlation,” and “local least squares matching” are applied to this pyramid level.

In the final level – the original stereo images – the detected correlations are densified using a region growing approach. Finally the result is a list of pixel coordinates in the first stereo image together with the sub-pixel positions in the second stereo image – their distances representing the disparities.

Using the sensor model, real 3D coordinates can be derived for every correlated point, and all these points can be interpolated to a final DSM as shown in Fig. 4, left.

Epipolar Geometry

As can be seen in Fig. 4, left, the classical approach is not suitable in urban areas. Since there remain only a few good “corner points” and these get correlated by a window with a size larger than one pixel, the result is always a smooth, interpolated DSM. In contrast Fig. 4, right, shows a DSM derived from the same images using a more sophisticated “dense” method.

In the next approach, the fact is used that any image stereo pair can be transformed to a so-called epipolar geometry in which the disparities are reduced to simple shifts in only row or column direction. We use here – without losing generality – the horizontal epipolar direction.

Figure 5 shows the principle of creating epipolar images. Two stereo images left and right represented in blue, respectively, and red together with their projection centers Z_L and Z_R see the same object point P in the left image in P_L and in the right image in P_R . Moving the object point to P' without changing P_R moves the projection P_L to P'_L in the left image. The line $P_L P'_L$ represents now the epipolar line in the left image. Doing the same with object point Q and the right image gives the epipolar line $Q_R Q'_R$ in the right image.

Now both original stereo images can be rotated around their center in a way they found epipolar lines $P_L P'_L$ and $Q_R Q'_R$ get both horizontally. Figure 6 shows again sections of the two stereo images of the center of Munich, and Fig. 7 shows the corresponding epipolar images.

Calculating the disparities now in the epipolar images requires at end of course the back projection to the original images for applying the sensor model and in turn calculating the real absolute ellipsoid heights.



Fig. 4 Small section $400\text{ m} \times 200\text{ m}$ from an Ikonos-Scene of Athens (acquired 2004), left, DSM derived using the classical approach; right, DSM derived using a simple dense stereo approach

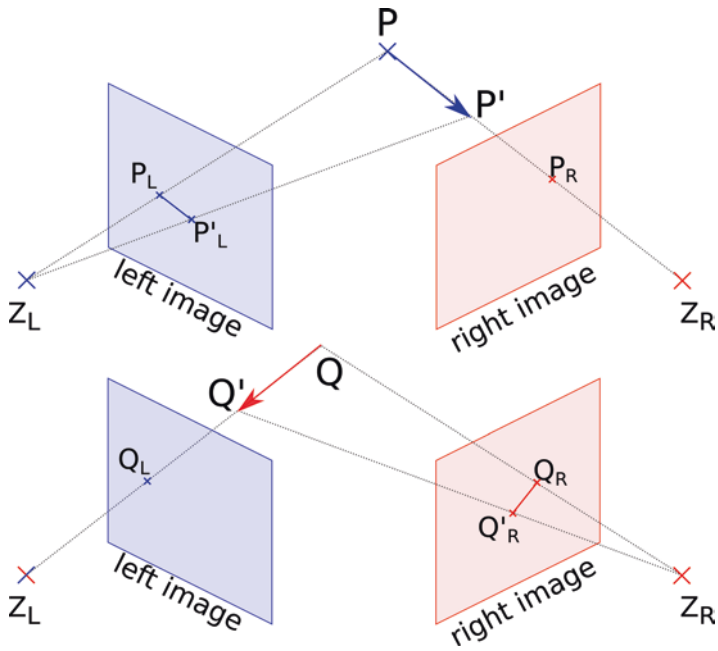


Fig. 5 Construction of epipolar geometry



Fig. 6 Original stereo images (750 m × 750 m, Center of Munich, Germany, 10 July, 2012, Worldview-2 (2012, European Space Imaging))

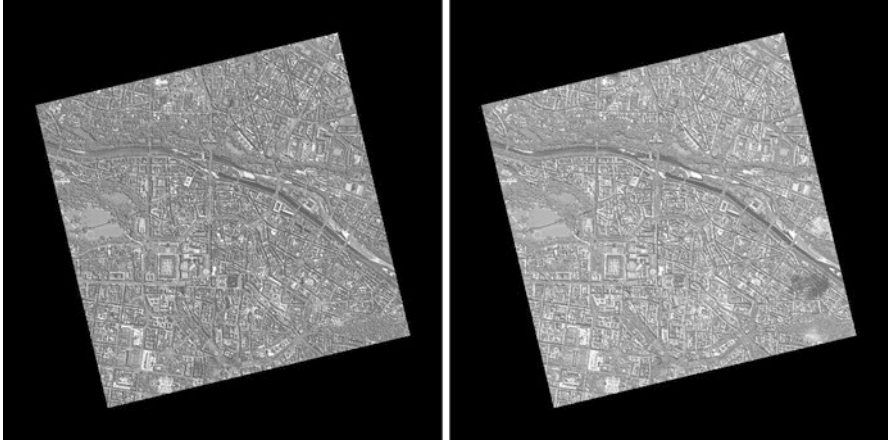


Fig. 7 Epipolar images transformed from Fig. 6

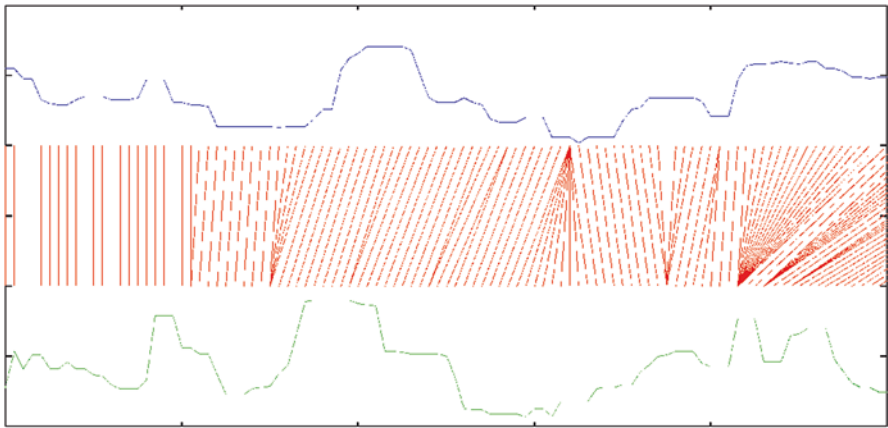


Fig. 8 Example of two gray value profiles of corresponding epipolar lines from two stereo images (top and bottom) together with the required shifts for warping one onto the other (middle)

Dynamic Programming

Using the epipolar geometry allows the reduction of a 2D correlation problem to a much simpler 1D problem by warping each epipolar line of one stereo image onto the corresponding line of the second epipolar stereo image (see Fig. 8).

A solution for the 1D correlation problem is applying the “dynamic programming” as described in (Birchfield and Tomasi 1998; Krauß et al. 2005; van Meerbergen et al. 2002). For finding the best local shifts between the epipolar lines in a $m \times n$ -matrix (m and n are the lengths of the epipolar lines in the left and right

stereo image) so-called costs C between pixel i of the epipolar line of image I_L and j of the epipolar line of image I_R will be stored in $C(i,j)$. The cost can be as simple as the absolute difference of the gray values of the image pixels.

Now a path from $(0, 0)$ to (m, n) in the matrix has to be found which minimizes the sum of all $C(i,j)$ on this path. The distances on this path to the main diagonal give the local shifts at this position. A recursive solution may look like

```
function getmin(i,j):
    minpos := None
    minc := 0
    (crek, posrek) := (0, [])
    for k in [max(0, j - d) . . . min(j + d, len(I^t)-1)]:
        if i < len(I)-1: (crek, posrek) := getmin(i + 1, k + 1)
        c = |I(i) - I^t(k)| + crek
        if minpos is None or c < minc:
            minpos := k
            minc := c
    return (minc, [minpos] + posrek) (totalmindist, minpath) = getmin(1,1)
(totalmindist, minpath) = getmin(1,1)
```

But a more sophisticated and easier solution gives the “dynamic programming.” In this method the cost matrix C is summarized in a special way up to an aggregated matrix D . $D(m, n)$ now contains the absolute minimum distance, and going back from (m, n) to $(0, 0)$ just by taking always the minimum upper or left neighbor gives the searched minimum path or the searched shifts between the two epipolar lines. D is derived from C by setting the first line and column to

$$D_{1,j} = \sum_{k=1}^j C_{1,k}, \quad D_{i,1} = \sum_{k=1}^i C_{k,1} \quad (1)$$

and the remaining $D_{i,j}$ ($i, j > 1$) to

$$D_{i,j} = C_{i,j} + \min(D_{i-1,j}, D_{i,j-1}, D_{i-1,j-1}) \quad (2)$$

The dynamic programming approach can be illustrated best using a simple example. Given are two gray value arrays (“epipolar lines” of the two stereo images) I and I' :

$$I = \begin{pmatrix} 1 \\ 0 \\ 2 \\ 1 \\ 0 \end{pmatrix} \quad \text{und} \quad I' = \begin{pmatrix} 0 \\ 1 \\ 0 \\ 2 \\ 1 \end{pmatrix} \quad (3)$$

From them the cost matrix C will be calculated to $C_{i,j} = |I_i - I'_j|$:

$$C = \begin{pmatrix} 1-0 & 1-1 & 1-0 & 1-2 & 1-1 \\ 0-0 & 0-1 & 0-0 & 0-2 & 0-1 \\ 2-0 & 2-1 & 2-0 & 2-2 & 2-1 \\ 1-0 & 1-1 & 1-0 & 1-2 & 1-1 \\ 0-0 & 0-1 & 0-0 & 0-2 & 0-1 \end{pmatrix} = \begin{pmatrix} 1 & 0 & 1 & 1 & 0 \\ 0 & 1 & 0 & 2 & 1 \\ 2 & 1 & 2 & 0 & 1 \\ 1 & 0 & 1 & 1 & 0 \\ 0 & 1 & 0 & 2 & 1 \end{pmatrix} \quad (4)$$

Aggregation of C following Eqs. 1 and 2 gives

$$D = \begin{pmatrix} \mathbf{1} & \mathbf{1} & 2 & 3 & 3 \\ 1 & 2 & \mathbf{1} & 3 & 4 \\ 3 & 2 & 3 & \mathbf{1} & 2 \\ 4 & 2 & 3 & 2 & \mathbf{1} \\ 4 & 3 & 2 & 4 & \mathbf{2} \end{pmatrix} \quad (5)$$

with the minimum path marked in bold in the latter. The total minimum distance is always the rightmost bottom element – in our case 2. Starting from there using always the smallest neighbor left, top, or top left results in the minimum path. The distance of the minimum path from the main diagonal gives the disparity d as

$$d = (1 \ 0 \ 0 \ 0 \ 1) \quad (6)$$

There are many image processing approaches for connecting the individually calculated disparities of each line. So it's possible to use small windows of diameter w instead of only one pixel for cost calculation like in

$$C_{i,j} = \sum_{\lambda=-w/2}^{w-w/2-1} \sum_{\mu=-w/2}^{w-w/2-1} |I_{i+\lambda,y+\mu} - I'_{j+\lambda,y+\mu}| \quad (7)$$

Also applying a median filtering with diameter m after the disparity calculation will help smoothing the result. Figure 9 shows four examples calculated with different window sizes w and median sizes m . But using such filtering approaches – especially window sizes w larger than one pixel – will result always in a smoothing of the resulting DSM in the same size, which is mostly not applicable particularly in reconstruction of building structures.

This leads to the actually best dynamic programming interconnection approach, the semi-global matching.

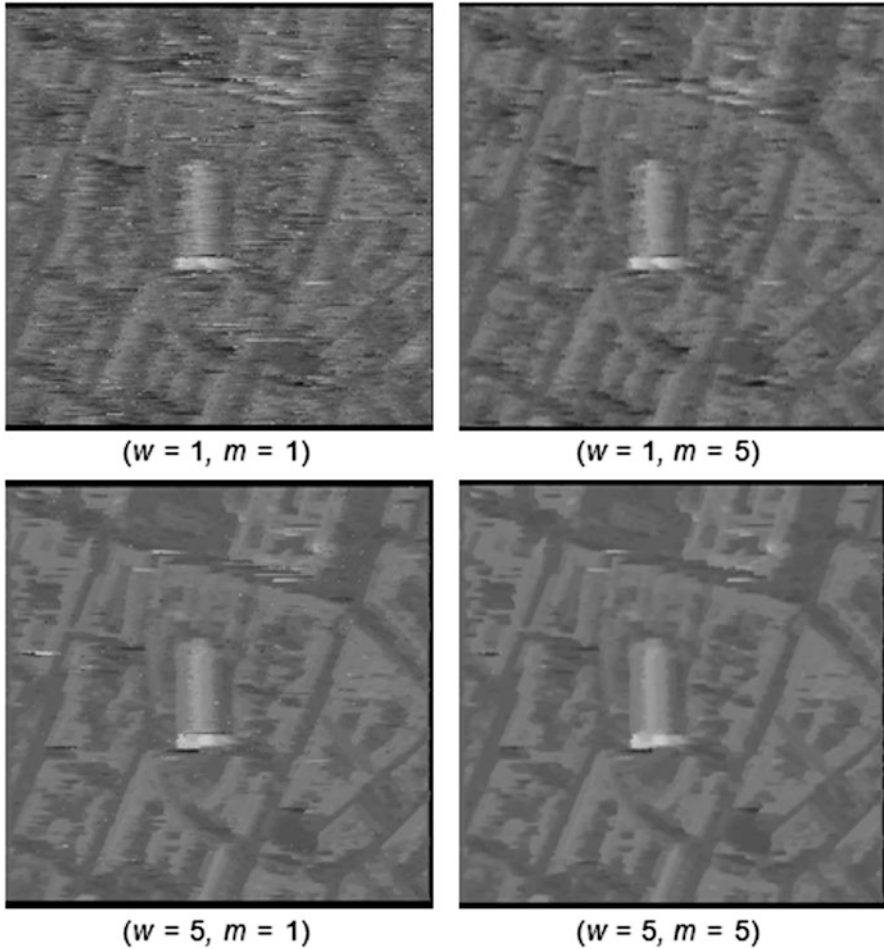


Fig. 9 DSMs calculated for given window sizes w and median sizes m (center of Munich, Frauenkirche 500 m \times 500 m)

Semi-global Matching (SGM)

The semi-global matching (Hirschmüller 2005) – SGM below – extends the simple dynamic programming approach described above by interconnecting the disparities of the epipolar lines already in the cost aggregation step and cutting down the matrices C and D to only a small band with size $\pm d_{\max}$ around the main diagonal using an estimated maximum disparity d_{\max} .

But this approach increases the memory needed for the calculation since now not only two matrices C and D of size w_l^2 are needed but three- dimensional matrices of size $w_l \times h_l \times (2d_{\max} + 1)$ using w_l and h_l as width and height of the epipolar images (Fig. 10).

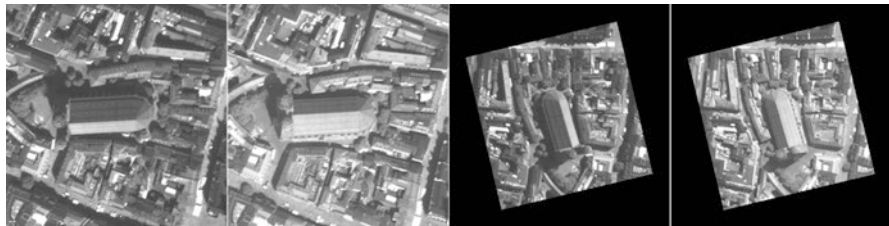


Fig. 10 Section 500 m \times 500 m around Frauenkirche, center of Munich, Germany, left, original images; right, epipolar images

In the first step, the cost matrix is calculated again for horizontal-oriented epipolar images I_1 and I_2 using any kind of cost function like

$$C(x,y,d) = |I_1(x,y) - I_2(x+d,y)| \quad (8)$$

Another – in urban areas or noisy images very useful – type of cost function is the “census” function. Census (Spangenberg et al. 2013; Zabih and Woodfill 1994) does not use differences of gray values but only the relative brightnesses in respect to the center position. For this a census value $c_i(x, y)$ is calculated in image I_i as

$$c_i(x,y) = \bigotimes_{h_c/2}^{\mu=-h_c/2} \bigotimes_{w_c/2}^{\lambda=-w_c/2} s(I_i(x,y), I_i(x+\lambda, y+\mu)) \quad (9)$$

with

$$s(u,v) = \begin{cases} 0 & \text{for } u \leq v \\ 1 & \text{for } u > v \end{cases} \quad (10)$$

using a small window of size $w_c \times h_c$ around each point (x, y) and \otimes as the bit concatenation operator. So a census window of size 3×5 will result in a 15 bit value or a more usual 7×9 in a 63 bit value. The cost for calculating the cost matrix is now the Hamming distance $\Delta_H(u, v)$ – how many bits differ in the bit strings u and v . So the cost matrix will calculate to

$$C(x,y,d) = \Delta_H(c_1(x,y), c_2(x+d,y)) \quad (11)$$

For aggregating C to D , not only one aggregation in epipolar line direction as shown in Eqs. 1 and 2 is used. Hirschmüller proposes in Hirschmüller (2005) using at least 8 or better 16 directions r for aggregation as shown in Fig. 11. Also he proposes the usage of two additional smoothness parameters p_1 and p_2 allowing for slanted and curved surfaces. The aggregated cost matrix D is now the sum of all aggregations from all directions:

$$D = \sum L_r \quad (12)$$

Fig. 11 SGM aggregation of 16 paths – each using again a dynamic programming 1D approach

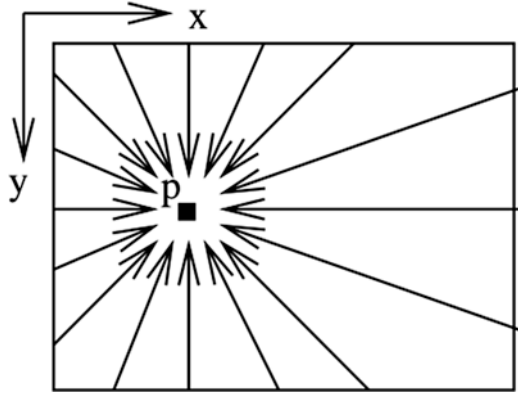
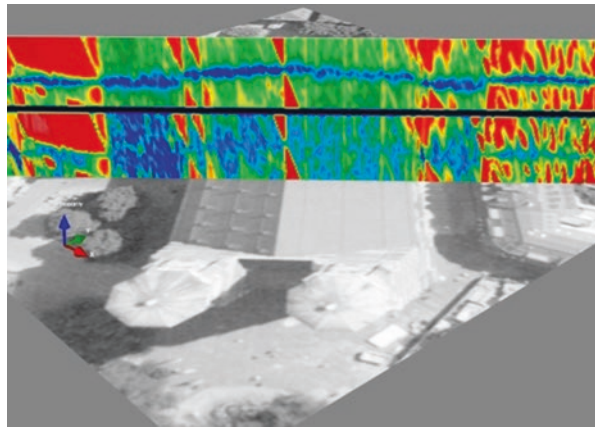


Fig. 12 Calculated cost C (bottom) and aggregated cost D (top) for one epipolar line, color-coded (blue to red from minimum to maximum cost)



with L_r being the aggregated cost matrix in direction r of $ndir$ directions ($ndir = 8$ or 16). The cost matrix L_r for direction $r = (r_x, r_y)$ is calculated as

$$\begin{aligned}
 L_{x,y,d} &= C_{x,y,d} + \min(L_{x-r_x,y-r_y,d}, \\
 &\quad L_{x-r_x,y-r_y,d-1} + p_1, \\
 &\quad L_{x-r_x,y-r_y,d+1} + p_1, \\
 &\quad \min_{i=-d_{max}}^{d_{max}} (L_{x-r_x,y-r_y,i}) + p_2)
 \end{aligned}
 \tag{13}$$

using the previously calculated disparity column $(x - r_x, y - r_y)$ and C . Figure 12 shows a section of the cost cube C and aggregated cost cube D for one aggregated epipolar line, disparities ranging from bottom to top from $-d_{max}$ to d_{max} .

In Fig. 13 the cost cube C and the aggregated cost cube D are shown for the example epipolar images from Fig. 10.

The calculation of the “minimum path” is now simply reduced to searching the disparity d of the minimum aggregated cost for each image pixel (x, y) in $D(x, y, d)$.



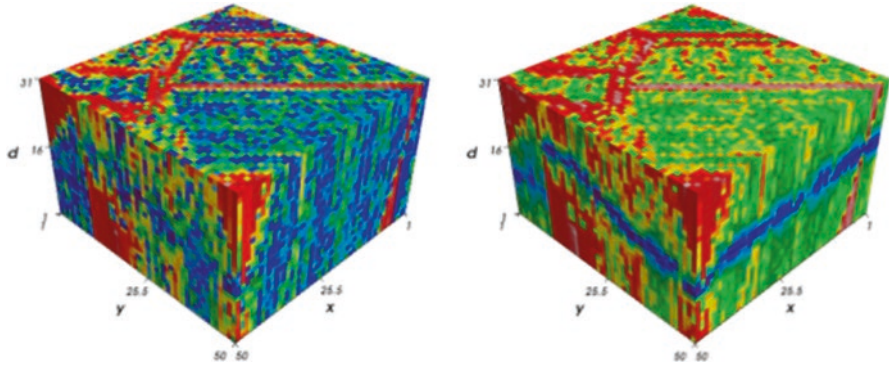
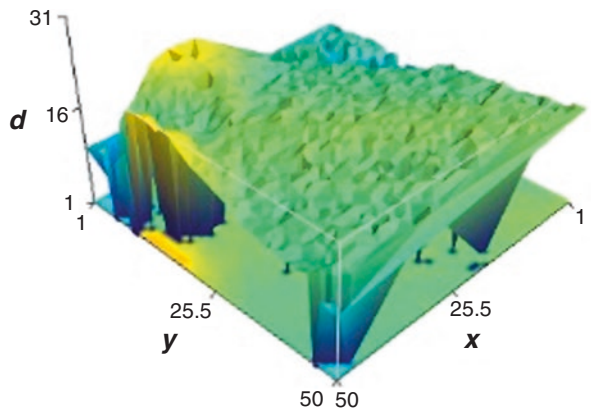


Fig. 13 Census cost cube C (left) and aggregated cost cube D (right) for the epipolar images from Fig. 10. (Images courtesy of Pablo d’Angelo)

Fig. 14 Resulting disparity image P in the same 3D view as the cost cubes in Fig. 13. (Courtesy Pablo d’Angelo)



In Fig. 13, right, these are the disparities marked in blue. The result is the disparity image $P(x, y)$ as shown in Fig. 14.

For better results the parallaxes can be calculated first from I_1 to I_2 giving a disparity image P_1 fitting exactly on I_1 and second vice versa from I_2 to I_1 giving P_2 fitting exactly on I_2 . Afterwards an outlier detection can be applied removing all disparities which differ by more than d_{lim} – usually about 1 px:

$$\Delta d(x,y) = \left| P_1(x,y) - (-P_2(x + P_1(x,y), y)) \right| < d_{lim} \tag{14}$$

The disparity at $P_1(x, y)$ tells us that the pixel (x, y) in the first epipolar image corresponds to pixel $(x + P_1(x, y), y)$ in the second image. Using this pixel in the second disparity map, P_2 should give the same but negative disparity if both are consistent.

Sensor Models: From Disparities to Absolute Heights

To calculate absolute heights from the disparities of the images, a so-called sensor model for the camera used is needed. Satellite imagery is mostly shipped with so-called RPCs (rational polynomial coefficients) (Grodecki et al. 2004; Jacobsen et al. 2005). These describe in a simplified third-order function the correlation of row (y) and column (x) of a pixel in the image with absolute longitude (λ) and latitude (φ) as a function of the absolute height h above the WGS84 ellipsoid:

$$x = \frac{f_{\text{samp,num}}(\lambda, \varphi, h)}{f_{\text{samp,den}}(\lambda, \varphi, h)} \quad \text{and} \quad y = \frac{f_{\text{line,num}}(\lambda, \varphi, h)}{f_{\text{line,den}}(\lambda, \varphi, h)} \quad (15)$$

or more generally as sensor model S_i for image i :

$$(x, y) = S_i(\lambda, \varphi, h) \quad (16)$$

Each of the functions $f()$ in Eq. 15 is a third-order polynomial in λ , φ , and h with 20 coefficients $c_i = \langle sl \rangle \langle nd \rangle \text{coeff} \langle i \rangle$ each with $\langle sl \rangle = \{\text{samp, line}\}$ $\langle nd \rangle = \{\text{num, den}\}$ and i ranging from 1 to 20. Together with 10 scale and offset parameters for x , y , λ , φ , and h , there are 90 parameters defining an RPC for a satellite image.

Each function $f_{\{\text{samp,line}\} - \{\text{num,den}\}}()$ is defined for its 20 coefficients c_i as

$$\begin{aligned} f(\lambda, \varphi, h) = & c_1 + c_2\lambda + c_3\varphi + c_4h + c_5\lambda\varphi + c_6\lambda h + c_7\varphi h + \\ & c_8\lambda^2 + c_9\varphi^2 + c_{10}h^2 + c_{11}\lambda\varphi h + c_{12}\lambda^3 + c_{13}\lambda\varphi^2 + c_{14}\lambda h^2 + \\ & c_{15}\lambda^2\varphi + c_{16}\varphi^3 + c_{17}\varphi h^2 + c_{18}\lambda^2 h + c_{19}\varphi^2 h + c_{20}h^3 \end{aligned} \quad (17)$$

Using this sensor model allows the direct calculation of pixel coordinates x and y if the absolute geographic longitude λ and latitude φ are known together with the ellipsoidal height h . Calculating λ and φ vice versa from x and y for a known h needs an iterative solution until the required accuracy is reached (Fig. 15).

The disparity image P describes the correlation of pixels in the epipolar image I_1 with pixels in the epipolar image I_2 . Let E_i be the epipolar transformation of image i and E_i^{-1} the inverted epipolar transformation of image i . For pixel (x, y) in the disparity image holds: pixel $I_1^{\text{orig}}(E_1^{-1}(x, y))$ is the same as $I_2^{\text{orig}}(E_2^{-1}(x + P(x, y), y))$, and for the sensor models, S_i can be stated

$$S_1(\lambda_1, \varphi_1, h) = E_1^{-1}(x, y) \quad \text{and} \quad S_2(\lambda_2, \varphi_2, h) = E_2^{-1}(x + P(x, y), y). \quad (18)$$

Varying the height h until $(\lambda_1, \varphi_1) = (\lambda_2, \varphi_2)$ provides the searched value of h for each point in I_1^{orig} creating a so-called “height map” M . This is an image fitting exactly on I_1^{orig} but containing the real absolute ellipsoidal heights h at each point.

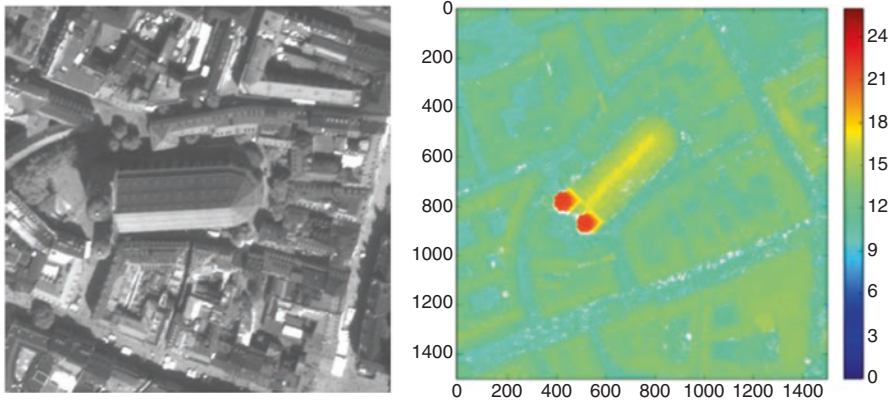


Fig. 15 Original satellite image (left) and the finally derived georeferenced DSM (right, courtesy Pablo d' Angelo)

The geographic referenced DSM is generated directly in the same step or later from this height map M by calculating λ and φ for each point (x, y) of the original image I_1^{orig} using the corresponding height $h = M(x, y)$ by iteratively inverting the sensor model.

Examples

Munich, Historic Center

The first example covers the historic city center from Munich, Germany. The stereo images were acquired 10 July 2012, 10:30 UTC by the satellite WorldView-2 (©2012 European Space Imaging). The whole images cover an area of about 20×20 square kilometers. In Fig. 16 the selected area of the historic city center is shown.

A WorldView-2 image consists always of a multispectral image with a ground resolution of about 2 m containing eight spectral bands (coastal, blue, green, yellow, red, red-edge, and two near-infrared bands) and one panchromatic image of 0.5 m resolution and one band. The pan bands of the two stereo images are usually used for the generation of the DSM. The satellite images are accompanied by the RPCs representing the sensor model. In the first step, the area of interest has to be cut from both of the stereo images and transformed to epipolar geometry as shown in Fig. 17.

Afterward the disparity map is calculated on the epipolar images using the SGM method and transformed back as height map to the original image. After filling occlusions and mismatches, the final DSM can be seen in Fig. 18, right.



Fig. 16 Section 1.75×1.75 km², Munich city center, left, panchromatic “left” image; right, multispectral (red, green, blue) “left” image

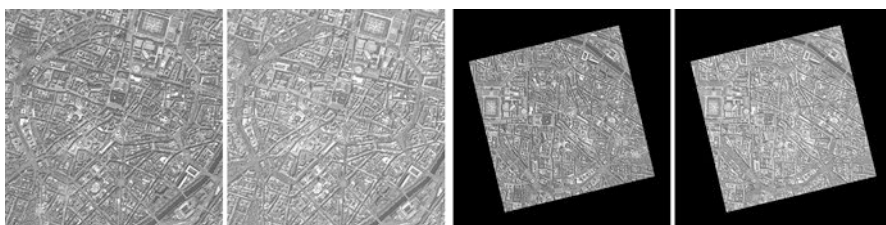


Fig. 17 Section 1.75×1.75 km², Munich city center, left and right original panchromatic images, left and right epipolar images used for DSM generation

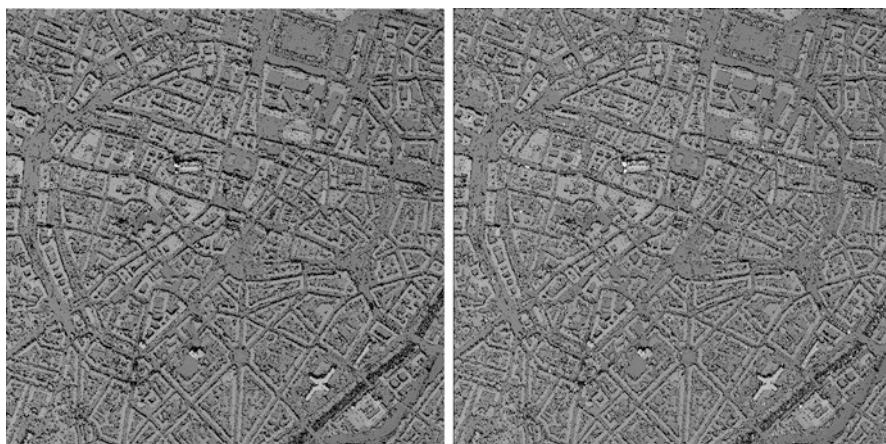


Fig. 18 Section 1.75×1.75 km², Munich city center, left, height map fitting on left original image; right, final DSM, UTM zone 32 north, WGS84 ellipsoid

Vaihingen, Historic Center

In the scope of a EuroSDR benchmark for generating DSMs and urban models from aerial imagery, stereo images were captured by a UltraCam-X at a height above ground of 2900 m and a ground sampling distance (GSD) of 20 cm over Vaihingen/Enz in Germany. The DSM is generated from the oblique view images as described above using the semi-global matching method. Figure 19 shows the two panchromatic stereo images together with the derived SGM height map fitting on the first of the images.

Athens, Acropolis

Another example for a DSM derived from satellite imagery is the area around the Acropolis in Athens as shown in Fig. 20. The stereo image was acquired by the former Ikonos-2 satellite at 24th of July 2004, 9:25 UTC with a ground resolution of about 1 m. The image was shipped already in epipolar format together with RPCs as sensor model.



Fig. 19 Section 400×400 m², Vaihingen city center, left/center, left and right stereo image; right, derived height map



Fig. 20 Section 1×1 km², Athens, Acropolis, satellite image Ikonos, 24 July 2004, left and right stereo image, height map and color-coded and shaded height map

Cairo, Pyramids

The last example is a stereo pair taken by the satellite GeoEye at 2nd of July 2009, 8:47 UTC over Cairo, Egypt. The ground resolution of the panchromatic sensor of this satellite is also about 0.5 m. Figure 21 shows a smaller section around the pyramids from the $12 \times 12 \text{ km}^2$ satellite scene.

From the section of Fig. 21, a small area around the pyramids was selected to calculate height maps using the SGM algorithm. Figure 22 shows the derived epipolar images.

Due to the large off-nadir angles of 14° and 21° of the stereo images, two SGM height maps were calculated to illustrate the differences, one fitting on the left epipolar image and the other fitting on the right epipolar image. The resulting height maps are shown in Fig. 23 and their color-coded and shaded counterparts in Fig. 24.

As can be seen in Fig. 23, left, the right (southern) surface of the Cheops pyramid has nearly the same inclination as the viewing angle of the south viewing stereo image of the satellite. In such cases where areas can only be nicely seen in one of the two stereo images, no stereo matching is possible, and the area is marked as “no data.” Such areas were also visible in all of the other (unfilled) height maps or dense DSMs presented in this chapter. But mostly these areas occur near steep walls in cities and can easily be filled using the nearby ground heights.



Fig. 21 Section $2.5 \times 2.5 \text{ km}^2$, Cairo, GeoEye, 2 July 2009, left and right stereo image



Fig. 22 Section $1 \times 0.5 \text{ km}^2$, Cairo, GeoEye, 2 July 2009, left and right stereo image

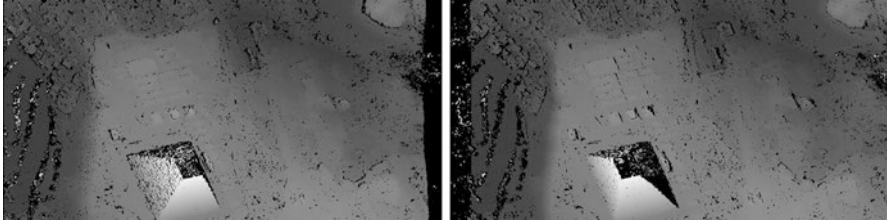


Fig. 23 Section $1 \times 0.5 \text{ km}^2$, Cairo, height maps fitting on first (left) and second (right) epipolar stereo image

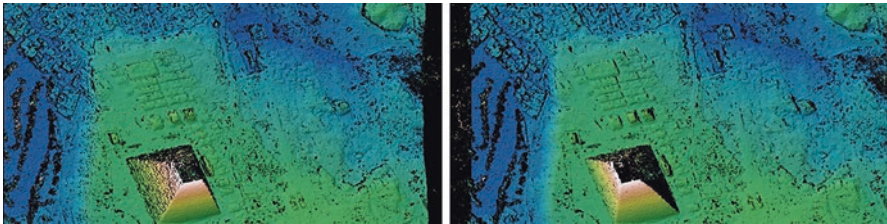


Fig. 24 Section $1 \times 0.5 \text{ km}^2$, Cairo, height maps fitting on first (left) and second (right) epipolar stereo image, shaded and heights color-coded

Conclusions

In this chapter we showed how dense digital surface models (DSMs) could be generated from (multi-)stereo satellite or airborne imagery. Starting with the basics, the key methods up to the actually best semi-global matching (SGM) were described and the whole chain of DSM generation explained. The presented methods can be applied to a wide range of stereo images. The only prerequisite is having a valid sensor model of the camera used. So starting from stereo images taken with hand-held or fixed cameras above an excavation pit over small drones covering only a small part of an archeological site to planes or even satellites mapping 16×16 square kilometers at once, high-quality surface models in all scales of resolution and coverage can be generated in reasonable good quality, mostly in the scale of the ground resolution of the camera used.

References

- Birchfield S, Tomasi C (1998) Depth discontinuities by pixel-to-pixel stereo. In: Proceedings of the 1998 IEEE international conference on computer vision, pp 1073–1080
- d'Angelo P, Lehner M, Krauß T, Hoja D, Reinartz P (2008) Towards automated DEM generation from high resolution stereo satellite images. In: IAPRS, vol 37, pp 1137–1142
- Grodecki J, Dial G, Lutes J (2004) Mathematical model for 3D feature ex-traction from multiple satellite images described by RPCs. In: ASPRS annual conference proceedings, Denver

- Hirschmüller H (2005) Accurate and efficient stereo processing by semi-global matching and mutual information. In: IEEE conference on computer vision and pattern recognition (CVPR), vol 2, pp 807–814
- Jacobsen K, Byksalih G, Topan H (2005) Geometric models for the orientation of high resolution optical satellite sensors. In: ISPRS workshop, Hannover, vol 36 (1/W3)
- Krauß T, Reinartz P, Lehner M, Schroeder M, Stilla U (2005) DEM generation from very high resolution stereo satellite data in urban areas using dynamic programming. In: ISPRS workshop, Hannover, vol 36 (1/W3)
- Lehner M, Gill RS (1992) Semi-automatic derivation of digital elevation models from stereoscopic 3-line scanner data. *Int Arch Photogramm Remote Sens* 29(B4):68–75
- Otto GP, Chau TKW (1989) Region growing algorithm for matching of terrain images. *Image Vis Comput* 2(7):83–94
- Scharstein D, Szeliski R (2002) A taxonomy and evaluation of dense two-frame stereo correspondence algorithms. *Int J Comput Vis (IJCV)* 47(1/2/3):7–42
- Spangenberg R, Langner T, Rojas R (2013) Weighted semi-global matching and center-symmetric census transform for robust driver assistance. *Comput Anal Images and Patterns* 8048:34–41
- van Meerbergen G, Vergauwen M, Pollefeys M, van Gool L (2002) A hierarchical symmetric stereo algorithm using dynamic programming. *Int J Comput Vis* 47(1/2/3):275–285
- Zabih R, Woodfill J (1994) Non-parametric local transforms for computing visual correspondence. In: *Computer vision – ECCV*, vol 1994, pp 151–158

Part III
Archaeology and Cultural Landscapes

Active Satellite Sensors in Cultural Heritage Research: The Use of SAR for Archaeological Prospection



Rosa Lasaponara and Nicola Masini

Abstract This paper provides an overview on the application of satellite synthetic aperture radar (SAR) technology in archaeology. The growing developments of space SAR technologies in terms of observational capabilities (spatial, spectral, radiometric, and temporal coverage) had made the use of these technologies very attractive for archaeological investigations. Although several achievements have been made in recent years on the basis of pioneering efforts addressed to the assessment of the potentiality of the L-, C-, and X-band SAR in archaeology, the full capability of these technologies for archaeological site detection is still incompletely evaluated until now. Moreover, significant advances are expected from the most recent satellite data available at 25 cm in X-band (TerraSAR) and at 1 m in multipolarized L-band (PALSAR). These enhanced characteristics, in terms of spatial resolution and radiometric quality, take the most recent SAR technologies to a new level for archaeological applications, addressed to object detection and target recognition.

Keywords Synthetic aperture radar · Archaeological mark · Satellite · Metaponto · Sabratha

R. Lasaponara (✉)

Institute of Methodologies for Environmental Analysis, CNR-IMAA (Italy),

Tito Scalo, Potenza, Italy

e-mail: rosa.lasaponara@imaa.cnr.it

N. Masini

Institute of Archaeological and Monumental Heritage, CNR-IBAM (Italy),

Tito Scalo, Potenza, Italy

e-mail: n.masini@ibam.cnr.it

© Springer Nature Switzerland AG 2020

D. G. Hadjimitsis et al. (eds.), *Remote Sensing for Archaeology and Cultural Landscapes*, Springer Remote Sensing/Photogrammetry,

https://doi.org/10.1007/978-3-030-10979-0_7

Introduction

Nowadays, the increasing availability of active and passive satellite sensors that provide very high-resolution data has opened new opportunities, unthinkable only a few years ago (Lasaponara & Masini 2008). The space technologies today available can provide extremely precise results for archaeological applications speeding up the work during the diverse phases of investigations ranging from survey, mapping, excavation, documentation, exploitation, and monitoring. Moreover satellite sensors offer data and information at diverse scales of interest, moving from small artefacts to architectural structures and landscape reconstruction. It is also possible to integrate ancient environment reconstruction, obtainable from space, with the mapping of past (even buried) and present (emerging) settlements and landscapes.

Synthetic aperture radar (SAR), in comparison with optical approaches, is an innovative microwave remote sensing technology characterized by penetration, polarization, and interferometry.

Satellite synthetic aperture radar (SAR) has entered into a golden age with a rich availability of data from both historical archives and numerous operative satellite platforms, which, compared to the past, offer advanced imaging mode capabilities available in diverse bands (L, C, and X). Moreover, the currently available satellite SAR systems provide data with a greater flexibility in the selection of incidence angles and polarizations, even in the scale of 1 meter and less. These advanced technical characteristics make the use of SAR data very attractive for numerous application fields, including archaeology (Lasaponara and Masini 2013; Chen et al. 2017).

The use of SAR data in archaeology can offer great potential for site detection (buried or emerging archaeological remains) and monitoring. Moreover, SAR enables us to overcome some limitations of optical imaging providing all weather acquisitions, at any time of day or night, also capable to “penetrate” (to some extents) vegetation and/or soil, depending on the antenna wavelength, surface characteristics (ice, desert sand, close canopy, etc.), and conditions (moisture content) (Wisemann and El-Baz 2007).

Even if the early applications of radar for archaeological purposes date back to the 1980s, later the use of SAR was historically limited by the low spatial resolution of the early sensors, as well as by the limited public availability of data and the complexity of data processing. This was and still is particularly relevant for archaeological investigations focused on the detection of subtle signals, often covered by noise, and only detectable in specific conditions depending on soil characteristics, moisture content, vegetation phenomenology, etc. The early applications of radar undoubtedly enabled numerous important archaeological discoveries and provided new insights in vast deserted areas, as in the case of the Sahara (McCauley et al. 1982). Nevertheless, the use of radar on both aerial and space platforms was mainly based on a few demonstrative experimentations made by NASA researchers, but, definitely, they were strongly limited for “operative” investigations. This means that, still today, there is a significant lack of studies and investigations conducted using SAR for archaeological purposes.

The availability of very high-resolution satellite radar data such as TerraSAR-X and COSMO-SkyMed, launched in 2007, as well as PALSAR L-band, launched in 2014, has opened a new era. Even if the use of satellite radar in archaeology is still in its experimental stage, it, undoubtedly, offers great potential for manifold applications ranging from the detection of features and sites, reconstruction of palaeo-landscape, documentation and monitoring of cultural heritage for site enhancement and preservation, etc.

One critical aspect, particularly pressing in archaeology and palaeoenvironmental studies, is still today linked with data processing issues, interpretation, and modeling approaches which should be adjusted or developed ad hoc for archaeological purposes as well as the lack of investigations in different archaeological environments.

A Brief Overview of Satellite Radar Missions

The early 1980s and 1990s were characterized by an intense experimentation of SAR systems. The USA launched four SAR demonstration missions designated as SIR (shuttle imaging radar): SIR-A (1981), SIR-B (1984), and two SIR-C/X-SAR (1994) with simultaneous acquisitions in L-, C-, and X-bands (see <https://directory.eoportal.org/web/eoportal/satellite-missions/s/sir-a>). European, Russian, Japanese, and Canadian space agencies launched a number of spaceborne SAR missions, such as (ERS)-1, ALMAZ-1, PALSAR/ALOS, and RADARSAT-1.

Later, in 2000 the NASA launched the Shuttle SAR Topography Mission (SRTM) designed for interferometric applications and for measuring large-scale surface changes. Digital elevation model (DEM) from SRTM data, today available at 30 m pixel resolution free of charge for almost 80% of the Earth's surface, has been and still is one of the most useful and used SAR-based products in archaeology and landscape studies.

The advent of the "2000" generation of spaceborne SAR sensors, such as ENVISAT/ASAR (2002–2012, C-band dual), ALOS/PALSAR (2005–2011, L-band), SARLupe (2006, X-band), COSMO-SkyMed (2007, X-band dual), TerraSAR-X (2007, X-band quad), and SARSAT-2 (C-band quad, 2007), provided advanced data acquired with greater flexibility in acquisition angles and polarization modes.

The launch on April 03, 2014, of Sentinel-1 started "the free availability" of SAR data (Berger and Aschbacher 2012). Sentinel-1, based on a long-standing heritage from the ERS, ENVISAT, and RADARSAT missions, operates in C-band and offers two acquisition modes (StripMap and Extra Wide Swath) with the possibility to sense data up to 5 × 5 m resolution (see Table 1).

Finally, ALOS-2, launched on May 24, 2014 with onboard PALSAR-2, opened a new era providing full polarization and high-resolution data in L-band (<http://www.eorc.jaxa.jp/ALOS-2/en/about/palsar2.htm>).

Table 1 SAR system parameters

SAR system	Band	Polarization	Incident angle (°)	Resolution (m)	Swath width (km)	Organization	Altitude (km)	Orbit Inclination (°)	Launch year
SEASAT	L	HH	23	25	100	NASA	790	108	1978
SIR-A	L	HH	45	30	50	NASA	225	57	1981
SIR-B	L	HH	20-60	30	50	NASA	225	57	1984
ALMAZ-1	S	HH	30-60	15	20-45	RSA (PKA)	300	72,7	1991
ERS-1	C	VV	24	25	100	ESA	790	97,7	1991
JERS-1	L	HH	35	18	76	NSDA/MITI	568	97,7	1992
SIR-C	C,L	All	17-60	25	15-100	NASA	225	57	1994
X-SAR	X	VV	17-60	25	15-40	DLR/ASI	228	57	1994
ERS-2	C	HH	24	25	100	ESA	785	97,7	1995
SARSAT	C	HH	17-50	10-100	50-170	CSA	790	98,6	1995
PRIRODA	S, L	HH	35	30	120	RSA/DLR	394	51,6	1995
ENVISAT	C	All	20-45	30	50-400	ESA	800	100	1998
SRTM	C	HH	20-60	30	60	NIMA/NASA	233	57	2000
PALSAR	L	HH; VV HV; VH	20-55	10-100	70-250	NASDA/ MITI	700	98	2002
Light SAR	L	All	20	25-100	50-500	NASA	790	97,7	2003
COSMO-SkyMed ScanSAR	X	One and two polarization modes (HH, VV, HV, or VH)	20-59	16-100	100-200	ASI	620	97,8	2007
COSMO-SkyMed StripMap	X		20-59	3-20	30-40	ASI	620	97,8	2007
COSMO-SkyMed Spotlight-2	X		20-59	1	10	ASI	620	97,8	2007
TerraSAR-X StripMap mode	X	(HH/VV), (HH/HV), VV/VH)	15-60	1.55-3.21	15-30	DLR-ASTIRUM	514	97,44	2007

TerraSAR-X spotlight mode	X	(HH, VV), (HH/VV)	15-60	1.34-3.21	10	DLR- ASTIRUM	514	97,44	2007	
TerraSAR-X ScanSAR mode	X	HH, VV	15-60	1.55-3.21	100	DLR- ASTIRUM	514	97,44	2007	
Sentinel-1 Strip Map	C	VV + VH HH + HV	20-45	5	80	ESA	693	98,18	2014	
Sentinel-1 Interferometric Wide		HH VV			250					
Sentinel-1 Extra Wide					400					
Sentinel-1 Wave Mode				5	20					
PALSAR-2 spotlight	L	HH, VV, HV	8-70	1-3	25	JAXA	636-639	97,92	2014	
PALSAR-2 StripMap		HH, VV, HV (HH + HV), (VV + VH) (HH + HV + VV + VH)			3/6/9					50-70
PALSAR-2 ScanSAR		HH, VV, HV (HH + HV), (VV + VH)			100					350-490

Satellite SAR Technologies in Archaeology

In the past, archaeological research based on satellite SAR data was constrained by low-resolution as well as complexity of data processing and interpretation. Today, abundant high-resolution, multimode satellite SAR, i.e., TerraSAR-/TanDEM-X, COSMO-SkyMed, RADARSAT-2, and ALOS PALSAR-2, as well as SAR data that are cost-free (Sentinel-1 from the European Space Agency) are available due to the technology development for acquiring multimode data. SAR data for archaeology definitely could step into a golden era; but applications still face challenges due to the lack of systematic methodologies for acquiring and interpreting data. For example, compared with optical approaches, performance of SAR data for archaeological applications is not fully understood and needs exploitation for further advancing the use of the technology.

The first applications of SAR in archaeology were made in desert areas by exploiting the penetration capability of the first shuttle imaging SIR-A. Herein we highlight the main results achieved such as the discovery of the palaeochannels in the desert area of northern Sudan and Southern Egypt (McCauley 1982; El-Baz 1998) and the buried river system in the Taklamakan (Holcomb and Shingiray 2007). Moreover, Mayas' ancient irrigation canals were discovered using SEASAT data in the Yucatan Peninsula (Adams 1980; Adams et al. 1981; Pope and Dahlin 1989).

The Lost City of Ubar was discovered in the desert of Oman by Blom et al. (1997). Sections of the ancient Great Wall of the Sui and Ming dynasties were identified by Guo (1997) using multiband and multi-polarization SIR-C/X-SAR data (Guo 1997). Settlements and river systems in the lower Mesopotamian Plain (Nippur archaeological sites in Iraq) were investigated by Richason III and Hritz (1998) using the Canadian SARSAT data.

In the 2000s, the easier (compared to the past) access to archive data and the availability of high-resolution data increased the interest in the use of spaceborne SAR in archaeology as evident by the publication of a dedicated book (Wiseman and El-Baz 2007) and a special issue in *Archaeological Prospection* (Lasaponara and Masini 2013). Inside this special issue, the archaeological landscape in the Nazca desert (Southern Peru) was investigated by Cigna et al. (2013) using ENVISAT C-band advanced SAR (ASAR). The archaeological site of Pelusium in the desert area of the northeastern edge of the Nile Delta (in Egypt) was investigated by Stewart et al. (2013) using multitemporal PALSAR data. A comparison between TerraSAR data and georadar survey conducted at a test site of a Roman fortress in Syria was made by Linck et al. (2013) in order to assess the penetration capability of the X-band in desert areas.

The quality and accuracy of TanDEM-X digital elevation models were specifically evaluated by Erasmi et al. (2014) for some archaeological sites in the Cilician Plain, Turkey. These analyses enabled the authors to identify and map palaeochannels in the investigated alluvial plain of Cilicia. Significant advances in SAR based investigations in presence of vegetation cover have been achieved by (Jiang et al. 2017; Stewart (2017). Jiang et al (2017) devised a model to use crop-

marks as proxy indicators in SAR imaging in Luoyang (China). Stewart (2017) demonstrated that SAR backscatter intensity, coherence and interferometry can be used to identify archaeological residues in vegetated areas over a number of areas in the vicinity of Rome. In desert environment, Comer et al. (2017) used in an integrated way the L-band data acquired by UAV NASA platform with C-band acquired by satellite sentinel-1 satellite to detect and measure landscape disturbance of Nasca geoglyphs. Finally, in oasis ecological niche X- and L-Band SAR Data proved to be effective in detecting palaeoenvironmental features related to ancient cultivations systems in China (Zhu et al. 2018).

It is undoubtedly that the improved observational capabilities of satellite SAR data opened new research lines; among them is the “radar archaeology,” namely, the detection of archaeological marks (Chen et al. 2015), herein discussed in section “Radar Space View of Archaeological Marks.”

Radar Space View of Archaeological Marks

A correct identification and interpretation of archaeological marks on the basis of radar images is not a straightforward task and requires knowledge about ground surface conditions as well as about the interaction mechanisms between radar waves and surface sensed. It is important to consider that there are significant differences between the interpretation of microwave and optical images including the radar penetration capability. Actually, from the historical points of view, as discussed in section “Satellite SAR Technologies in Archaeology,” one of the main important applications of SAR data for archaeology has been focused on the exploitation of radar penetration capability particularly significant in drought desert areas. Compared with optical imagery, penetration is one of the main merits of SAR remote sensing for archaeology. This capability is useful for detection of relics in rainforests and buried remains (settlements and ancient water systems) in deserts. The depth of penetration depends on the wavelength (the longer the wavelength, the deeper penetration), as well as on surface properties (roughness and moisture content) and imaging geometry. Until today, the lack of high-resolution data with greater penetration capability (i.e., L-band) has limited the use of SAR data in archaeology. The recent launch of ALOS-2, with onboard PALSAR-2 operating in L-band and capable to acquire at higher resolution (1×3 m per pixel in spotlight mode), can open encouraging perspectives.

The reconnaissance of typical archaeological marks (such as crop, shadow, and soil/damp marks) by using radar is more complex with respect to optical imaging due to a greater number of parameters that characterize SAR data, including the following:

- (i) Characteristics of the radar system such as operating frequency, polarization, angles, viewing geometry (ascending or descending), etc.

- (ii) Characteristics of the surface, in terms of land cover type, topography, relief, dielectric constant, moisture content, and conductivity
- (iii) Archaeological features in terms of buried or emerging remains, their geometric structure, orientation, building material, etc.

Many of these characteristics or parameters are closely interrelated so that the brightness of features and in turn the visibility of archaeological marks is usually linked to several variables.

The parameters that have a key role in the interactions between radar and target are (i) surface roughness, (ii) radar viewing and surface geometry relationship, and (iii) moisture content and dielectrical properties of the target.

The roughness is usually the dominant factor in a radar picture, but it is very important to consider that it is not an absolute characteristic but it depends on the wavelength and on the incidence angle of radar signal which is another crucial parameter. As a general rule, for the same target in the same conditions, there are significant variations of backscattering by changing the incidence angle of the illuminating wave.

One more very important parameter is moisture content which strongly affects the electrical properties of soil, and therefore, it influences the absorption, transmission, and reflection of microwave energy. Generally, radar image brightness tends to increase with the increasing of moisture content (Cigna et al. 2013; Jiang et al. 2016). The acquisition of SAR data in different polarization modes can help in discriminating and estimating the different contributions due to (i) moisture content and (ii) roughness.

On the basis of the previous physical basis consideration, we can argue that, in radar data, the detection of *crop marks*, *soil marks*, and *shadow marks* (viz., microtopographic relief) is strongly conditioned by the acquisition frequency, view geometry (incidence angle), and moisture conditions.

In optical images, *crop marks* linked to the presence of buried walls and/or filled ditches in vegetated areas produce local variations in moisture and nutrient content and, consequently, in the growth of vegetation that can be revealed by spectral variations in specific spectral channels more sensitive to vegetation (as near infrared) or spectral indices (i.e., mathematical combinations of different spectral channels) as NDVI, etc. In radar data, the understanding and modeling of the interaction radar/surface in the case of crop marks is much more complex compared to optical image due to the great number of factors and interaction mechanisms which affect the backscattering. A promising approach is based on the multitemporal amplitude data processing particularly when SAR image acquisition covers an entire plant growth cycle (Stewart et al. 2013; Chen et al. 2015; Stewart 2017). However, single data analysis can provide good results with the use of adequate filtering methods. In this case, as for optical images, it is important to select data acquired in the most favorable period for crop-mark observation.

In optical images, *damp marks* that occur when archaeological deposits induce local changes in the drainage capability of the soil can be revealed by spectral variations in specific channels more sensitive to moisture or spectral indices (i.e., math-

ematical combinations of different spectral channels as NDWI, etc.). In a radar image, the changes in moisture content induce variations in the dielectric property of the soil and consequently in the scattering of radar signal. In this case, as for optical image, it is important to select data acquired in the most favorable period, and single data analyses can provide good results with the use of adequate filtering methods. From a theoretical point of view, damp marks should be enhanced by specific polarization (or combination of polarization) more sensitive to moisture.

Finally, regarding *shadow marks*, it should be considered that in optical images, micro-/medium-*topographic relief* linked to archaeological remains, such as earthworks, platforms, ditches, and shallow remain, can be revealed by the presence of *shadow*. In radar data, only very steep slopes cause shadows which are generally not linked to archaeological remains. From the theoretical point of view, *microtopographic relief* linked to archaeological remains should be easier detected using SAR data acquired in X and C bands. In this context, previous experiences of the authors in sites located in Peru and Northern Africa confirmed that the use of COSMO-SkyMed was very effective for the identification of emerging archaeological remains. In this case, shapes and geometric patterns can also facilitate the interpretation of surface roughness as potential archaeological patterns.

As a general rule, the discriminability of archaeological marks is a complex issue linked both to the signal-to-noise ratio and to the differential scattering behavior between target/feature and its surrounding. Some recent applications suggest a strategy based on the use of (i) adequate filtering techniques, (ii) multitemporal data processing, including coherence and interferometry (Stewart 2017) and (iii) knowledge of the problem/site to select the best data and period of observation (Chen et al. 2015)

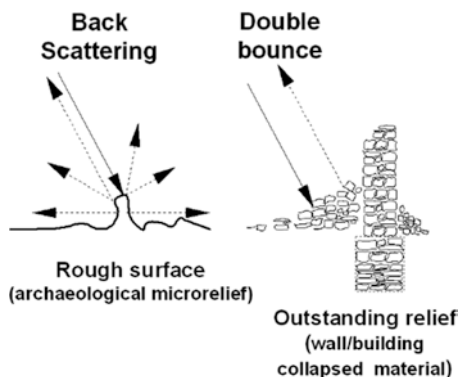
Practical Examples of Archaeological Marks Detection Based on Radar Data

Microtopography as Archaeological Proxy Indicator: the Case of Sabratha

The second study area is the archaeological site of Sabratha, on the coast of Libya (Fig. 2 upper left), 64 km west of Tripoli, characterized by an arid climate in a desert environment.

Sabratha was founded in the seventh century BC by the Phoenicians of Tyre in one of the few natural harbors of Tripolitania and soon became a trading post at the mouth of a major caravan route (Matthews and Cook 1957). Because of its strategic location, Sabratha experienced a rapid development and soon fell under the control of Carthage. Passed briefly to the Kingdom of Numidia under Masinissa, Sabratha was later taken by the Romans in 46 BC, under which it enjoyed a new prosperity. The city was rebuilt under Roman period when it achieved its greatest prosperity

Fig. 1 Interaction between radar and some typical archaeological features



during the second and third centuries AD. Later the city was negatively affected by religious quarrels which probably induced also a decline in the commerce activities, and later on it was destroyed by an earthquake in AD 365. The rebuilding activities were only carried out for a smaller area. In 455 Sabratha was invaded by Vandals, later reconquered by Byzantine and definitively abandoned after the Arab invasions (seventh to eleventh centuries).

The processing and interpretation of remote sensing data focused on an area of about 3 Ha between the Roman town and the amphitheater which is characterized by lesser known archaeological features. They consist of microrelief attributable to shallow remains (walls, foundation) close to the Sabratha amphitheater.

These features are well visible from the COSMO-SkyMed spotlight scene acquired on 12 December 2012 (see Fig. 2b), thanks to the high resolution of the image and the effect of double bounce in backscattering as shown in Fig. 1. The same microrelief could be observed from a multitemporal image set available from Google Earth. However, compared with the spotlight image, the visibility of microrelief is reduced in three of them (10.2009, 20 August 2011, 26 May 2012), and a significant improvement of the spotlight scene in terms of the visibility of archaeological microrelief was achieved using some filtering methods to reduce noise and to enhance the microreliefs of archaeological interest (Chen et al. 2015).

Crop and Damp Marks: Metaponto

The archaeological site of Metapontum is located between the Basento and Bradano rivers, near the Ionian Sea. It has the typical Mediterranean climate. In the Corinne land cover maps, the investigated area is classified as arable with prevailing wheat cultivations. It is one of the most important archaeological areas in the south of Italy. Several archaeological campaigns (Adamesteanu 1973; Carter 1990) have established human presence there since the mid-eighth century BC, when Metapontum was founded by Greeks coming from the Achaean region. Between Greek colonization (700 BC to 200 BC) and the Roman age (200 BC to 400 AD),

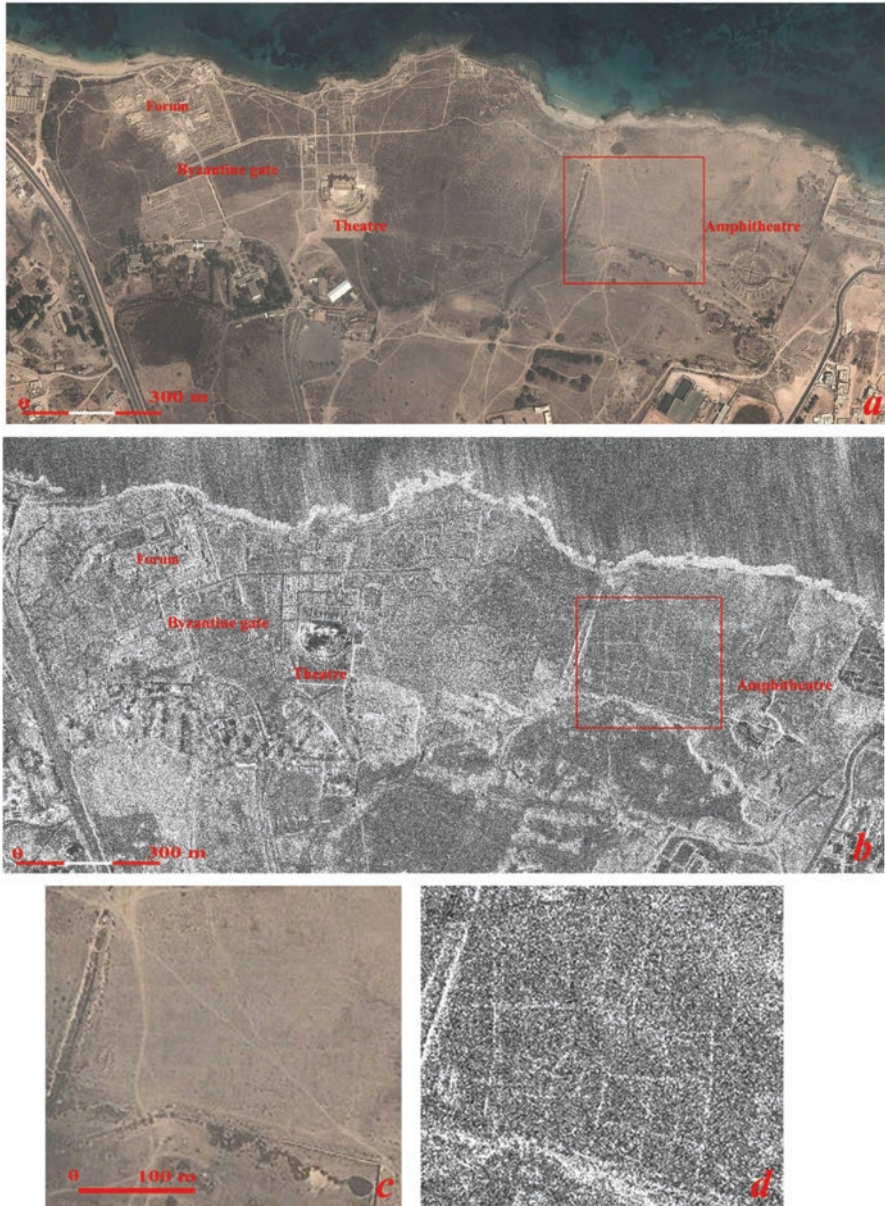


Fig. 2 The archaeological site of Sabratha: comparison between of satellite optical and SAR images (**a** and **b**, respectively). The zooms on an area near the amphitheatre evidence the added value of SAR (**2d**) data respect to optical one (**2c**) in terms of visibility of archaeological features linked to shallow remains.

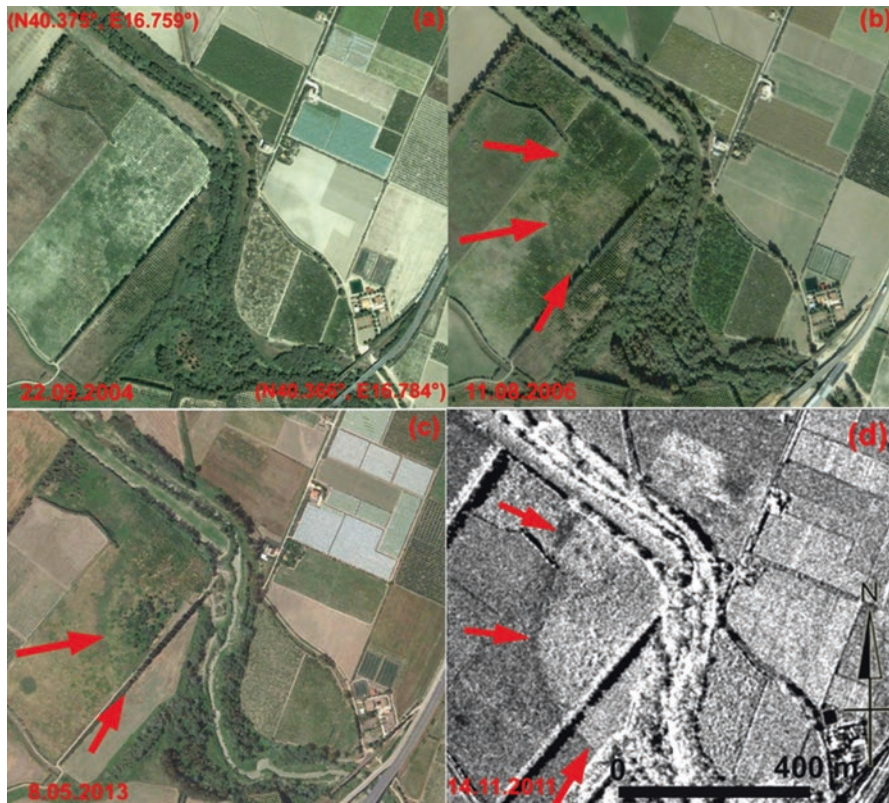


Fig. 3 Multitemporal imaging of a palaeo-riverbed in Metapontum. (a, b, c) RGB imagery acquired on 22.09.2004, 11.08.2006, and 8.05.2013 (Google Earth courtesy). (d) Cosmo SkyMed (Enhanced Spotlight) acquired on 14.11.2011. The visual comparison evidences a better visibility of the palaeo-riverbed from SAR (d) respect to optical data (a–c)

the territory was characterized by an intensive use of soil as revealed by the several rural sites that can be observed from surface surveys and excavations and also the presence of an extensive system of parallel land divisions (Adamesteanu 1973; Carter 1990). Another important element in the history of Metapontum is the spatial and temporal relationship between the hydrography and the human settlements. The rivers Bradano and Basento between which Metapontum is located changed their floodplains several times, influencing the settlement pattern. These spatial features linked to ancient human transformations of the landscape represent one of the most significant traces of ancient human activities which need to be protected. Unfortunately, due to the destructive effects of mechanized agriculture, these traces of the human and geological past are increasingly difficult to identify using solely optical images. For this reason, it has been decided to also use SAR data, such as COSMO-SkyMed acquired in enhanced spotlight mode, in order to assess their ability to detect archaeological and palaeoenvironmental features, in particular roads, palaeoriverbeds, and palaeochannels (see Fig. 3a–d).

In particular, a number of features related to palaeochannels, palaeoriverbeds, ancient roads, and land divisions were investigated. They are very clearly visible from the available COSMO-SkyMed spotlight image processed using (as also for Sabratha) filtering methods to reduce noise and to enhance the microreliefs of archaeological interest (Chen et al. 2015).

Conclusions

This paper offers a brief note to orientate archaeologists in the use of radar technology for applications aimed at identifying the typical marks of archaeological interest (crop, soil, damp, and shadow marks).

A brief history of the use of satellite radar in archaeology coupled with an overview of current satellite missions with main technological characteristics is presented. A correct identification and interpretation of archaeological marks on the basis of radar images is not a straightforward task and requires knowledge about ground surface conditions as well as about the interaction mechanisms between radar waves and surface sensed. It is important to consider that there are significant differences between the interpretation of microwave and optical images including the radar penetration capability.

Firstly, archaeological sites with regular and observable topological traces on the landscape, e.g., crop, shadow, soil, and damp marks (Lasaponara and Masini 2013; Chen et al. 2015), create anomalies on the images, implying the potential of remote sensing for archaeology, particularly when high-resolution SAR data, e.g., TerraSAR-/TanDEM-X, COSMO-SkyMed, RADARSAT-2, and ALOS PALSAR-2, are used. Archaeological features, such as unknown palaeochannels buried under the desert, can be detected by SAR data taking advantage of SAR's penetration capability. In general, penetration is stronger as radar wavelength and subsurface porosity increase. In view of the complicated scenario, the quantitative penetration depth of SAR data however needs to be further estimated through a sufficient number of case studies.

Scaling effect related to the resolution of SAR images is another scientific issue. The optimization of image scaling contributes for cost savings and for improving detection performance in archaeological applications; for example, moderate-resolution SAR data are suitable for large-scale heritage sites and their surrounding paleoenvironment, and high-resolution data are critical for specific local-scale ruins.

The geometry of SAR imaging (i.e., incidence angle together with satellite flight path) has close relationship to surface backscattering. Compared with incidence angle, the impact of satellite flight path (ascending and descending acquisitions) is more significant in archaeological applications because of the interactions between the sensitivity of radar echoes and linear features on the earth's surface. Strong linear backscattering anomalies on SAR images can be observed when the flight path is approximately parallel with linear archaeological features.

Images from multimode (e.g., multifrequency, multitemporal, and multi-polarization) SAR platforms provide different sensed parameters, which are benefi-

cial for the detection of archaeological remains. However, the heterogeneity of data brings in the complexity of image processing and interpretation. For instance, the scattering mechanism that determines the relationship between radar waves and surface/subsurface echoes needs to be investigated for the SAR data optimization. Moreover, the normalization of multimode SAR data is also essential for the performance comparison and assessment.

Apart from the local-scale archaeological signs (crop, soil, and shadow), ancient ruins alter regional landscape that could be observed by remote sensing images and derived added-value products, resulting in the rise of a new subdiscipline of landscape archaeology. Landscape analysis became an irreplaceable component in SAR remote sensing for archaeology. Considering the relationship between the occurrence of ancient ruins and topography, such as those located in high-level wetland platforms, SAR interferometry (InSAR)-derived DEM can be used for identifying potential site.

References

- Adamesteanu D (1973) Le suddivisioni di terra nel Metapontino. In: Finley MI (ed) *Problèmes de la terre en Grèce ancienne*. Mouton, Paris, pp 49–61
- Adams REW (1980) Swamps, canals, and the locations of ancient Maya cities. *Antiquity* 54(212):206–214
- Adams R, Brown W, Culbert T, Mapping SAR (1981) Archeology, and ancient Maya land use. *Science* 213:1457–1463
- Berger M, Aschbacher J (2012) Preface: the sentinel missions-new opportunities for science. *Remote Sens Environ* 120:1–2
- Blom R, Clapp N, Zarins J, Hedges G Space technology and the discovery of the Lost City of Ubar. Paper read at IEEE Aerospace Conf. February 1-8, 1997
- Carter JC (1990) Between the Bradano and Basento: archaeology of an ancient landscape in. In: Kelso W, Most R (eds) *Earth patterns. Essays in landscape archaeology*. University of Virginia Press, Charlottesville, pp 227–243
- Chen F, Masini N, Yang R, Milillo P, Feng D, Lasaponara R (2015) A space view of radar archaeological marks: first applications of COSMO-SkyMed X-band data. *Remote Sens* 7:24–50
- Chen F, Lasaponara R, Masini N (2017), An overview of satellite synthetic aperture radar remote sensing in archaeology: From site detection to monitoring, *Journal of Cultural Heritage*, <http://dx.doi.org/10.1016/j.culher.2015.05.003>
- Cigna F, Tapete D, Lasaponara R, Masini N (2013) Amplitude change detection with Envisat ASAR to image the cultural landscape of the Nasca region, Peru. *Archaeol Prospect* 20:117–131
- Comer DC, Chapman BD, Comer JA (2017) Detecting Landscape Disturbance at the Nasca Lines Using SAR Data Collected from Airborne and Satellite Platforms. *Geosciences*, 7, 106
- El-Baz F (1998) Prehistoric artifacts near paleo-channels revealed by radar images in the western desert of Egypt. *Remote sensing in archaeology from spacecraft, aircraft, on land, and in the deep sea*. Boston University, Boston
- Erasmí S, Rosenbauer R, Buchbach R, Busche T, Rutishauser S (2014) Evaluating the quality and accuracy of TanDEM-X digital elevation models at archaeological sites in the Cilician plain, Turkey. *Remote Sens* 6(10):9475–9493. <https://doi.org/10.3390/rs6109475>
- Guo H (1997) Spaceborne multifrequency, polarimetric and interferometric radar for detection of the targets on earth surface and subsurface. *J Remote Sens* 1:32–39

- Holcomb DH, Shingiray IL (2007) Imaging SAR in archaeological investigations: an image processing perspective. In: Wisemann J, El-Baz F (eds) Remote sensing in archaeology. Springer, Verlag, Berlin/Heidelberg, pp 11–45
- Jiang A, Chen F, Masini N, Capozzoli L, Romano G, Sileo M, Yang R, Tang P, Cheng P, Lasaponara R, Liua G (2016) Archeological crop marks identified from Cosmo-SkyMed time series: the case of Han-Wei capital city, Luoyang, China. *International Journal of Digital Earth*, <http://dx.doi.org/10.1080/17538947.2016.1254686>
- <http://www.eorc.jaxa.jp/ALOS-2/en/about/palsar2.htm>
- <https://directory.eoportal.org/web/eoportal/satellite-missions/s/sir-a>
- Lasaponara R, Masini N (eds) (2008) Advances in remote sensing for archaeology and cultural heritage management. In: Proceedings of I international EARSeL workshop “Advances in remote sensing for archaeology and cultural heritage management”. Rome 30 September–4 October, 2008. Aracne: Roma. ISBN: 978-88-548-2030-2
- Lasaponara R, Masini N (2013) Satellite synthetic aperture radar in archaeology and cultural landscape: an overview. *Archaeol Prospect* 20:71–78
- Linck R, Busche T, Buckreuss S, Fassbinder JWE, Seren S (2013) Possibilities of archaeological prospection by high-resolution X-band satellite radar—a casestudy from Syria. *Archaeol Prospect* 20:97–108
- Matthews Jr KD, Cook AW (1957) *Cities in the sand: Leptis Magna and Sabratha in Roman Africa*. University of Pennsylvania Press, Philadelphia
- McCauley JF, Schaber GG, Breed CS, Grolier MJ, Haynes CV, Issawi B, Elachi C, Blom R (1982) Subsurface valleys and geoarchaeology of the eastern Sahara revealed by shuttle radar. *Science* 218:1004–1020
- Pope KO, Dahlin BH (1989) Ancient Maya wetland agriculture: new insights from ecological and remote sensing research. *J Field Archaeol* 16:87–106
- Richason III FB, Hritz C (1998) The use of digitally enhanced SARsat SAR imagery in the interpretation of archaeological sites in the Nippur, Iraq, area of the lower Mesopotamian plain. Proceedings of the international conference on remote sensing in archaeology from spacecraft, aircraft, on land and in the deep sea, Boston
- Stewart C, Lasaponara R, Schiavon G (2013) Alos palsar analysis of the archaeological site of pelusium. *Archaeol Prospect* 20:109–116
- Stewart C (2017) Detection of Archaeological Residues in Vegetated Areas Using Satellite Synthetic Aperture Radar. *Remote Sens* 9(2): 118; <http://dx.doi.org/10.3390/rs9020118>
- Wisemann J, El-Baz F (eds) (2007) *Remote sensing in archaeology*. Springer-Verlag, Berlin
- Zhu X, Chen F, Guo H (2018) Reconstruction of the Water Cultivation Paleoenvironment Dating Back to the Han and Tang Dynasties Surrounding the Yangguan Frontier Pass Using X- and L-Band SAR Data. *Remote Sens* 10:1536.

Recent and Past Archaeological Looting by Satellite Remote Sensing: Approach and Application in Syria



Nicola Masini and Rosa Lasaponara

Abstract Illegal excavations represent one of the main risks which affect archaeological heritage throughout the world. Actions oriented to quantify damage and prevent looting can be supported by satellite technologies which can provide reliable information to detect and map devastation phenomenon in particular for remote or non-accessible sites. In these cases, it is desirable to use satellite-based semiautomatic or automatic approaches for the mapping and quantification of looting patterns. In this paper, an automatic method for archaeological looting feature extraction approach (ALFEA) has been applied to an archaeological site in Syria, Tell Sheikh Hamad, affected by archaeological looting before and during the civil war. The aim is to evaluate the capability of ALFEA to extract past and recent looting features and patterns using Google Earth images. The results have been assessed through visual inspection, which shows that the rate of success was higher than 90% for recent looting and around the 80% for past archaeological disturbance.

Keywords Satellite remote sensing · Past and recent archaeological looting · Automatic feature extraction · Texture analysis · Google Earth · Syria

N. Masini (✉)

Institute of Archaeological and Monumental Heritage, CNR-IBAM (Italy),
Tito Scalo, Potenza, Italy

e-mail: n.masini@ibam.cnr.it; nicola.masini@cnr.it

R. Lasaponara

Institute of Methodologies for Environmental Analysis, CNR-IMAA (Italy),
Tito Scalo, Potenza, Italy

e-mail: rosa.lasaponara@imaa.cnr.it

© Springer Nature Switzerland AG 2020

D. G. Hadjimitsis et al. (eds.), *Remote Sensing for Archaeology and Cultural Landscapes*, Springer Remote Sensing/Photogrammetry,

https://doi.org/10.1007/978-3-030-10979-0_8

Introduction

Illegal excavations of archaeological sites are part of a global crime system of trafficking in antiquities (Bowman 2008) whose activity tends to grow dramatically during armed conflicts causing irreversible damages to archaeology and history on the human past (Gibson 1997; Brodie et al. 2001). In fact a number of important archaeological areas are located in countries involved in armed conflicts and civil wars, as in the case of Syria, where looting activities have exponentially increased (UNESCO 1956, 1970; United Nations Security Council 2015) since the beginning of the conflict as in many other countries of the Middle East.

Unfortunately, important cultural property disappeared in many countries across the world even in areas not involved in armed conflicts or politic unrest, where looting is phenomenon (Looted Heritage 2016), fed by demand of private collectors and those museums that do not take measures to control the provenance of artefacts (Ganciu 2018; Hart and Chilton 2015). According to analyses conducted by Proulx (2013), 'the archaeological site looting is [...] a globally pervasive problem and is not limited to certain parts of the world respect to others'. This occurs despite the UNESCO recommendations and the repressive measures adopted by many countries which impose the returning of looted objects (UNESCO 1956, 1970; United Nations Security Council 2015). Nevertheless, it must be considered that even returning the refund looted artefacts, the damage to archeology research and the study of the human past cannot be anymore recovered due to the loss of cultural context.

Since the first decade of 2000s, very-high-resolution (VHR) satellite images have shown great potentiality (Lasaponara & Masini 2008) for the identification and the quantification of damage of looting in Syria (Casana and Panahipour 2014; Casana 2015; AAS 2015; Danti et al. 2017), in Iraq (van Ess et al. 2006; Stone 2008, 2015; Danti et al. 2017), in Egypt (Parcak 2007; Bowen et al. 2017), in Afghanistan (Lauricella et al. 2017), in Jordan (Vella et al. 2015), in China (Caspari 2018), and in Peru (Contreras 2010; Lasaponara and Masini 2010; Lasaponara et al. 2012, 2014). Satellite technologies proved to be particularly effective in addressing the current cultural heritage crisis in the conflict zones, as Iraq and Syria, where the worst catastrophe for archaeological heritage is occurred since the Second World War (Danti et al. 2017; Matthiae 2015). In such scenarios, the effectiveness of satellite remote sensing could increase through the application of automatic extraction procedures. Nevertheless, up to now, only a few investigations have been specifically focused on the automatic extraction of archaeological looting features using remote sensing. In particular, van Ess et al. (2006) applied a semiautomatic object-oriented approach based on the segmentation and subsequent supervised classification to the archaeological site of Uruk-Warka in Iraq. Bowen et al. (2017) used a hierarchical categorization and localization algorithm for partially supervised classification of looted areas in Egypt. Lauricella et al. (2017) used a semiautomatic procedure based on principal component analysis for the detection of looting. Cerra et al. (2016) performed an automatic change detection in two archaeological sites in

Syria and Iraq analysing texture features through Gabor filters. Agapiou et al. (2017) used an object-oriented classification for the detection of looted tombs in Cyprus.

Lasaponara and Masini (2010) firstly introduced the use of local indicators of spatial association (LISA) for the identification of looting patterns, near Nasca (in Southern Peru), and later added an unsupervised classification (Lasaponara et al. 2014) step for the automatic extraction of looting features in Ventarron (Northern Peru). This approach was further improved (Lasaponara and Masini 2016) adding a segmentation step, similarly to a feature extraction procedure (Lasaponara et al. 2016), developed for Hierapolis in Turkey. The final refinement of the procedure, recently published (Lasaponara and Masini 2018) and named archaeological looting feature extraction approach (ALFEA), has been applied in desert environment, in two different test cases: Dura-Europos in Syria and Cahuachi (near Nasca) in Peru. These test sites were chosen because they are the representative for two looting features diverse in morphological characteristics and temporal dynamics: frequent in the past for Cahuachi and still ongoing in Dura-Europos.

In this paper, ALFEA has been applied to Tell Sheikh Hamad in western Syria, located in the lower Khabur River and affected by clandestine excavation activities started before the beginning of the civil war (March 2011) and continued with renewed intensity during the years of conflict. Tell Sheikh Hamad has been chosen because it is representative of two looting features/patterns referable to the past and recent looting. The reliability of the results was estimated using both visual inspection and independent investigations (Cunliffe et al. 2014).

Study Area

The Syrian cultural heritage dates back millennia considering that human settlement was recorded at least from around 9000 BC. It is one of the richest and complex heritages in human history being that over the centuries Syria homed a long succession of civilizations starting from the Bronze Age to the Ottoman Empire (Akkermans and Schwartz 2003).

Syria (Abdulkarim 2014; Cunliffe et al. 2014) was strongly affected by clandestine excavations during the ongoing conflict which began 2011 with anti-government protests (BBC 2016) and later enlarged into a full-scale civil war which also facilitated the escalation of the so-called Islamic State (IS). The latter has conducted a systematic destruction of cultural heritage with the aim of erasing the vestiges of the pre-Islamic past and using illegally excavated artefacts to finance their criminal activities (Conversation 2016).

The selected test case is Tell Sheikh Hamad, the modern name of the ancient Assyrian city of Dūr-Katlimmu, which lies on a limestone terrace on the lower Khabur River, tributary of the Euphrates, between the cities of Hassake and Deir ez-Zor in western Syria (North Mesopotamia). Although the oldest remnants of settlements dated back to the end of the fourth millennium BC, Dūr-Katlimmu was founded during the reign of Shalmaneser I (1274 BC–1245 BC), King of Assyria

during the Middle Assyrian Empire (1365 BC–1050 BC). The identification of the ancient name was made possible by the discovery of 30 inscribed tablets of the Middle Assyrian period, found in 1977. The excavations, carried out since 1978, have unearthed the remains of a large city, extending over an area of over 100 hectares, and articulated in various suburbs around the tell. Dūr-Katlimmu had its major development in the Middle Assyrian period. In the Neo-Assyrian period, the city was enlarged with the construction of the lower city. At this time, it was an important military base for the Assyrian expeditions towards Syria and countries facing the Mediterranean Sea. In the Persian period, Dūr-Katlimmu lost importance: from the sixth to the fourth century, the lower city was only partially inhabited. Occupancy levels are still attested on the main tell of the site at Parthian and Roman times, after which it was deserted.

Tell Sheikh Hamad compared to other sites in Syria, such as Palmyra and Dura-Europos, was less damaged during the civil war even if it presents many areas plundered and destroyed by bombing, such as an Assyrian temple, collapsed after shell fire, and other monumental structures heavily damaged when the site was transformed into a battlefield between deserters and army (Cunliffe 2012, p. 6). Two satellite images acquired on March 2011 and March 2014, respectively, show looted areas between the tell and the ancient city (see Fig. 1b, c). The comparison between the two images exhibits changes in terms of looted area and different visibility of past looting. Figure 2 shows details of 2011 and 2014 image. An orange box denotes the area of interest which includes three groups of looting features named A, B and C. The visual comparison between the two images put in evidence two different shapes of looting features:

- (i) The first one, in cluster A (in Fig. 2b), is characterized by quadrangular shape with size ranging from 1.5 to 4 m, referable to recently dug pits, completely shadowed (see also zoomed picture in Fig. 2b bordered by red box).
- (ii) The second one, in B and C, exhibits rounded-shape holes, partially shadowed and with size ranging from 2 to 5.5 m, which are related to looting activities occurred before 2011. These features are characterized by different visibility of the edges depending on the different depth and consequently excavation phases. In particular, two types of features, named 'x' and 'y', with different edge visibility have been identified. Type 'x' refers to the holes with greater edge contrast, having size ranging from 3.5 to 5 m (as measured from Google Earth). Type 'y' refers to the holes with lower contrast with a size ranging from 2.5 to 4 m. The comparison between the two satellite images (see in particular zooms of cluster B in Fig. 2a, b) evidences a significant decrease in terms of visibility of the looting features in B and C.

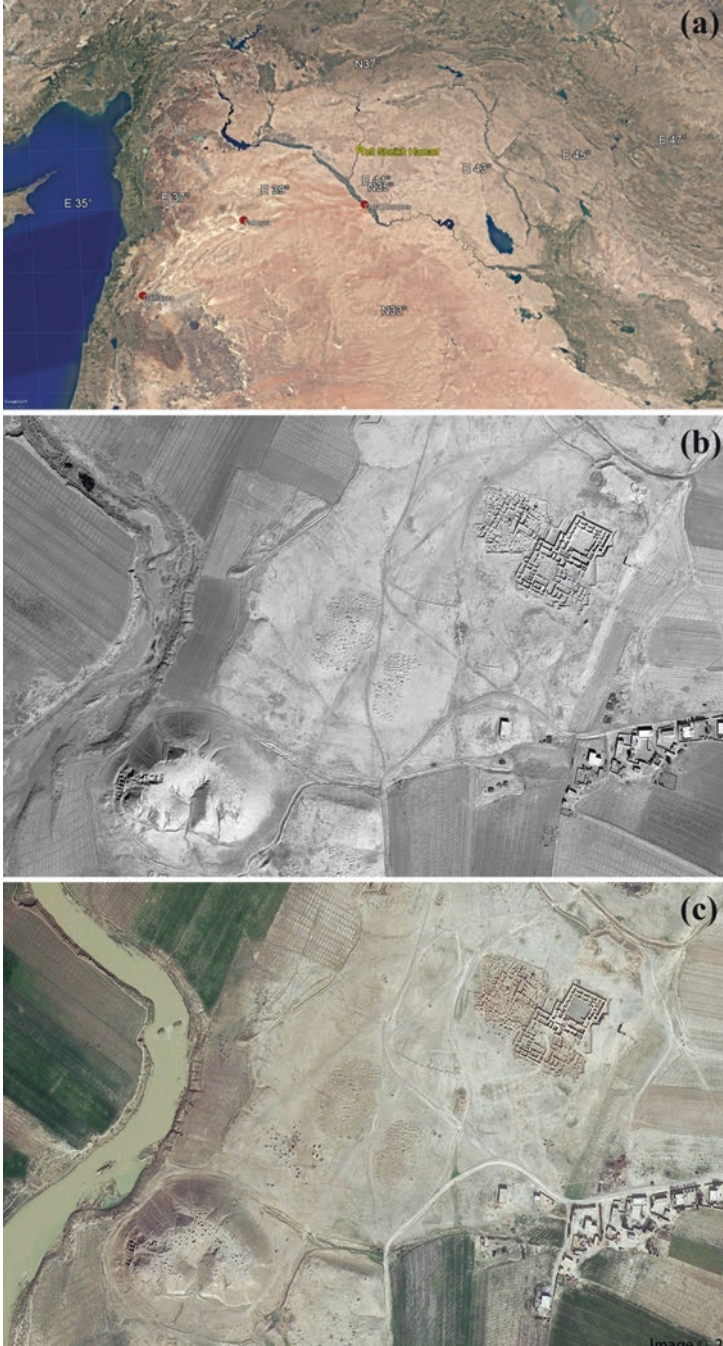


Fig. 1 (a) Location of Tell Sheikh Hamad, modern name of the ancient Dūr-Katlimmu, in Eastern Syria, located in one of the tributaries of the Euphrates River; (b–c) satellite images of Tell Sheikh Hamad acquired on March 1, 2011, and on March 3, 2014. (Courtesy by Google Earth)

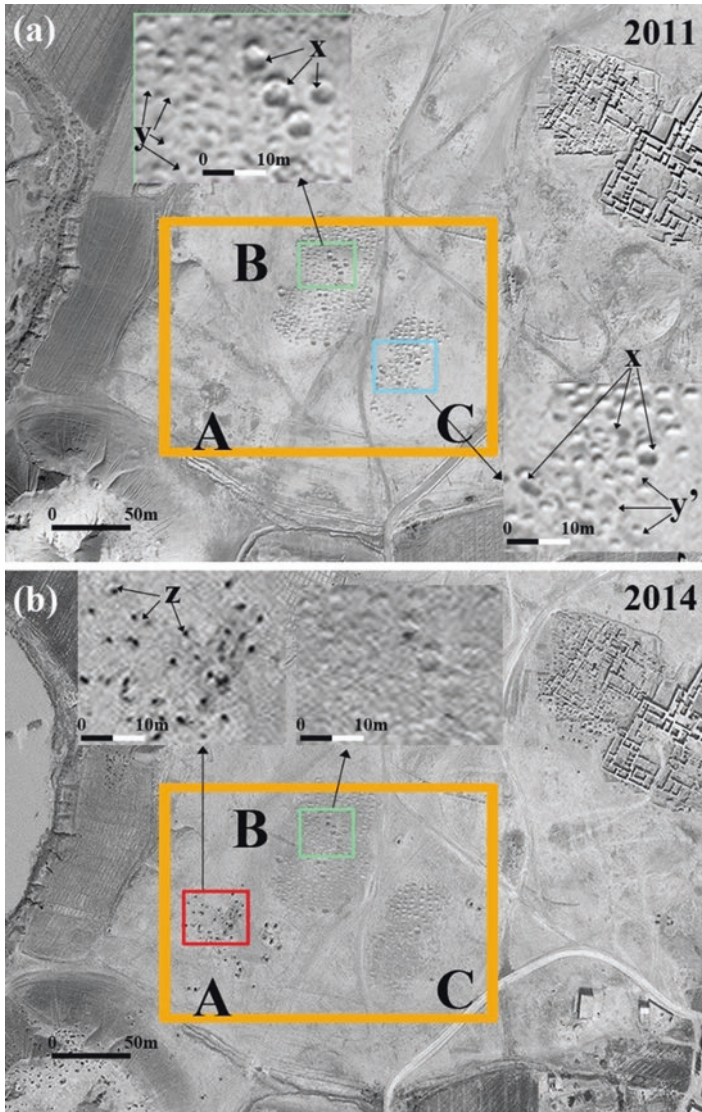


Fig. 2 Details of 2011 and 2014 images (**a** and **b**, respectively). The orange box denotes the test site which ALFEA has been applied to. A, B and C indicate three groups of holes and pits related to two diverse looting phases, before the 2011 (B and C) and in 2014 (A). The holes in B and C are less visible in 2014 than in 2011. In (**a**) zooms of B and C (bordered by green and light blue box, respectively) evidence two different looting features (labelled 'x' and 'y') which exhibit a different visibility of their circular edges, being that they were probably excavated in different periods. In (**b**) the same zoom of B evidences a less significant discriminability of the holes in 2014 with respect to 2011. Finally, the red box denotes a zoomed image of A which depicts the presence of rectangular pits excavated some month before the satellite image acquisition

Material and Method

Satellite Dataset

The automatic extraction of looting features (explained in section ‘[Method](#)’) has been done using Google Earth images to encourage the use of automatic procedures to a wide community of users, also considering the opportunity of civic crowd sourcing activities (Pringle 2010; Ur 2006).

The Google Earth images available for Tell Sheikh Hamad were acquired in 1.03.2011, 12.08.2013, 3.03.2014, 6.11.2016, and 30.09.2017. They make possible to observe a plundering activity before the civil war which continued between 2013 and 2014 and is still today ongoing. For testing the ALFEA method, we used the satellite image acquired in 2011 and 2014 which evidences a variety of looting features in terms of shapes, dimensions and depth, and consequently visibility of edges.

Method

Remote sensing-based identification of looted areas of archaeological interest poses serious challenges related to data processing and interpretation due to the diverse physical characteristics from one site to another one, from one image to another one of the same site or from an area to another in the same image. The complexity of the problem is more evident in case of weak spatial/spectral signals which affect the edge visibility as in the case of archaeological sites located in desert environment. Actually, the holes and pits, created by grave robbers to plunder past treasures, are partially covered over time by desert sand, especially in windy areas, making the detection of looting features by remote sensing difficult (Lasaponara and Masini 2016). In this context, procedures based on textural analysis which take into account both the pixel spectral values and the spatial relationships among the neighbouring pixels may be more effective (Richards and Jia 2006). A similar approach has been recently proposed by Lasaponara and Masini (2018) and applied to two archaeological sites in Syria and in Peru for extracting in an automatic way looting features and patterns. It is based on three steps: (i) local spatial autocorrelation to provide a first clusterization of features, (ii) unsupervised classification to categorize classes linked to looting features, and, finally, (iii) segmentation to refine the feature extraction.

Spatial autocorrelation measures the degree of dependency among pixel reflectance values, considering at the same time their similarity and distance relationships (Bao 1999). The basic formulation of the presence of autocorrelation in a spatial distribution is based on two contributions, generally denoted as first- and second-order effects that could be well defined, but not easily separated (Gatrell et al. 1996). Both of them produce clustering and smooth variations in density, but

their relationships and interaction mechanisms with other variables are very different. The first-order effects measure how the expected value (mean of pixel number) varies in the space, and the second-order effects concern local interactions between pixels and are measured by covariance variations. There are many indicators of spatial autocorrelation generally denoted as global and local indicators, the latter are more suitable to identify second-order effects. Global statistics inform us (by a single value) about the magnitude of autocorrelation for the whole region under investigation. The local statistics relies on the information distance captured in distance matrix and informs us about edges and clusters. These indicators measure if and how much the dataset is autocorrelated on the basis of distance used to define the neighbourhood of a given region (Anselin 1995; Getis et al. 1992). The widely local indicators are Getis-Ord G_i^* , Moran's I , and Local Geary's C . They allow us to uncover hidden local patterns that global statistics may lose. Results from these indices provide diverse maps which, for each pixel, inform us about the presence of local clusters, as well as variations in texture or the presence of edges (Anselin 1995; Getis et al. 1992; Geary 1954). For the purpose of our investigations, we used Local Geary's C index which identifies edges and areas characterized by a high variability compared to the values of its neighbouring pixels and determines if adjacent observations of the same phenomenon (in our case looting features) are correlated (Geary 1954).

Local Geary's C index is defined according to formula 1.

$$C = \frac{n-1}{\sum_{i=1}^n (X_i - \bar{X})^2} \frac{\sum_{i=1}^n \sum_{j=1}^n w_{ij} (X_i - X_j)^2}{2 \sum_{i=1}^n \sum_{j=1}^n w_{ij}} \quad (1)$$

where n is the total number of pixels, X_i and X_j are intensity in points i and j (with $i \neq j$), \bar{X} is the average value, and w_{ij} is an element of the weight matrix.

After the edge extraction, using Local Geary's C , textural analysis has been focalized on looting features carried out by unsupervised classification and segmentation.

Unsupervised classifications enable not only to obtain an automatic clusterization but also to overcome the need of a priori predefining known classes. A number of unsupervised classification approaches can be found in literature, even if the most common used algorithms are (i) K-means clustering and (ii) ISODATA (Iterative Self-Organizing Data Analysis Technique). These two approaches are quite similar. Both of them require a few parameters to be set, as (i) the number of predefined classes (clusters) and (ii) the number of iterations to be carried out. In the K-means classification, the number of clusters is known a priori, whereas in the ISODATA approach, the number of clusters is 'dynamically assigned'. Compared to the K-means method, ISODATA is considered more flexible (Memarsadeghi et al. 2007).

A segmentation tool was applied to the classification maps, to select among all the clusters those that exhibited a roughly circular shape (according to the expected looting features). The output from the classification is the input of the segmentation step made to obtain meaningful feature classes as well as to improve the interpretation. Each segment is characterized by a set of attributes, which enable the extraction of specific features characterized by (i) close proximity on the basis of the Geary analysis and (ii) similar spectral characteristics, on the basis of the classification. The processing steps based on the sequence of Local Geary's *C*, ISODATA, and segmentation have been performed by using routines of ENVI software.

With respect to Local Geary's *C*, it is crucial to select two parameters, (i) neighbourhood rule and (ii) maximum lag:

- (i) Neighbourhood rule is the adjacency rule used in the calculation; therefore, it defines which adjacent pixels must be compared to the central pixel.
- (ii) Maximum lag (pixels) specifies the maximum distance in pixels at which autocorrelation statistics must be calculated.

Given the texture to be extracted, linked to the morphology of the looting features and their dimensions (1.5–4 m on average), we used, respectively, (i) Queen rule, because it selects all eight neighbouring pixels, (ii) and lag distance equal to 1.

As regards ISODATA the following parameters were selected: the number of classes ranging from 5 to 10, change threshold = 5%, and minimum class distance = 5.

The final step is the segmentation aimed at partitioning the ISODATA classes to facilitate the texture discrimination. To this aim it is crucial:

- (i) To adequately select the ISODATA classes which better represent the texture to be extracted.
- (ii) To set the minimum population (MP) and the number of neighbours (NN) in order to enhance the 'looting texture'. Given the dimension of the looting pits and their shape (most of them roughly circular), we assumed the following values of MP and NN equal to 10 and 4, respectively.

Results and Discussion

Figures 3 and 4 show the results of different steps of the data processing chain for the subset, bordered in orange depicted in Fig. 2a, b for 2011 and 2014 images, respectively. As regards the 2011 image (Fig. 3), the result of Local Geary's *C* index (Fig. 3b) enables the extraction of clusters related to looting holes in areas indicated as B and C (subarea A does not exhibit any disturbance). Local Geary's *C* index also enables the removal of some tracks on the desert pavement. Output from ISODATA classification, shown in Fig. 3c, provides seven classes, among them one (class 7, magenta coloured) refers to looting holes. Consequently, this class has been selected for the following step of segmentation that enabled the extraction of looting pits and the removal of other features not related to looting activity (see Fig. 3d).

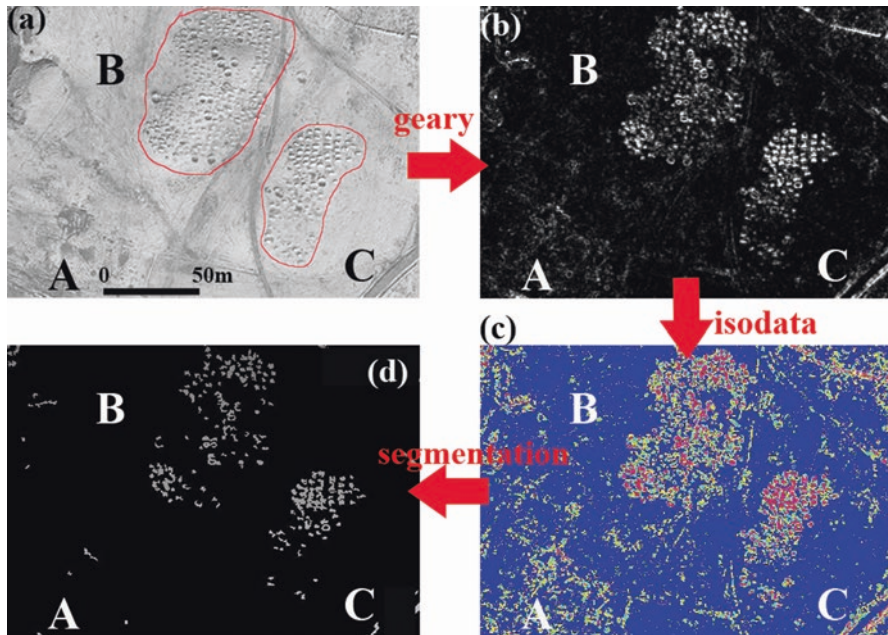


Fig. 3 Results of data processing chain applied to the subset, indicated in Fig. 2a, b, of 2011 image. From up left to bottom left clockwise: non-processed image, Geary result, ISODATA map, and segmentation. Parameters assumed: number of ISODATA classes, 5–10; segmentation applied to classes 6 and 7, population minimum, 10; number of neighbouring, 4

Being that the classification is unsupervised, it is not possible to have statistics related to the assessment that is performed by visual inspection, using the following parameters:

- NH is the number of holes identified from observing Google Earth image.
- TD indicates the number of targets (looting pits) detected.
- TnD is given by the number of targets not detected.
- FA are the false alarms.
- N_{FA} is the normalized false alarm index given by $FA/(FA + TD)$.

Table 1 summarizes the results from the assessment procedure. In particular, the rate of success of targets detected is between 79.41% and 83.58% for clusters C and B, respectively; NFA is around 5%.

Considering that the visual discriminability of looting features is in some points not good, the results of automatic procedure of feature extraction in terms of targets detected and false alarms are to be considered satisfactory.

The rate of success of targets detected strongly increases for the most recent looting pits observed in A of the 2014 image as shown in Fig. 4 and Table 2. In particular, the percentage of targets detected is around 95%. On the contrary the rate of

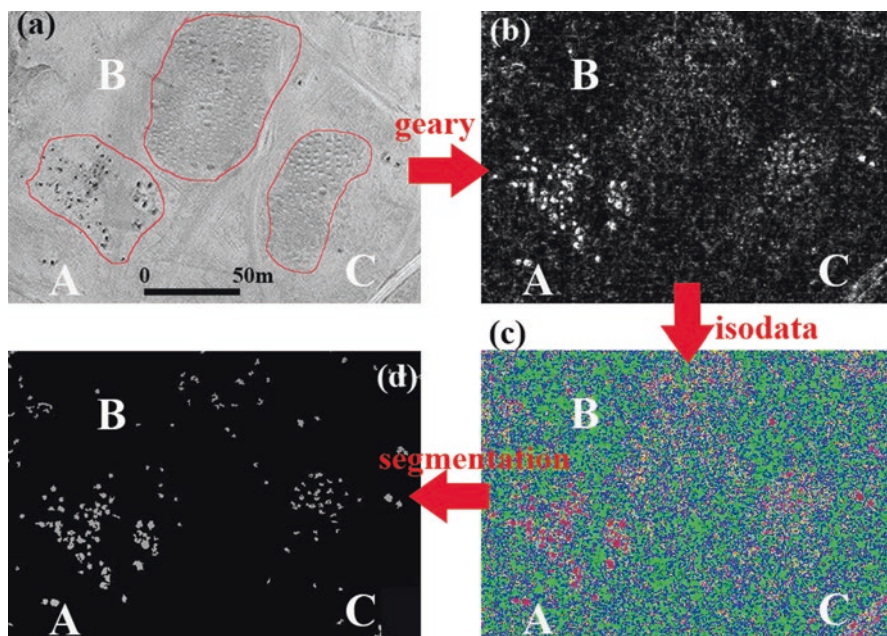


Fig. 4 Results of data processing chain applied to the same subset of Fig. 3 of 2014 image. From up left to bottom left clockwise: non-processed image (a), Geary result (b), ISODATA map (c), and segmentation (d). Parameters assumed: number of ISODATA classes = 5–10; segmentation applied to classes 6 and 7, population minim = 10; number of neighbouring = 4

Table 1 Assessment carried out in the test sites of 2011 image

2011					
Group	NH	TD	TnD	FA	$N_{FA} = FA/(FA + TD)$
A	0				
B	134	112	22	5	
	100.00%	83.58%	16.42%		4.27%
C	102	81	21	5	
	100.00%	79.41%	20.59%		5.81%

Legend. *NH* number of holes identified from visual interpretation, *TD* target (holes/pits) detected, *TnD* target not detected, *FA* false alarms, N_{FA} normalized false alarm index ($N_{FA} = FA/(FA + TD)$)

Table 2 Assessment carried out in the test sites of 2014 image

2014					
Sector	NH	TD	TnD	FA	$N_{FA} = FA/(FA + TD)$
A	78	74	4	3	
	100.00%	94.87%	5.13%		3.90%
B	23	16	7	5	
	100.00%	69.57%	30.43%		23.81%
C	36	31	5	3	
	100.00%	86.11%	13.89%		8.82%

Legend. *NH* number of holes identified from visual interpretation, *TD* target (holes/pits) detected, *TnD* target not detected, *FA* false alarms, N_{FA} normalized false alarm index ($N_{FA} = FA/(FA + TD)$)

success of the automatic feature extraction is much lower for the looted areas B and C whose discriminability strongly reduced from 2011 to 2014.

Conclusions

Looting represents one of the main risk factors which affects the archaeological heritage throughout the world. The damage is not only the loss of artefacts and monuments but also of the archaeological context, thus denying the knowledge of human past to new generations (O'Neil 1972). To contrast and limit this phenomenon, a systematic monitoring is required. The protection of archaeological heritage from illegal diggings is generally very complex to be approached using only direct (in situ) surveillance. Moreover, it is expensive, time-consuming, and not operatively applicable to desert areas or regions involved in wars and conflicts as, for example, in Syria. In these cases, the use of VHR satellite remote sensing is mandatory along with the use of automatic procedures for the reconnaissance of looting features.

In this paper, we applied a procedure (ALFEA by Lasaponara and Masini 2018) devised for the automatic identification of archaeological looting performed using Google Earth images. This method is made up of three steps: (i) spatial autocorrelation based on Geary index for the extraction of edges, (ii) unsupervised classification, and (iii) segmentation which enabled us to focalize the texture analysis on the targets of interest. The procedure was already tested in desert conditions (Lasaponara and Masini 2018) for two sites located in different geographic areas (Dura-Europos in Syria and Cahuachi in Peru) and characterized by diverse looting features and temporal dynamics. In this paper, ALFEA has been again applied to the site of Tell Sheikh Hamad (in Syria) selected because it is affected by a long plundering activity conducted before and during the civil war.

ALFEA has been assessed in three test areas of Tell Sheikh Hamad characterized by diverse looting features and patterns and, consequently, by different visibility and complexity in the identification of looting edges. As a whole, the adopted methodology provided satisfactory results for the diverse looting features, and it is important to highlight that the methodology is easy and can promptly be reapplied to other geographic areas. This can provide a reliable low-cost tool for a preliminary identification and quantification of clandestine excavations in desert areas. ALFEA represents a contribution to set automatic approaches for looting monitoring using Google Earth operationally.

References

- AAS (2015) Ancient history, modern destruction: assessing the current status of Syria's World Heritage Sites using high-resolution satellite imagery. <https://www.aas.org/page/ancient-history-modern-destruction-assessing-current-status-syria-s-world-heritage-sites-using>. Accessed 26 Nov 2016

- Abdulkarim M (2014) Directorate general of antiquities and museums annual report 2013. Damascus: Ministry of Culture, Directorate General of Antiquities and Museums
- Agapiou A, Lysandrou V, Hadjimitsis DG (2017) Optical remote sensing potentials for looting detection. *Geosciences* 7(4):98. <https://doi.org/10.3390/geosciences7040098>
- Akkermans PMMG, Schwartz GM (2003) The archaeology of Syria: from complex hunter-gatherers to early urban societies (ca. 16,000–300 BC). Cambridge University Press, Cambridge
- Anselin L (1995) Local indicators of spatial association LISA. *Geogr Anal* 27:93–115
- Bao S (1999) An overview of spatial statistics. University of Michigan, USA, China Data Center
- BBC (2016) The Syria: the story of the conflict. <https://www.bbc.com/news/world-middle-east-26116868>. Accessed on 12 Sept 2017
- Bowen FW, Tofel BB, Parcak S, Granger R (2017) Algorithmic identification of looted archaeological sites from space. *Front ICT* 4, article 4. <https://doi.org/10.3389/fict.2017.00004>
- Bowman N (2008) Transnational crimes against culture: looting at archaeological sites and the ‘grey’ market in antiquities. *J Contemp Crim Justice* 24(3):225–242
- Brodie NJ, Doole J, Renfrew C (2001) Trade in illicit antiquities: the destruction of the world’s archaeological heritage. McDonald Institute, Cambridge
- Casana J (2015) Satellite imagery-based analysis of archaeological looting in Syria. *Near East Archaeol* 8(3):142–152
- Caspari G (2018) Assessing looting from space: the destruction of early iron age burials in northern Xinjiang. *Heritage* 1:320–327
- Casana J, Panahipour M (2014) Satellite-based monitoring of looting and damage to archaeological sites in Syria. *J East Mediterr Archaeol Herit Stud* 2(2):129–152
- Cerra D, Pank S, Lysandrou V, Tian J (2016) Cultural heritage sites in danger—towards automatic damage detection from space. *Remote Sens* 8:781. <https://doi.org/10.3390/rs8090781>
- Contreras DA (2010) Huaqueros and remote sensing imagery: assessing looting damage in the Viru Valley, Peru. *Antiquity* 84(324):544–555
- Conversation (2016) Inside ISIS’ looted antiquities trade. Available at <http://theconversation.com/inside-isis-looted-antiquities-trade-59287>. Accessed on 31 July 2017
- Cunliffe E (2012) Damage to the soul: Syria’s cultural heritage in conflict, Global Heritage Fund, 2012. http://ghn.globalheritagefund.com/uploads/documents/document_2107.pdf. Accessed on 31 July 2017
- Cunliffe E, Pedersen W, Fiol M, Jellison T, Saslow C, Bjørgo E, Boccardi G (2014) Satellite-based damage assessment to cultural heritage sites in Syria. UNITAR/UNOSAT. <http://www.unitar.org/unosat/chs-syria>. Accessed on 31 July 2017
- Danti M, Branting S, Penacho S (2017) The American Schools of Oriental Research cultural heritage initiatives: monitoring cultural heritage in Syria and Northern Iraq by geospatial imagery. *Geosciences* 7:95. <https://doi.org/10.3390/geosciences7040095>
- Ganciu I (2018) Heritage for sale! The role of museums in promoting metal detecting and looting in Romania. *Heritage* 1(2):437–452. <https://doi.org/10.3390/heritage1020029>
- Gatrell AC, Bailey TC, Diggle PJ, Rowlingson BS (1996) Spatial point pattern analysis and its application in geographical epidemiology. *Trans Inst Br Geogr* 21:256–271
- Geary RC (1954) The contiguity ratio and statistical mapping. *Inc Stat* 5(3):115–145
- Getis A, Getis O, Keith J (1992) The analysis of spatial association by the use of distance statistics. *Geogr Anal* 24:189–206
- Gibson M (1997) Iraq Since the Gulf War. The loss of archaeological context and the illegal trade in Mesopotamian antiquities. *Culture Without Context. The Newsletter of the Near Eastern Project of the Illicit Antiquities Research Centre*, 1, pp 6–8
- Hart SM, Chilton ES (2015) Digging and destruction: artifact collecting as social practice. *Int J Herit Stud* 21:318–335
- Lasaponara R, Masini N (eds) (2008) Advances in remote sensing for archaeology and cultural heritage management. In: Proceedings of I international EARSeL workshop “Advances in remote sensing for archaeology and cultural heritage management”. Rome 30 September–4 October, 2008. Aracne: Roma. ISBN: 978-88-548-2030-2

- Lasaponara R, Masini N (2010) Facing the archaeological looting in Peru by local spatial autocorrelation statistics of very high resolution satellite imagery. In: Taniar D et al (eds) Proceedings of ICSSA, the 2010 international conference on computational science and its application, Fukuoka-Japan, March 23–26, 2010. Springer, Berlin, pp 261–269
- Lasaponara R, Masini N (2016) Combating illegal excavations in Cahuachi: ancient problems and modern technologies. In: Lasaponara R, Masini N, Orefici G (eds) The ancient Nasca world new insights from science and archaeology. Springer International Publishing, pp 605–633. https://doi.org/10.1007/978-3-319-47052-8_25
- Lasaponara R, Masini N (2018) Space-based identification of archaeological illegal excavations and a new automatic method for looting feature extraction in desert areas. *Surv Geophys.* <https://doi.org/10.1007/s10712-018-9480-4>
- Lasaponara R, Danese M, Masini N (2012) Satellite-based monitoring of archaeological looting in Peru. In: Lasaponara R, Masini N (eds) Satellite remote sensing: a new tool for archaeology. Springer, Berlin/Heidelberg, ISBN 978-90-481-8800-0, pp 177–193. https://doi.org/10.1007/978-90-481-8801-7_8
- Lasaponara R, Leucci G, Masini N, Persico R (2014) Investigating archaeological looting using satellite images and GEORADAR: the experience in Lambayeque in North Peru. *J Archaeol Sci* 42:216–230. <https://doi.org/10.1016/j.jas.2013.10.032>
- Lasaponara R, Leucci G, Masini N, Persico R, Scardozzi G (2016) Towards an operative use of remote sensing for exploring the past using satellite data: the case study of Hierapolis (Turkey). *Remote Sens Environ* 174:148–164. <https://doi.org/10.1016/j.rse.2015.12.016>
- Lauricella A, Cannon J, Branting S, Hammer E (2017) Semi-automated detection of looting in Afghanistan using multispectral imagery and principal component analysis. *Antiquity* 91(359):1344–1355
- Looted Heritage (2016) Looted heritage monitoring the illicit antiquities trade. <https://heritage.crowdmap.com/main>. Accessed on 31 July 2017
- Matthiae P (2015) Distruzioni, saccheggi e rinascite. Gli attacchi al patrimonio artistico dall'antichità all'Isis. Mondadori Electa, Florence
- Memarsadeghi N, Netanyahu NS, LeMoigne J (2007) A fast implementation of the ISODATA clustering algorithm. *Int J Comput Geom Appl* 17(1):71–103
- O'Neil T (1972) Archaeological looting and site destruction. *Science* 176:353–355
- Parcak S (2007) Satellite remote sensing methods for monitoring archaeological tells in the Middle East. *J Field Archaeol* 32(1):65–81
- Pringle H (2010) Google Earth shows clandestine worlds. *Science* 329:1008–1009
- Proulx BB (2013) Archaeological site looting in global perspective. *Nature, scope and frequency.* *Am J Archaeol* 117:111–125
- Richards JA, Jia X (2006) Remote sensing digital image analysis – hardback. 4th edn. Springer, Berlin/Heidelberg
- Stone EC (2008) Patterns of looting in southern Iraq. *Antiquity* 82:125–138
- Stone EC (2015) An update on the looting of archaeological sites in Iraq. *Near East Archaeol* 78(3):178–186
- UNESCO (1956) Recommendation on international principles applicable to archaeological excavations. http://portal.unesco.org/en/ev.php-URL_ID=13062&URL_DO=DO_TOPIC&URL_SECTION=201.html. Accessed on 31 July 2017
- UNESCO (1970) Convention on the means of prohibiting and preventing the illicit import, export and transfer of ownership of cultural property. http://portal.unesco.org/en/ev.php-URL_ID=13039&URL_DO=DO_TOPIC&URL_SECTION=201.html. Accessed on 31 July 2017
- United Nations Security Council (2015) Unanimously adopting resolution 2199, security council condemns trade with Al-Qaida associated groups, threatens further targeted sanctions. <https://www.un.org/press/en/2015/sc11775.doc.htm>. Accessed on 31 July 2017

- Ur J (2006) Google Earth and archaeology. *SAA Archaeol Rec* 6:35–38
- van Ess M, Becker H, Fassbinder J, Kiefl R, Lingenfelder I, Schreier G, Zevenbergen A (2006) Detection of looting activities at archaeological sites in Iraq using Ikonos imagery. *Angewandte Geoinformatik, Beiträge zum* (18). Wiechmann-Verlag, Heidelberg, pp 668–678
- Vella C, Bocancea E, Urban TM, Knodell AR, Tuttle CA, Alcock SE (2015) Looting and vandalism around a World Heritage Site: documenting modern damage to archaeological heritage in Petra's hinterland. *J Field Archaeol* 40(2):221–235

Identification of Buildings Damaged by Natural Hazards Using Very High-Resolution Satellite Images: The Case of Earthquake in L'Aquila, Italy



Luigi Barazzetti and Branka Cuca

Abstract Earth observation technologies are becoming increasingly important not only in monitoring practice in environmental domain, but also for detecting changes in urban areas caused by natural hazards such as earthquakes, floods or landslides. A range of high- and very high-resolution sensors useful for this purpose have been implemented as equipment of several missions launched since the year 2000, mostly by private companies. This chapter proposes a methodology for identification of damages in urban fabric of L'Aquila, caused by an earthquake in 2009. The images employed for assessment of such damages are Quickbird images with less than 1 m resolution, providing inputs for an advanced visualisation technique. The results of this process were discussed within a larger framework of emergency management cycle for possible thematic mapping, useful especially for response and recovery planning strategies.

Keywords L'Aquila · Earthquake · Quickbird · HR satellite imagery · Remote sensing · Historic centre

Introduction

A timely damage evaluation and risk assessment is becoming increasingly more important not only for humanitarian and social but also economic reasons and management purposes. Already in the 1990s, the benefits of the geographic information systems were explored for purposes of the comprehensive emergency management

L. Barazzetti (✉)

Department of Architecture, Built Environment and Construction Engineering (ABC),
Politecnico di Milano, Milan, Italy
e-mail: luigi.barazzetti@polimi.it

B. Cuca

Department of Civil Engineering and Geomatics, Faculty of Engineering and Technology,
Cyprus University of Technology, Limassol, Cyprus

© Springer Nature Switzerland AG 2020

D. G. Hadjimitsis et al. (eds.), *Remote Sensing for Archaeology and Cultural Landscapes*, Springer Remote Sensing/Photogrammetry,
https://doi.org/10.1007/978-3-030-10979-0_9

139

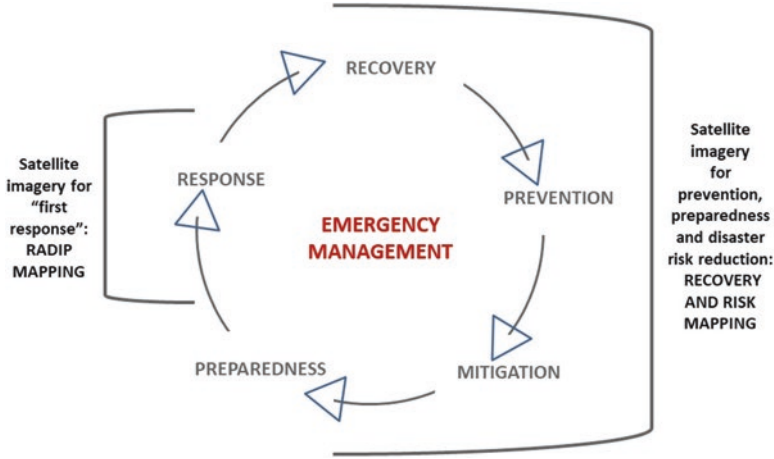


Fig. 1 Phases of emergency management cycle and types of services that can be provided by satellite remote sensing

(CEM) that relies on the temporal dimension of disasters to organise the emergency management process into a cycle of often overlapping phases (Cova 1999).

The European Copernicus Emergency Management Service (EMS) provides a set of mapping services using the satellite data provided by the Copernicus programme, to address the emergency situations resulting from natural or man-made disasters. In particular, mapping provided by EMS follows two temporal modes: rapid mapping to support emergency management activities immediately after a hazard has occurred and risk and recovery mapping in support of activities successive to immediate response, i.e. prevention, preparedness, risk reduction and recovery phases (Copernicus EMS 2018). According to this logic, Fig. 1 illustrates a schema proposal of services based on satellite earth observation (EO) technologies matching the phases of emergency management cycle.

Unlike fire or in some cases even flooding events (Alexakis et al. 2014), earthquakes cannot be prevented and cannot be controlled. For this reason, the focus of emergency management strategies in these cases is on phases of preparedness and response, i.e. on measures aimed at (i) reducing the risk, (ii) enhancing earthquake resistance, (iii) improving earthquake detection and monitoring and (iv) developing a response plan (Stovel 1998). In case of an earthquake in fact, the phase regarding damage evaluation is highly important for the first emergency response for securing of people, animals and structures and during the recovery phase in order to support assistance and inspection teams. Furthermore, such evaluations can be valuable also to reconsider the phases preceding the event (such as prevention, mitigation and preparedness) providing inputs to evaluation of economic damage and future urban planning and resilience strategies.

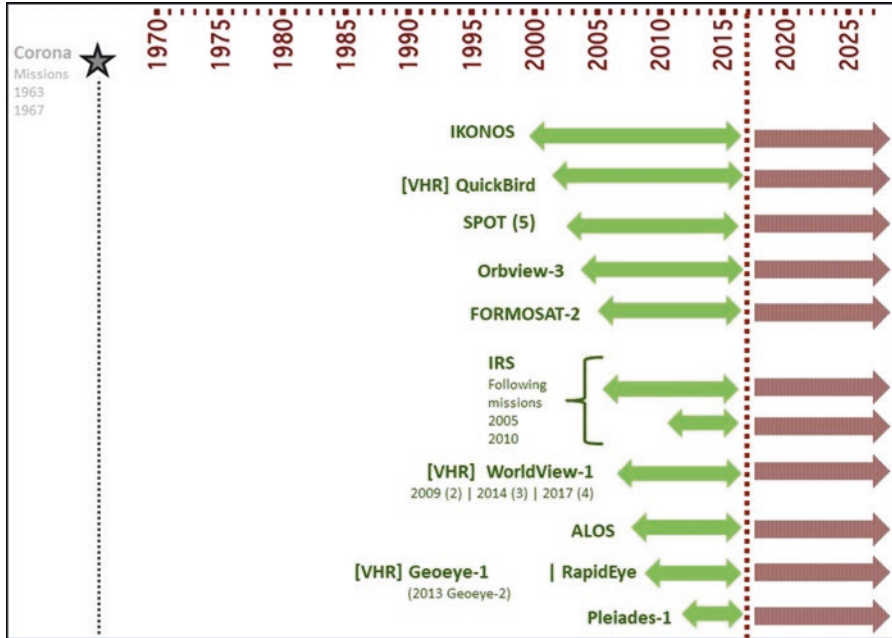


Fig. 2 Satellites with high- and very-high (indicated as VHR) resolution sensors for monitoring of urban environment: a timeline overview according to image availability

For cultural heritage and historic buildings, assessment and mapping of damage conducted by professionals become of extreme importance not only due to their cultural and social value, but also economic value for the community. Historic district and historic centres, for example, in addition to damages of buildings, can suffer also significant damages to their systems such as destruction of municipal infrastructure system (electrical and communication systems, water, gas and sewerage systems) and damage to transport infrastructures (including bridges, underpasses or elevated passages) potentially compromising the access to threatened or damaged areas (Stovel 1998). Timely and updated information is hence needed already in the first phases of emergency management in order to proceed with the quick and efficient response and recovery planning phases.

Damage assessment using satellite remote sensing has already been widely applied, especially cases of destruction occurring in urban areas (Rezaeian 2010; Pacifici et al. 2010; Dong and Shan 2013). The use of high- and very high-resolution images has proven to be valuable not only for visual inspection (Yamazaki et al. 2005) but also for pixel-based methods and classification focusing on the roofs of the buildings to access the damages (Chesnel et al. 2007). Fig. 2 illustrates selections of satellites with high- and very high-resolution sensors currently active, organised according to their year of launch. For a more exhaustive description on the civilian satellite systems, the reader is referred to Belward and Skøien (2015).



Fig. 3 Several scenes of L'Aquila historic centre, severely damaged during the earthquake occurred in 2009

Case Study: Town of L'Aquila in Italy

The case study examined by this chapter is the town of L'Aquila located in the central Italy, in Abruzzo Region. L'Aquila is erected on a soil with such a structure that amplifies seismic waves. In the past, the city was struck by earthquakes in 1315, 1349, 1452, 1501, 1646, 1703, 1706 and 1958 (Antonini 2010).

The earthquake that has struck L'Aquila on 6 April 2009 had an intensity of 5.8–5.9 on the Richter scale, and it has caused 309 human victims in the area. Quite a few buildings, especially in the historic centre that are still surrounded by the mediaeval walls, have undergone serious structural damages (Fig. 3).

As a consequence, almost complete evacuation of the historic centre has been imposed by the civil protection and is still in force for majority of the residential buildings. More than 65,000 inhabitants were forced to leave their homes. Many of the



Fig. 4 Perimeter of L'Aquila historic centre shown in white (a); damages of Santa Maria Paganica (b) and of L'Aquila Duomo cathedral (c), background images ©Google

buildings that have undergone damages were churches or other monuments of historic and cultural relevance to the citizens of L'Aquila and the whole region (Fig. 4).

The damages caused by the earthquake opened discussions about the anti-seismic building standards adopted in Italy. Although many buildings in L'Aquila have been built before the adoption of modern anti-seismic regulations, serious damages have been found also for recent buildings.

According to the Italian National Institute of Geophysics and Volcanology (INGV), in 2003 the whole territory of the country has been classified into four main categories in relation to the intensity and frequency of observed past events and according to application of specific normative construction measures in the seismic areas. These categories (sorted by decreasing risk intensity), are: Zone 1, area at major risk where strong earthquakes can occur; Zone 2, area where strong earthquakes can occur; Zone 3, area where earthquakes may occur but rarely; and Zone 4, less dangerous areas where earthquakes are rare.

An important fact is that, with this new classification conducted after the legislation measure has been introduced, the category “non-classified” has been cancelled and a new category Zone 4 has been introduced, thus bringing to consider the whole Italian territory as possibly subjected to the consequences of an earthquake. For Zone 4, it has been left up to single regional authorities to recommend measures for anti-seismic construction (for more details, reader is referred to Gazzetta Ufficiale n.105 2003). Regarding all categories, a base value of risk has been taken into account and defined considering a matrix of 5 km by 5 km, independently of administrative boundaries (Fig. 5c). Figure 5 shows illustration of seismic risk as provided by INGV, with reference to the values of the maximum acceleration of the soil. It can be noticed that the town of L'Aquila has been classified among the areas at the highest risk even before the tragic event occurred in 2009.

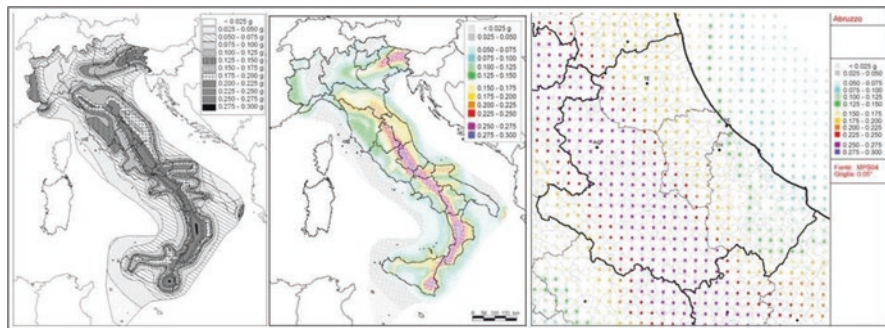


Fig. 5 Seismic risk reference in Italy: (left) the map in black and white, Official Gazette n.108; (middle) ag values on a 0.05° grid for the whole national territory; (right) ag values on a 0.05° grid, closeup on Abruzzo Region. (Source © INGV)

Dataset Description and Image Classification

The methodology proposed was focused on imagery collected above the historic centre of L'Aquila. The dataset is composed of two Quickbird images termed Ipre and Ipost provided by DigitalGlobe Inc., acquired on 4 September 2006 and 8 April 2009, respectively, with a ground resolution (GSD) of about 0.6 m. They also have a different off-nadir angle (10.65° and 5.6°), which is a significant issue for automated change detection. Indeed, the use of variable off-nadir angles allows reducing revisit time, but, in the case of tall objects, the top is leaning away from its base. In other words, there is a lack of overlap between objects, especially when large off-nadir angles are used.

The research work carried out concerns a procedure for comparing images with such additional spatial inconsistency, in which specific algorithms allow the user to handle geometrically inconsistent data. Here, the comparison of two images is not a pixel-to-pixel approach: objects in the images are extracted through object-based classification (Blaschke 2010) and are then compared after aligning classification shapefiles. The method assumes that residual misalignments are mainly caused by elongated features (not by areas indicating damage), which are then removed through object-based image analysis. The schema of the overall workflow is shown in the Fig. 6.

Preliminary data processing consists in pan-sharpening and orthorectification with the provided RPC coefficients. It is well known that VHR images suffer for the estimation of the true spatial orientation of every scan line for the direct measurement of sensor orientation. Orthorectification requires accurate grid models of the ground and 3D points with known coordinates to correct orientation biases. Quickbird has a geolocation accuracy of 23 m (CE90%), whereas panchromatic and multispectral images have a ground sampling distance (GSD) of 0.6/0.7 m and 2.4/2.5 m, respectively (DigitalGlobe 2013).

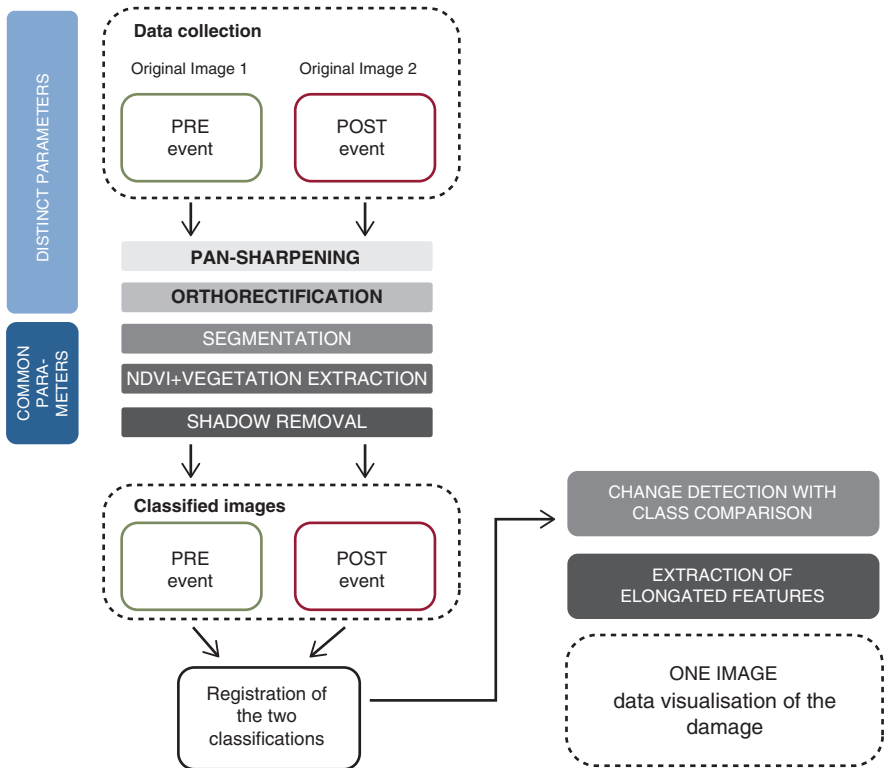


Fig. 6 The overall workflow for processing of single images and the couple (before/after the event)

Object-based image analysis can improve the classification accuracy of VHR satellite images. The proposed approach is based on three layers, which were assumed as sufficient for L’Aquila. Segmentation was carried out with the multi-resolution tool available in eCognition; areas with vegetation were then detected and excluded from data processing. The NDVI is computed for both images; then a threshold is used to classify objects as vegetation for both pre- and post-event images. Classification layers are termed V_{pre} and V_{post} .

The second class used is related to shadows, which are classified using brightness $BRI = [R + G + B]/3$. This has provided two new classes (S_{pre} , S_{post}). Finally, a class “object” is assigned to pixel which does not belong to the previous classes, obtaining two new layers termed O_{pre} and O_{post} . Results for a selected area close to the Spanish Fortress in L’Aquila (district of the church Santa Maria Paganica) are shown in Fig. 7. As it can be seen, the class object does not discriminate between buildings and roads that appear in the same class (Fig. 7b, in red colour).



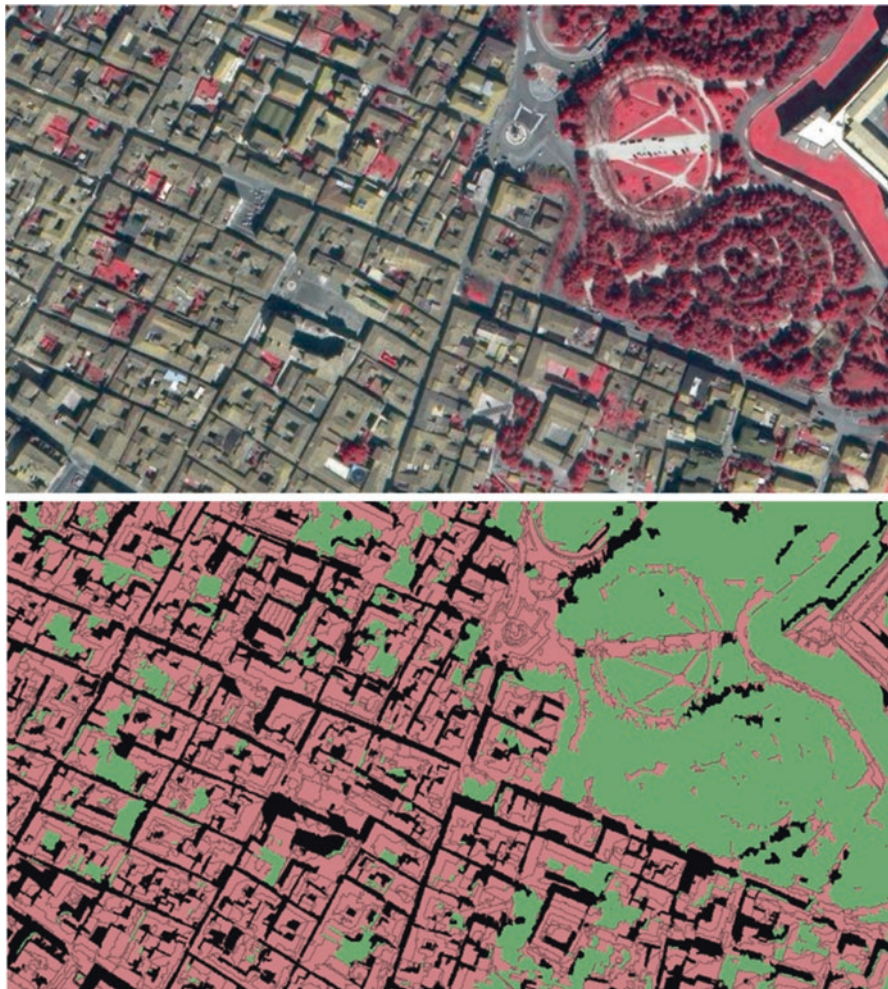


Fig. 7 The Quickbird image after the earthquake and classification results of segmented elements

Change Detection with Variable Off-Nadir Angle

Change detection requires the vector layers generated in the previous object-based classification. The method does not consider those buildings that have completely collapsed during the earthquake. The main assumption is that if the shadow of a building is found only in the post-event image, that shadow indicates a local damage like the collapse of the roof. The idea is to identify only those areas of shadow found in the post-event satellite image; hence the proposed procedure allows the identification of partially damaged buildings.

Change detection with images acquired with a different off-nadir angle does not allow a direct pixel-to-pixel comparison. After preliminary data processing, images exhibit a significant lack of pixel also caused by the digital elevation model (DEM) and the rational polynomial coefficients (RPC) without bias compensation (Hanley et al. 2002; Fraser and Hanley 2003). On the other hand, quick data processing after the earthquake can be guaranteed only if the analysis is based on the available products, without a mission on-site in order to avoid that operators are exposed to any possible risks. For instance, correcting the bias in the RPC coefficients would require some ground control points measured with GNSS receivers. This practice is not always feasible, especially in areas with a potential risk for the safety of human operators, such as in case of earthquakes and areas that might be subject to so-called aftershocks.

In order to overcome this problem, an additional registration procedure was developed to reduce the geometric discrepancy between the classification shapefiles. The final result is not a perfect correspondence between different vector layers. However, a strong reduction of the initial misalignment can be achieved. For these procedures, images are divided into tiles, and matching is carried out to detect corresponding points between the images. Then, an additional check has been added to remove wrong image correspondences through robust estimation of homographic transformations. The threshold between inliers and outliers is set to geolocalisation accuracy of Quickbird data (CE90%). The use of small tiles (instead of the full image) allows one to locally reduce deformities, and the estimation of the homography is more consistent with the global error due to RPC coefficients without bias compensation. The computer parameters are then applied to the classification.

Before running the change detection algorithm (comparison of classification layers), the intersection between the shadow layers after the earthquake S_{post} and both vegetation V_{pre} and shadows S_{pre} before the earthquake is carried out, and the identified areas are excluded from data processing. This can be written as $S_{post} \cap (V_{pre} \cup S_{pre})$. Then, the intersection written as $(S_{post} \setminus S_{post} \cap (V_{pre} \cup S_{pre})) \cap O_{pre}$ is computed to find partial damages. This second intersection is affected by the variable off-nadir angle, which has caused an additional generation of elongated elements in areas close to the polygon edges of classification shapefiles. Removing such elements from the analysis is mandatory to improve change detection results and hence to identify only those areas that depict shadows of buildings in post-event image.

As such errors have an elongated shape, geometric parameters based on their geometry can separate them from effective damages, which have a more circular form. Given a generic element E_i , the index $T_i = \sqrt{P_i} / (\sqrt{\sigma_{x_i}^2 + \sigma_{y_i}^2} + 1)$ has low value for elongated feature and large values for squared objects. $\sqrt{P_i}$ is the diameter of a square object made up of P_i pixels, and $\sigma_{x_i}^2$ and $\sigma_{y_i}^2$ are the variances. The interactive manual setting of the threshold $[T_{min}, T_{max}]$ allows one to find the proper parameters for extracting only local damages.



Fig. 8 The area around the church of Santa Maria Paganica: (a, c) Pre- and (b, d) post-event images. The comparison of classification shapefiles provide several errors shown in red colour (e), which are automatically filtered out with the removal of elongated features showing only shadows that indicated the damage, shown in yellow colour (f)

An example of a damaged building examined by this method is the church of Santa Maria Paganica. Figure 8 shows the building and the neighbourhood area before (a, c) and after (b, d) the earthquake. The comparison of classification shapefiles provides several errors (e), which are automatically filtered out with the removal of elongated features, showing only those shadows that with the highest probability indicate the damage caused by the earthquake (f).

Discussion of Work

The proposed solution is based on different steps, in which several parameters have to be set, firstly considering the two images separately and then as a couple. The whole workflow can be easily automated as it is made up of consequential steps. Most operations do not require a significant computation cost, apart from the multiresolution

segmentation which could become quite slow for big images. The method proposed is to be considered as an advanced visualisation technique rather than a method to compute the number of damaged buildings. Hence, the threshold can be interactively modified by the user to enhance the visualisation of the damaged building. Indeed, it is not simple to define a priori all the thresholds in the different steps of the workflow, especially in case of replication of the methodology in other areas. At the moment, the method has been tuned for the specific case for the town of L'Aquila.

The logic behind the whole procedure is similar to the grading maps provided by Copernicus EMS rapid mapping products. For example, in the case of another disastrous earthquake event which occurred in Amatrice (Italy) in 2016, the service has provided “grading maps” – thematic maps derived from post-event images that provide an assessment of the damage grade. Such maps include the extent, magnitude or damage grades specific to each disaster type. In case of earthquakes, the grading map can be shown taking into account the number of destroyed damaged buildings in each cell of a regular grid.

In fact, the method proposed has also a strong connection with the logic of the geographic information systems (GIS) and spatial data infrastructures (SDI) in general. It provides vector shapefile layers as output, which can be further inspected and handled in GIS software, also in combination with other types of geospatial open data such as roads or other infrastructures for accessibility and danger verification. For example, an integration with the open-source QGIS platform can be performed (Fig. 9). The results can be further manipulated in an GIS software to enhance the visibility of damaged buildings.

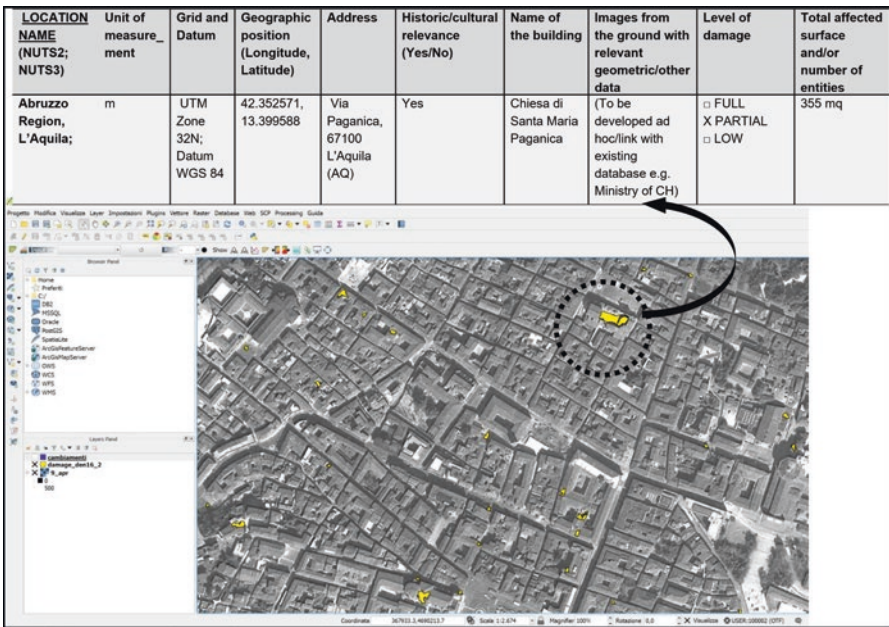


Fig. 9 The results of change detection with variable off-nadir angle very high-resolution imagery can be exported, manipulated and visualised in GIS software: L'Aquila case study

Figure 9 (below) shows the case in which only the feature with an elongation in a predefined range using the attribute table associated to the shapefile. As explained, the results here illustrated do not take into account fully destroyed buildings but rather those which have undergone partial damage. The table of Fig. 9 linked to the polygon of the undergone damage contains important information about the building itself such as geographic position (cartographic coordinates), projection and datum of the map, building address, name of the building (if any), historic/cultural relevance as “yes/no” (information provided by the regional public authority geoportal), images of the building from the ground with relevant geometric/other data (to be developed “ad hoc”), level of damage of the building (qualitative assessment in terms of low/partial/high level of damage) and total affected surface and/or number of entities damaged.

Conclusion

Since 2016 an official document issued by MiBACT (Italian Ministry of Cultural Heritage and Activities and of Tourism) has put into place a “Procedure of the Implementing Officer of 21 September 2016: management of activities on the securing of movable and immovable cultural heritage” (ordinanza n. 393 del 13 settembre 2016), nominating a body “Funzione Beni Culturali” as a responsible party with a one member of MiBACT and one member of civil protection as main representatives. Such initiative declares a great public commitment, and attention is currently on heritage affected by extreme earthquake events and sets the ground for a larger framework of intervention on built cultural heritage in a period of postcrisis such as in the case of L’Aquila here presented. This chapter illustrates how a methodology relying in photogrammetric and visualisation investigation techniques applied on high- and very high-resolution EO satellite data can contribute to the mapping of the damaged buildings in case of earthquake, providing both qualitative and quantitative information of a specific building, district or even entire complex (e.g. a historic centre of the city). The method could hence support the action of identification and quantification of such buildings and affected areas, both for processing of grading maps (in case of rapid mapping) and thematic mapping for risk and recovery purposes at the later stages of emergency management cycle.

Acknowledgement The authors would like to thank the DigitalGlobe Foundation (www.digitalglobe.com) for providing the Quickbird images used in this work.

References

- Alexakis DD, Gryllakis E, Koutroulis A, Agapiou A, Themistocleous K, Tsanis I, Michaelides S, Pashiardis S, Demetriou C, Aristeidou K, Retalis A, Tymvios F, Hadjimitsis DG (2014) GIS and Remote Sensing Techniques for the Assessment of Land Use Changes Impact on Flood

- Hydrology: the Case Study of Yialias Basin in Cyprus, *Natural Hazards and Earth System Sciences* 14:413–426
- Antonini O (2010) *I terremoti aquilani*, Tau Editrice, 48 pages
- Belward AS, Skøien JO (2015) Who launched what, when and why; trends in global land-cover observation capacity from civilian earth observation satellites. *ISPRS J Photogramm Remote Sens* 103:115–128
- Blaschke T (2010) Object based image analysis for remote sensing. *ISPRS J Photogramm Remote Sens* 65:2–16
- “Copernicus Emergency Management Service.” Directorate Space, Security and Migration, European Commission Joint Research Centre (EC JRC). Accessed 2 Aug 2018. <http://emergency.copernicus.eu/>
- Cova TJ (1999) GIS in emergency management. *Geogra Inf Syst* 2:845–858
- Chesnel AL, Binet R, Wald L (2007) Quantitative assessment of building damage in urban area using very high resolution images. In: 2007 urban remote sensing joint event. IEEE, pp 1–5
- DigitalGlobe (2013) Geolocation accuracy of worldview products
- Dong L, Shan J (2013) A comprehensive review of earthquake-induced building damage detection with remote sensing techniques. *ISPRS J Photogramm Remote Sens* 84:85–99
- Fraser CS, Hanley HB (2003) Bias compensation in rational functions for Ikonos satellite imagery. *Photogramm Eng Remote Sens* 69(1):53–57
- Gazzetta Ufficiale n. 105, 8 May 2003, Supplemento Ordinario n. 72, Ordinanza del Presidente del Consiglio dei Ministri n.3274, March 20th, 2003 “Primi elementi in materia di criteri generali per la classificazione sismica del territorio nazionale e di normative tecniche per le costruzioni in zona sismica”
- Hanley HB, Yamakawa T, Fraser CS (2002) Sensor orientation for high-resolution satellite imagery. *Int Arch Photogramm Remote Sens* 34(1):69–75. (on CD-ROM)
- Pacifici F, Chini M, Bignami C, Stramondo S, Emery WJ (2010) Automatic damage detection using pulse-coupled neural networks for the 2009 Italian earthquake,” *International Geoscience and Remote Sensing Symposium 2010*, Honolulu, USA, July 25–30
- Rezaeian M (2010) Assessment of earthquake damages by image-based techniques, Diss.. ETH Zurich N. 19178, 149 pages
- Stovel H (1998) Risk preparedness: A management manual for World Cultural Heritage, Rome: ICCROM, 153 pages
- Yamazaki F, Yano Y, Matsuoka M (2005) Damage detection in earthquake disasters using high-resolution satellite images. *ICOSSAR 2005*:1693–1700

Remote Sensing Roman and Byzantine Eastern Frontier Zone in Landscape: Case Studies from Syria and Turkey



Minna Silver, Kenneth Silver, Markus Törmä, Milton Nuñez, Jari Okkonen, and Tuula Okkonen

Abstract The Euphrates and the Tigris valleys in greater Mesopotamia provide a treasure trove for archaeologists studying the Roman and Byzantine eras. There existed some parts of the eastern frontier zone of the Roman and Byzantine empires, remains of which are in modern Syria and Turkey. This was also the stage where some of the first steps in archaeological remote sensing were taken in aerial archaeology in the Near East in the beginning of the twentieth century. It also became an arena in which the Finnish project SYGIS and the Finnish-Swedish Archaeological Project in Mesopotamia (FSAPM) applied satellite imagery, cartographic data, historical sources and Geographic Information Systems (GIS) in archaeological prospecting, surveying and mapping. Declassified CORONA satellite photographs from the 1960s were used in prospecting and environmental studies. Landsat-7 ETM, QuickBird and GeoEye images were also purchased. The spatial resolution of the images provided means to trace Roman sites and roads. SPOT images were acquired as well, and they revealed settlements and agricultural fields in the neighbourhood of the Euphrates valley. Landscape models were produced fusing satellite imagery with DEM (digital elevation model) data, either from the SRTM mission or ASTER imagery to visualize and study the contexts in different types of environments and landscapes. Contrasts appeared between dry mountainous areas and flat irrigated agricultural areas in the river valley of Syria to hilly agricultural areas in mainly rain-fed eastern Turkey. In a multiperiod survey in Syria concentrating on nomadic and settled cultures, it was realized that the area comprised plenty of Roman and Byzantine remains that we integrated into the survey and studied in the context of the region. This Roman Limes area provided sites that reflected the network and military strategy. Visibility and viewshed analyses were able to be carried out with DEM data from X-SAR shuttle mission and ASTER-DEM data. They provided

M. Silver (✉) · M. Nuñez · J. Okkonen · T. Okkonen
University of Oulu, Oulu, Finland
email: minna.silver@helsinki.fi

K. Silver
Independent researcher, Oulu, Finland

M. Törmä
Aalto University, Espoo, Finland

© Springer Nature Switzerland AG 2020
D. G. Hadjimitsis et al. (eds.), *Remote Sensing for Archaeology and Cultural Landscapes*, Springer Remote Sensing/Photogrammetry,
https://doi.org/10.1007/978-3-030-10979-0_10

military aspects for defending the eastern frontier zone. In Turkey the landscape modelling provided means to understand the hilly and fertile landscape and positions of fortified Roman/Byzantine towns on hills in the Parthian/Persian frontier.

Keywords Archaeology · Roman · Byzantine · Remote sensing · Aerial photographs · Satellite imagery · Prospecting · Surveying · CORONA · X-SAR mission · SRTM · Landsat · SPOT · QuickBird · GeoEye · ASTER-DEM

Introduction

The Near East was a stage where some of the first steps in aerial archaeology were taken, especially in the area of the Roman eastern frontier zone. The Euphrates and the Tigris valleys proved to be treasure troves for archaeologists studying Roman and Byzantine remains in the Near East. There in modern Syria and Turkey, in ancient greater Mesopotamia, once existed parts of the eastern frontier zone of the Roman and Byzantine empires. Here in this article we do not deal with other parts of the frontier zone that continued from Syria to modern Israel and Jordan as far as Arabia but concentrate on areas that have been studied by Finnish and Finnish-Swedish projects in central Syria and eastern Turkey.

The natural frontiers between the west and east, including the twin rivers, mountains, agricultural areas and deserts, became cultural boundaries between the classical and oriental worlds. Beside the enemies in Parthia/Persia, natural features in environment and nomads living in the area clearly had been driving forces in creating the boundaries and frontiers. According to one theory, the pressure of nomads to the Roman Empire was one of the reasons for fortifying the frontier area, especially the so-called Outer Limes that protected the empire from desert forces. But more major enemies lurked in the mountainous areas of Parthia/Persia in the east. The Silk Road formed a vein connecting these worlds to each other. Also various other roads were laid in the desert for military reasons and trade purposes. The roads such as the *Via Nova Traiana* and the *Strata Diocletiana* became expressions of Roman border politics connecting military installations (Lönnqvist et al. 2011).

This article concentrates on two projects the Finnish project SYGIS (the Syrian GIS) for surveying and mapping Jebel Bishri in Central Syria and the Finnish-Swedish Archaeological Project in Mesopotamia (FSAPM) in modern Turkey. The present authors have carried out these projects applying satellite photographs/imagery, cartographic data and historical sources as well as field surveying including ground-penetrating radar (GPR) in tracing, recording and documenting sites in the Eastern Frontier of the Roman and Byzantine empires. The project in Syria took place in the mountainous region of Jebel Bishri in the Palmyrides (Fig. 1), located between the Euphrates river and the Syrian Desert, in 1999/2000–2010. Although the primary goal of the SYGIS project was to study the relationship of pastoral nomads and village people in the area from the survey data through the ages, the regional approach of the survey took into account all the periods and revealed the



Fig. 1 The project areas in the mountainous regions of Jebel Bishri and Tūr Abdin in Mesopotamia

unexpected amounts of Roman sites (see Lönnqvist et al. 2006). The second project was started in 2014 in the mountainous area of Tūr Abdin in the Tigris valley in eastern Turkey (Fig. 1). Both areas in Syria and Turkey belong to the greater area of Mesopotamia in the valleys of the Euphrates and the Tigris.

The preliminary reports of the Finnish project SYGIS have appeared in the journal *KASKAL* (Vol. 3, 2006, and Vol. 6, 2009), and the first volume of the final publication *Jebel Bishri in Context: Introduction to the Archaeological Studies and the Neighbourhood of Jebel Bishri in Central Syria* (Lönnqvist 2008) came out following several other publications after 2010. The larger last volume of the final publication of SYGIS is *Jebel Bishri in Focus: Remote sensing, archaeological surveying, mapping and GIS studies of Jebel Bishri in central Syria by the Finnish project SYGIS* appeared in 2011 (Lönnqvist et al. 2011). A preliminary report of the Finnish-Swedish FSAPM project in Turkey is concentrating on remote sensing and documentation by photographing and was published in *ISPRS Annals* (Silver et al. 2017).

What is important is to note that the area where the Finnish project SYGIS in Syria worked became the central scene of the administration of ISIS/ISIL, Raqqa beneath Jebel Bishri as its capital in 2013–2017, and heavy looting of archaeological sites including those of the Finnish project was to follow. Already in the first year of the Syrian civil war, the Syrian General Directory of Antiquities and Museums reported damage to the Roman/Byzantine fort of Tabūs that the Finns had earlier documented. Satellite imagery, such as UNOSAT, has been the source of data to follow the destruction and looting of sites without access during the occupation of ISIS.

In Turkey the areas where the Finnish-Swedish project FSAPM worked the threats for archaeological remains were different. The Tigris dam projects, agricultural works and heavy building endeavours endanger sites and their future. Therefore documentation of sites was urgent. In both cases, in Syria and Turkey, the coordinate information has been essential to locate and map sites, also for their further monitoring and visits. UTM coordinates have been used in both cases either based on satellite imagery, maps or capturing GPS points on the ground. The coordinate information is essential for identification of archaeological sites and protecting them.

First Steps in Remote Sensing: From Air to Space in the Near East

Such pioneers as L.W.B. Rees (1929), Antoine Poidebard (1934) and Sir Aurel Stein (Gregory and Kennedy 1985) started aerial studies in Syria (Fig. 2), Iraq and Jordan after the First World War. In the use of historical photograph archives, also German aerial photographs from the First World War have proved to be useful in archaeological remote sensing studies in the Near East later on (Bewley and Kennedy 2013). Poidebard and Aurel Stein concentrated in their studies on the Roman Eastern Frontier zone, or the so-called Eastern Limes, tracing fortresses, forts, military posts and roads. They mapped sites but did not check and verify in all the cases the nature of sites and roads on the ground.

Balloons and kites were mounted with cameras in the nineteenth century before the invention of aeroplanes, and also Aurel Stein already used balloons for aerial photographing of archaeological sites in the beginning of the twentieth century. The benefits of the bird's eye view were gradually recognized in detecting ancient remains. The capture of the sight from the air opened a new approach for reconnais-

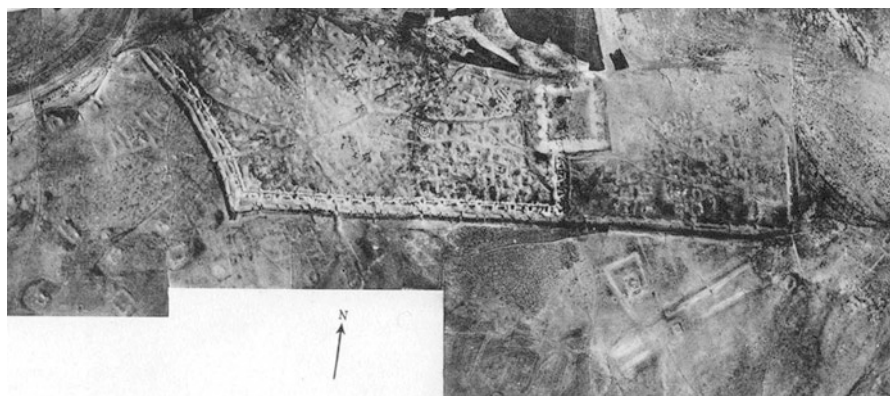


Fig. 2 The Roman site of Sura on the Euphrates in Syria photographed by A. Poidebard (1934) from air

sance. The optimal conditions revealed features that were not visible on the ground level, especially using certain light conditions of a day and changes in vegetation cover during various seasons. The so-called crop marks also have become indicators of ancient sites and monuments that can be identified from the air and space. The scale of the approach also provided a new view to the environmental and landscape contexts. Landscapes and signs of human traces were detected from various heights and angles. After R. Mouterde's and A. Poidebard's (1945) work in Syria, aerial photographs were especially used by archaeologists in Jordan, and David Kennedy (see, e.g. Kennedy 1982; Kennedy and Bewley 2004) became a major promulgator of their use in archaeology in his studies of the Roman frontier zone in Jordan.

After aerial photographing, new technologies to find archaeological sites using remote sensing from space and under the ground have revolutionized the archaeological prospection in recent decades. Aerial photographs were followed by satellite imagery, and space archaeology became a field of double meanings: either meaning remote sensing archaeological sites from various platforms from space or studying space junk that has landed on earth. Remote sensing by aerial photography and satellite imagery has benefited from ideal cloudless conditions to which the Near East with desert and steppe regions and length of sunny seasons has been useful for visibility.

Satellite imagery had been used in archaeological prospecting already in the 1970s (see Lönnqvist and Stefanakis 2009, 1230). But the satellite imagery and radar data for archaeological prospecting in the Near East were especially applied by NASA's Jet Propulsion Laboratories in California in the 1980s. It resulted in such claimed discoveries as Ubar, a lost city in Oman in Southern Arabia mentioned in the tales of the Arabian Nights, the Bible and the Koran. The site had been covered by desert sands through time. The city was on the caravan trail for transporting frankincenses made of aromatic resins but had remained unrecovered for centuries (Evans et al. 1994; Space Today Online 2006).

Global positioning system (GPS), total stations and Geographic Information Systems (GIS) had brought additional ways to capture site data combining location information from satellites to the ground and spatially analysing the information (Lönnqvist and Stefanakis 2009). Like capturing radar data SAR (synthetic aperture radar) has provided means to have digital elevation model (DEM) data in tiles. Laser scanners like LiDAR (light detection and ranging) have brought even more ways to trace sites that are covered by vegetation. Digitalization revolutionized the field. The digital image has offered new ways to analyse and model information (see Harrower and Comer 2013).

The Data Sources of SYGIS, the Finnish Project in Syria and the Finnish-Swedish FSAPM Project in Turkey

The Finnish archaeological surveying and mapping project SYGIS was established to study Jebel Bishri in central Syria in 1999/2000. The project applied satellite imagery and Geographic Information Systems (GIS) in prospecting and mapping

archaeological sites. In 1999 the project was accepted to NASA's world monitoring program through the German Aerospace Center. Due to this program, the project was able to get the X-band DEM of NASA's Shuttle Radar Shuttle Topography Mission which was to serve as a basis for the future landscape modelling of Jebel Bishri and the Euphrates valley (Lönnqvist et al. 2011).

SYGIS first acquired both Landsat-7 ETM satellite image data and black and white declassified CORONA satellite photographs to be used as data sources for prospecting, surveying and mapping archaeological sites in the Jebel Bishri region (Lönnqvist and Törmä 2003). Landsat images were especially useful in studying environment and landscapes in colour making a spatial contrast between the river valley, oases and the desert-steppe environment. Cluster analysis, for example, revealed various environmental features invisible with a naked eye from the tessellated images before clustering. Also Landsat images from various years, taken in various seasons, provided means for environmental analysis over years and in specific seasonal circumstances. The orthorectified panchromatic channel of Landsat-7 with 15 m resolution was used for field mapping with MapSheets Express software. Ground survey took equally place in 15 m interval field walking (Lönnqvist et al. 2011) (Fig. 3).

David Kennedy (1998) had used CORONA declassified satellite photographs to study archaeological sites in Turkey in the 1990s. These CIA photographs on film dated back to the 1960s, and the spatial resolution of them reached up to 1.8 metre that was better than other satellite imagery that had been available in civil markets

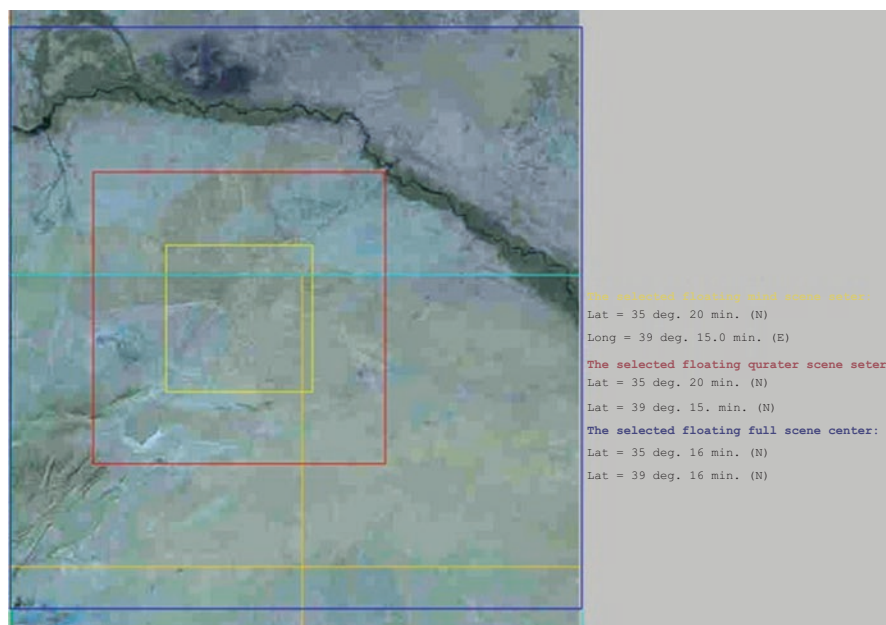


Fig. 3 Landsat-7 satellite image zooming in over Jebel Bishri

before. The benefits have been in their low price, the high spatial resolution and date in detecting sites and features in the landscape before some constructions and changes in the environment had taken place. The use of CORONA photographs opened a new view to study the evolution of landscapes and sites through decades beginning from the 1960s. The application of CORONA by Jason Ur (2003) in Turkey was published in the same year as the first reports of the Finnish project using the respective photographs in Syria came out (Lönnqvist and Törmä 2003).

The cartographic data that the SYGIS project utilized consisted of UK aerial military maps and Russian topographic maps. The Syrian officials refused to provide local military maps of detailed information and offered only tourist maps to be used. A. Poidebard's and R. Mousterde's aerial photographs and maps as well as Alois Musil's (1927, 1928) itineraries were valuable sources of information. Ancient cartographic data and site names from the Roman and Byzantine times, such as available in Ptolemy's Geography, *Notitia Dignitatum* and *Tabula Peutingeriana* were needed as the source of reference and identification for ancient sites. Interviews with local Bedouins were valuable source of information of sites as well. The Bedouins were used as informants prior and during the field campaigns.

The Syrians published *Space Image Atlas: Syria* and *Syria, Archaeology from Space* just in the turn of the new millennium and before the first publications by the Finnish project SYGIS came out in 2003. The atlases were published by the General Organisation of Remote Sensing (GORS) in Damascus which in 2004 also organized a conference on remote sensing and development in which SYGIS was invited to give a presentation on archaeology, remote sensing and cultural heritage. Beside various subjects in the field of developing studies, some colleagues from Britain and Iraq also dealt with archaeology.

Furthermore in 2003 the Finnish project purchased QuickBird satellite imagery with high spatial resolution of 0.60 m, and later SPOT images were acquired. No Google Earth was available yet at that time. Google created the program in 2005, and it soon became common as an open source for prospecting archaeological sites. However, still in the mid of the first decade of the twenty-first century, its coverage and spatial resolution were not sufficient for the Finnish project. On the other hand, it needs to be mentioned that the applicability of Google Earth for various analyses is limited, and therefore it does not allow all the photogrammetric and analytical benefits needed in GIS, compared to the use of tessellated satellite imagery. After the end of the Finnish project in 2010, the Google Earth 3D became already available (Lönnqvist et al. 2012).

The Finnish-Swedish project in eastern Turkey in Mesopotamia has used comparable data sources to those of SYGIS. The leaders of the project in Turkey were largely the same as in SYGIS. Now the Google Earth was applied for preliminary studies, and CORONA photographs were acquired for environmental studies and landscape prospection. Local administrators helped to locate some Roman sites that were known but that still lacked proper documentation and study. The sites that we documented in Turkey laid outside Poidebard's maps of the eastern frontier zone, and no reconnaissance had been published of them and their location before. As availability of QuickBird had ceased, we ordered GeoEye-1 satellite image with

even higher spatial resolution of 0.46 m covering an area that we had visited and chosen for closer studies (Silver et al. 2017).

Landscapes as Contexts: Spatial Boundaries and River Channel Changes

To understand cultures and their development, one needs to study their environmental and landscape contexts. Jebel Bishri belongs not only to the desert-steppe areas but also to the mountain chain of the Palmyrides in Syria. That part of the Palmyrides is geologically named as the “Bishri block”. Brew et al. (2003) have produced a map providing a digital elevation model that visualizes the geological nature of the block, the Euphrates trough and the Jezira plains reaching the Mardin highs of Tūr Abdin in eastern Turkey.

The Finnish project SYGIS utilized satellite imagery in studying the spatial differences in the nature between the desert, the mountain and the sown between the Syrian Desert and the Euphrates. Landsat images clearly provided the visual data of the contrast between the brown desert and desert-steppe compared to the irrigated and agricultural green river valley and desert oases (Lönnqvist and Törmä 2004). Water is the source of human activities, cultures and civilizations, and in desert areas especially oases have attracted people from early times. Indeed the El Kowm oasis on the western piedmont of Jebel Bishri is providing evidence of long-term human impact (Lönnqvist et al. 2011). But also the Euphrates with its fans has provided an early stage for agriculture (Moore et al. 2000).

We were able to study the changes in the Euphrates valley landscape, especially extracting visible information of the old channels with CORONA satellite photographs and also analysing the changes in Landsat images (Fig. 4). The river channels had changed their courses by time. More recent changes were able to be studied and analysed with Landsat images. It was clear that some of the ancient sites had become buried in silt along the channel changes through millennia, and some that had been at the river bank as harbours had become remote in their location to the river (Lönnqvist et al. 2007).

It was also the interest of the Finnish-Swedish project FSAPM to understand Roman and Byzantine sites in the undulating landscape of the Tigris valley. The annual precipitation in the higher altitudes of Tūr Abdin area in the Tigris valley is considerably higher than in the Euphrates valley in Syria. Vine is flourishing in the neighbourhood, and Ömerli is still famous for its vines and grape production (Silver et al. 2017). Landscape models were produced fusing GeoEye satellite imagery with Aster-DEM data. These provided views for using natural hills as bases for fortified sites (Silver et al. 2017).

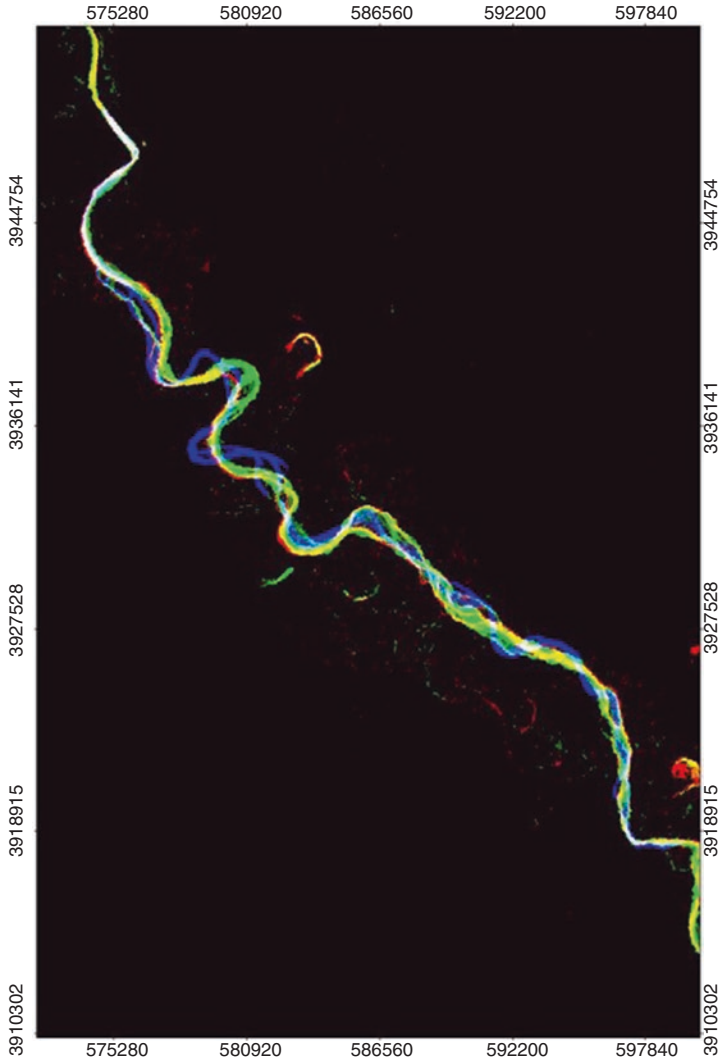


Fig. 4 The analyses of the Euphrates river channel changes over decades CORONA and Landsat images

Studying Roman and Byzantine Sites with Satellite Imagery

Before the Finnish project Jebel Bishri had largely remained an empty spot in the maps and atlases of the Roman empire. CORONA photographs and Landsat images appeared to be valuable data sources in general prospection and mapping. Sites were explored at the edges of the mountain and inner regions. In the eastern piedmont, Poidebard's aerial photographs and maps led to study the surrounding oases

on the ground in 2000. They were visited, and Roman activities were confirmed at Shukhna and Taibe (Lönnqvist et al. 2011).

Not far from Taibe the surroundings of the Umayyad castle known as Qasr al-Hayr ash-Sharqi were studied. It appeared that the site had been already occupied during the Roman times and offered quarries as well as tombs in the neighbourhood dating from the Late Roman and Byzantine times. The tombs were documented and associated pottery recorded for the dating purposes. The existence of Bedouin tent camps in the eastern piedmont appeared in Poidebard's aerial photographs from the 1920s and 1930s, and CORONA photographs revealed the earlier environmental conditions of the neighbourhood with orchards. At Darakhlia, in the central areas of the mountain, a large Roman water harvesting site with a barrage or a dam and a stepped pool associated with a watchtower was traced with the local informants and documented in 2000–2004 (Lönnqvist et al. 2011).

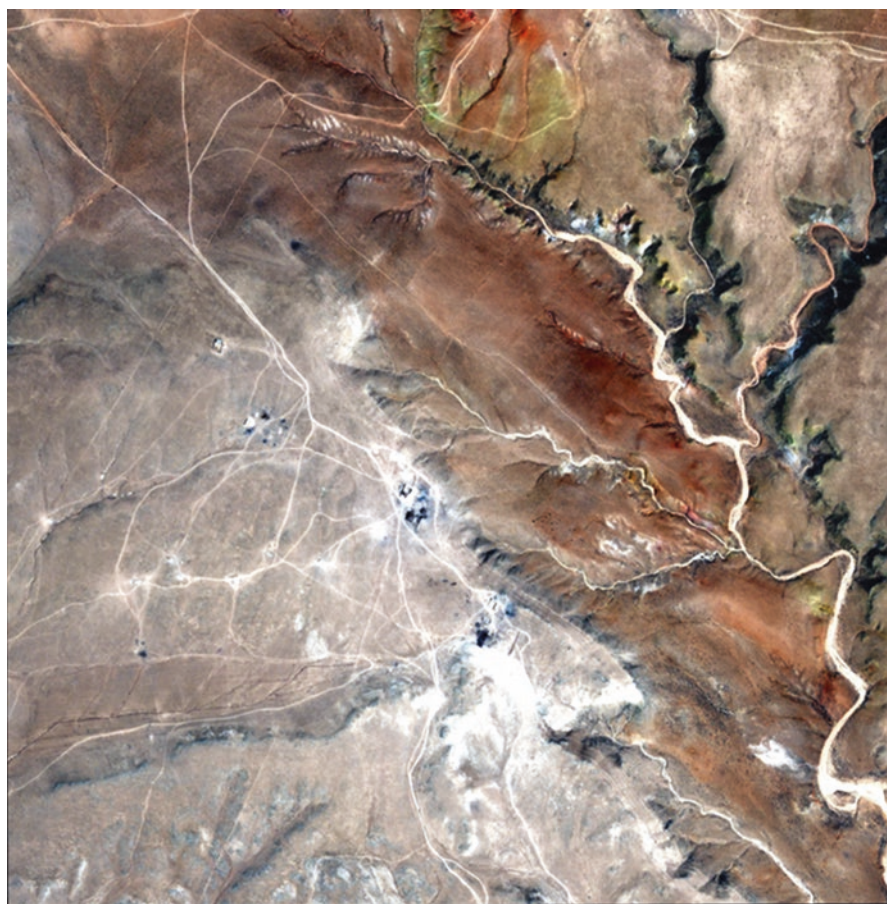


Fig. 5 A Roman military camp on Jebel Bishri identified on a QuickBird image



Fig. 6 A Roman camp originally identified on a QuickBird image and studied on the ground on Jebel Bishri. Note the Via principalis running through it. (Photo: Kenneth Lönnqvist 2005)

Beside informants consisting of local Bedouins, the purchase of QuickBird imagery in 2003 covering parts of the central areas of the mountain proper of Jebel Bishri provided 0.6 m spatial resolution in panchromatic channel. The resolution was able to reveal very interesting sites that had not been able to be seen on the ground before. In the images, we found a temporary Roman military camp of a play card shape (Figs. 5 and 6), near the barrage that led to concentrated searches in the area in question. Furthermore a Roman military posts and dwelling sites in the central areas of the mountain were visited on the ground and mapped with Landsat imagery. It became clear that there had been a special corridor for military supply for the Roman troops, possible including Palmyrenes, through Jebel Bishri towards the Euphrates. We have called this “Bishri corridor” that fills some gap on cartographic sources and in our knowledge of Roman presence between Palmyra and the Euphrates. The Euphrates forms a border area, called the Euphrates Limes that had been also temporarily under Palmyra while it was a client kingdom under Rome (Lönnqvist et al. 2011).

There on the Euphrates border, CORONA photographs and Landsat images appeared to be useful in mapping forts and fortresses (Figs. 7 and 11). A military post with Roman houses was mapped in Qseybe in central northeastern parts of Jebel Bishri. It needs to be emphasized that besides remote sensing, experimental studies on the ground are essential in identifying sites and their nature. Misinterpretation can take

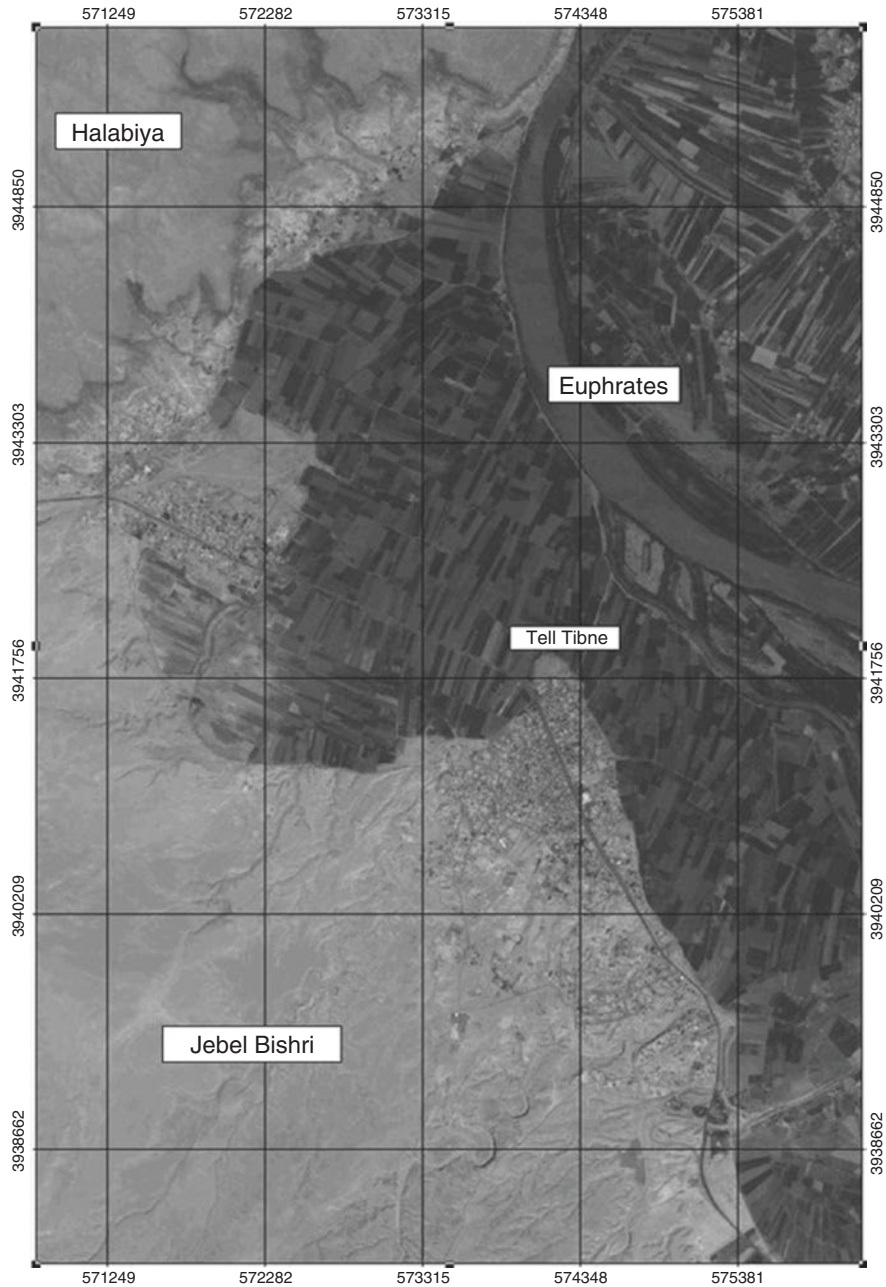


Fig. 7 Tell Tibne, possible Roman site of Mambri, visible at the edge of the Euphrates valley and mapped on Landsat-7 image with ERDAS MapSheets Express software. (Mapping Minna Lönnqvist)

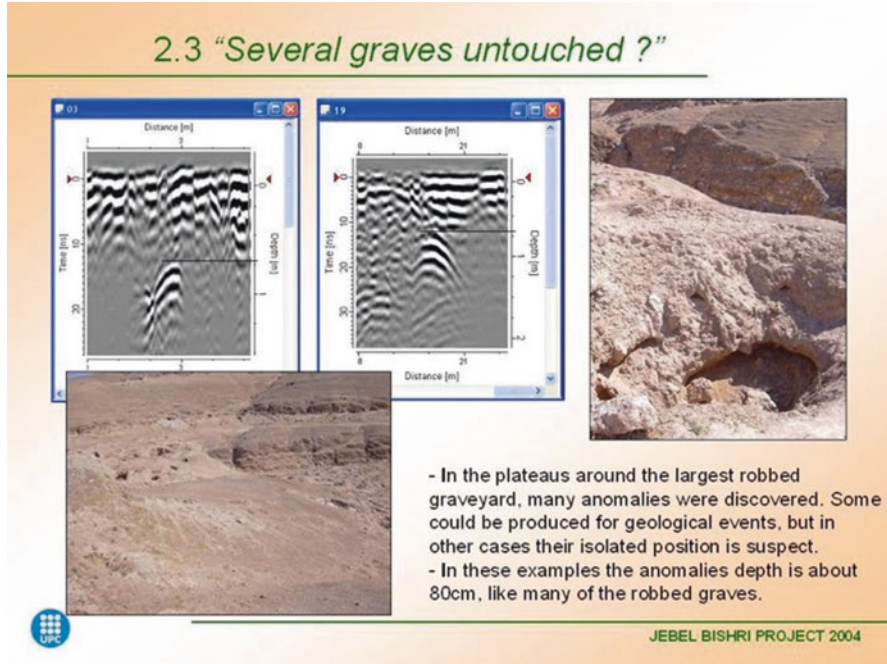


Fig. 8 Prospecting eventual graveyards near the Roman fort of Tabūs with ground-penetrating radar (GPR). (Prospection by Josep Pedrez Rodes)

place without studies on the ground and collection of surface finds. In all the cases of the forts and fortresses, military posts and camps, we collected Roman pottery and glass for the site identification and reference for the dating (Lönnqvist et al. 2011).

The Late Roman/Byzantine fort of Tell Tabūs that had been earlier studied by Friedrich Sarre and Ernst Herzfeld (1911, 1920) was documented by SYGIS with satellite mapping and on the ground by tacheometry in 2004. The nearby cemetery was also documented by drawing and remote sensing by using ground-penetrating radar (GPR) (Fig. 8). It appeared that there were still unidentified underground tombs with galleries. A number of tombs had been looted resulting in a moon-like landscape. Tell Tibne (Fig. 7) near Halabiya and the fortress of Zenobia that dates from the Byzantine era was also mapped with satellite imagery and documented with a tacheometry. The DEM model of the site was created from tacheometry measurements on the ground, and a special map showing the visible structures on the surface was produced. The stamped pottery indicated Parthian influence as well as Late Roman and Byzantine occupation of the site. It is possible that the site can be identified as Mambri, the fortress site built by Diocletian (Lönnqvist et al. 2011).

Also ground-penetrating radar (GPR) was used as a remote sensing device during the Finnish project on the Euphrates side in 2004. Important remote sensing studies with geophysical methods on the ground had earlier been carried out by Andreas Schmidt-Colinet in the Palmyra district. These studies led to the discovery

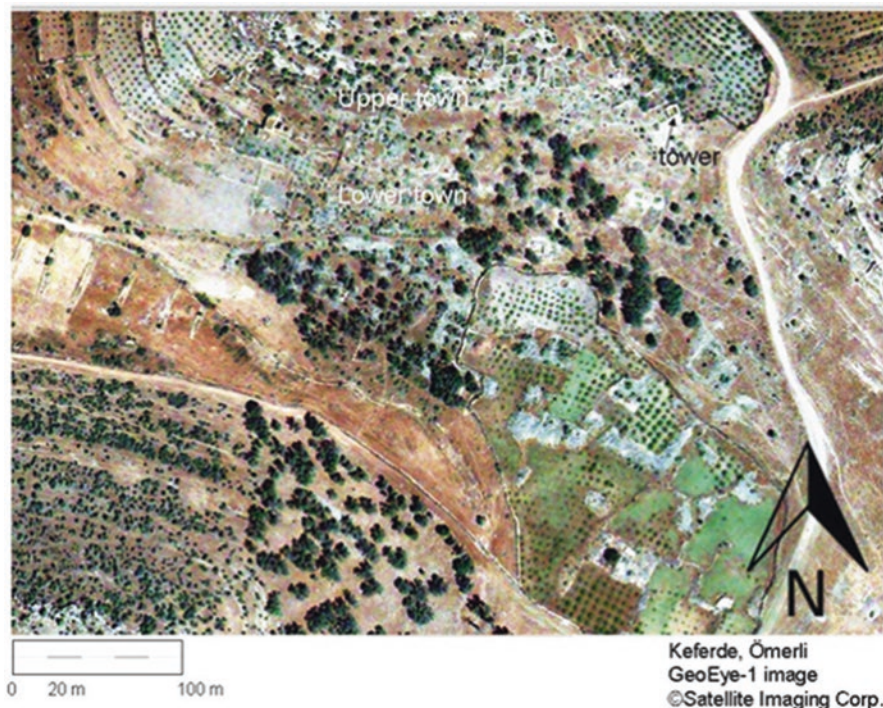


Fig. 9 Visualizing the Roman/Byzantine site of Keferde in Turkey with a GeoEye satellite image. (Mapping Minna Silver 2017)

of the subsurface ruins of Hellenistic Palmyra (see Schmidt-Colinet et al. 2016). The studies were indicated in the new archaeological atlas published by GORS. While the Finnish project was working in the desert, German team with Syrians also used geophysical means to study a Roman fortress of Qreiye in the village of Ayyash, near Deir ez-Zor on the Euphrates (Gschwind and Hasan 2008).

GeoEye satellite imagery appeared to be very useful for identifying Roman and Byzantine structures of a town of the so-called oppidum type and named Keferde in the Tūr Abdin mountains of eastern Turkey. The upper and lower towns were identified, and structures were photographed including a large polygonal tower (see Fig. 9). Pottery from the Late Roman and especially Byzantine era was identified on the surface for dating purposes. A possible wine pressing area and cultic caves with tombs were observed. Further to the northeast, a larger fortified town was found at Besikkaya and tentatively identified as Beioubaiitha. The fortification systems at both sites, especially in the last one, were imposing. At Besikkaya a massive tower governed the site, and curtain walls ran along the slopes. Inside the walls, there were houses that belonged to a present-day village. Remains of a church of a basilica type were encountered as a reused barn. There fine *sigillata* pottery dating from the Roman era was found (Silver et al. 2017).

Fig. 10 Measuring and mapping the Roman/ Byzantine fort of Tabūs on Jebel Bishri with a tacheometre and a prism. (Photo: Eivind Seland 2004)



Networks of Ancient Roads in Syria

Already Poidebard (1934) had documented Roman roads from the air in the Syrian Desert. We were also able to delineate such with satellite photographs and imagery associated with ground identification. Photogrammetric and spatial studies have been earlier carried out by Finns in studying ancient roads from the Roman period in Petra in Jordan (Haggrén et al. 2002, 2005), and others at the same time in various areas in the Near East (Gates 2006) (Figs. 11 and 12).

The location of the Roman/Byzantine fort of Tabūs on Jebel Bishri above the Euphrates in association of an ancient road was detected. The road was clearly aligned so that it could have been observed from the tower of the fort (Fig. 10). The Roman origin of this paved road was observed not only in its alignment but also in its structure and based on associated pottery. Quarrying for pavement stones was convenient beside the mountain. Also the local officials were on the opinion that the road that could be observed from the tower of the fort of Tabūs was of Roman origin, at least in its alignment. That road was also documented with a tacheometre, GPS waypoints and hand drawing, and its structure was studied by remote sensing methods with a ground-penetrating radar (GPR). The GPS waypoints were also laid on a Landsat-7 image to create a map (Fig. 11). Another ancient road cut through the mountain slope beneath Tabūs was also detected on the ground and on a Landsat-7 image (Lönnqvist et al. 2005b, 2011; Silver et al. 2015b).

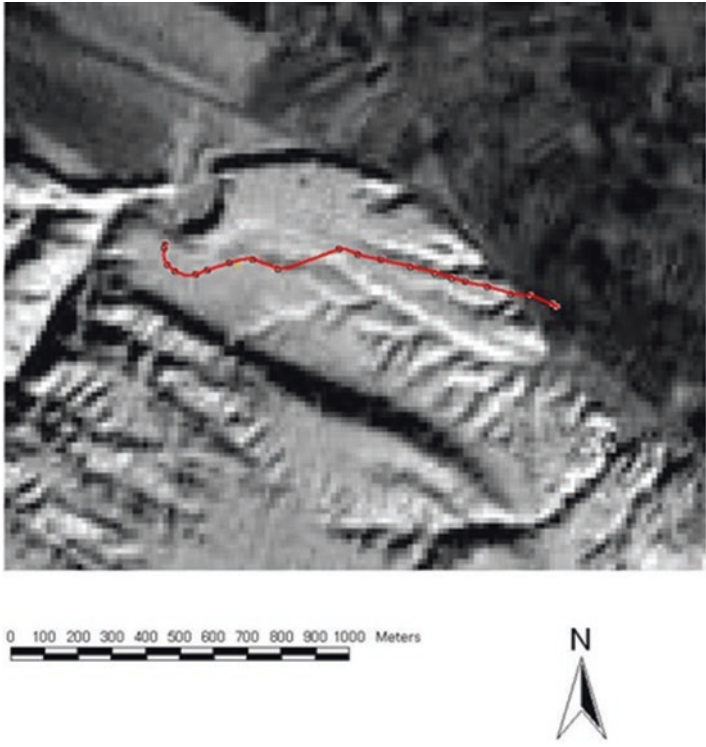


Fig. 11 Ancient road mapped with GPR waypoints on Landsat-7 satellite image. (Mapping by Jari Okkonen 2004)

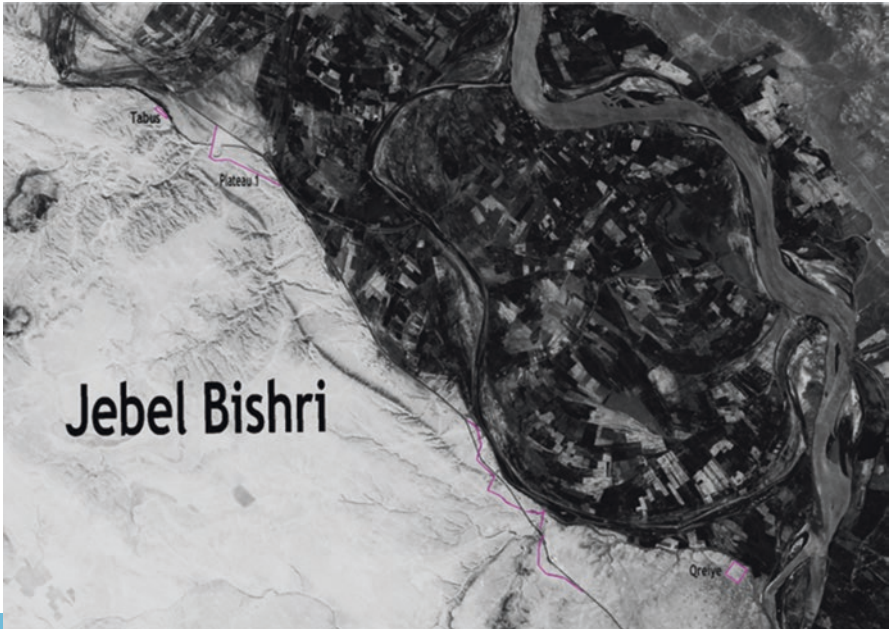


Fig. 12 Finding the continuation of the Roman road alignments on CORONA satellite photograph between the Roman sites of Tabus and Qreiyeh at the edge of Jebel Bishri on the Euphrates in 2005

The continuation of the road from Tabūs along the Euphrates to the fort of Qreiye was detected near the area of the village of Ayyash with the help CORONA satellite photographs (Fig. 12), and the studies to verify the road alignment were continued on the ground in 2005. It was clear that the CORONA photographs from the 1960s were able to reveal the road that had since been affected by agriculture, traffic and new road constructions (Lönnqvist et al. 2011; Silver et al. 2015b). Hollow ways had been earlier studied by Jason Ur (2003) with CORONA. In our case it was clear that the sound stony terrace that belonged to the piedmont of Jebel Bishri had been used for a road in the area that was vulnerable for flooding. The stretches of this paved road connected Roman sites in the Euphrates frontier, and there also were ancient and more recent bridge points. The vital way to verify the findings was to study the remains of the detected stretches on the ground (Lönnqvist et al. 2011).

Roman dirt roads were further identified on the mountain, especially one crossing a camp like a straight *via principalis* visible on our QuickBird satellite imagery and studied on the ground (Lönnqvist et al. 2009, 2011; Silver et al. 2015b).

Landscape Modelling, Visibility and Viewshed Analyses

Landscape studies using satellite imagery have increased in the past decade (see Comer and Harrower 2013). As previously mentioned, the Finnish project SYGIS had started applying satellite imagery also for landscape studies from the beginning of the project first using Landsat images and CORONA photographs. As previously mentioned, the X-SAR 2000 mission (Rabus et al. 2003) provided DEM data from the region of Jebel Bishri enabling the construction of landscape models fusing the radar data with Landsat-7 imagery in 2003 (Fig. 13). A fly-over animation was used so that one can approach the Euphrates and Jebel Bishri from various directions, both from the southeast and the Jezira (see www.helsinki.fi/hum/arla/sygis). The satellite data also allowed to capture a 3D scene mosaic over the peninsula of Halabiya with a Landsat-4 MSS (Lönnqvist et al. 2011, 55).

GIS has provided means to study visibilities in landscape (see Wheatley and Gillings 2000). On the southwestern edge of Jebel Bishri, prehistoric and Bronze Age sites were met in numbers, and visibilities toward the eastern oases were studied with landscape models that were constructed by using Russian topographic maps and Landsat-7 image data using Image drape software (Lönnqvist et al. 2011) (Fig. 14). Landscape models of desert-steppe areas to study the environmental contexts were also created fusing QuickBird imagery with ASTER-DEM data (Fig. 15). That fusion produced natural kind of models because of the high spatial resolution of QuickBird imagery. (Lönnqvist et al. 2012).

The same visibility obviously served the Romans and Palmyrenes in inspecting the areas (the plains and the *wadis*) (Silver et al. 2017, 2018). Special attention was paid to the visibilities between various forts and fortresses on the Euphrates. A viewshed analysis (see Wheatley 1995) was carried out between three forts, namely, Tabūs, Qreiye and Mambri on the Euphrates using SRTM data (Fig. 16). Attention was especially paid on intervisibility. The location of the Tabūs fort in the middle of

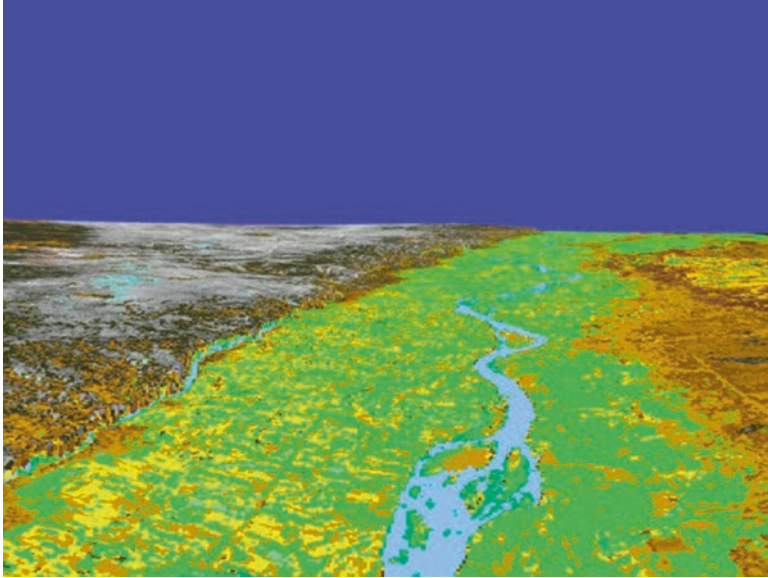


Fig. 13 A 3D landscape model displaying Jebel Bishri and the Euphrates valley from east to west constructed fusing Landsat-7 image with X-SAR-mission data. (Constructed by Markus Törmä 2003)

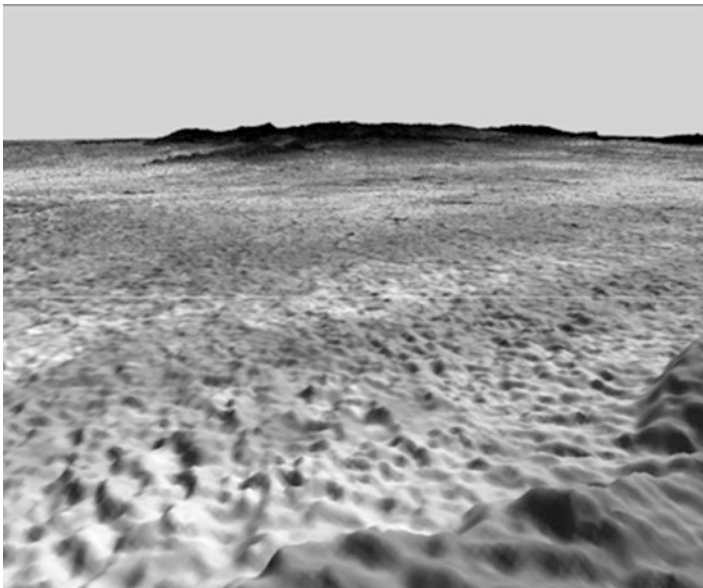


Fig. 14 Visibility analyses from the western edge of Jebel Bishri fusing Landsat images with topographic data. (3D modeling by Markus Törmä 2010)

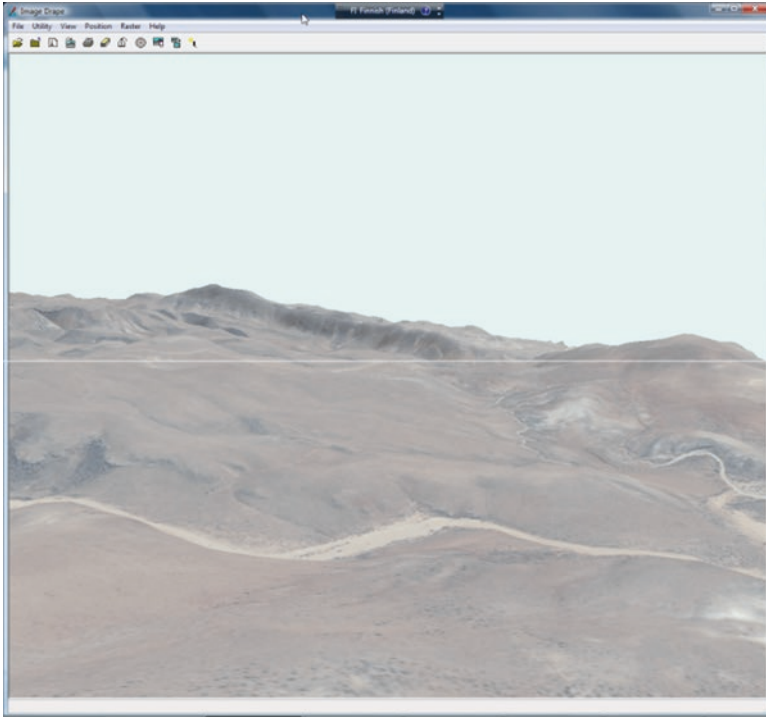


Fig. 15 Modelling the steppe landscape in 3D on Jebel Bishri fusing QuickBird imagery with ASTER-DEM data. (Constructed by Markus Törmä 2012)

the three forts and on higher elevation compared to the sites lower in the river valley made it a kind of a relay station (Lönnqvist et al. 2005a).

In our more recent study, after the SYGIS project ended in 2010 and the Syrian civil war started in 2011, we studied visibility from ancient tower tombs. The most famous ones are situated in Palmyra, but the structures are met in the Syro-Mesopotamian region in general. We wished to find out whether tombs had also been used as watch towers. The locations of the tombs and viewshed analyses indicated double function for these and their staircase towers: both as watchtowers and as tombs. There were more evidences to reinstate the hypothesis of defensive purpose in Palmyra and Hatra where tombs were also integrated in the walls surrounding the cities (Silver et al. 2015a, 2018).

In eastern Turkey in the area of Tūr Abdin, landscape models (Fig. 17) were produced fusing GeoEye-1 imagery with EU-DEM (European Digital Elevation Model data using SRTM and ASTER-DEM) with ERDAS ER Mapper 2016. They provided a way to visualize the potentials for visibility from the fortified sites of Keferde to Beioubaita. The traffic could have moved in valleys that provided natural contours to walk. Visibility and means for movement were useful or even essential in the border zones in the Roman and Byzantine times, when the threat of Parthians

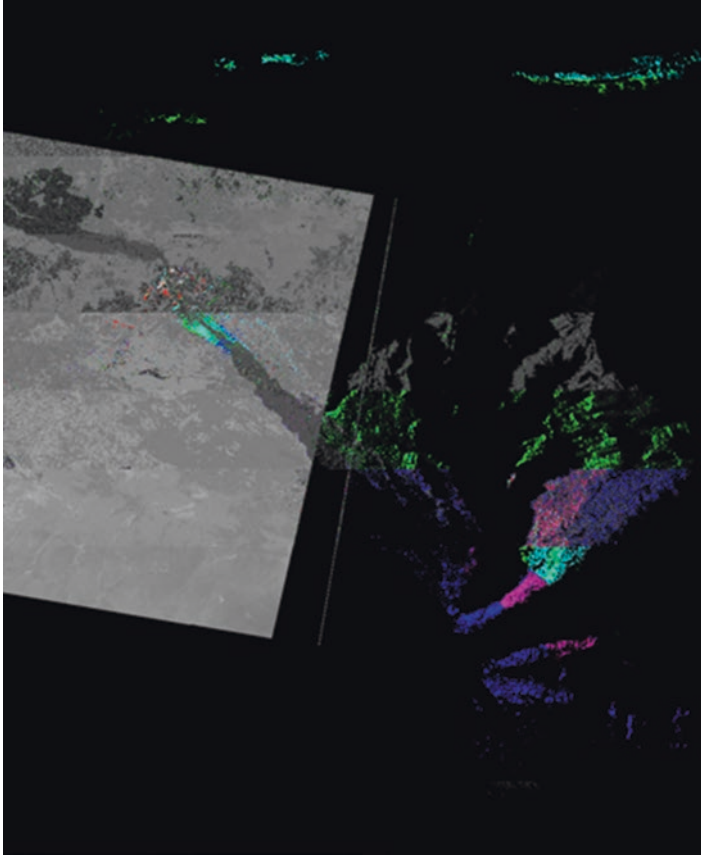


Fig. 16 A viewshed analysis between Roman forts on Jebel Bishri and along the Euphrates applying Landsat satellite imagery and SRTM data. (Analysis by Markus Törmä 2005)

or Persians was imminent (Silver et al. 2017). The landscape of sites in Tūr Abdin in the respective models is visibly fertile and agricultural compared to the models of the steppic and desert areas of Jebel Bishri (Fig. 15) that is and has been the realm of pastoral nomads.

Final Remarks

It needs to be mentioned that the areas that the Finnish project SYGIS and the Finnish-Swedish project FSAPM in greater Mesopotamia have studied are located in the areas where heritage has been at risk. Sites on Jebel Bishri in Syria have suffered from the military interference, destruction and heavy looting since the civil

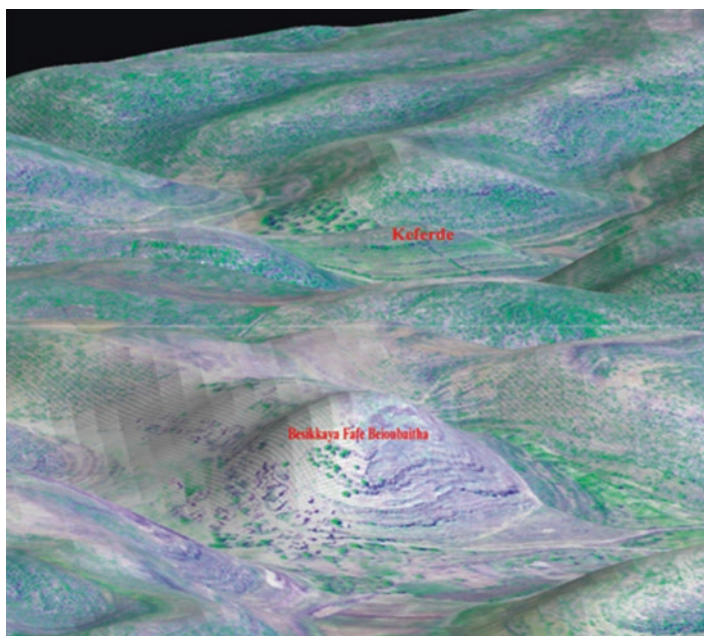


Fig. 17 A 3D landscape model displaying Roman/Byzantine sites in Tūr Abdin constructed by fusing GeoEye imagery with EU-DEM data from SRTM and ASTER- DEM. (Constructed by Markus Törmä 2017)

war started in 2011. Tūr Abdin is in the region of Turkey that is affected by large Tigris dam projects and agricultural development and building. Therefore, the swift documentation of sites and monuments has been of utmost value. New sites and monuments were detected by prospecting with satellite imagery and combining the results with experimental field work by surveying on the ground, also using GPS and GPR in Syria.

Unclassified CORONA satellite photographs have been widely used in archaeological prospecting in the Near East during the past decades. The benefits have been in their low price, high spatial resolution for detecting sites and features in the landscape before some constructions and changes in the environment had taken place. Landsat images have been valuable data sources for environmental studies, also enabling to see changes through the years and carrying out various analyses to extract environmental information. They have also been used in mapping archaeological sites and carrying out landscape modelling by fusing the data with DEM tiles from SRTM and ASTER-DEM or with topographical map information. Landscape models have also provided means for visibility studies and viewshed analyses.

Google Earth and other higher spatial resolution images such as QuickBird and GeoEye have revealed Roman sites such as military camps, roads and forts in detail. Because of their higher spatial resolution, the images have also provided more natural type of landscape models when fusing them with radar data. The environmental differ-

ences between the Syrian and Turkish sites are clear; those in Syria were in the steppe landscape, while those in Turkey were in areas of rain-fed agriculture.

The manifold advantages of remote sensing have become evident in archaeology in recent decades. Now when the Near East has been in turmoil, the remote sensing is in some cases the only way to carry out studies and monitoring sites. That we have location information, like UTM coordinates, is of utmost importance in saving the location information and eventually the sites with heritage value. For research new mappings of the Roman frontier, modellings and analyses have opened wider views for understanding of military strategies and social, economic and cultural lives in the region.

References

- Bewley R, Kennedy D (2013) Historical aerial imagery in Jordan and the Wider Middle East. In: Hanson SW, Oltean IA (eds) *Archaeology from historical aerial and satellite archives*. Springer, New York, pp 221–242
- Brew G, Best J, Barazangi M, Sawaf T (2003) Tectonic evolution of the NE Palmyride mountain belt, Syria: the Bishri crustal block. *J Geol Soc* 160:677–685
- Comer DC, Harrower MJ (eds) (2013) *Mapping archaeological landscapes from space*. Springer, New York
- Evans DL, Stofan ER, Jones TD, Godwin LM (1994) Earth from sky: radar systems carried aloft by the space shuttle endeavour provide a new perspective of the Earth's environment. *Sci Am* 271(6/Dec):70–75
- Gates J (2006) Hidden passage: Graeco-Roman roads in Egypt's eastern desert. In: by Robertson EC, Seibert JD, Fernandez DC, Zender MU (eds) *Space and spatial analysis in archaeology*. The University of Calgary Press, Calgary, pp 315–322
- Gregory S, Kennedy D (1985) *Sir Aurel Stein's limes report, Part I and II*, BAR International Series 272 (I–II). BAR, Oxford
- Gschwind M, Hasan H (2008) Das römische Kastell Qreiye-'Ayyāš, Provinz Deir ez-Zor, Syrien, Ergebnisse des syrisch-deutschen Kooperations-projektes. *Zeitschrift für Orient-Archäologie* 1:316–334
- Haggrén H, Nuikka M, Junnilainen H, Järvinen J (2002) Photogrammetric approach for archaeological documentation of an ancient road, CIPA heritage documentation. In: Albertz J (ed) *Proceedings of the XVIIIth international symposium of CIPA*, Potsdam (Germany) Sept. 18–21. The ISPRS international archives of photogrammetry, remote sensing and spatial information sciences, vol XXXIV-5/C7. CIPA, Berlin, pp 108–113. H
- Haggrén H, Koistinen K, Junnilainen H, Erving A (2005) Photogrammetric documentation and modelling of an archaeological site: the Finnish Jabal Haroun project. www.isprs.org/proceedings/XXXVI/5-W17/pdf/39.pdf. Accessed 19 Oct 2017
- Harrower MJ, Comer DC (2013) Introduction: The history and future of geospatial and space technologies in archaeology. In: Harrower MJ, Comer DC (eds) *Mapping archaeological landscapes from space*, springer briefs in archaeology, archaeological heritage management. Springer, New York, pp 1–10
- Kennedy D (1982) *Archaeological explorations on the Roman frontier in north east Jordan: The Roman and Byzantine military installations and road network on the ground and from the air (Including unpublished work by Sir Aurel Stein and with a contribution by D. N. Riley)*, BAR, International Series 132. BAR, Oxford
- Kennedy D (1998) Declassified satellite photographs and archaeology in the Middle East: case studies from Turkey. *Antiquity* 72:553–561
- Kennedy D, Bewley R (2004) *Ancient Jordan from the air. The Council for the British Academy in the Levant*, Dorset: The British Academy

- Lönnqvist M (ed) (2008) *Jebel Bishri in context: introduction to the archaeological studies and the neighbourhood of Jebel Bishri in Central Syria*. In: Proceedings of a Nordic research training seminar in Syria, May 2004. BAR International Series 1817. Archaeopress, Oxford
- Lönnqvist M, Stefanakis E (2009) GIScience in archaeology: ancient human traces in automated space. In: Madden M (ed) *Manual of geographic information systems*. ASPRS, Bethesda, pp 1221–1259
- Lönnqvist M, Törmä M (2003) SYGIS – the Finnish archaeological project in Syria. In: Altan MO (ed) *Proceedings of the XIXth international symposium CIPA 2003 (The ICOMOS & ISPRS Committee for Documentation of Cultural Heritage): new perspectives to save cultural heritage, Antalya, Turkey, The ISPRS international archives of the photogrammetry, remote sensing and spatial information sciences, vol XXXIV-5/C15, Istanbul, pp 609–614*
- Lönnqvist M, Törmä M (2004) Different implications of a spatial boundary, Jebel Bishri between the Desert and the Sown in Syria. In: Orhan Altan M (ed) *The ISPRS XXth congress proceedings, The ISPRS international archives of the photogrammetry, remote sensing and spatial information sciences, vol XXXV. Part B, Istanbul, pp 897–902*
- Lönnqvist M, Lönnqvist K, Whiting MS, Törmä M, Nuñez M, Okkonen J (2005a) Documenting, identifying and protecting a late Roman – Byzantine Fort at Tabus on the Euphrates. In: Dequal S (ed) *International cooperation to save the world's cultural heritage, proceedings of the XX international symposium CIPA 2005, Turin (Italy) 26 September – 01 October, 2005, vol 1, The international archives of photogrammetry, remote sensing and spatial information sciences, vol XXXVI-5/C34, CIPA – The ICOMOS/ISPRS Committee for Documentation of Cultural Heritage. CIPA, Turin, pp 427–432*
- Lönnqvist M, Lönnqvist K, Stout Whiting M, Törmä M, Nuñez M, Okkonen J (2005b) Tracing new dimensions in the Roman military organization of the Eastern Limes, International cooperation to save the world's cultural heritage. In: Dequal S (ed) *Proceedings of the XX international symposium CIPA 2005, Turin (Italy) 26 September – 01 October, 2005, vol 2, The international archives of photogrammetry, remote sensing and spatial information sciences, vol XXXVI-5/C34, CIPA–The ICOMOS/ISPRS Committee for Documentation of Cultural Heritage, Italy, pp 1074–1079*
- Lönnqvist M, Törmä M, Lönnqvist K, Stout Whiting M, Nuñez M, Okkonen J (2006) An ethical overview of long-term perspectivism: experiences from an archaeological survey on Jebel Bishri in Syria. In: Ioannides M, Arnold D, Niccolucci F, Mania K (eds) *The evolution of information communication technology in cultural heritage, where Hi-Tech touches the past: risks and challenges for the 21st century, short papers from the joint event CIPA/VAST/EG/EuroMed 2006, 30 October – 4 November 2006, Nicosia, Cyprus. EPOCH Publication, Budapest, pp 108–113*
- Lönnqvist M, Törmä M, Nuñez M, Lönnqvist K, Okkonen J, Latikka J (2007) The Euphrates channel changes and archaeology along Jebel Bishri in Syria. In: Georgopoulos A (ed) *Proceedings of the XXI symposium, CIPA 2007, Athens, anticipating the future of the cultural past, vol 1, The international archives of photogrammetry, remote sensing and spatial information sciences, vol XXXVI-5/C53, pp 465–470*
- Lönnqvist M, with the contributions by Törmä M, Lönnqvist K, Okkonen J, Herles M, Königsdörfer M. (2009) *Archaeological surveys of Jebel Bishri, the preliminary report of the Finnish Mission to Syria, 2005–2006. KASKAL, Rivista di storia, ambienti e culture del Vicino Oriente Antico 6:1–42*
- Lönnqvist M, Markus Törmä M, Lönnqvist K, Nuñez M (2011) *Jebel Bishri in focus: remote sensing, archaeological surveying, mapping and GIS studies of Jebel Bishri in central Syria by the Finnish project SYGIS. British Archaeological Reports International Series 2230*
- Lönnqvist, M., Törmä, M., Lönnqvist, K., Nuñez, M. (2012) *Satellite perspective on highland – lowland human interaction in ancient Syria*. In: Madden M, Shortis M (eds) *International archives of photogrammetry, remote sensing and spatial information sciences, vol XXXIXB4, XXII ISPRS congress 25 August – 01 September 2012, Melbourne, Australia, pp 455–460*
- Moore AMT, Hillman GC, Legge AJ, Huxtable J (2000) *Village on the Euphrates: from foraging to farming at Abu Hureyra*. Oxford University Press, Oxford

- Mouterde R, Poidebard A (1945) *Le Limes de Chalcis: Organisation de la steppe en Haute Syrie Romaine*. Bibliothèque archéologique et historique. Documents aériens et épigraphiques. Texte and Atlas. Paul Geuthner, Paris
- Musil A (1927) *The middle Euphrates: a topographical itinerary*. American Geographical Society. Oriental Explorations and Studies No 3. American Geographical Society, New York
- Musil A (1928) *Palmyrena: a topographical itinerary*. American Geographical Society. Oriental Explorations and Studies No 4. American Geographical Society, New York
- Poidebard A (1934) *La trace de Rome dans le désert de Syrie. Le limes de Trajan à la conquête arabe*. Recherches aériennes (1925–1932), Bibliothèque arch, et hist, du Service des Antiquités de Syrie, tome XVIII, Texte and Atlas, in two volumes, Paris: Paul Geuthner
- Ptolemy = Claudius Ptolemy, the geography. Translated and edited by Stevenson EL. Dover Publications, New York
- Rabus B, Eineder M, Roth A, Bamler R (2003) The shuttle radar topography mission—a new class of digital elevation models acquired by spaceborne radar. *ISPRS J Photogramm Remote Sens* 57:241–262
- Rees LWB (1929) *The Transjordan Desert*. *Antiquity* III:389–407
- Sarre F, Herzfeld E (1911) *Archäologische Reise im Euphrat- und Tigris-Gebiet Band I*. Forschungen zur islamischen Kunst I. Dietrich Reimer (Ernst Vohsen), Berlin
- Sarre F, Herzfeld E (1920) *Archäologische Reise im Euphrat- und Tigris-Gebiet. Band II*. Forschungen zur islamischen Kunst I. Dietrich Reimer (Ernst Vohsen), Berlin
- Schmidt-Colinet A, Al-As'ad K, Al-As'ad W (2016) Palmyra, 30 years of Syro- German/Austrian archaeological research (Homs). In: by Kanjou Y, Tsuneki A (eds) *A history of Syria in one hundred sites*. Archaeopress, Oxford, pp 339–348
- Silver M, Törmä M, Silver K, Okkonen J, Nuñez M (2015a) The possible use of ancient tower tombs as watchtowers in Syro-Mesopotamia. In: Yen Y-N, Weng K-H, Cheng H-M (eds), *ISPRS annals (II-5/W3)*, pp 287–293
- Silver M, Törmä M, Silver K, Okkonen J, Nuñez M (2015b) Remote sensing, archaeology and landscape: tracing ancient tracks and roads between Palmyra and the Euphrates in Syria. In: Yen Y-N, Weng K-H, Cheng H-M (eds) *ISPRS annals (II-5/W3)*, pp 279–285
- Silver K, Silver M, Törmä M, Okkonen J, Okkonen T (2017) Applying satellite data sources in the documentation and landscape modelling for Graeco-Roman/Byzantine Fortified sites in the Tur Abdin Area, Eastern Turkey. In: *ISPRS annals of the photogrammetry, remote sensing and spatial information sciences*, vol IV-2/W2, 2017, 26th international cipa symposium 2017, 28 August–01 September 2017, Ottawa, Canada, pp 251–258
- Silver M, Fangi G, Denker A (2018) *Reviving Palmyra in multiple dimensions: Images, Ruins and Cultural Memory*. Whittles Publishing, Caithness
- Space Today Online (2006) Accessed <http://www.spacetoday.org/SolSys/Earth/Ubar.html>. Access date 7 Sept 2017
- Tabula Peutingeriana (see, e.g., *Itineraria Picta, Contributo allo Studio della Tabula Peutingeriana*, by Levi, A. and Levi, M. 1967. Roma: L'Erma)
- Ur J (2003) CORONA satellite photography and ancient road networks: a Northern Mesopotamian case study. *Antiquity* 77:102–115
- Wheatley D (1995) Cumulative viewshed analysis: a GIS-based method for investigating intervisibility, and its archaeological application. In: Lock G, Stančić Z (eds) *Archaeology and geographic information systems*. Taylor & Francis, London-Bristol, pp 171–185
- Wheatley D, Gillings M (2000) Vision, perception and GIS: developing enriched approaches to the study of archaeological visibility. In: Lock G (ed) *Beyond map, archaeology and spatial technology series a: life sciences*, vol 321. IOS Press, Amsterdam, pp 1–27

Archaeological Landscapes and Built Heritage: Climate Risk and Contribution of Remote Sensing Technologies



Petros Patias, Charalampos Georgiadis, and Dimitrios Kaimaris

Abstract The focus of this chapter is the contribution of remote sensing (RS) technologies in climate risk mainly for archaeological landscapes and built heritage. It will study the use of RS technologies for sea level rise scenario risk assessment and the use of multi-temporal multisource data and statistical indices for the detection of changes in built heritage. This chapter is divided in two sections: the first one focuses on sea level rise and potential threats, while the second one focuses on monitoring of temporal changes in built heritage using multisource multi-temporal data and indices.

Keywords Remote sensing · Sea level rise · Built heritage · Change detection · DEM production · UAV

Introduction

The focus of this chapter is the contribution of remote sensing (RS) technologies in climate risk mainly for archaeological landscapes and built heritage. Global climate changes due to various factors are causing risk not only to human life but also to cultural heritage. One of the most significant consequences of climate change is sea level rise. Sea level rise due to climatic change is evolving during the last decades

P. Patias (✉)

School of Rural and Surveying Engineering, Aristotle University of Thessaloniki,
Thessaloniki, Greece
e-mail: patias@auth.gr

C. Georgiadis

School of Civil Engineering, Aristotle University of Thessaloniki, Thessaloniki, Greece
e-mail: harrisg@civil.auth.gr

D. Kaimaris

School of Spatial Planning and Development (Eng.), Aristotle University of Thessaloniki,
Thessaloniki, Greece
e-mail: kaimaris@auth.gr

© Springer Nature Switzerland AG 2020

D. G. Hadjimitsis et al. (eds.), *Remote Sensing for Archaeology and Cultural Landscapes*, Springer Remote Sensing/Photogrammetry,
https://doi.org/10.1007/978-3-030-10979-0_11

177

posing a threat to all coastal sites. A large number of cultural and natural heritage sites are either underwater or coastal at the moment. A search at the UNESCO World Heritage Center site (<http://whc.unesco.org/en/list/>) returned a total of 110 coastal or underwater heritage sites out of a total of 1073 sites, representing roughly 10% (September 2017). On the other hand, climatic changes have an effect in built heritage. In order to be able to monitor changes in built environments either historical city centers or settlements, the use of multi-temporal and multisource data is almost mandatory. The new remote sensing satellites coupled with historical maps and aerial photographs can provide a very powerful tool for the detection of such changes. Another effective methodology to monitor and document these changes is by using indices in order to study certain features and characteristics. This chapter is divided in two sections: the first one focuses on sea level rise and potential threats, while the second one focuses on monitoring of temporal changes in built heritage using multisource multi-temporal data and indices. Each section is complemented with the presentation of implemented case studies. For the first section “Sea Level Rise and Potential Threats to Heritage,” a case study presenting the use of remote sensing satellite data and UAV imagery for the production of DEMs and orthoimages is presented. For the second section “Monitoring of Temporal Changes in Built Heritage Through Indices,” two case studies are presented. The first one presents the identification of changes in the historic center of Nicosia using multi-source and multi-temporal data, while the second one examines the changes that occurred in the settlement of New Mesibria using statistical indices applied to aerial photographs.

Sea Level Rise and Potential Threats to Heritage

This section focuses on methodologies and tools that deal with sea level rise (SLR) potential threats to underwater and heritage sites. According to (UNESCO 2007), SLR will threaten the coastal area with coastal erosion and permanent submersion of low-lying areas along with an increase in sea-salt chloride load in the coastal soils. Recent projections of SLR are predicting an increase of approximately 1 m in sea level globally based on different types of scenario (Carson et al. 2016; Kopp et al. 2014; Jorda 2014). In order to assess the impacts of SLR to coastal areas, most of the studies (SLR scenarios) can be divided in two categories: (a) aggregation of global exposure surveys that can quantify the impact and (b) high-resolution site-specific studies that target specific areas and their results cannot be extrapolated to predict global estimates with respect to coastal impact (Diaz 2016). Different studies regarding SLR scenarios have been performed in the recent years. (Anzidei et al. 2017) performed a flooding scenario for the Lipari Island in Italy. Their study revealed that an area of 12,500 m² or 17,500 m² is going to be flooded by 2100 AD in a coastal strip of about 700 based on a 1.36 m and 1.60 m potential SLR scenario, respectively. Wardell-Johnson et al. (2015) performed a study for the K’gari-Fraser Island. They concluded that although K’gari-Fraser Island is

unlikely to experience coastal flooding due to SLR over the next century, even small rises could result in saline contamination of low-lying areas of the island. (Marzeion and Levermann 2014) performed a study focused on loss of cultural world heritage due to SLR. In their study, they used a global DEM (SRTM and ETOPO1) to run a scenario and predict coastal flooding over the next two millennia. Their study predicted that out of the 720 sites listed in UNESCO World Heritage List in October 2012, 136 sites will be impacted by SLR if a warming of $\Delta T = 3$ K is sustained over the next two millennia.

In order to be able to assess potential threats and run SLR scenarios, a detailed (high resolution) and accurate DEM of the region is required. The technological advancements along with the new very high-resolution satellites provide the answer for fast and accurate 3D modeling. In this chapter, the methods and resources that can be used to provide accurate mapping are going to be presented. Remote sensing data or global DEMs derived from satellites can help to predict vulnerable areas globally.

Cultural Heritage Mapping with Remote Sensing

For SLR disaster assessment, the coastal line and the area's DEM are enough in order to create risk assessment maps. Depending on the SLR scenario, short- or long-term one must choose the proper resolution and accuracy of the DEM. Remote sensing is widely used for mapping large areas. The new satellites provide very high-resolution data down to 0.30 m pixel size, thus being able to map heritage sites, and create high-resolution DEMs. In the following table, an indicative list of high and very high satellite data that can be used for the production of DEMs suitable for risk assessment with respect to SLR and coastal disasters is presented.

In Table 1, the current satellites with a resolution of 2.5 m or better are presented. Other satellite data can be also used for the temporal and historical monitoring of heritage sites. The Landsat mission can provide a very thorough source of data for temporal analysis. Another source of potential historical data which can provide satellite photos of high resolution but with limited global coverage is the declassified intelligence satellite photographs (DISP). Their resolution ranges from 1 to 140 m and was part of the CORONA, ARGON, LANYARD, GAMBIT, and HEXAGON satellite programs (USGS 2008). Detailed information about the DISP archive can be found in (Fowler 2013).

Existing global DEMs can be used to produce SLR risk assessment maps in small scales but for covering larger areas. The following table presents and indicates list of existing free/proprietary global or regional DEMs.

The Shuttle Radar Topography Mission (SRTM) used two SARs, a C band system (5.6 cm, C radar) and an X band system (3.1 cm, X radar) (Farr et al. 2007). SRTM collected radar data over 80% of the Earth's land surface between 60° north and 56° south latitude with data points posted every 1 arc-second (approximately 30 meters) (<https://lta.cr.usgs.gov/SRTM>). The accuracy of the SRTM data was assessed by Rodriguez et al. (2005) (Table 2).

Table 1 Current 2.5 m and better resolution land imaging satellites (Stoney 2007)

Satellite	Country	Launch date	Panchromatic resolution (m)	Multispectral resolution (m)	
1	WorldView-3	USA	08/13/14	0.3	1.2
2	WorldView-4	USA	11/11/16	0.3	1.2
3	GeoEye-1	USA	03/16/07	0.4	1.6
4	WorldView-1	USA	07/01/07	0.5	
5	WorldView-2	USA	07/01/08	0.5	1.8
6	Quickbird-2	USA	10/18/01	0.6	2.4
7	Gaofen 2	China	08/19/14	0.8	3.2
8	Pleiades-1	France	03/01/09	0.5	2.0
9	Pleiades-2	France	09/01/10	0.5	2.0
10	KOMPSAT 3	Korea	05/17/12	0.7	2.8
11	KOMPSAT 3A	Korea	03/25/15	0.5	2.2
12	EROS B1	Israel	04/25/06	0.7	
13	EROS C	Israel	03/21/08	0.7	2.5
14	TripleSat	India	07/10/15	0.8	3.2
15	SkySat 1	USA	11/21/13	0.9	2.0
16	SkySat 2	USA	7/8/14	1.1	2.0
17	TanDem-X	Germany	06/30/09	1.0	
18	TerraSAR-L	Germany	08/15/08	1.0	
19	TerraSAR-X	Germany	10/31/06	1.0	
20	IRS Cartosat 2	India	03/15/07	1.0	
21	COSMO-Skymed-1	Italy	11/12/07	1.0	
22	COSMO-Skymed-2	Italy	05/01/08	1.0	
23	COSMO-Skymed-3	Italy	11/01/08	1.0	
24	COSMO-Skymed-4	Italy	05/01/09	1.0	
25	Arirang-2 (KOMPSAT-2)	Korea	07/28/06	1.0	4.0
26	Resurs DK-1 (01-N5)	Russia	06/15/06	1.0	3.0
27	IKONOS-2	USA	09/24/99	1.0	4.0
28	OrbView 3	USA	06/26/03	1.0	4.0
29	SPOT 6	France	09/09/12	1.5	6.0
30	SPOT 7	France	06/30/14	1.5	6.0
31	EROS A1	Israel	12/05/00	1.8	
32	FormoSat (RocSat 2)	Taiwan	04/20/04	2.0	8.0
33	TH 01	China	2010,12,15	2.0	10.0
34	THOES	Thailand	06/30/07	2.0	15.0
35	Alsats-2A	Algeria	12/01/08	2.5	10.0
36	Alsats-2B	Algeria	12/01/09	2.5	10.0
37	SPOT-5	France	05/04/02	2.5	10.0
38	IRS Cartosat 1	India	05/04/05	2.5	
39	ALOS	Japan	01/24/06	2.5	10.0
40	CARTOSAT-1	India	05/05/05	2.5	
41	RazakSat	Malaysia	11/01/06	2.5	5.0
42	Spain Sat	Spain	07/01/10	2.5	
43	TopSat (SSTL)	UK	10/27/05	2.5	5.0

Table 2 Free global or regional DEMs

Dem	Grid (m)	Positional accuracy (m)	Vertical accuracy (m)	Free or proprietary
SRTM	30 × 30	8.8–12.6	5.6–9	Free
ASTER GDEM	30 × 30	18–20	15–17	Free
DLR SRT	25 × 25	20	16	Free
EU-DEM	25 × 25	<5	2.9	Free
ALOS world 3D 30	30 × 30	<10	5	Free
ALOS World 3D	5 × 5	<5	5	Proprietary
Elevation 30	30 × 30		8	Proprietary
Elevation 8	8 × 8		3	Proprietary
WorldDEM (TerraSAR-X and TanDEM- X)	12 × 12		4	Proprietary
Elevation 4	4 × 4		2	Proprietary
Elevation 1	1 × 1		1.5	Proprietary

The ASTER Global Digital Elevation Model Version 2 (GDEM V2) was jointly released on October 17, 2011, by the Ministry of Economy, Trade, and Industry (METI) of Japan and the US National Aeronautics and Space (NASA). Its coverage spans from 83 degrees north latitude to 83 degrees south, encompassing 99 percent of Earth's landmass. (Tachikawa et al. 2011) published a report that validated the ASTER GDEM v2 results. According to their study, the ASTER GDEM v2 demonstrates a positional accuracy of approximately 18–20 m and an absolute vertical accuracy of approximately 15–17 m.

The X band radar measurements of SRTM were processed by DLR creating a global DEM with a grid size of approximately 25 × 25 meters.

The ALOS world DEM was generated by the Japan Aerospace Exploration Agency (JAXA). The DEM was generated using the archived data of the Panchromatic Remote sensing instrument (PRISM) on board the Advanced Land Observing Satellite (ALOS). ALOS operated from 2006 to 2011 acquiring approximately 6.5 million scenes covering the entire globe (Tadono et al. 2014). PRISM was an optical sensor consisting of 3 radiometers for Nadir, forward and backward looking with a 2.5 m spatial resolution and 35 km swath width.

The ALOS world 3D 30 m mesh was produced by the ALOS world 3D. The ALOS world 3D is a fine resolution DEM with a grid size of 5 m covering the +/- 80 degrees latitude regions. The ALOS World 3D 30 m DEM was generated by resampling 7 × 7 pixels on the AW3D DEM dataset (Tadono et al. 2016). Tadono et al. (2016) evaluated the achieved accuracies of the AW3D30DEM and concluded that it can provide a height RMSE of 4.4 m.

The EU-DEM was generated based on SRTM, ASTER GDEM, and public available Russian Maps. It provides Pan European elevation data with a grid of 25 meters. Based on the validation of Tottrup (2014), the EU-DEM has an overall vertical accuracy of 2.9 m RMSE and a horizontal accuracy better than 5 m.

In addition, several licensed global or regional DEMs exist. One of the major distributors of medium- to very high-resolution DEM data is Airbus (<http://www.intelligence-airbusds.com/en/66-geo-elevation-and-dem>). Elevation 30, 8, 4, and 1 and the WORLDDDEM are distributed by them. Their DEMs are produced either by optical satellites (SPOT 5/6, Pleiades) or radar (TerraSAR-X, TanDEM-X). Global DEMs can be used to assess potential threats when examining long- or medium-term sea level rise scenarios. When one needs to assess potential short-term sea level rise threats in a small area, then aerial or UAV imagery can be used for DEM production. UAV imagery can achieve ultrahigh-resolution DEM reaching 2–4 cm with an accuracy of 1–2 cm.

Lefkas Case Study

In order to demonstrate the use of remote sensing and UAVs in the production of 3D models of heritage sites, a case study performed in the Lefkas island is presented. Two different regions were mapped: one in the north part and one in the south part of the island. The north part of the island includes a part of the city of Lefkas and the adjoining lagoon, while the south part is a mapping of the coastal town of Vassiliki. Two different approaches were demonstrated for the production of high-resolution DEMs and orthoimages. The first approach was based on satellite imagery (WorldView-1 and WorldView-3) and the second one on UAV image acquisition.

Remote Sensing Mapping

In this section, the study case regarding the production of DEM and orthoimages for the two areas of the Lefkas island using WorldView-1 and WorldView-3, satellite imagery is going to be presented. Two different WorldView stereopairs were acquired, one for each area.

For the north area covering part of the Lefkas city and the adjoining lagoon, two WorldView-1 panchromatic images, with 0.50 m resolution and acquisition date 11 April 2017, were acquired. In addition, a multispectral WorldView-3 image with 0.30 m panchromatic resolution and 1.2 m MS resolution with acquisition date 16 April 2009 was acquired. A total of 26 ground points (16 used as ground control points and 10 as check points) were measured using GNSS RTK with a 0.05 m accuracy and used for the processing of the images (Fig. 1).

The triangulation yielded an accuracy of 0.31 m in X, 0.39 m in Y, and 0.45 m in Z. Using the panchromatic stereopair, a DEM of the area was created with a grid of 2×2 m. The DEM production yielded the following results (Tables 3 and 4).

The orthoimage was produced using data fusion between the MS and the PAN image. The registration was performed using the DEM and GCPs and satellite resection. The total RMS error of the orthoimage was 1.26 pixel or 0.38 m.

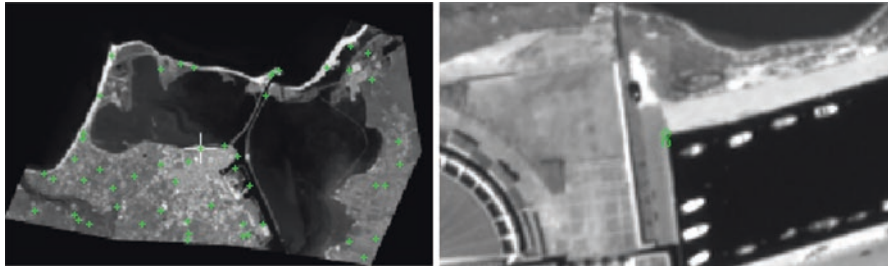


Fig. 1 Ground control points and check point distribution (left) and control point detail. (WorldView 1© 2017DigitalGlobe, Inc)

Table 3 North area DEM accuracy information: general mass point quality











DEM (2 × 2 m)		
Excellent	74.13%	
Good	14.00%	
Fair	0.000%	
Isolated	0.000%	
Suspicious	11.87%	

Table 4 North area vertical accuracy

Total # of 3D reference points used	10
Min, max error	-2.52, 0.75
Mean error	-0.77
Mean absolute error (RMSE)	0.96
LE90	1.21
	1.59

Table 5 South area DEM accuracy information: general mass point quality

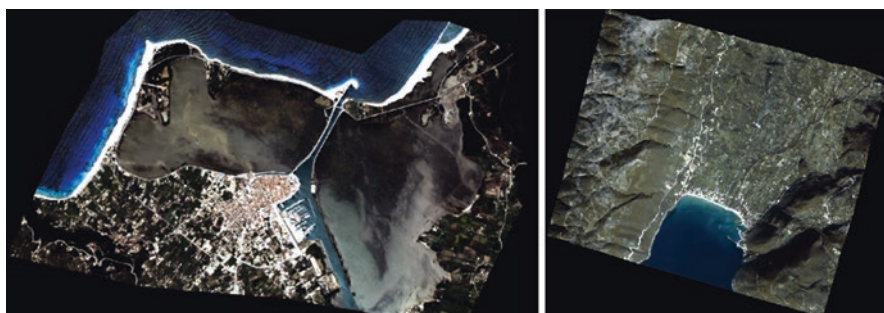
DEM (2 × 2 m)		
Excellent	74.47%	
Good	14.61%	
Fair	0.000%	
Isolated	0.000%	
Suspicious	8.92%	

For the second area, a WorldView-3 stereopair (PAN-MS) with a resolution 0.30 m PAN, and 1.20 m MS acquired on 28 December 2015, was used. A total of 27 ground points (17 used as ground control points and 10 as check points) were measured using GNSS RTK with a 0.05 m accuracy and used for the processing of the images. The triangulation yielded an accuracy of 0.12 m in X, 0.15 m in Y, and 0.29 m in Z. The produced 2 × 2 grid DEM yielded the following results (Tables 5 and 6).

The total RMS of the produced orthoimage was 0.86 pixel or 0.26 m. Figure 2 presents the produced orthoimages.

Table 6 South area vertical accuracy

Total # of 3D reference points used	10
Min, max error	-1.83, 0.56
Mean error	-0.24
Mean absolute error (RMSE)	0.54
LE90	0.72
	0.67

**Fig. 2** The produced orthoimages (Lefkas city left, Vassiliki right). (WorldView 1© 2015 Digital Globe, Inc)

UAV Mapping

The UAV mapping was performed using an eBee fixed-wing UAV equipped with the 1 inch 20 megapixel SODA sensor. The field surveys were realized in May–June 2017. A total of 2702 images were used for the DEM and orthoimage production for the north area, while a total of 1056 images were used for the south area. Ground control points were measured using GNSS RTK with an accuracy of 0.02 m. 37 control points and 6 check points were used for the photogrammetric processing of the north area, and 20 control points and 5 check points were used for the south area. The results provided a check points RMSE of 0.03 m, 0.04 m, and 0.03 m in the X, Y, and Z axes, respectively, for the north area and 0.03 m, 0.01 m, and 0.04 m for the south area. The final DEM was produced with 0.04×0.04 m grid and the orthoimages produced with a pixel size of 0.04 m (Fig. 3).

Conclusion

SLR is an effect of the climatic change that can potentially threaten cultural heritage. Global sea level rise scenarios predict a rise in the sea level of approximately 1–1.2 m for the next 100 years. Furthermore, area-specific SLR scenarios predict rises up to 5–7 mm/year. In order to be able to assess potential threats (flooding, coastal erosion, etc.) to cultural heritage, the area's topography, namely, the DEM

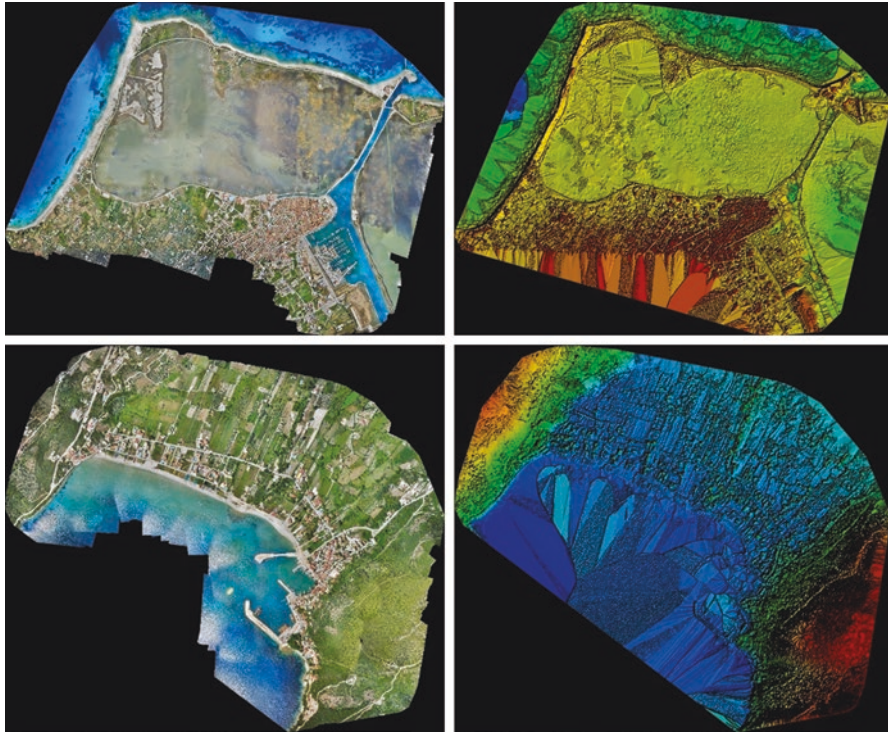


Fig. 3 The UAV imagery produced orthoimages and DEMs (the north area, top; the south area, bottom)

and the coastline, should be known. For very long-, long-, and medium-term SLR scenarios, very high-, high-, or medium-resolution and very high-, high-, and medium-accuracy DEMs are adequate for the assessment of potential threats. For short-term scenarios, ultrahigh-resolution and ultrahigh-accuracy DEMs are needed. Global DEMs, either free or proprietary, produced by remote sensing satellites, can be used for the assessment of risk in very long-, long-, and medium-term SLR scenarios. High- and very high-resolution satellite images can be used for the production of DEMs for the assessment of SLR risks in long- and medium-term scenarios because they can provide the adequate resolution and accuracy. Free global DEMs have a grid resolution of either 25 m or 30 m, while their horizontal and vertical accuracy span between 5 and 20 m and 3–17 m, respectively. Finally ultrahigh-resolution DEMs produced by UAV imagery can help assess SLR threats for short-term scenarios as they can provide resolution down to 2 cm with an accuracy of 1–2 cm. Furthermore, a case study demonstrating the results that can be achieved in DEM production using VHR satellite data and UAV was presented. VHR satellite images processing can achieve DEM production with an accuracy of 0.3–0.4 m horizontally and 0.5–1.0 m vertically, while UAV imagery can achieve DEM production with an accuracy of 0.01–0.02 m horizontally and 0.02–0.04 vertically creating DEMs with a resolution of 0.04 m.

Monitoring of Temporal Changes in Built Heritage Through Indices

Multi-temporal Data Sources for Monitoring Changes

Nowadays, the use of various data from several sources is almost mandatory for the analysis and documentation of historical city centers and their temporal evolution. The diversity of the data can be easily identified when maps and images are used. These two data sources refer to different but specific phases of evolution in time represent the technology used at that time through their unique geometric integrity, and have their own thematic or radiometric content.

Due to the fact that no source alone can provide the necessary information, the use of data from several sources is obligatory for studying certain features and characteristics. As a result, the use of multi-temporal data, such as aerial photography (old method) and satellite imagery (recent method), is unavoidable especially when dealing with changes over time.

Finally, manual or automated processes are used to extract the necessary (buildings, streets, green, etc.) geospatial information from the abovementioned multi-temporal data, to study the changes of historical city centers. Indices that recognize and document the percentage and type of urban change are used, identifying their systematic or non-systematic nature, as well as their concentration pattern.

Historical Maps

Maps are the oldest form of spatial representation, whereas satellite imagery and aerial photography are newer. It is easily understood that the accuracy of oldest maps is inversely proportional to their age: the older they are, the less accurate they are. In general, old maps represent a view of the reality emphasizing on the viewpoint the cartographer wished to communicate. Therefore, the amount of information and its geometric integrity can be reflected on their scale.

Another very important setback in dealing with old maps is their hard copy form. As a result, only through scanning they can only be compared to new digital maps. With respect to their geometric integrity, old maps display large material distortions, which combined with scanning distortions create difficulties in their use and study (Kaimaris et al. 2006).

Aerial Photography

More than 200 years have passed since the first appearance of aerial photography which provided a useful tool for studying historical changes.

Film and lens distortions, along with scanning errors, are the basic disadvantages of aerial photography as well. However, due to their solid geometric model (i.e., central projection), they can be processed easier, thus being more preferable than maps. Finally, they are a representation of the reality without any generalization, unlike maps.

The visible range of the electromagnetic spectrum, represented as gray values, is usually the radiometric content of aerial photography. Photographs of historical archives only use the visible range of the electromagnetic spectrum. On the other hand, color aerial photography and digital sensors sensitive to the infrared or thermal part of the spectrum are widely used nowadays.

Satellite Imagery of High and Very High Resolution

In 2017, 43 satellites of various mode types are operational (see Table 1). Specifically, these satellites are categorized as follows:

- Fifteen satellites with a spatial resolution of less than 3.2 m in multispectral mode and less than 1 m (GSD) in panchromatic mode (No. 1–15)
- Thirteen satellites with a spatial resolution of less than 4 m in multispectral mode and 1 m in panchromatic mode (No. 16–28)
- Fifteen satellites with a spatial resolution from 5 to 15 m in multispectral mode and from 1.5 to 2.5 m in panchromatic mode (No. 29–43)

Change Detection Procedure

The most important step toward any analysis, in this case monitoring temporal changes in built heritage, is the transformation of all the available data to a common reference frame, a procedure called georeferencing. Georeferencing is a mathematical transformation, which takes into consideration the scale and projection of the map, the central projection of the aerial photographs, and the “quasi”-central projection of the satellite images. The result of the georeference procedure is the definition of a common reference frame for all the available maps or images selected for analysis. In addition, the georeferenced data are free of any sensor or scanner distortions.

Urban areas are composed of constructions, roads, urban green, water bodies, etc. Selecting the proper feature for study is one of the basic steps toward the analysis. Automatic or semiautomatic techniques are preferred when compared with manual image analysis techniques as the latter are time-consuming, erroneous, and costly (Kaimaris and Patias 2016a, b).

Qualitative and Quantitative Indices of Historical Changes: A Review

Many studies (Ji and Gallo 2006; Sun et al. 2006; Shekhar 2004; Li 2005) suggest that qualitative and quantitative indices are a useful tool for continuous analysis of urban changes.

Urban environment's formation through time is affected by various characteristics and factors. Therefore, several radiometric (the effect of the atmosphere, the reflectance of the materials, etc.) and spatial (spatial homogeneity or concentrations, systematic or non-systematic appearance of features in certain points or linear paths, etc.) parameters must be taken into account when analyzing urban changes over time.

Qualitative and quantitative indices are computed using raster data. As a result, the radiometry of the used data should be normalized, the data sources should have the same pixel size and scale, and last but not least, the data should be georeferenced in a common reference frame.

Identification of the Amount of Changes

The first step in change identification is to set a specific threshold value in order to establish a minimum amount of change, during the elapsed time between multi-temporal data, which when exceeded the changes would be considered important. The assessment of the amount of urban changes during the study's temporal interval constitutes a very important step, as it determines whether to continue with the analysis or not.

The identification of urban changes is implemented through the computation of a general index. The index is computed based to the reflectance (intensity) values of the pixels using the sensor or scanner captured values, without assessing any spatial relations since at this stage no spatial relationships are available or needed. It must be noted that this index is computed using the full extent of a map or images.

This type of index can measure the similarity of datasets captured at different time instances. In 2006, Ji and Gallo presented a set of such indices found in literature. The most common indices of agreement are presented in Table 7.

As seen in the Table 7, Ji and Gallo (2006) created the agreement coefficient, Eq. 9 (AC) index which is validated through an in-depth analysis of other indices. AC is non-dimensional, bounded, symmetric, and capable of separating systematic and non-systematic differences.

Specifically, AC is non-dimensional as its nominator and denominator are canceled out. It is also bounded in the interval (0,1). A value equal to 1 ($AC = 1$) applies to a perfect agreement of images, whereas a value of 0 ($AC = 0$) indicates the perfect disagreement. Lastly, it is symmetric, as the interchange of g_1 and g_2 result to the same AC value.

Table 7 Measures of image agreement

Index	Formulation Description
Mean difference	$\Delta\bar{g} = \frac{1}{NM} \sum_{i=1}^N \sum_{j=1}^M \Delta g(i,j)$ <p>(1)</p> <p>Where: $\Delta g(i,j) = g_1(i,j) - g_2(i,j)$ (2) g_1 = the image/map at time t_1 g_2 = the image/map at time t_2 N = number of pixel rows M = number of pixel columns</p>
	<p>The average difference between two images is measured, without categorizing positive from negative differences</p>
Mean absolute difference	$ \Delta\bar{g} = \frac{1}{NM} \sum_{i=1}^N \sum_{j=1}^M \Delta g(i,j) $ <p>(3)</p>
	<p>Same as above but in absolute terms</p>
Mean absolute percent difference	$ \Delta\bar{g} _{\%} = \frac{1}{NM} \sum_{i=1}^N \sum_{j=1}^M 100 \frac{ \Delta g(i,j) }{g_1(i,j)}$ <p>(4)</p>
	<p>Same as above but expressed in percentages (Ramanathan 1995)</p>
Mean variance	$\sigma^2 = \frac{1}{NM} \sum_{i=1}^N \sum_{j=1}^M (\Delta g(i,j) - \Delta\bar{g})^2$ <p>(5)</p>
	<p>It measures the density or dispersion of the differences</p>
Mean percent variance	$\sigma_{\%}^2 = \frac{1}{NM} \sum_{i=1}^N \sum_{j=1}^M \left[100 \frac{(\Delta g(i,j) - \Delta\bar{g})}{(g_1(i,j) - \bar{g}_1)} \right]^2$ <p>(6)</p>
	<p>Where:</p>
	$\bar{g}_1 = \frac{1}{NM} \sum_{i=1}^N \sum_{j=1}^M g_1(i,j)$ <p>(7)</p>
	<p>Same as above but expressed in percentages</p>
Covariance	$\sigma_{12} = \frac{1}{NM} \sum_{i=1}^N \sum_{j=1}^M (g_1(i,j) - \bar{g}_1)(g_2(i,j) - \bar{g}_2)$ <p>(8)</p>
	<p>The similarity between two images is measured without being standardized nor bounded in value</p>
AC (after Ji and Gallo 2006)	$AC = 1 - \frac{\sum_{i=1}^N \sum_{j=1}^M \Delta g(i,j)^2}{\sum_{i=1}^N \sum_{j=1}^M [(\bar{g}_1 - \bar{g}_2 + g_1(i,j) - \bar{g}_1) \cdot (\bar{g}_1 - \bar{g}_2 + g_2(i,j) - \bar{g}_2)]}$ <p>(9)</p>
	<p>It measures the agreement of two images and is non-dimensional, bounded, symmetric and capable of separating systematic and non-systematic differences</p>

(continued)

Table 7 (continued)

Index	Formulation Description
Correlation coefficient	$r = \frac{\sigma_{12}}{\sigma_1 \sigma_2} = \frac{\sum_{i=1}^N \sum_{j=1}^M (g_1(i,j) - \bar{g}_1)(g_2(i,j) - \bar{g}_2)}{\sqrt{\sum_{i=1}^N \sum_{j=1}^M (g_1(i,j) - \bar{g}_1)^2 \sum_{i=1}^N \sum_{j=1}^M (g_2(i,j) - \bar{g}_2)^2}} \quad (10)$ <p>It measures the co-variance of the two images and is bounded to the interval (0,1). It explains only the linear covariation of the data and the actual difference</p>
Willmott's index of agreement (Willmott et al. 1985)	$d = 1 - \frac{\sum_{i=1}^N \sum_{j=1}^M \Delta g(i,j)^2}{\sum_{i=1}^N \sum_{j=1}^M [(g_1(i,j) - \bar{g}_1) \cdot (g_2(i,j) - \bar{g}_2)]} \quad (11)$
Mielke's measure of agreement (Mielke 1991; Mielke et al. 1997)	$\rho = 1 - \frac{\frac{1}{NM} \sum_{i=1}^N \sum_{j=1}^M \Delta g(i,j)^2}{\frac{1}{(NM)^2} \sum_{k=1}^{N \times M} \sum_{\lambda=1}^{N \times M} [(g_3(k,1) - g_4(\lambda,1))^2]} \quad (12)$ <p>where $g_3(k, 1)$ is the column matrix with dimensions $(N \times M) \times 1$, resulting from the placement of all elements of matrix $g_1(i, j)$ in a column, starting from the elements of the first line ($i = 1$) to those of line N. Matrix $g_4(\lambda, 1)$ is also a column matrix of dimensions $(N \times M) \times 1$ whose all elements λ are the same and equal to those in table $g_2(i, j)$ for $i = 1, 2, \dots, N$ and $j = 1, 2, \dots, M$</p>
Robinson's coefficient of agreement (Robinson 1957, 1959)	$A = 1 - \frac{\sum_{i=1}^N \sum_{j=1}^M (g_1(i,j) - g_3(i,j))^2 + \sum_{i=1}^N \sum_{j=1}^M (g_2(i,j) - g_3(i,j))^2}{\sum_{i=1}^N \sum_{j=1}^M (g_1(i,j) - \bar{g}_3)^2 + \sum_{i=1}^N \sum_{j=1}^M (g_2(i,j) - \bar{g}_3)^2} \quad (13)$ <p>where</p> $g_3(i,j) = \frac{1}{2}(g_1(i,j) + g_2(i,j))$ <p>and</p> $\bar{g}_3 = \frac{1}{2}(\bar{g}_1 + \bar{g}_2)$

Identification of the Possible Systematic Nature of Changes

In order to express systematic or non-systematic changes, a statistical metric is needed. Index AC (Eq. 9) can serve this purpose, once expressed in two terms.

The unique and most useful characteristic of AC is its ability to separate systematic and non-systematic differences. One should note that in least squares regression (which by the way is asymmetric), g_1 is assumed with errors, whereas g_2 is error free. While this is reasonable for comparing actually observed data to model-

predicted values, when both datasets are actually measured, we must assume that both are equally subject to measurement errors. Unlike least squares estimators, AC uses the geometric mean functional relationship (GMFR) regression model (Ricker 1980; Laws and Archie 1981; Draper and Smith 1998), expressed by:

$$\hat{g}_2(i,j) = a + b g_1(i,j) \quad (14)$$

where the estimated coefficients are given as follows:

$$b = \frac{\sqrt{\sum_{i=1}^N \sum_{j=1}^M (g_2(i,j) - \bar{g}_2)^2}}{\sqrt{\sum_{i=1}^N \sum_{j=1}^M (g_1(i,j) - \bar{g}_1)^2}} \quad (15)$$

$$a = \bar{g}_2 - b \bar{g}_1 \quad (16)$$

AC has the ability of identifying systematic and non-systematic patterns. To this respect, two parts of the AC can be created: the AC_s representing the systematic patterns and the AC_{ns} representing the non-systematic patterns (Ji and Gallo 2006).

$$AC_s = 1 - \frac{\sum_{i=1}^N \sum_{j=1}^M [g_1(i,j) - g_2(i,j)]^2 - \sum_{i=1}^N \sum_{j=1}^M [|g_1(i,j) - \hat{g}_1(i,j)| \cdot |g_2(i,j) - \hat{g}_2(i,j)|]}{\sum_{i=1}^N \sum_{j=1}^M [(|\bar{g}_1 - \bar{g}_2| + |g_1(i,j) - \bar{g}_1|) \cdot (|\bar{g}_1 - \bar{g}_2| + |g_2(i,j) - \bar{g}_2|)]} \quad (17)$$

$$AC_{ns} = 1 - \frac{\sum_{i=1}^N \sum_{j=1}^M [|g_1(i,j) - \hat{g}_1(i,j)| \cdot |g_2(i,j) - \hat{g}_2(i,j)|]}{\sum_{i=1}^N \sum_{j=1}^M [(|\bar{g}_1 - \bar{g}_2| + |g_1(i,j) - \bar{g}_1|) \cdot (|\bar{g}_1 - \bar{g}_2| + |g_2(i,j) - \bar{g}_2|)]} \quad (18)$$

Identification of Possible Concentration Patters of Changes

Urban changes appear with several types of patterns due to different urban/environmental characteristics and neighborhood factors. Thus, when studying those changes, one must bear in mind the fact that concentrations or dispersions may appear. The estimation of possible concentrations or dispersions can be achieved by the entropy (E) index which is ideal for this type of analysis (Table 2). The relative Shannon's entropy is another index that can be used. It can be calculated following the creation of buffer zones/circles in GIS software. Its values range between 0 and 1 (see, e.g., Shekhar 2004; Li 2005).

The methodology for calculating the spatial attractiveness indices (SA1 and SA2) is the following: the index SA1 of a city subcenter is calculated by counting

the number of pixels belonging to buildings within a circular buffer zone of radius R around a city subcenter, and the index SA2 of a road is calculated by counting the number of pixels belonging to buildings within a buffer zone of width D from the center line of a major road (Li 2005).

Euclidean and fractal geometry are two different approaches to describe the shapes of natural features and complement each other. More analytically, Euclidean geometry uses dimensions in integers (e.g., 1 for lines, 2 for areas, and 3 for volumes), which are constant despite any irregularities or anomalies of any element line or volume. On the contrary, the dimensions in fractal geometry are continuous. For example, a curve's dimension can take any value between 1 and 2, or a surface's dimension can take any value between 2 and 3 according to their forms' irregularity.

In the case of images, fractal dimensions can (a) characterize their spatial complexity, (b) provide textual data to image classification, (c) describe the geometric complexity of the feature classes' shape in image classification, and (d) investigate the scaling behavior of environmental phenomena (Sun et al. 2006; Wu et al. 2006; Myint et al. 2004).

In other words, fractal geometry explains any irregularities of fragments of the shapes of natural features that Euclidean geometry fails to achieve (Table 8).

Table 8 Measures of concentration of changes

Index	Formulation
	Description
Shannon's relative entropy	$E = \frac{\sum_{i=1}^n D_i \cdot \log \left[\frac{1}{D_i} \right]}{\log(n)}$ <p>where: BA_i = number of Building pixels in i^{th} zone A_i = Total number of pixels in i^{th} zone $D_i = BA_i/A_i$ = Build Density in i^{th} zone n = the number of zones</p> <p>This is the relative Shannon entropy index. It is normalized and bound to the interval (0,1). It measures the level of spatial dispersion of changes. The larger the entropy value, the less concentrated and according to some pattern are the changes</p>
Spatial attractiveness	<p>SA1 = Number of building pixels within a buffer circle of radius R from a city center (or sub-centers) SA2 = Number of building pixels within a buffer zone of width D from main road(s)</p> <p>These two indices are distance-metrics and can be calculated through GIS software "cost-distance" functions</p>
Fractal dimension	$E[(\Delta g(i, j) - \Delta g(i + d, j + d))^2] \propto d^{2H}$ <p>When $\log\{E[\dots]\}$ is plotted vs $\log\{d\}$ the slope is $2H$, and the fractal dimension is $D = 3 - H = 3 - \text{slope}/2$</p> <p>The fractal dimension here is computed with the variogram method (Sun et al. 2006) This index estimates the irregularity or complexity of the changes. D values are non-integer numbers in the interval (2,3)</p>

The Case Study of Nicosia, Cyprus

Nicosia, also known as Lefkosia, is located in the center of Cyprus and is the capital and largest city of the island. The city is the economic, business, and governmental center. In ancient times, Nicosia was known as Ledra. Its name “Lefkosia” originated by the fact that Lefkos, the son of Ptolemy I, rebuilt the city around 300 BC. At that time, the city was small of little importance, and it was also called Lefkothea.

Unfortunately, its historical course was not so calm. Although it has been destroyed by conquerors, there are historical traces that reveal its past. A great example is the Venetian city wall (Fig. 4). It was constructed between 1567 and 1570 with a 4,5 m thick wall and three gates. The center of the city rested within the walls at that time. Clearly, the city has grown since then, and the city’s modern center grows beyond the walls’ boundaries (Patias et al. 2011).

Multisource and Multi-temporal Data and Their Georeferencing

An orthorectified satellite image QuickBird-2 (pixel size, 0.6 m; local coordinate system, LTM (Local Transverse Mercator)) of 2006 was used for the georeferencing of the historical geographical data (Patias et al. 2011, Fig. 4).

The 1:2000 scale (Geographical Section General Staff No. 4861, published by D. Survey, War Office and Air Ministry, 1956, Fig. 5) historical map of Nicosia was scanned in 400dpi resolution (1pixel = 13 cm GSD). The control points were selected among several well-preserved constructions (streets, buildings, etc.). For its georeference, a second-grade polynomial transformation was used with a transformation accuracy of ~1,5 m.

Four historical aerial photographs (dated 02/10/1963, scale 1:5400, source: Department of Lands and Surveys, scanning resolution 1200 dpi (0,11 m GSD)) were also used. The control points for their projective transformation were selected



Fig. 4 Quickbird panchromatic satellite imagery with resolution of 0.6 m of 2006. (a) A general view, (b) a view in detail, (c) panchromatic and multispectral (fused) imagery (resolution = 0.6 m). It must be mentioned that the infrared band has replaced the red band so that the vegetation (blue color) is portrayed more clearly in the image

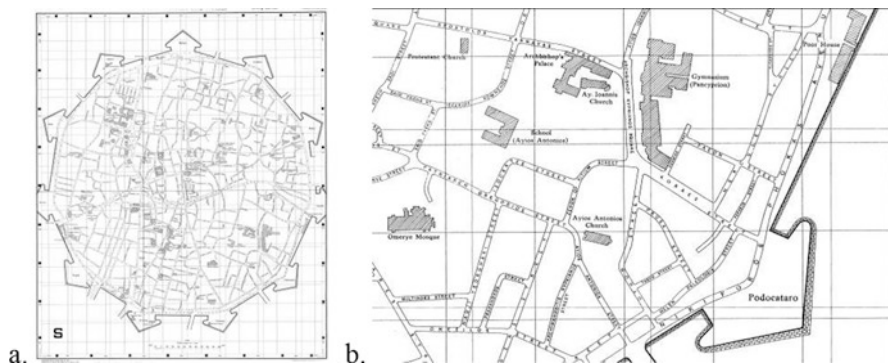


Fig. 5 Map of Nicosia, 1956, scale 1:2000. (a) A general view, (b) a view in detail

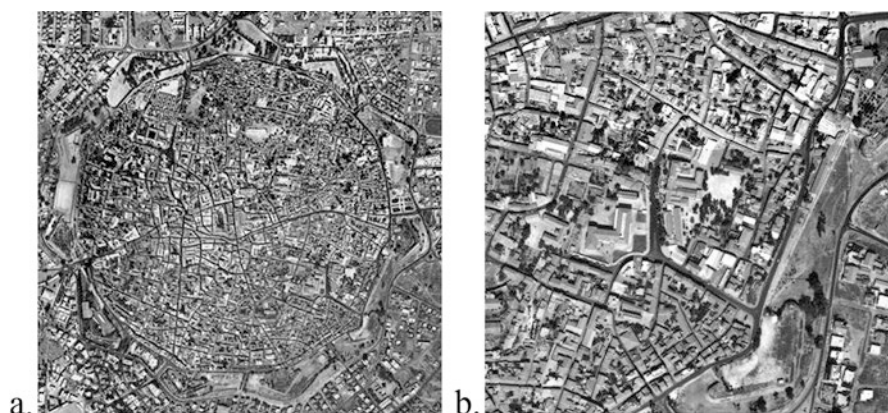


Fig. 6 Mosaic rectified aerial photographs of Nicosia, 1963. (a) An overall view, (b) detail view

from the contemporary orthorectified QuickBird-2 satellite image (accuracies of transformation 0.4–0.7 m). The images were combined to create a mosaic with a spatial resolution of 0.7 m (Fig. 6) (Patias et al. 2011).

Image Classification Procedure

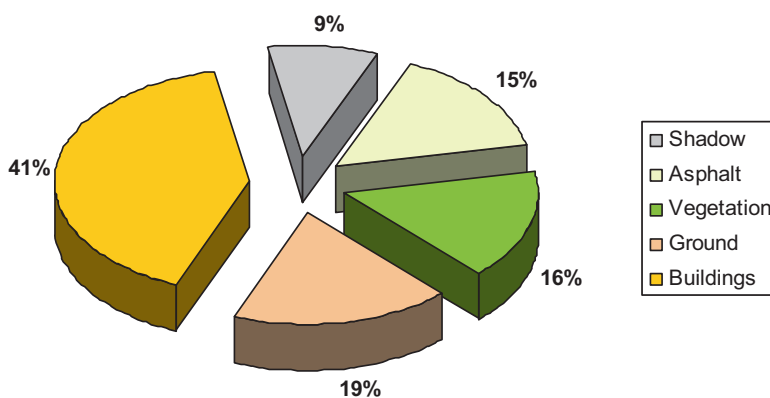
At this step, features belonging to different classes should be identified. Shadow, asphalt, vegetation, ground, and buildings were the five object classes selected for the implementation of a supervised classification using the QuickBird-2 satellite image (Table 9). The Overall Classification Accuracy (OCV) was 85.71%, and the Overall Kappa Statistics (OKS) was 0.8539. The accuracy assessment was based to a total of 203 pixels (Patias et al. 2011).

Table 9 Classification accuracy assessment report

Class name	Reference totals	Classified totals	Number correct	Producers accuracy	Users accuracy
Vegetation	16	16	16	100,00%	100,00%
Asphalt	30	27	26	86,67%	96,30%
Ground	38	44	34	89,47%	77,27%
Buildings	108	106	89	82,41%	83,96%
Shadow	11	10	9	81,82%	90,00%
Totals	203	203	174		

Table 10 Land use and number of pixels

Type of Land use	Number of pixels
Shadow	776,993
Asphalt	1,300,826
Vegetation	1,334,783
Ground	1,564,770
Buildings	3,455,840
Total	8,433,212

**Fig. 7** Classification of land use

The three classes representing the built area (asphalt, buildings, and shadow) cover 65% of the study area (Table 10, Fig. 7), while the other two representing natural ground (vegetation and ground) cover 35% of the study area.

Detection of Changes by Photo Interpretation

The comparison of urban changes revealed very interesting findings. The comparison was made between the historical map of 1956 and the aerial photographs of 1963 (Fig. 8). Changes were detected on buildings and roads. As far as buildings are concerned, 6 from 106 religious, administrative, and commercial buildings were



Fig. 8 Comparison of geographical data. (a) Map of 1956, (b) aerial photograph of 1963 in scale 1:5400, (c) overlay: inside the blue circle, there is a preserved building and with a green line, a new road



Fig. 9 Comparison of geographical data. (a) Map of 1956, (b) QuickBird-2 2006, (c) overlay: blue circle, a preserved building; red circle, a demolished building; green line, a new road

destroyed, giving their place to new constructions or to unstructured areas (Fig. 10). On the other hand, seven new roads were constructed, and one road was destroyed transforming into built area (Patias et al. 2011).

A second comparison was made between the historical map of 1956 and the satellite image QuickBird-2 (Fig. 9). This comparison revealed the destruction of nine buildings, which also gave their place to new constructions or unbuilt areas. Roads changed at a larger scale. After 1963, 7 new roads were constructed, and 15 roads were destroyed becoming new buildings or unbuilt areas.

The Case Study of Nea Mesimvria (Municipality of Thessaloniki), Greece

The settlement of New Mesibria was established by refugees arriving in the area in the beginning of the twentieth century. The scope of this study was to define, analyze, and detect the possible systematic nature of changes in the settlement of New Mesibria (municipality of Thessaloniki) by applying statistical indices in pairs of panchromatic aerial photographs of 1951 and 1990. When studying changes in an urban/structured environment using photographs or images, several radiometric and spatial/geometric factors have to be considered. To this end, a series of available data (maps, photographs, statistics) were collected and processed in order to compute statistical indices that would help to define the changes that occurred in the settlement (Stamnas 2013). It must be noted that the analysis, data, and results presented in this case study are part of the PhD Thesis of Dr. Anastasios Stamnas.

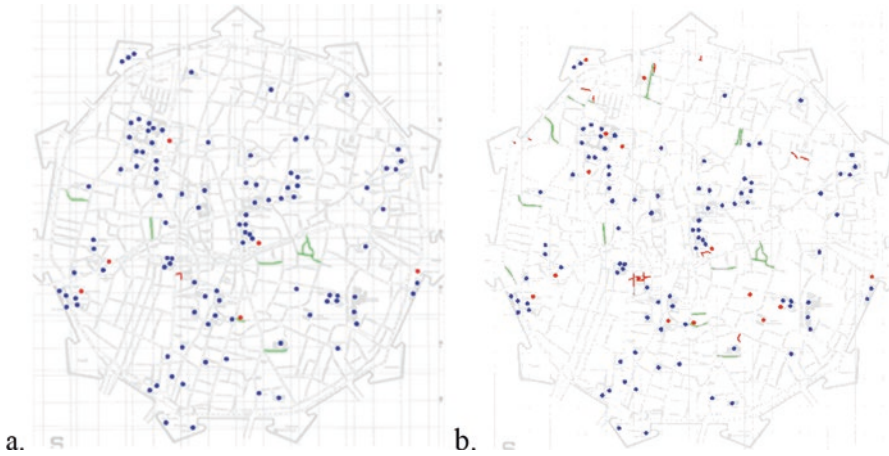


Fig. 10 Transformation of the built area, (a) 1956–1963 and (b) 1956–2006. Background is the historical map of 1956, in scale 1:2000. Blue circles, the preserved buildings; red circles, buildings that do not exist; green lines, new roads; red lines, roads that do not exist

Multisource and Multi-temporal Data and Their Georeferencing

For the refugee settlement of Nea Mesimbria, several old maps of the Ministry of Agriculture were collected. The maps included the cadastral allotment of the settlement in 1: 1000 scale for the years 1969 and 1971 and the cadastral allotment of the agricultural area (farms) in 1: 5000 scale for the years 1935, 1957 και 1966.

In addition, aerial photographs (1951, 1:13000 scale) (1990, 1:15000 scale) acquired by the Hellenic Military Geographical Service (HMGS) were also used. The aerial photographs (0.23 m × 0.23 m) were scanned at 1200dpi resolution resulting in 0.28 m GSD for the 1951 images, and 0.32 m GSD for the 1990 images. Orthoimages (Fig. 11) of 1:3000 scale were produced from the photogrammetric processing of the abovementioned aerial photographs. The accuracy of the bundle adjustment aerotriangulation was less than 0.5 pixel for both pairs.

The Implementation of the Statistical Indices

Statistical indices were calculated (Table 11) for both the original pair of digital images of the settlement of Nea Mesimvria (Fig. 11) and on processed pairs of images resulting from applying median filters with window sizes of 5 × 5, 10 × 10, 15 × 15, and 20 × 20 pixels. The median filters were used to reduce random noise due to georeferencing errors in the images.

The most important findings of Table 11's analysis taking into consideration the results observed in the pairs that the 20 × 20 pixels median filter was applied are:



Fig. 11 Pair of orthoimages of the settlement of Nea Mesimvria (a) 1951 and (b) 1990, where statistical indicators were applied

Table 11 Application of statistical indices on pairs of images of New Mesimbria in 1951 and 1990

Indices	Initial images	5 × 5	10 × 10	15 × 15	20 × 20
Δg (Eq. 2)	1.0440	1.0423	1.0390	1.0332	1.0279
AC (Eq. 9)	0.0710	0.0762	0.0930	0.1047	0.1220
AC_s (Eq. 17)	0.7785	0.7768	0.7725	0.7663	0.7602
AC_{nc} (Eq. 18)	0.2925	0.2994	0.3178	0.3384	0.3618
Corr (Eq. 10)	0.1466	0.1496	0.1587	0.1660	0.1776
Willmott (Eq. 11)	0.3400	0.3393	0.3385	0.3332	0.3305
Mielke (Eq. 12)	0.2511	0.2596	0.2822	0.2789	0.2983
Robinson (Eq. 13)	0.5060	0.5064	0.5082	0.5083	0.5101

- The very low value (0.122) of the AC reflects a great variation between the pixels of the two images.
- The very high value (0.7602) of the systematic AC_s reflects low systematic variation between the two images.
- The low value (0.3618) of the non-systematic AC_{ns} agreement coefficient represents a very large non-systematic variation between the two images.
- The non-systematic difference ($AC_s > AC_{ns}$) contributes more to the “inconsistency” of the two images. In this case, there is a significant difference between the coefficient of agreement (0.122) and the average difference (1.0279), while the correlation coefficient (0.1776) is very close to the agreement (0.1220).
- The above “mismatch” of the two images is similarly expressed by the low values of Willmott (0.3305), Mielke (0.2893) and Robinson (0.5101).

Conclusion

The use of diachronic and geospatial data is almost mandatory for the analysis and documentation of built heritage's evolution. Mostly, however, the use of multi-temporal data, such as aerial photographs (older data) and satellite images (recent data), is unavoidable, especially when changes must be documented over time.

When studying urban changes of historical city centers, manual or automated processes for the extraction of the necessary geospatial information (e.g., buildings, streets, green, etc.) are used. In addition, qualitative and quantitative indices are used, which can estimate and document the amount of urban changes in historical centers, identify their systematic or non-systematic nature, and their concentration pattern (presenting concentrations or dispersions).

In the case of the historical center of Nicosia, Cyprus, findings revealed a very interesting fact. During 1956 to 2006, historical buildings inside the boundaries of the walls were preserved up to 86%, whereas road network system also remained significantly the same. Consequently, the historical urban design remained almost completely unchanged during the course of the years preserving part of our rich cultural heritage. In the case of the refugee settlement of Nea Mesimbria, the application of the statistical indices determined the large variation between the respective pixels of the images, which expresses the significant changes of the underlying settlement's components (road network, building areas, land parcels, etc.) as well as the changes in the area around it.

Acknowledgment Part of this work was funded by the European research project SAVEMEDCOASTS (Seal level rise scenarios along the Mediterranean coasts GA No. ECHO/SUB/2016/742473/PREV16). SAVEMEDCOASTS is a cooperation European project co-funded by the ECHO European Commission Unit (EU Humanitarian Aid and Civil Protection).

The author would like to thank Dr. A. Stamnas for providing material from his PhD thesis that was used for the presentation of the New Mesimbria case study and Prof. P. Patias for making available his unpublished notes on indices.

References

- Anzidei M, Bosman A, Carluccio R, Casalbore D, D'Ajello Caracciolo F, Esposito A, Nicolosi I, Pietrantonio G, Vecchio A, Carmisciano C, Chiappini M (2017) Flooding scenarios due to land subsidence and sea-level rise: a case study for Lipari Is-land (Italy). *Terra Nova* 29(1):44–51
- Carson M, Köhl A, Stammer D, Slangen ABA, Katsman CA, Van de Wal RSW, Church J, White N (2016) Coastal sea level changes, observed and projected during the 20th and 21st century. *Clim Chang* 134(1-2):269–281. <https://doi.org/10.1007/s10584-015-1520-1>
- Diaz DB (2016) Estimating global damages from sea level rise with the Coastal Impact and Adaptation Model (CIAM). *Clim Chang* 137(1-2):143–156
- Farr TG, Rosen PA, Caro E, Crippen R, Duren R, Hensley S, Kobrick M, Paller M, Rodriguez E, Roth L, Seal D (2007) The shuttle radar topography mission. *Rev Geophys* 45(2):RG2004
- Draper NR, Smith H (1998) *Applied regression analysis*. Wiley, New York, p 706

- Fowler MJ (2013) Declassified intelligence satellite photographs. Archaeology from historical aerial and satellite archives. Springer, New York, pp 47–66. https://doi.org/10.1007/978-1-4614-4505-0_4
- Ji L, Gallo K (2006) An agreement coefficient for image comparison. *Photogramm Eng Remote Sens* 72(7):823–833
- Jordà G (2014) Detection time for global and regional sea level trends and accelerations. *J Geophys Res Oceans* 119(10):7164–7174. <https://doi.org/10.1002/2014JC010005>
- Kaimaris D, Georgoula O, Karadedos G (2006) Historical maps and archaeological research. Proceedings of 8th national conference of cartography cartography and good leaving, Thessaloniki, Greece, November 2006, pp 51–62
- Kaimaris D, Patias P (2016a) Population estimation in an urban area with remote sensing and geographical information systems. *Int J Adv Remote Sens GIS* 5(6):1795–1812
- Kaimaris D, Patias P (2016b) Identification and area measurement of the built-up area with the Built-up Index (BUI). *Int J Adv Remote Sens GIS* 5(6):1844–1858
- Kopp RE, Horton RM, Little CM, Mitrovica JX, Oppenheimer M, Rasmussen DJ, Strauss BH, Tebaldi C (2014) Probabilistic 21st and 22nd century sea-level projections at a global network of tide-gauge sites. *Earth's Future* 2:383–406. <https://doi.org/10.1002/2014EF000239>
- Laws EA, Archie JW (1981) Appropriate use of regression analysis in marine biology. *Mar Biol* 65:13–16
- Li X (2005) A four-component efficiency index for assessing land development using remote sensing and GIS. *Photogramm Eng Remote Sens* 71(1):47–57
- Marzeion B, Levermann A (2014) Loss of cultural world heritage and currently in-habited places to sea-level rise. *Environ Res Lett* 9(3):034001
- Mielke Jr PW, Berry KJ, Landsea CW, Gray WM (1997) A single-sample estimate of shrinkage in meteorological forecasting. *Weather Forecast* 12:847–858
- Myint SW, Lam NS-N, Tyler JM (2004) Wavelets for urban spatial feature discrimination: comparisons with fractal, spatial autocorrelation, and spatial co-occurrence approaches. *Photogramm Eng Remote Sens* 70(7):803–812
- Patias P, Kaimaris D, Stylianidis E (2011) Change detection in historical city centers using multi-source data: the case study of historical center of Nicosia-Cyprus. Proceedings of the CIPA XXIII Symposium, Prague, Czech Republic, CIPA Archives for Documentation of Cultural Heritage, Vol XXIII-2011, ISBN 978-80-01-04885-6, CD
- Ricker WE (1980) Computation and use of central lines. *Can J Zool* 62:1897–1905
- Ramanathan R (1995) *Introductory econometrics with applications*. 3rd edn. Harcourt Brace College Publishers, Fort Worth, 800 p
- Robinson WS (1957) The statistical measurement of agreement. *Am Sociol Rev* 22(1):17–25
- Robinson WS (1959) The Geometric interpretation of agreement. *Am Sociol Rev* 24(3):338–345
- Rodríguez E, Morris CS, Belz JE, Chapin EC, Martin JM, Daffer W, Hensley S (2005) An assessment of the SRTM topographic products (p. 143). Technical Report JPL D-31639. Jet Propulsion Laboratory, Pasadena
- Mielke Jr PW (1991) The application of multivariate permutation methods based on distance functions in the earth science. *Earth-Sci Rev* 31:55–71
- Shekhar S (2004) Urban sprawl assessment entropy approach. *GIS Dev* 8(5):43
- Stamnas A (2013) Temporal study of geometric and cartographic features of Thessaloniki's refugee settlements (Greece) using photogrammetric and cartographic methods and aiming their spatial documentation and classification. PhD Thesis, Aristotle University of Thessaloniki, Greece (in Greek), pp 47, 49, 52, 55, 88–93
- Stoney W (2007) ASPRS guide to land imaging satellites, www.asprs.org
- Sun W, Xu G, Gong P, Liang S (2006) Fractal analysis of remotely sensed images: a review of methods and applications. *Int J Remote Sens* 27(22):4963–4990
- Tachikawa T, Kaku M, Iwasaki A, Gesch DB, Oimoen MJ, Zhang Z, Danielson JJ, Krieger T, Curtis B, Haase J, Abrams M (2011) ASTER global digital elevation model version 2-summary of validation results. NASA

- Tadono T, Ishida H, Oda F, Naito S, Minakawa K, Iwamoto H (2014) Precise global DEM generation by Alos Prism. *ISPRS Ann Photogramm Remote Sens Spat Inf Sci* 2(4):71
- Tadono T, Nagai H, Ishida H, Oda F, Naito S, Minakawa K, Iwamoto H (2016) Generation of the 30 M-Mesh global digital surface model by Alos Prism. *Int Arch Photogramm Remote Sens Spat Inf Sci* 41:157–162
- Tøttrup C (2014) EU-DEM statistical validation report, DHI GRAS c/o Geocenter Denmark
USGS Fact sheet 2008-3054, 2008. <https://pubs.usgs.gov/fs/2008/3054/pdf/fs2008-3054.pdf>
- UNESCO World Heritage Centre, Case studies on climate change and World Heritage. ISBN 978-92-3-104125-9, 2007
- Wardell-Johnson G, Schoeman D, Schlacher T, Wardell-Johnson A, Weston MA, Shimizu Y, Conroy G (2015) Re-framing values for a World Heritage future: what type of icon will K'gari-Fraser Island become?. *Australasian Journal of Environmental Management* 22(2):124–148
- Willmott CJ, Ackleson SG, Davis RE, Feddema JJ, Klink KM, Legates DR, O'Donnell J, Rowe CM (1985) Statistics for the evaluation and comparison of models. *J Geophys Res* 90(C5):8995–9005
- Wu S-S, Xu B, Wang L (2006) Urban land-use classification using Variogram-based analysis with an aerial photograph. *Photogramm Eng Remote Sens* 72(7):813–822

Interpreting Archaeological Features on the Wieprza River Floodplain, West Pomerania, Poland



Lukasz Banaszek and Włodzimierz Rączkowski

Abstract Application of remote sensing techniques in archaeology makes both the detection of new features and the rethinking of previous results possible. Additionally, integration of heterogeneous datasets provides better means of understanding past landscapes. However, similarities between anthropogenic structures and natural landforms hamper interpretation. In this paper, we present some interpretative difficulties related to the integration of data acquired by means of different prospection methods. We use a case study of the middle Wieprza River basin to discuss the role of archaeological pre-understanding and the challenging location of sites within a fluvial landscape. We demonstrate that distinction between natural and anthropogenic features is conditioned by the characteristics of the studied area and the capabilities of the applied methods to represent archaeological information.

Keywords Archaeology · Airborne laser scanning · Aerial reconnaissance · Interpretation · Floodplain relief · Wieprza River

Introduction

Settlement pattern and landscape studies in the middle Wieprza River basin (Fig. 1) have been ongoing since the 1980s (Rączkowski 1998), and several archaeological prospection methods have been applied in this area. Subsequently to field-walking surveys, aerial reconnaissance was employed (Rączkowski 1995), whereas a few sites were investigated by means of near-surface geophysics and terrestrial lidar

Ł. Banaszek (✉)

Historic Environment Scotland, Edinburgh, United Kingdom

Institute of Archaeology, Adam Mickiewicz University, Poznań, Poland

e-mail: lukasz.banaszek@hes.scot

W. Rączkowski (✉)

Institute of Archaeology, Adam Mickiewicz University, Poznań, Poland

e-mail: wlodekra@amu.edu.pl

© Springer Nature Switzerland AG 2020

D. G. Hadjimitsis et al. (eds.), *Remote Sensing for Archaeology and Cultural Landscapes*, Springer Remote Sensing/Photogrammetry,

https://doi.org/10.1007/978-3-030-10979-0_12

203

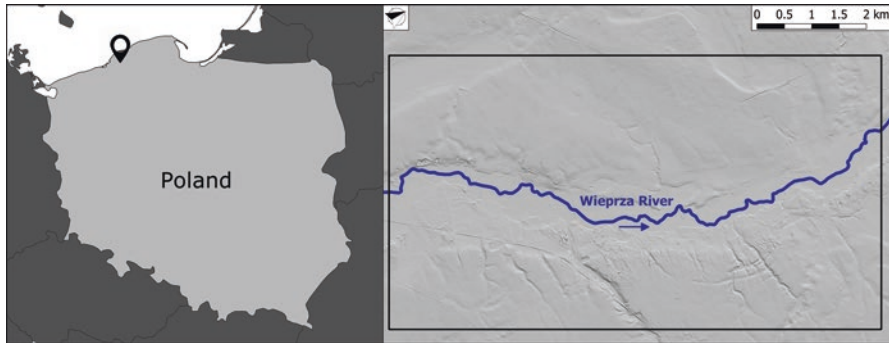


Fig. 1 Location of the study area

(Banaszek and Wróblewska 2013; Rączkowski et al. 2013). Additionally, airborne laser scanning (ALS) and satellite imagery served the interpretation on a landscape level (Banaszek 2015; Ruciński et al. 2015).

Noteworthy, the use of different prospection methods requires more than just a straightforward interpretation of isolated datasets. Instead of simply comparing the results, these numerous and heterogenic data have to be put together and contrasted (Rączkowski 2006; Salisbury et al. 2013). A divergence of outputs should not be taken as a reason to disqualify any particular method. Quite the opposite, such a situation should encourage archaeologists to seek deeper understanding of the applied procedures, and the processes of knowledge construction (Halliday 2013; Michalik 2014). In this position, we share the perspectives in contemporary archaeology, which are critical of the existence of any ultimate and conclusive method (Trigger 2007). Archaeological techniques are tied up with cultural discourse, and all should be understood as cultural activities and, thus, subjective approaches. Hence, a convergence of the results (interpretative outcomes) obtained by means of different methods does not confirm any ultimate ‘truth’. Indeed, it may be no more than pure coincidence. Nevertheless, there is a difference between good and bad interpretation (Doneus and Kühnle 2013).

In this paper, we demonstrate particular interpretative difficulties for the integration of various sources of archaeological prospection data. New, complex and distinctive datasets shed light on additional aspects of the analysed landscape; however, these give rise to a number of doubts, and a case study of the middle Wieprza River basin illustrates the problem. Although subsequent prospection methods provided new details concerning anthropogenic structures, we believe that archaeological pre-understanding is the lifeblood of any interpretation. Here, we discuss the challenging location of archaeological features within the fluvial landscape. We demonstrate that distinction between natural and anthropogenic features is conditioned by characteristics of the studied area as well as the capabilities of the applied methods to represent archaeological information. Thus, although individual objects are recorded within the analysed datasets, their recognition is a complex phenomenon.

The Archaeology of the Wieprza Floodplain: Issues of Traditional Approaches

Polish archaeologists often recognise field-walking survey of ploughed land looking for artefacts as the most reliable prospection technique (Rączkowski 2011). However, the method has been barely used in fluvial areas, and even if it was, no significant results would have been expected for two reasons. Firstly, the complexity of the alluvial environment (Bridge 2005) seems to be a serious challenge, and a pedestrian survey in such unfriendly environs does not appeal to the researchers.

Secondly, if earthworks are not being recorded, only artefacts that could have been collected will allow archaeologists to define a site (Mazurowski 1980). However, no archaeological material is to be found on the ground surface unless either ploughing or other activities bring them to the top. Since many floodplains have not been cultivated recently, in this case it is only animal activities (e.g. molehills, rooting in turf by wild boar) and water system maintenance (drainage and riverbed regulation) that might bring the material to the surface. In most cases, though, the regulation took place some time ago, whilst dredging of the riverbed happens rarely. For instance, Wieprza River (Fig. 2) was regulated mainly between 1900 and 1920 (Florek 2002), long before the first pedestrian survey, which happened in 1981. Additionally, unlike ploughing, the character of water system maintenance is linear. Whilst molehills appear very often and in different places every year, their activity is also restricted and on a much localised scale. Therefore, encountering of archaeological finds on floodplains is less likely than in arable lands.

Even though several field-walking surveys in the middle Wieprza River basin purposely included the Holocene floodplain, no significant archaeological data concerning the fluvial environment have been acquired. As a result, only the numerous levelled sites that are scattered across the arable moraine uplands of the region have been detected along with abundant barrows located in the woodland. To date, in the immediate vicinity of the river, only two medieval complexes have been recognised (Fig. 3): a structure in Sławsko occupied between the tenth and fifteenth centuries AD

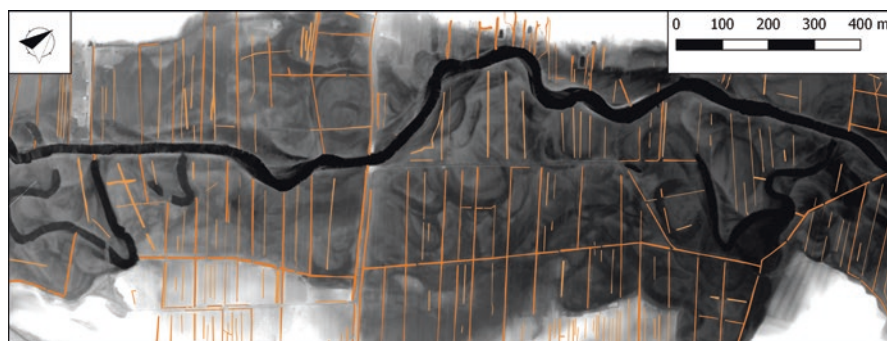


Fig. 2 Drainage brought order and regularity to the floodplain, with straightening of the Wieprza River major trunk stream

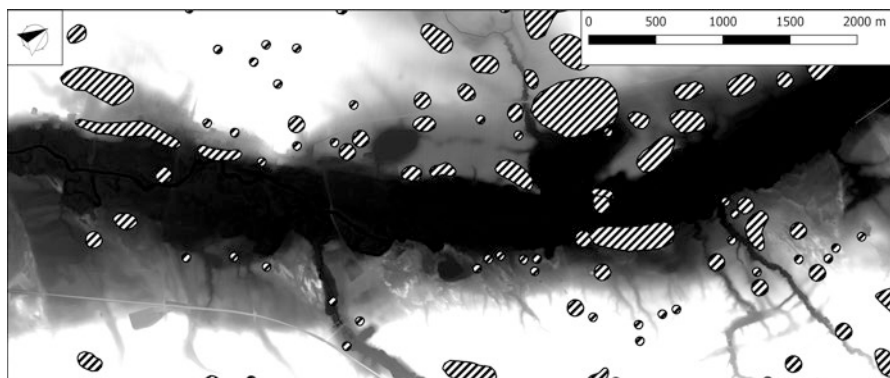


Fig. 3 Does this distribution of evidence for settlement in the middle Wieprza basin represent the remains of a settlement pattern or is it the result of field-walking prospection limits? The locations of archaeological sites as hatched polygons are shown against the background of an ALS-derived DTM. Notice the height difference between the Holocene floodplain (the darkest area), the Pleistocene terrace (greyish strips on the both sides of the Holocene plain) and the moraine uplands (white regions), and the varying disposition of archaeological sites across these zones

and a stronghold in Wrześnica of eighth and ninth/tenth century AD date (Łosiński et al. 1971; Rączkowski and Sikorski 1996). Yet, both these fortified sites had been archaeologically recorded already in nineteenth century (Skrzypek 2008), and, by means of field-walking survey, some archaeological finds have been identified only in one new location on the floodplain. Found upstream of the fortified site in Wrześnica, these were interpreted as the remains of an open settlement contemporary with the stronghold. A number of potsherds were discovered in molehills, whilst some others were collected from a layer of sand deposited on the surface from dredging which had taken place a few months earlier. Noteworthy, the finds were due to two independent factors: firstly, intensive and repeated investigation in the immediate vicinity of the stronghold, which eventually brought unexpected results; and secondly, the survey was luckily performed a short time after the occasional dredging. Thus, the discovery was caused by a combination of consistent research decisions (potsherds were identified because of regular surveys) and purely coincidental factors (the dredging conducted short time before the survey).

Due to the discovery, one should expect further archaeological evidence within the Holocene floodplain. However, the results of excavations that took place in the 1990s near the fortified site in Wrześnica to some extent explain the limitations of the field-walking surveys. Remains of a timber-paved road and a possible pier, which were found outside the stronghold, were clearly covered by a layer of flood deposits that accumulated since the Early Middle Ages, when the accelerating deforestation intensified soil erosion by water (Kaczmarzyk et al. 2008). The layer is omnipresent along the floodplain, including within the interior of the fortified site in Wrześnica. Its thickness is typically 20–60 cm, and unsurprisingly, it is greater wherever negative relief features (swales on point bars, palaeochannels, tributary channels and irregular depressions) are located. Silty sands were being deposited

due to frequent and presumably annual inundation of the Holocene plain (Florek et al. 1998), in a pattern that would have continued as a matter of routine if the river was not regulated. Today, only very occasionally do the gradually rising waters cover (in a non-violent manner) broader areas of the Holocene plain.

Alternative Approach to Prospecting the Fluvial Environment of Wieprza River

It is clear that further field-walking surveys are not going to bring any significant change in understanding the fluvial landscape. Both, the cultural and environmental factors, which were described above, cause that the traditional survey strategy is inappropriate for such an environment. Thus, the patterning of the evidence for past settlement in the middle Wieprza River basin (Fig. 3) is not a result of decisions made in the past. Rather it is the outcome of biased traditional data collection strategy (Cowley 2013). Therefore, a question has to be asked whether the use of remote sensing techniques would bring any improvement and recognition of features that not necessarily draw the attention of pedestrian prospection. After all, strong tradition of field-walking in Poland induces particular research interest, classification and terminology (Rączkowski 2005; Cowley 2016). On the one hand, there is a serious need to develop knowledge about the young fluvial landscape, which is traditionally marginalised. On the other hand, acquisition of new information, which would allow interpretation of multifaceted past actions on floodplains, is prerequisite.

Aerial Reconnaissance: Improved Understanding and Further Bias

Several observer-directed aerial reconnaissance campaigns have covered the study area, yet only a limited number of archaeological features have been identified. These poor results are due to several independent factors. Firstly, nearly all flights took place in late June and July. In general, at this time variegation in crops due to vegetation stress should already be noticeable, whilst harvest yet not started. However, due to its proximity to the Baltic Sea, the study area enjoys a relatively mild climate, and usually damp summers (Table 1). Hence, the occurrence of cropmarks in such conditions is less likely (Cowley 2015). Secondly, poor postglacial Pomeranian soils are vastly uncultivated, whilst crop types, which are resistant to stress, are often planted in the arable lands (Wilson 2000). Thirdly, even if some faint marks occurred, they might be omitted since observer-directed reconnaissance was being undertaken, and oblique photographs were taken only if the archaeologist had observed any marks from the air (Palmer 2005; Rączkowski 1999). In this context, all of the identified cropmarks are situated within arable uplands, whilst no

Table 1 A comparison of the soil moisture deficit that was registered in the middle Wieprza River basin and maximum values noted in the same time (May 21 – July 20) in Poland. © Institute of Soil Science and Plants Cultivation in Puławy (<http://www.susza.iung.pulawy.pl/KBW> accessed October 6, 2016)

Year	Soil moisture deficit values in the study area (mm)	Maximum value of the soil moisture deficit index in Poland (mm)
2016	> -50	-179 to -170
2015	-119 to -110	-179 to -170
2014	-139 to -130	-189 to -180
2013	> -109 to -100	-129 to -120
2012	> -50	-119 to -110
2011	-109 to -100	-179 to -170
2010	-169 to -160	-239 to -230
2009	> -50	-69 to -60

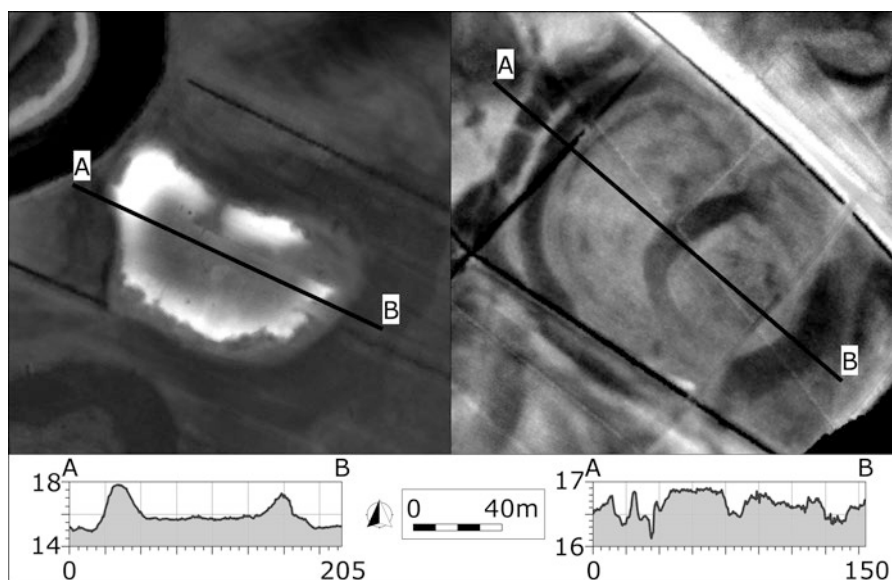


Fig. 4 Remains of the fortified site in Wrześnica embankments are clearly visible against the negative relief of Wieprza River floodplain, whereas in Sławsko only slight relief differences are to be noticed. ALS-derived DTM, profile distance and height in metres

new sites were detected across the damp and grassy fluvial environment. Nevertheless, being recorded earlier, the two strongholds located within the floodplain were photographed from the air.

In the case of Wrześnica, the preserved ramparts are relatively straightforward to interpret (Fig. 4), whereas in Sławsko no significant earthworks can be observed today. However, one should expect some relief features, whilst a former princely seat is being investigated, and slight remains of an annular structure (Fig. 5a) were identified in the 1960s (Łosiński et al. 1971). In July 1996, intensive precipitation

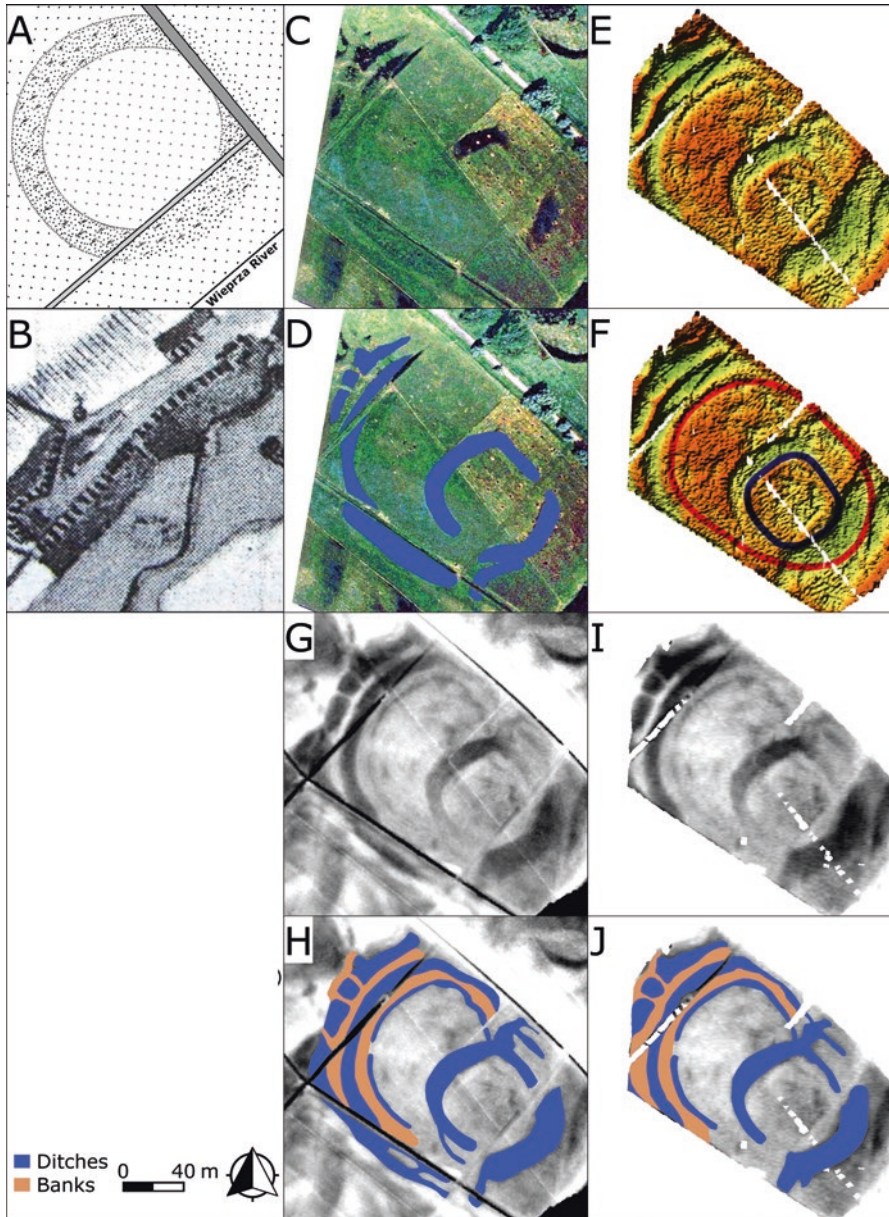


Fig. 5 Different approaches to the site in Slawsko resulted with alternative interpretations. (a) Site extent (Łosiński et al. 1971). (b) Double ramparts illustrated on the Schmettausches Karten (out of scale). (c, d) Rectified oblique aerial photography and its interpretation. (e, f) The 2011 DTM and the site extent interpretation (Rączkowski et al. 2013). (g, h) ALS-derived DTM and its interpretation. (i, j) Reprocessed and reinterpreted 2011 DTM

caused the increase of the water level and highlighted various negative relief features within the floodplain as watermarks, and amongst palaeochannels of Wieprza River, the moats surrounding the princely seat got submerged (Fig. 5c, d). Whilst in the air, a small annular part of the stronghold was detected next to the Wieprza River. Due to its regularity, and thus similarity to the structure that had been documented nearly 30 years earlier, initially, it was assumed that the earlier archaeologists had misinterpreted the site location. However, later, during a desk-based assessment, features that were not perceived during the flight were derived from the photograph. Additional ring, most likely representing second moat, was attached to the central part of the site (Rączkowski 2008). It seems that, at least partially, a double ditch had surrounded the adjoining segment, since two parallel curved dips located westwards were under water when the photograph was taken.

Apparently, it is the larger enclosure that was partially identified during the 1960s survey, and, at the time, it was assumed that the missing section created a circle. Whilst only the smaller enclosure was identified during the aerial reconnaissance, luckily, the photograph included the remnants of the second segment of the fortified site. Since the outer moats in the west were not perceived from the airplane, identification of the entire site extent was a matter of a coincidence. If the photograph of the small part was taken from another angle, it might have not included the western ditches. Noteworthy, in the 1990s, analogue cameras were in use, and thus, the number of photographs that were taken during a single flight was limited, and each shot had to be legitimated. If the photograph did not include the outer moats, the site would be still understood as a simple, annular feature. Moreover, based on the photography, it could be assumed that earlier archaeologists had misinterpreted site location. In this case, deceitfully, the ‘objective’ photographic evidence could gain power over the enigmatic results of the interpretative mapping undertaken in the 1960s (Rączkowski 1999).

A few years later, previously inaccessible historic maps were analysed. Although no topographic features were noticed in Sławsko, when Messtischblätter map was created (1897), a simple, elevated and annular form is clearly visible on an Urmesstischblätter map (1831), with an earlier chart (Schmettausches Karten, 1767–1787) showing that additional, adjoining ring of ramparts was still observable (Fig. 5b) in the second half of the eighteenth century (Hinkel 1959). Therefore, interpretation of the photograph was confirmed by information derived from historic maps.

Tradition in Power

Discovery of the adjoining ring in Sławsko raises issues regarding data collection strategy and knowledge construction process. Firstly, one should ask whether the site would have been registered at all, if the remains of the ramparts had not been observable in nineteenth century. Analysis of historic maps shows that early archaeologists had noticed the elevated structure within the floodplain shortly

before it was levelled. At the time, available prospection methods were used to a limited extent, and researchers paid attention either to distinguishable earthworks or to sites located in arable lands, which were often incidentally detected by farmers (Trigger 2007). Therefore, it is very likely that the stronghold would not have been identified if the ramparts had been levelled before first archaeologists penetrated the area and/or the local community had not informed the researchers about the once existing earthworks. As a result, the survey conducted in the 1960s (Łosiński et al. 1971) would also presumably omit the indistinct site. The reasons are twofold: Polish archaeologists have not developed skills required to undertake elaborate topographic survey, as presented by, e.g. Gannon (1999), and the floodplain had not been studied for decades due to the limitations of traditional approach. Noteworthy, no archaeologist was present during the regulation of Wieprza River, what explicitly show the power of research tradition and its impact on the range of questions which may be approached (Rączkowski 2005).

Secondly, one should ask whether aerial photographs of the watermarks would have been taken if the site had not been registered in nineteenth century. Instant interpretation, which characterises observer-directed aerial reconnaissance and causes taking photographs of the spotted marks, limits acquired data (Verhoeven and Sevara 2016). In the case of site not being registered, unless the flight director had immediately identified the moats, there would be no photographs to assess afterwards. Since submerged remains of former moats are nearly indistinguishable from other negative relief features within the floodplain, detecting them from the air is a challenge (Fig. 6). After all, the moats were constructed most likely by rearrang-



Fig. 6 Complexity of negative relief features within floodplains is challenging for observer undertaking aerial reconnaissance. (Photograph by W. Rączkowski)

ing palaeochannels, and the second segment was not identified during the flight, yet whilst the aerial photography sorties were interpreted. Area coverage could provide photos for desk-based assessment and thus eliminate the pitfalls of subjective visual experience, which characterises observer-directed aerial reconnaissance (Verhoeven and Sevara 2016); however, in case of Pomerania, such attempts have never been made.

Thirdly, the case study of the stronghold in Sławsko clearly shows the immense potential of archaeological information kept in the archives (Cowley and Stichelbaut 2012). The adjoining ring of ramparts is marked on historic maps; however, the information could be derived only after the access to these resources was opened. Noteworthy, many archives are still inaccessible, and the ongoing declassification will undoubtedly trigger further discoveries (Fowler 2016). The historic maps demand critical examination (Kiarszys 2016), yet undoubtedly, archives should be assessed whenever possible (Burks 2010).

Geophysical Prospection and Topographic Survey: Site Level Approach

In 2011, the strongholds in Sławsko and Wrześnica were surveyed by means of Bartington 601 dual fluxgate gradiometer and Magmapper G858 caesium magnetometer combined with a GPS RTK unit (Rączkowski et al. 2013). Geophysical and height data were used to determine location, depth, character and preservation state of the remains, and based on these, the site's structure was interpreted. A new linear feature running parallel to the external moats was identified in Sławsko (Fig. 5e, f), and it was assumed that it limited the site in north and west. In general, the survey confirmed information derived from aerial photographs; however, it is discussed in the following section that the collected height data were partially misinterpreted.

Airborne Laser Scanning: Total Area Coverage Approach

ALS survey, which was undertaken for archaeological purposes in 2012 (Table 2), included arable lands and pastures, Wieprza River floodplain and woodland (Banaszek 2015). For the first time, a total area coverage approach substituted selective data collection strategies. Although the resulting dataset is not truly bias-free, its subjectivism is constant since laser beams do not discriminate cultural and natural aspects of the landscape (Banaszek 2014). As a result, beside areas, which were accessible for pedestrian surveys, and the selected parts of the land that were photographed from the air, the topography of the entire study area was examined.

Clearly, there are many factors that determine the way, in which airborne lidar data are being examined (Opitz and Cowley 2013). The interpretation results from a tension between the analysed data, eyes, mind, accumulated knowledge,

Table 2 Characteristic of the ALS survey and data

Survey date	April 26, 2012
Sensor	Riegl LMS-680i
Aircraft	Vulcanair P68 Observer
Flying height (m a.g.l.)	950
Laser frequency (kHz)	360
Wavelength (nm)	1550
Strip overlap (%)	60
Mean point density – last echo (pts/m ²)	12.15
Gridded derivatives resolution (m)	0.5

professional experience and research design, whereby working with ALS derivatives demands also a level of understanding the roles of data acquisition, processing and visualisation, as well as skills in reading the topography (Palmer 2013; Mlekuż 2013; Kokalj et al. 2013). Although developing best practices in dealing with airborne lidar data is important (Kokalj and Hesse 2017), to understand interpreter's background and to improve observation skills are equally required.

Noteworthy, in the case of middle Wieprza River basin, reading the ALS-derived digital terrain and surface models (DTM and DSM, respectively) was structured by previous approaches and prospection results that were discussed above. This fundamentally affected the interpretation, though such impact is unavoidable. If known to the interpreter, registered archaeological sites that are covered by airborne lidar force particular approach. Therefore, round barrows that were identified earlier in woodland drew immediately attention of DTM reader, whilst arable lands, where sites identified mainly due to field-walking surveys, were unsuccessfully examined in pursuit of earthworks. Needless to say, strongholds situated on the banks of Wieprza River were in the centre of interest.

Alike in the case of other prospection methods, the presence of well-preserved ramparts in Wrześnica decidedly makes them stand out against other features of the floodplain whilst interpreting ALS-derived DTM (Fig. 4). Thus, identification of the site does not demand serious interpretative skills. In fact, due to its characteristic form, location and state of preservation, the fortified site represents an example of deceptive thinking, according to which ALS derivatives are straightforward to read. Additionally, early medieval strongholds are amongst the iconic sites of Polish archaeology. These attract much attention, very often at the expense of other, less spectacular locations. Therefore, even if the site was somehow omitted by earlier archaeologists, it would have been most likely noticed either as a result of interpreting the 2012 ALS survey data or by other researchers immensely exploring the available national lidar dataset (Wroniecki et al. 2015).

Unquestionably, the capacity of ALS to represent subtle fluvial landforms depends on the resolution (Notebaert et al. 2009), and fortunately, in the case of middle Wieprza River basin, high-quality data have been collected (Table 2). Therefore, identification of various negative relief features within the floodplain was possible (Fig. 7). However, location and condition of the Sławsko stronghold in



Fig. 7 The maze of negative relief within the floodplain of the middle Wieprza River basin identified through interpretation of ALS data

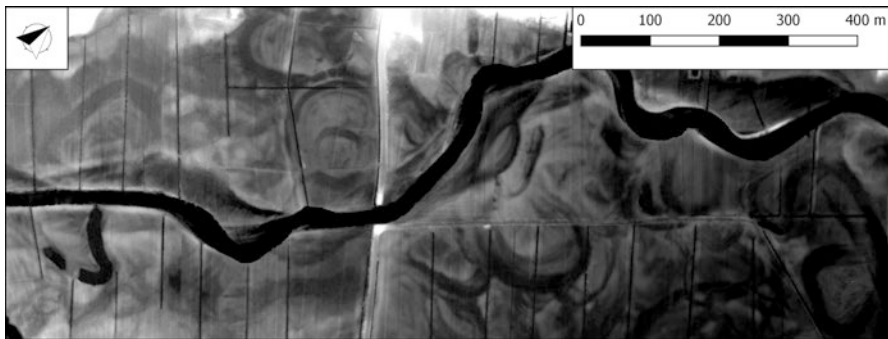


Fig. 8 The remains of the fortified site in Slawsko conceal themselves amongst the negative relief of Wieprza River floodplain

such a context illustrate an interpretative problem with the remotely acquired data. Undoubtedly, being aware of the site's presence made it to be distinguished from the surrounding maze of negative relief features within the floodplain. In this case, particular knowledge and experience played an important role and structured the interpretation. However, moats flanking both parts of the stronghold follow the course of the ancient river channels, and the topography of the site strongly resembles the omnipresent and natural remains of former oxbow lakes (Fig. 8). Thus, it is important to ask whether the site would be detected due to interpretation of ALS-derived DTM if it was not registered earlier. Definitely, it would require an experienced eye to discriminate it from natural negative relief features. However, unlike the case of the observer-based aerial reconnaissance, the area coverage approach makes that the data have already been collected and can be used on various occasions and the interpretation does not need to be made as quickly as during the observer-based reconnaissance flight. Hence, even if the stronghold was not identified immediately whilst interpreting ALS derivatives, it could be recognised during some other assessment that could be performed by an independent observer or for alternative purposes.

Besides highlighting the difficulty in separating archaeological earthworks from natural landforms, the stronghold in Sławsko illustrates that skills of reading the topography and 3D data are indispensable. The narrow ditch that was detected and partially understood as a site border during the surveying, which accompanied the geophysical prospection (2011), was examined in detail through interpretation of the ALS-derived DTM (2012) that was undertaken by a different archaeologist. Whereby the site extent drew by the geophysical surveying team presents an idealised and/or simplified picture, the ALS derivatives shows that the adjoined western sector resembles an oval indented at the south east corner (Fig. 5g, h). The most evident discrepancies are located in the northern and northeastern sector. Instead of drawing the site extent next to a modern causeway that leads towards a bridge over the Wieprza River, the narrow ditch curves sharply and joins the annular moat surrounding the central part of the princely seat.

Noteworthy, the same outline of the ditch was recorded in the height data collected in 2011 (Rączkowski et al. 2013), yet it was not properly identified at the time. However, after reading the ALS derivatives, previous data were re-examined (Fig. 5i, j), and thus, it became clear that the ditch was misinterpreted, most likely due to a few reasons. Firstly, as said above, studying topography has been underestimated in Polish archaeology, and researchers usually treat it without esteem. Although site topographic maps have been created, these have not been thoroughly studied. Secondly, the height data collection was not the main purpose of the 2011 survey, and thus it was not prioritised during processing and interpretation. Thirdly, the stronghold was not covered equally with GPS measurements since a few linear obstacles made some areas inaccessible. Actually, one fence cuts across the narrow ditch and made the DTM interpretation slightly more demanding. Fourthly, the 2011 height data seem to be more noisy than the classified ALS point cloud. Most likely, it is a result of the data collection strategy and the irregular surface of the meadow, where every step caused inclination of a GPS unit. Lastly, it seems that a simple hill-shade visualisation technique was used to interpret the DTM. Whilst illumination source was situated beyond top-left corner of the imagery, a part of the ditch that leads towards the annular moat surrounding the central sector of the site was occluded. Using alternative visualisation method (Challis et al. 2011a) could help to eliminate this bias; however, in this case, there is no evidence for using any other technique.

Besides investigating the relief of the princely seat in Sławsko, thanks to the area coverage approach, a desk-based assessment of the entire floodplain was undertaken, which resulted with a discovery of previously unknown archaeological earthworks. Presumably, these features are related to a historic road network, which used to cut the fluvial landscape. Possible remains of a causeway were identified few hundred metres from the stronghold in Sławsko (Fig. 9). Within the maze of palaeochannels and drainage system, a L-shaped object is located. Its shorter part is almost parallel to the contemporary riverbed and lies on an irregular, quasi-trapezoidal and slightly elevated platform, whereas the longer section runs across a former oxbow lake. It is clear that the feature was constructed intentionally and should not be understood as a natural deposit. Its shape and orientation is exceptional within the floodplain, where no other palaeochannel has been cut by an elevated strip of land.

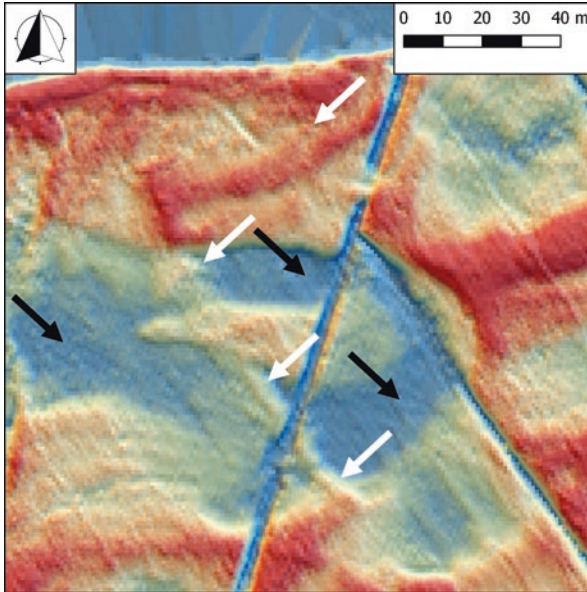


Fig. 9 Supposed relief remains of a causeway (white arrows) crossing a former oxbow lake (black arrows) of Wierpra River as visible in the ALS-derived DTM visualisation

Interpretation of the ALS derivatives gave also a significant, yet indirect, indicator of other roads within the floodplain. Moraine upland near the fortified site in Wrześnica is cut by a medieval route (Banaszek 2015). Although it leads towards the stronghold, the relief feature can be tracked only to a place where uplands meet the floodplain. Nevertheless, the course of the road, and the fact that the identified section was partly constructed as a causeway, suggests that the track was intentionally maintained. Hence, organic remains of a sunken causeway that could cut across the floodplain, and thus making an extension of the road towards the fortified site, are most likely to be hidden underneath the accumulated river deposits.

Discussion

Undoubtedly, fluvial landscape has far greater potential than the set of archaeological information that has been already extracted from it. However, the characteristics of the floodplain do not derive only from the data collected by the researchers. It is the archaeological pre-understanding that formulates the scope of this complex phenomenon. A contextualised set of theories, methods, questions to be answered and prospection traditions determines the scope of actions that are being performed to meet the actual research expectations. Depending on the background of an individual archaeologist, particular features are defined as interesting, whilst the others are left

unnoticed. Moreover, the fluvial landscape is a distinct area, where solutions that are successfully applied for other regions do not bring any significant evidence. Therefore, it has to be treated individually. Otherwise, it would remain a gap on archaeological map as it used to be from the limited field-walking perspective.

The case study of the middle Wieprza River basin illustrates some interpretative issues. Early archaeologists and the practice of the pedestrian survey developed a particular research and interpretative model. This caused a significant redundancy in the classification of past human activities performed in particular environments. Therefore, the gaps in the settlement pattern that are often situated within the river terraces should not be treated as the result of past human actions. On the contrary, these should be understood as a consequence of decisions made by the researchers. The practice clearly shows that continuous application of the same prospection method is not going to qualitatively alter our understanding of the past landscape. Therefore, to include previously marginalised areas into the scope of landscape studies is a serious challenge, and a profound change in approaching the subject of the research is required.

We demonstrated that archaeological pre-understanding is a crucial aspect of any research. A conscious and experienced mind is required to identify the archaeological features and extract them from other objects within the analysed landscape. Both the natural structures and the results of the contemporary human actions constitute a puzzle in which individual elements intertwine, and untangling such a knot is a challenge.

Although nearly levelled, the former princely seat in Sławsko resembles in plan the other early medieval strongholds scattered across Pomerania (Łosiński et al. 1971). However, due to its condition, the site is an excellent example showing that although archaeological information is being recorded within different datasets, it is the matter of human mind to extract it from other palaeoenvironmental features. This mind has to be aware of deceitfulness of the acquired data, processing methods and archaeological practice. It is hard to say how many other sites like Sławsko have not yet been registered and are hidden within floodplains. However, undoubtedly, these will not be identified without an experienced interpreter, and if the problem is going to be approached traditionally.

Moreover, we illustrated that the maze of negative relief features on the Wieprza River floodplain can be deciphered. It might be useful in planning further surveys (Carey et al. 2006), which, instead of taking the whole area into account, would focus on slightly elevated and thus dryer spots and platforms that were not cut by any noticeable palaeochannel. Such information can be treated as an indicator to predict areas, where archaeological finds are more likely to be detected on ground surface if mole or drainage activity occurs, and if, actually, any settlement took place within the floodplain. In this sense, the use of ALS data would be quite different from detecting spots that are characterised by greater moisture as it is investigated through the ALS intensity data (Challis et al. 2011b, c). Therefore, the proposed usage of airborne lidar derivatives would rather focus on knowledge-based mapping of the areas within the floodplain where settlement was more likely to happen.

Acknowledgements The authors are indebted to Dave Cowley for his comments on the early draft of the paper. This research was sponsored by Polish Ministry of Science and Higher Education through the Mobility Plus program (1088/MOB/2013/0). Data discussed in the text were collected due to a financial support provided by the Ministry of Science (N N109 160 140) and the Ministry of Culture and National Heritage (1548/11) of the Republic of Poland, as well as thanks to the EU sponsored ArchaeoLandscapes Europe project (2010-1486/001-001).

References

- Banaszek Ł (2014) Lotniczy skaniny laserowy w polskiej archeologii. Czy w pełni wykorzystywany jest potencjalny prospekcyjny metody? *Folia Praehistorica Posnaniensia* 18:481–525
- Banaszek Ł (2015) *Przeszłe krajobrazy w chmurze punktów*. Wydawnictwo Naukowe UAM, Poznań
- Banaszek Ł, Wróblewska L (2013) Teledetekcja archeologicznych krajobrazów Ziemi Sławieńskiej. In: Rączkowski W, Sroka J (eds) *Historia i kultura Ziemi Sławieńskiej*, T. 11, Ośrodki miejskie. Fundacja Dziedzictwo, Darłowo-Sławno, pp 45–79
- Bridge JS (2005) *Rivers and floodplains: forms, processes, and sedimentary record*. Blackwell Publishing, Malden-Oxford-Carlton
- Burks J (2010) Rediscovering prehistoric earthworks in Ohio, USA: it all starts in the archives. In: Cowley DC, Standring RA, Abicht MJ (eds) *Landscapes through the lens: aerial photographs and historic environment*. Oxbow Books, Oxford, pp 77–87
- Carey CJ et al (2006) Predictive modelling of multiperiod geoarchaeological resources at a river confluence: a case study from the Trent-Soar, UK. *Archaeol Prospect* 13:241–250
- Challis KC, Forlin P, Kinsey M (2011a) A generic toolkit for the visualization of archaeological features on airborne LiDAR elevation data. *Archaeol Prospect* 18:279–289
- Challis KC, Carey CJ et al (2011b) Airborne lidar intensity and geoarchaeological prospection in river valley floors. *Archaeol Prospect* 18:1–13
- Challis KC, Carey CJ et al (2011c) Assessing the preservation potential of temperate, lowland alluvial sediments using airborne lidar intensity. *J Archaeol Sci* 38:301–311
- Cowley DC (2013) What kind of gaps? Some approaches to understanding bias in remote sensing data. In: Ceraudo G (ed) *Archeologia aerea*, vol 7. Claudio Grenzi Editore, Foggia, pp 76–88
- Cowley DC (2015) Aerial photographs and aerial reconnaissance for landscape studies. In: Chavarría Arnau A, Reynolds A (eds) *Detecting and understanding historic landscapes*. SAP Società Archeologica s.r.l., Mantova, pp 37–66
- Cowley DC (2016) What do the patterns mean? Archaeological distributions and bias in survey data. In: Forte M, Campana S (eds) *Digital methods and remote sensing in archaeology*. Archaeology in the age of sensing. Springer, Cham, pp 147–170
- Cowley DC, Stichelbaut BB (2012) Historic aerial photographic archives for European archaeology. *Eur J Archaeol* 15(2):217–236
- Doneus M, Kühleiber T (2013) Airborne laser scanning and archaeological interpretation – bringing back the people. In: Opitz R, Cowley D (eds) *Interpreting archaeological topography. 3D data, visualisation and observation*. Oxbow Books, Oxford, pp 32–50
- Florek W (2002) Geomorfologiczne walory doliny Wieprzy w rejonie Sławska i Staniewicz. In: Rączkowski W, Sroka J (eds) *De rebus futuris memento: przyszłość przeszłego krajobrazu kulturowego Ziemi Sławieńskiej*. Fundacja Dziedzictwo, Sławno, pp 151–165
- Florek E, Florek W, Kaczmarzyk J (1998) Studia nad paleohydrologicznymi zmianami koryta Wieprzy i jej równi zalewowej w okresie subatlantyckim w kontekście funkcjonowania wczesnośredniowiecznego grodziska we Wrześnicy. In: Dworaczyk M, Krajewski P, Wilgocki E (eds) *Acta Archaeologica Pomoranica*, T. 1, XII Sesja Pomorzoznawcza, Szczecin 23-24 października 1997 r. Materiały. Stowarzyszenie Naukowe Archeologów Polskich, Szczecin, pp 185–194

- Fowler MJF (2016) The archaeological potential of declassified HEXAGON KH-9 panoramic camera satellite photographs. *AARG News* 53:30–36
- Gannon AR (1999) Challenging the past: the resurvey of Braidwood Hillfort. In: Frodsham P, Topping P, Cowley DC (eds) 'We were always chasing time.' Papers presented to Keith Blood. *Northern Archaeology* 17/18, pp 105–111
- Halliday S (2013) I Walked, I Saw, I Surveyed, but what did I see?... and what did I survey? In: Opitz RS, Cowley DC (eds) *Interpreting archaeological topography. 3D data, visualisation and observation*. Oxbow Books, Oxford, pp 63–75
- Hinkel H (ed) (1959) *Historischer Atlas von Pommern*. Böhlau, Köln-Graz
- Kaczmarzyk J, Florek W, Olszak IJ (2008) Górnoholocięskie i współczesne formy i osady pozakorytowe w dolinie środkowej Wieprzy. *Landform Anal* 7:80–94
- Kiarszys G (2016) Why are maps often misleading about archaeological sites. In: Ivanišević V et al (eds) *Recovering lost landscapes*. Institute of Archaeology in Belgrade, Aerial Archaeology Research Group, Belgrade, pp 21–34
- Kokalj Ž, Hesse R (2017) Airborne laser scanning raster data visualization. A guide to good practice. Založba ZRC, Ljubljana
- Kokalj Ž, Zakšek K, Oštir K (2013) Visualizations of lidar derived relief models. In: Opitz RS, Cowley DC (eds) *Interpreting archaeological topography. 3D data, visualisation and observation*. Oxbow Books, Oxford, pp 100–114
- Łosiński W, Olczak J, Siuchniński K (1971) Źródła archeologiczne do studiów nad wczesnośredniowiecznym osadnictwem grodowym na terenie województwa koszalińskiego, T. 4. Wydawnictwo Naukowe UAM, Poznań
- Mazurowski R (1980) *Metodyka archeologicznych badań powierzchniowych*. Powszechnie Wydawnictwo Naukowe, Warszawa-Poznań
- Michalik T (2014) Between the eye and the mind. Technology, cognition and knowledge development – eye-tracking study report. *AARG News* 48:24–34
- Mlekuż D (2013) Skin deep: LiDAR and good practice of landscape archaeology. In: Corsi C, Słapšak B, Vermeulen F (eds) *Good practice in archaeological diagnostics*. Springer, Cham, pp 113–129
- Notebaert B et al (2009) Qualitative and quantitative applications of LiDAR imagery in fluvial geomorphology. *Earth Surf Process Landf* 34:217–231
- Opitz RS, Cowley DC (2013) Interpreting archaeological topography: lasers, 3D data, observation, visualisation and application. In: Opitz RS, Cowley DC (eds) *Interpreting archaeological topography. 3D data, visualisation and observation*. Oxbow Books, Oxford, pp 1–12
- Palmer R (2005) If they used their own photographs they wouldn't take them like that. In: Brophy K, Cowley DC (eds) *From the air: understanding aerial archaeology*. Tempus, Stroud, pp 94–116
- Palmer R (2013) Reading aerial images. In: Opitz RS, Cowley DC (eds) *Interpreting archaeological topography. 3D data, visualisation and observation*. Oxbow Books, Oxford, pp 76–87
- Rączkowski W (1995) Aerial archaeology and the study of settlement systems: some examples from the Middle Pomerania (Poland). In: Kunow J (ed) *Luftbild archaeologie in Ost- und Mitteleuropa*. Forschungen zur Archaeologie im Land Brandenburg, vol. 3. Brandenburgisches Landesmuseum für Ur- und Frühgeschichte, Potsdam, pp 265–270
- Rączkowski W (1998) Między programem a przypadkiem: badania osadnictwa w dorzeczu środkowej Wieprzy. In: Dworaczek M, Krajewski P, Wilgocki E (eds) *Acta Archaeologica Pomoranica*, T. 1, XII Sesja Pomorzoznawcza, Szczecin 23–24 października 1997 r. Materiały. Stowarzyszenie Naukowe Archeologów Polskich, Szczecin, pp 157–165
- Rączkowski W (1999) Power of image: some ideas on post-processual aerial archaeology. *AARG News* 19:10–14
- Rączkowski W (2005) Tradition in power: vicious circle(s) of aerial survey in Poland. In: Brophy K, Cowley DC (eds) *From the air: understanding aerial archaeology*. Tempus, Stroud, pp 151–167
- Rączkowski W (2006) Towards integration: two prospection methods and some thoughts. In: Campana S, Forte M (eds) *From space to place. 2nd international conference on Remote Sensing in Archaeology*. Proceedings of the 2nd international workshop, CNR, Rome, Italy, December 4–7, 2006, pp 203–205

- Rączkowski W (2008) Antropogeniczne formy krajobrazowe powstałe w pradziejach i wczesnym średniowieczu w dorzeczu środkowej Wieprzy. *Landform Anal* 7:143–153
- Rączkowski W (2011) Integrating survey data – the Polish AZP and beyond. In: Cowley DC (ed) *Remote sensing for archaeological heritage management. Proceedings of the 11th EAC heritage management symposium, Reykjavik, Iceland, 25–27 March 2010. Europae Archaeologia Consilium, Association Internationale sans But Lucratif, Siège Social, Brussels*, pp 153–160
- Rączkowski W, Sikorski A (1996) Datowanie grodziska wczesnośredniowiecznego we Wrześnicy, gm. Sławno, stan. 7. *Geochronometria* 14:169–181
- Rączkowski W et al (2013) Sławsko – the prince’s worthy seat? Non-invasive archaeological surveys. In: Neubauer W et al (eds) *Archaeological prospection, proceedings of the 10th international conference – Vienna. Ludwig Boltzmann Institute, Austrian Academy of Sciences Press, Vienna*, pp 77–79
- Ruciński D, Rączkowski W, Niedzielko J (2015) A Polish perspective on optical satellite data and methods for archaeological sites prospection. In: Hadjimitsis DG et al (eds) *Proceedings of the SPIE 9535, third international conference on Remote Sensing and Geoinformation of the Environment (RSCy2015), 95350U, June 19, 2015*, pp 1–8
- Salisbury RB, Bertók G, Bácsmegi G (2013) Integrated prospection methods to define small-site settlement structure: a case study from Neolithic Hungary. *Archaeol Prospect* 20:1–10
- Skrzypek I (2008) Najdawniejsze dzieje gminy Sławno. In: Rączkowski W, Sroka J (eds) *Historia i kultura Ziemi Sławieńskiej. T. 8, Gmina Sławno. Fundacja Dziedzictwo, Sławno*, pp 109–183
- Trigger B (2007) *A history of archaeological thought. Cambridge University Press, Cambridge*
- Verhoeven GJJ, Sevara C (2016) Trying to break new ground in aerial archaeology. *Remote Sens* 8(918):1–29
- Wilson DR (2000) *Air photo interpretation for archaeologists. The History Press, London*
- Wroniecki P, Jaworski M, Kostyrko M (2015) Exploring free lidar derivatives. A user’s perspective on the potential of readily available resources in Poland. *Archaeol Pol* 53:612–616

Towards Early Warning for Damages to Cultural Heritage Sites: The Case of Palmyra



Daniele Cerra and Simon Plank

Abstract The intentional damage to local cultural heritage sites carried out in recent months by the Islamic State has received wide coverage from the media worldwide, raising the awareness for the need of prompt, safe, non-invasive damage detection and assessment surveys. Earth observation data represents the only reliable, non-invasive information source in areas which are not accessible due to conflicts or natural disasters. In order to provide a fast response, automated image processing techniques are needed to speed up the analysis. This chapter shows a comprehensive case of study for damage detection and monitoring in time through a series of satellite images acquired over the city of Palmyra, Syria, which suffered huge losses related to its cultural heritage in a time span longer than a year. Maps highlighting potential damages are derived from robust change detection techniques, based on changes in the textural features characterizing pre- and post-disaster satellite data. Such information could help experts at timely assessing the damages to cultural heritage sites of interest, and a chronological study of the different damages can be produced if a satellite image time series is available on the site of interest. Furthermore, the idea of marking sensitive areas characterized by different criticality is introduced: early damage detection routines could thus be restricted to the most important or threatened sites or expanded to larger areas or surrounding urbanizations. For this purpose, a pair of images acquired on the city of Sirwah, Yemen, are analysed, and the change detection results are discussed in this frame.

Keywords Cultural heritage · Palmyra · Earth observation monitoring · Change detection techniques · Damage assessment

The original version of this chapter was revised. The correction to this chapter is available at https://doi.org/10.1007/978-3-030-10979-0_17

D. Cerra (✉) · S. Plank
Earth Observation Center (EOC), German Aerospace Center (DLR), Münchner str. 20,
Weßling, Germany
e-mail: Daniele.Cerra@dlr.de

© Springer Nature Switzerland AG 2020
D. G. Hadjimitsis et al. (eds.), *Remote Sensing for Archaeology and Cultural Landscapes*, Springer Remote Sensing/Photogrammetry,
https://doi.org/10.1007/978-3-030-10979-0_13

221

Introduction

When the Islamic State (IS) was rumoured in the media to have destroyed cultural heritage (CH) sites in Syria—in particular in the city of Palmyra—the sites of interest were inaccessible to any legal authority in order to confirm the damage through an in situ visual inspection by traditional means. Therefore, the Orient Department of the German Archaeological Institute (DAI) tasked the experts of the remote sensing department of the German Aerospace Center (DLR) to assess any damage using high-resolution satellite data. A visual analysis confirmed the destructions claimed by the IS, confirming damages to the Temple of Bel and several tower tombs within Palmyra's ancient necropolis (Plank et al. 2015). The availability of high-resolution satellite images is steadily increasing, along with their quality and temporal resolution. Remote sensing is therefore capable of providing the only non-invasive way of observing and recording changes in the archaeological landscape for conflict areas and inaccessible sites (Lasaponara and Masini 2011).

If several images of the same site are available, of which at least one acquired before a given event and one afterwards, a change detection analysis can be carried out to assess the damages caused by a natural disaster or as a consequence of human conflicts. Usually such task is performed by visually verifying the integrity of critical sites and relevant infrastructures in the area of interest. Whenever the affected area is large and a rapid response is desired, however, this manual approach presents several drawbacks. On the one hand, it becomes a difficult and time-consuming activity; on the other hand, damaged areas could remain undetected for an observer, if the time available for the analysis is limited. Therefore, an approach with a certain degree of automation would be preferable.

Automatic analysis of Earth observation (EO) data has been successfully employed for several archaeological applications, especially the systematic detection of CH sites. In Lasaponara and Masini (2007), pan-sharpened multispectral QuickBird (DigitalGlobe, Westminster, CO, USA) images are exploited to detect crop marks related to buried archaeological remains. An image-based methodology for the detection of archaeological buried relics using multi-temporal satellite imagery was derived in Agapiou et al. (2013) observing the phenological cycle of the crops. Automatic detection of ancient Arabian tombs through high-resolution satellite imagery was proposed in Schuetter et al. (2013), while an automatic detection of ancient circular structures based on VHR QuickBird images in Southeast Norway has been described in Trier et al. (2009). Recently, previously undocumented cities in Cambodia have been mapped beneath vegetation using airborne LIDAR (Evans 2016). Monitoring and risk assessment of CH sites at landscape scale have been proposed in Agapiou et al. (2016) by integrating a variety of satellite sensors bearing different spatial and spectral resolutions, using geographic information systems (GIS) to cluster cultural heritage sites and monuments with similar characteristics.

Although automatic methods are often used as in the examples listed above, damage detection to CH sites is usually carried out by visual analysis: see Casana and Panahipour (2014) for an example in Syria or other cases of study in Contreras (2010) and Cunliffe (2014). In Lasaponara and Masini (2012), the need of expanding

automatic or semi-automatic procedures to a wider range of archaeological applications is discussed.

In this chapter we apply a change detection algorithm based on differences of textural features in order to go towards the automatic production of maps where areas suspected of having suffered damages are highlighted.

Results are based on robust differences of texture features, yielding reliable change maps with a certain tolerance to co-registration errors and geometric distortions caused by different acquisition angles. The map contains a potential set of sensitive areas on which a more detailed analysis should be carried out by the experts.

The change detection workflow has been tested on images acquired in Palmyra in Cerra et al. (2016). In the present work, two additional images are added to the set of the three available acquisitions previously processed. The different change detection maps are merged in order to successfully visualize the evolution in time of the detected damages in the area and validated against official reports.

An automatic or semi-automatic early warning system would ideally work as follows: at first, sensitive areas containing endangered CH sites should be selected; subsequently, whenever a new acquisition from an optical satellite is available, an automatic change detection procedure would take place. If a relevant change is detected within any area of interest, an alert would be raised and analysed by an operator, who in the end will determine if the change could really correspond to damage to the site.

In periods of war, civil unrest, political instability or after a natural disaster, the sensitivity of a given area could change. Therefore, we analyse a second case of study in Sirwah, Yemen, to introduce the possibility of a configurable selection of sensitive areas with different priority. The user can select beforehand larger areas in which it would be of interest to receive alerts on newly produced damages, but only if one of the aforementioned cases arise. In this case, areas with lower priority such as urbanizations in the immediate proximities of the CH sites and infrastructures would be added to the sites under observation. Once it becomes necessary to increase the attention in an area of interest, this would be done immediately using the preselected areas, increasing the timeliness of the analysis and facilitating a quick response.

The paper is structured as follows. Section “[Change Detection Based on Textural Differences](#)” describes the features used to carry out the damage detection. Results of multi-temporal analysis on the archaeological sites of Palmyra are described in section “[Case Study: Palmyra](#)”, while section “[Damage Detection: 2015](#)” proposes a possible configurable early warning system for damage detection to CH sites. We conclude in section “[Conclusions](#)”.

Change Detection Based on Textural Differences

Change detection aims at providing a map of changes given as input two or more images acquired at different times over the same area. For the applications described in this chapter, the desired output should highlight the locations of monuments that

suffered damage or changes in the time span between the two acquisitions. Automatic change detection techniques may be difficult to apply in practice. For example, the differences between pre- and post-event images may be difficult to obtain in a reliable way if the acquisition dates of the two images are too far away. Even if this is not the case, a pixel-based analysis is difficult to carry out even after an accurate co-registration step, as often no high-resolution digital surface model (DSM) is available. In this case, images may exhibit orthorectification errors, and the differences in view angle introduce, in turn, pronounced geometric distortions.

Gabor features are robust to two-dimensional shifts in space and are traditionally employed in edge detection and edge characterization tasks (Manjunath and Ma 1996). They can be described as a windowed Fourier analysis, compensating for the lack of spatial dependency of features in the frequency domain. They are therefore able to capture the interactions between neighbouring pixels in a local window by quantifying the roughness or smoothness in a specific point, along with its scale and orientation. A bank of Gabor filters usually consists of a set of complex linear filters encompassing the characteristics that stand out for the human eye and agreeing well with how the human visual system's 2D receptive fieldworks (Grigorescu et al. 2002). Each element in the filter bank is derived by transforming in time domain two-dimensional impulses in the frequency domain and multiplying the result by a Gaussian function, which acts as an envelope. In Fig. 1 different orientations and scales of the two-dimensional waves are reported, with the envelope being the weighting function suppressing the response of the filter as a function of the distance from its centre. The higher the frequency of the captured texture, the smaller the envelope can be. Therefore, each component in the filter bank can be defined in its discrete form by varying the frequency f and the orientation θ of the plane waves as proportional to:

$$G_c[k,l] = e^{-\frac{k^2+l^2}{2\sigma^2}} \cos(2\pi f(k \cos \theta + l \sin \theta)), \quad (1)$$

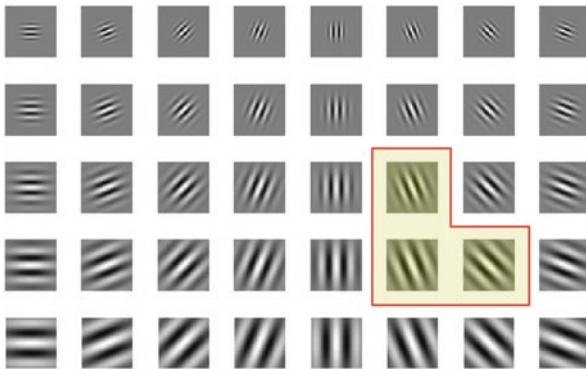


Fig. 1 Real parts of the Gabor filter bank used in the experiments in this paper according to the different orientations and scales. Highlighted are the filters giving the highest contribution to the detection to be described in the next section

$$G_s[k,l] = e^{-\frac{k^2+l^2}{2\sigma^2}} \sin(2\pi f(k \cos \theta + l \sin \theta)), \quad (2)$$

where k and l are the extension in number of pixels of the filter, usually with $k = l$, and σ^2 the variance of the Gaussian function used to define the envelope: the smaller the σ , the smaller the effective area in which a specific texture detector for one orientation and scale is applied. An example for the real parts of the filter bank used in the experiments contained in this paper is reported in Fig. 1. Before their application, the filters should be multiplied by a normalization factor chosen in order to have the sum of the responses of the filter to the same sinusoidal function as 1 (Ramakrishnan et al. 2002). The filter banks in Eqs. (1) and (2) are convolved with the image to generate the response centred at each pixel as R_c and R_s . The final value for the response of a pixel to a specific filter in the filter bank is then computed as:

$$B[i,j] = \sqrt{R_c[i,j]^2 + R_s[i,j]^2}. \quad (3)$$

This value is proportional to the similarity of the observed area with the grey-value distribution for a given frequency and orientation in the filter bank. Some generic experiments on damage detection using Gabor features have been carried out in Vijayaraj et al. (2008). In our case, for two co-registered images acquired at t_1 and t_2 , the difference in texture for an image element at location (i, j) for a given frequency f , rotation θ and spread σ is quantified as:

$$D_G(i,j) = abs(R_{t_1}[i,j] - R_{t_2}[i,j]). \quad (4)$$

$R_{t_1}[i, j]$ and $R_{t_2}[i, j]$ are the results of independently applying Eq. (3) to the same image element in the two images.

To produce a final binary change map, all pixels with textural difference larger than a selected threshold can be selected. Morphological filtering (opening and closing) is subsequently applied to the binary thresholded image to produce the final results.

Case Study: Palmyra

We analysed the archaeological site of Palmyra in Syria, which has been reported to have suffered damage from terrorist activities from 2015 to the beginning of 2017, and the case of Sirwah in Yemen. The latter will inspire a configurable selection for sensitive areas to be monitored with different priority. The locations of these two sites are reported in Fig. 2.

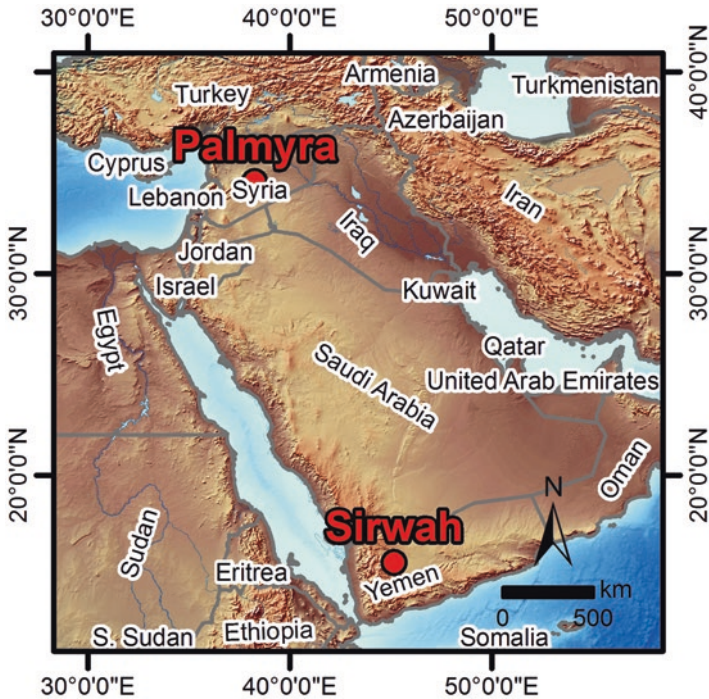


Fig. 2 Map showing the locations of the two sites analysed in this paper

Damage Detection: 2015

Most of the experiments contained in this chapter are carried out on the large archaeological site of Palmyra, situated in the Syrian Desert northeast of Damascus, which have been listed as UNESCO World Heritage site since 1980. One of the most important monuments within the walled city is known as Sanctuary of Bel, on which the first excavation missions took place in the area (Starcky and Munajjed 1960), dedicated to the Gods Bel, Iarhibol and Aglibol in the first century A.D. (Cantineau 1934). The Temple dedicated to the Semitic God Bel (Fig. 3a), whose worship was dominant in the Palmyrene religious cult (Danti 2001), is located in the centre of the Sanctuary. It dates back to the Hellenistic period and received several architectural modifications throughout the first two centuries A.D., which make it of great importance according to scholars for its rich and diverse architectural details (Cantineau 1934; Danti 2001). Sadly, the Temple of Bel became famous on a planetary scale for being among the CH sites in the area to have suffered the worst damage from terrorist activities perpetrated by the IS.

Important vestiges of rich Palmyra's cultural heritage are to be found outside the walls of the city. The western part of Palmyra's ancient necropolis contains what are known as tower tombs (Fig. 3b), erected during the first and second centuries A.D.,

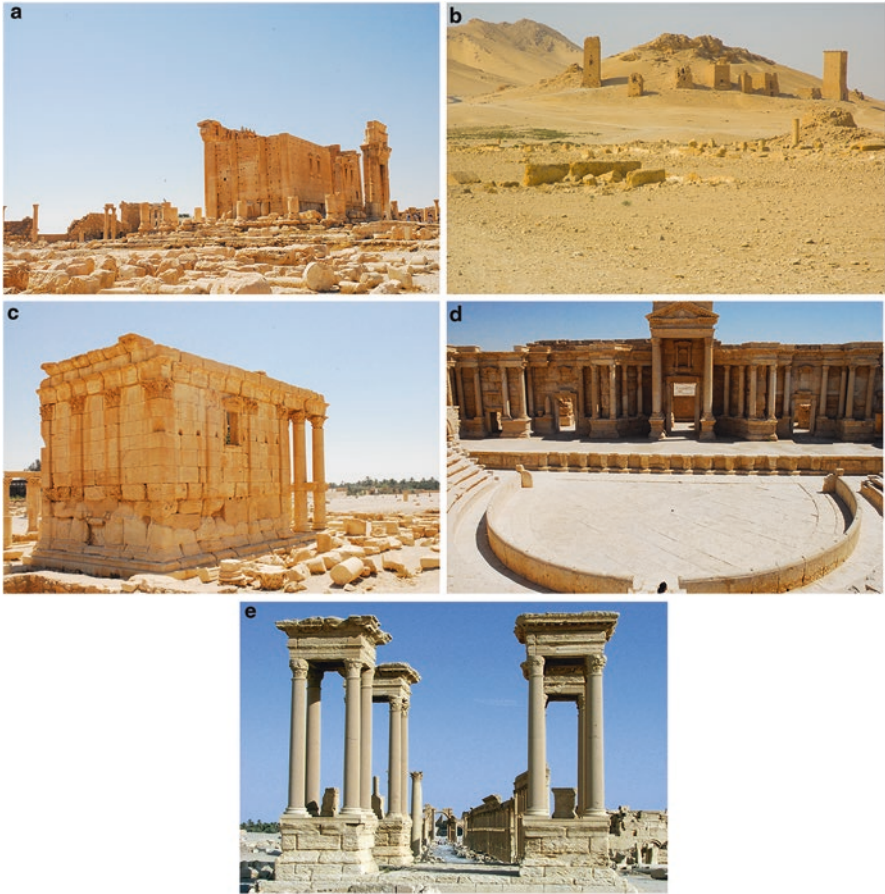


Fig. 3 Palmyra's archaeological sites discussed in this work: (a) Temple of Bel @ Michael Danti; (b) tower tombs in the background @ szymanskim; (c) Temple of Baalshamin @ Michael Danti; (d) Roman theatre @ Michael Danti; (e) tetrapylon @ DGAM

which contained burial items, decorations and wall paintings representing an important source of information related to the cultural habits of the ruling class of the city. The tower tombs underwent severe damages in the last years, part of which will be analysed in the next section.

Other important monuments (Bryce 2014) include the Temple of Baalshamin, dating back to the second century B.C. (Fig. 3c), a Roman theatre founded in the second century A.D. (Fig. 3d), and the tetrapylon, a cubic monument with four gates usually placed on important crossroads (Fig. 3e).



Fig. 4 Subset of the WorldView-2 image acquired on the 27th of August 2015 (European Space Imaging/DigitalGlobe)



Fig. 5 Subset of the WorldView-2 image acquired on the 2nd of September 2015 (European Space Imaging/DigitalGlobe)

Figures 4 and 5 report the subsets of two WorldView-2 datasets acquired outside the city centre of Palmyra on the 27th of August and on the 2nd of September 2015, dates that henceforth we denote with t_1 and t_2 , respectively. At time t_1 , the IS had already destroyed several CH sites in the area, such as the Temple of Baalshamin. This loss must be added to the huge number of artefacts destroyed or illegally sold to finance IS activities (ref. the companion book chapter “Recent Destructions in Palmyra/Syria, Looting and Illegal Antiquities Trade”). Between t_1 and t_2 , other tower tombs and the Temple of Bel were damaged. In the figures, the Temple of Bel is located in the southeast, while the tower tombs are scattered in the north-western part of the image. In our first step, the co-registration of the images has been refined by automatically deriving 1000 Ground Control Points by matching of scale-invariant feature transform (SIFT) features (Lowe 2004) between the two images and by warping the image acquired at time t_1 using as reference the image acquired at time t_2 .

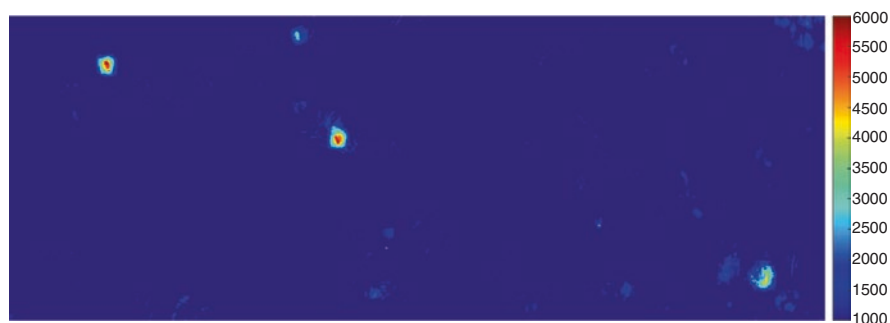


Fig. 6 Change detection map between the two images reported in Figs. 4 and 5. The four targets which stand out clearly represent detected damages to three clusters of tower tombs (upper left) and to the Temple of Bel (lower right)

We employ a standard Gabor filter bank, capturing the texture information in a geometric grid having any combination of 5 different scales with 8 possible orientations, analysed in a window of size 39×39 , for a total of 40 filters (Haghighat et al. 2015). Figure 1 reports the real parts of the filters: the most important features for the analysis carried out in the rest of this section are highlighted and are related to the scale of the objects of interest and the shadow orientation, dependent on the sun's elevation angle.

As textural features are usually computed on a single spectral band, we choose in all cases the red band as it has a high quality for the WorldView sensors which is independent from the off-nadir acquisition angle (Aguilar et al. 2013).

To derive a change map, also the brightness information is taken into account in this case, and brightness robust difference (RD) features (Tian et al. 2014) are computed using a window of size 9×9 , which was found to give more robust results. As the contribution to the change map of RD was smaller than the robust texture differences, we did not compute RD in the experiments reported in the next sections.

The overall change map in Fig. 6 is produced by normalizing and averaging the textural and brightness differences. If a binary map showing the locations of possible damages is desired, the final changes are highlighted from a manually thresholded version of the change map, after applying a single pass of morphological opening and closing. The structuring element of choice for the morphological filter was a disc of size 3, corresponding to a 3×3 square window filled with ones, with zeros in the four corners.

The binary map is overlaid on the image acquired over Palmyra at time t_2 in Fig. 7.

The map indicates the destruction between t_1 and t_2 of several tower tombs and of the central part of the Temple of Bel on the right of Fig. 7. The validation of these changes will be discussed at the end of this section: to have a complete frame, it is of interest to consider also the additional damages to cultural heritage sites in the area which had been carried out before t_1 , time for which we have our first available image.



Fig. 7 Red: Post-processed change map from Fig. 6 overlaid on the 2nd of September 2015 WorldView-2 image reported in Fig. 5. All the main damaged areas are correctly identified (European Space Imaging/DigitalGlobe)

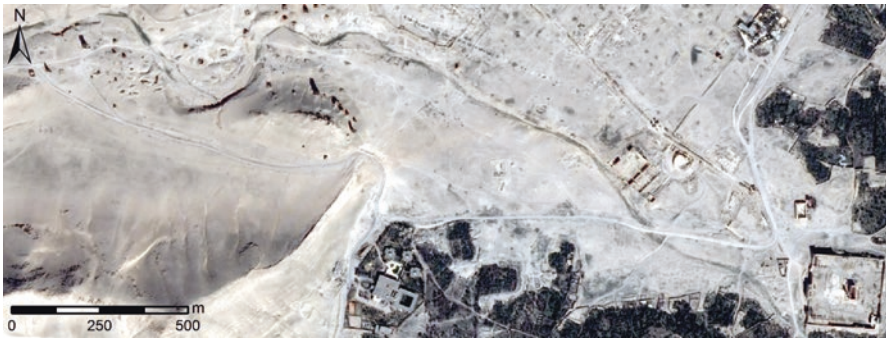


Fig. 8 Pre-disaster image acquired on the 20th of February 2014, screenshot from Google Earth (DigitalGlobe)

In order to ideally travel back in time, we extracted an image available on Google Earth (version 7.1.5.1557, Google Inc., Mountain View, CA, USA) which was acquired on the 20th of February 2014. We refer to this date as time t_0 . The image reported in Fig. 8 shows all relevant monuments still intact.

In this and the next experiments, only textural differences have been considered: on the one hand, they proved to be the most meaningful and robust; on the other hand, blending together the results obtained through textural and brightness robust differences requires the tuning of additional parameters which should be ideally skipped, if a certain degree of automation is desired in the workflow. The image extracted from Google Earth is co-registered to the image acquired at time t_2 , and differences based on Gabor features are computed in the same way as in the previous experiment. The final results are reported in Fig. 9. All the relevant damaged areas are detected, including the Temple of Bel and the tower tombs: the most meaningful result is represented by the additional detections which correctly correspond to the Temple of Baalshamin (in the north-eastern part of the image), the tombs of



Fig. 9 Red: post-processed changes overlaid on the 2nd of September 2015 WorldView-2 image reported in Fig. 5. All the main damaged areas are correctly identified with two small false alarms in the southern part of the image (European Space Imaging/DigitalGlobe)

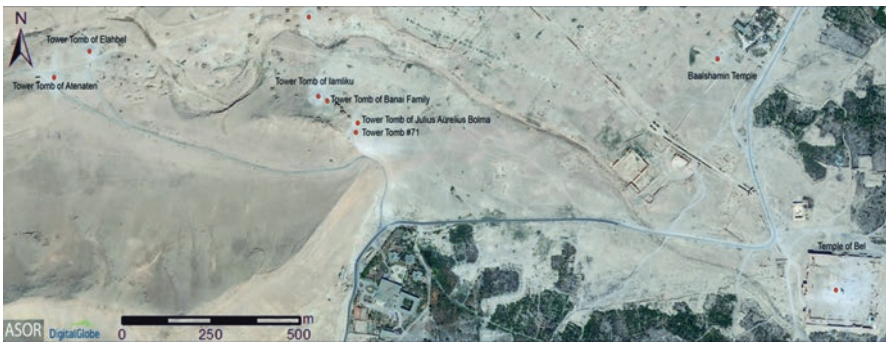


Fig. 10 Report from Cuneo et al. (2015) showing destroyed CH sites in Palmyra. This map was used as validation for the detected damaged areas (ASOR CHI/DigitalGlobe)

Iamluku with the tomb of the Banai family directly to its east (merged in a single area in the centre-left of the image) and the tomb of Atenaten (in the northwest). Only two false alarms are visible in the lower central part of the image.

The final damage detection can be validated against a map representing all relevant CH sites destroyed produced by the American School of Oriental Research (ASOR) in the report on the situation in Palmyra (Cuneo et al. 2015) depicted in Fig. 10. According to the report, between t_1 and t_2 the following monuments have been destroyed: the Temple of Bel, the tomb of Elahbel, the tomb of Kithoth in the northern part of the necropolis, the tomb of Julius Aurelius Bolma and the tomb #71 near the tomb of Iamluku. The damages carried out between t_0 and t_1 affected instead the Temple of Baalshamin and the tombs of Atenaten, Iamluku and the Banai family. All of such damages are correctly detected both in time and space.

It is interesting to consider the correspondence between the most useful Gabor features highlighted in Fig. 1 and the damaged buildings in the image. Regarding the scale, Gabor filters in the filter bank are comparable to the damaged objects.

But also the orientation of the filters plays a key role, as it seems to agree with the sun's position and therefore with the direction of shadows on the ground. Variations in the latter could raise false alarms; therefore, it is recommended whenever available to use for the change detection images acquired by a satellite operating in a heliosynchronous orbit.

Analysis of Recent Damage: 2017

On 20th of January, Syria's Director General of Antiquities and Museums confirmed that the IS had destroyed the tetrapylon and part of the facade of the Roman theatre (Danti et al. 2017). Two images are available over this area: one WorldView-3 and one WorldView-2 multispectral images. The former was acquired on the 26th of December 2016 and the latter on the 10th of January 2017. Henceforth, we refer to the mentioned dates as t_3 and t_4 , respectively.

The two images were not accurately co-registered, so an additional pre-processing step was needed as texture change detection is robust to small co-registration errors but only up to a certain extent. A procedure based on the extraction of SIFT features was therefore carried out as described in previous section. The texture-based change detection applied to the two images results in the change map overlaid in Fig. 11.

Due to the pronounced differences in acquisition angles, some false alarms are present, but the damages to the tetrapylon are clearly detected. Regarding the theatre, only the changes in the central part are detected over a small area. The changes in the Temple of Bel do not correspond to a new damage, as they are caused by the different shapes of the shadows on the ground in the two images.

A subset of the two images is reported in Fig. 12. The tetrapylon and the Roman theatre, which are to be found, respectively, in the top left and bottom right of each image, are visibly preserved at time t_3 . The severe damages suffered by these two CH sites are clearly shown in the image acquired at time t_4 .

Multi-temporal Analysis

A multi-temporal representation of the systematic destructions affecting the cultural sites of Palmyra can be derived by merging the detected damaged areas between images acquired at times t_0 , t_1 and t_2 with the most recent damages detected between times t_3 and t_4 , representing different time spans with different colours. An example is reported in Fig. 13, in which the older damages are highlighted in blue, subsequent destroyed buildings in red and more recent changes in green.

Such multi-temporal analysis cannot exactly determine the exact date in which damages occurred, but can help in reconstructing the evolution of events in sensitive areas.



Fig. 11 Subset of the WorldView-2 image acquired on the 26th of December 2016 (t_3). Reported in black and white in the yellow square is a subset of the WorldView-3 image acquired on the 10th of January 2017 (t_4). Damage that occurred between t_3 and t_4 is highlighted in light blue

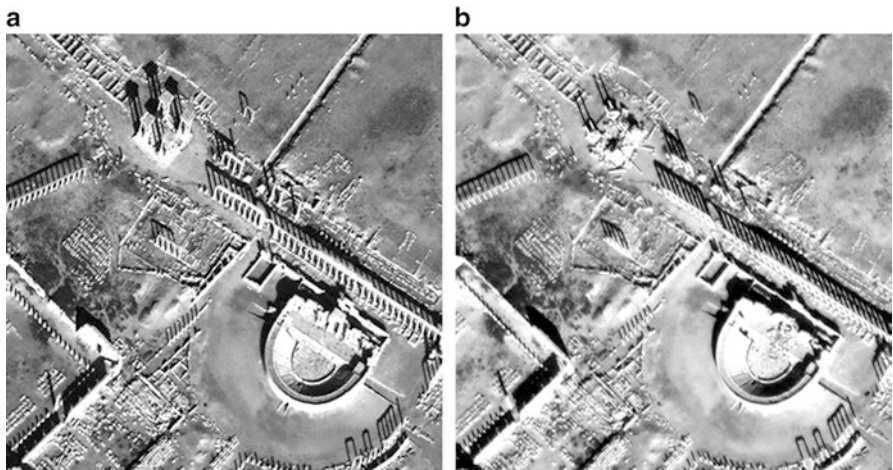


Fig. 12 Detail of image in 11: Theatre (bottom right) and tetrapylon (top left) still intact in an image acquired at time t_3 (a) and appearing destroyed or damaged in an image acquired at time t_4 (b)

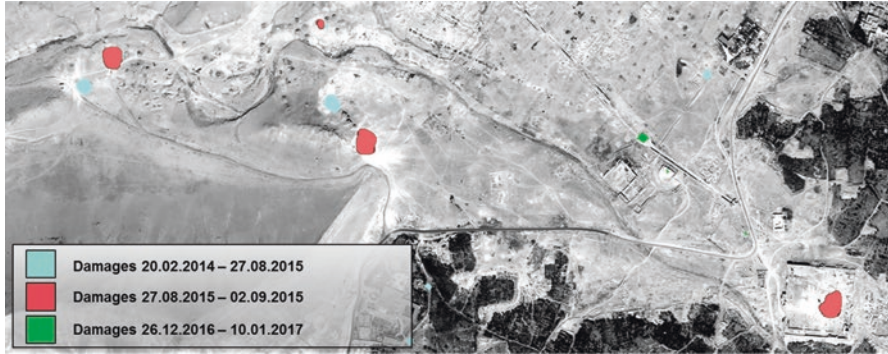


Fig. 13 Multi-temporal representation of damage overlaid on the 2 September 2015 WorldView-2 image reported in Fig. 5 (European Space Imaging/DigitalGlobe). Damage that occurred between $t0$ and $t1$, between $t1$ and $t2$ and between $t3$ and $t4$ is highlighted in blue, red and green, respectively

Setting Up an Early Warning System for Endangered Cultural Heritage Sites

The Sabaean city of Sirwah is located about 40 km to the west of Marib in Eastern Yemen, and it represented the second most important economical and political centre of the Kingdom of Saba in the first century B.C. The historical part of the city comprises several CH sites of particular interest, such as the 780-m-long outer protection wall, the Almaqah temple dating back to the seventh century B.C. and the Athtar temple. Part of these sites has been discovered only recently, with several still ongoing excavations (Gerlach 2017).

In spring 2015 a civil war took place in Yemen, with Sirwah being placed at the frontline between the Houthi rebels and the Arabic alliance supporting the president of the country, making access to the sites difficult and further excavations almost impossible (Al Masdar News 2017). The conservation of Sirwah's CH sites became a concern as air strikes of the Arabic alliance against the Houthi rebels caused massive damages to the modern part of the city, which is located very close to the ancient part, and were assessed by a visual analysis of satellite images before and after the event. This real scenario suggests a possible configuration setting for the monitoring of specific areas rich in CH sites located in sensitive areas.

Whenever human-driven events as in the aforementioned case (e.g. civil war, terrorism) or natural ones (e.g. earthquake, fire, flood) are taking place, it may be of interest to monitor not only the most important CH sites but also the surrounding areas. If the latter would result in damage, the vulnerability of nearby CH sites would probably increase. This leads to the proposed configurable early warning system, in which different priorities could be set to monitor critical areas.

If the ingestion of newly acquired satellite images is constantly being delivered on an area of interest, the user could select the CH sites at risk as areas having maximal

criticality, but also indicate any nearby territory which would need to be monitored in case of dangerous (foreseeable or not) events. Whenever desired, the user could then switch on the monitoring in areas denoted by a lower priority as needed. The negative consequence would be a higher number of raised false alarms not indicating real changes, which should be examined by the user. On the other hand, such analysis would quickly raise awareness on the overall damages, as the areas to analyse would have been set beforehand, speeding up the process.

In the case of Sirwah, comparative analysis of very high-resolution WorldView-2 imagery acquired on the 8th of April 2014 and the 23rd of May 2015 showed no clear changes (possible damages) within the ancient part of the city. However, several damages were detected in the modern area surrounding the CH sites: for instance, the government's palace was completely destroyed. Figure 14 reports a possible definition of areas with different priority in Sirwah and a subset of the comparative analysis results derived from difference in textural Gabor features. On the top of Fig. 14, the area of higher priority containing most of the CH sites of interest in Sirwah is delimited by a red circle denoted by 'CH'. The area around in yellow may represent the surrounding area which it may be desired to monitor in extreme situation, such as the aerial bombings carried out in 2015. If the yellow area would be activated, meaning that it is added to the automatic change detection analysis, the destruction of a building in the modern area of Sirwah would be detected. This is depicted in the lower part of the image, along with the change detection results.

In the case of Palmyra, a possible definition for such areas is reported in Fig. 15. In this example, the main CH sites have been selected for the high priority zone, while a secondary one has been derived by including any object within a 200 m distance from any of the CH sites. Automatic change detection techniques as described in previous sections could be applied only on the high priority zones in absence of ongoing conflicts or to all areas otherwise.

Conclusions

Recent historical events put cultural sites of universal interest under serious threats, with Earth observation data playing an important role in their monitoring, as detailed damage assessment maps are paramount for authorities and stakeholders (Council of Europe 2000). The number of operating spaceborne sensors systems is steadily increasing, along with the imaging capabilities and revisit time of each sensor. The pre-processing steps for a single image (e.g. atmospheric, radiometric, geometric correction) are carried out automatically, thus making these data readily available in the aftermath of a natural or man-made event threatening a cultural heritage site.

The usual way of assessing damages is change detection, in which a pre-event image available in the archive is compared by image analysts to a new acquisition. Such process is often carried out by visual analysis (Plank et al. 2015), decreasing the timeliness in production and sometimes the completeness of a damage assessment or risk estimation map. It would therefore be desirable to increase the automation

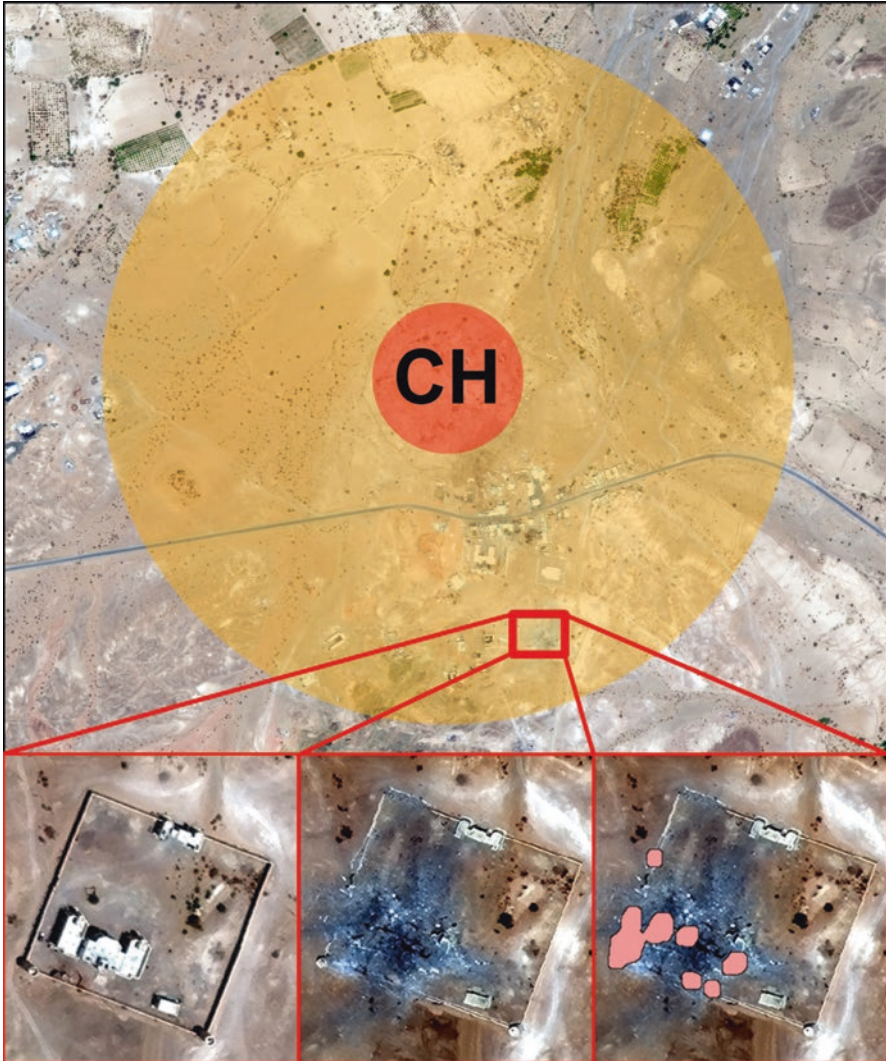


Fig. 14 Top: Possible definition of high-sensitivity (red) and medium-sensitivity (yellow) areas in Sirwah. Bottom: change detection analysis based on Gabor features of a building in the medium-sensitivity area; from left to right, image acquired before the event, image acquired after the event and change detection results

degree of such response (Lasaponara and Masini 2012). This chapter illustrates the use of absolute differences in Gabor texture features in order to derive robust change maps, which can provide image analysts with a valuable input to speed up their anyway necessary verification of the entity of damages in a sensitive area.

The case of study of Palmyra in Syria, which became unfortunately well-known for the recent destruction to its cultural heritage carried out by the so-called

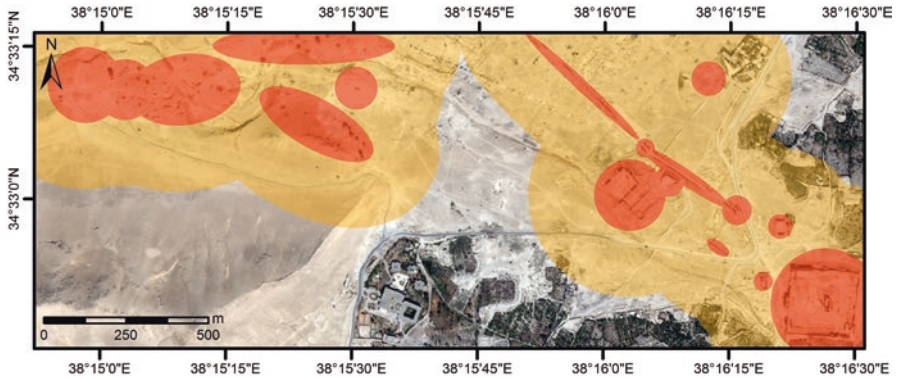


Fig. 15 Possible definition of high- and medium-sensitivity areas in Palmyra: high priority zones rich in CH sites are represented in red, while surrounding areas which could be monitored during critical events are marked in yellow

Islamic state, is analysed to demonstrate the capabilities of such computer-aided system. A reference map verified by authorities reporting all sites which suffered damages in the last years is used as ground truth: this is almost identical to the results of the described change detection algorithm.

The analysis of the most useful Gabor features employed suggests that more reliable change detection maps could be achieved by preselecting the orientation of texture filters as a function of image resolution and of the sun’s position, if the images are acquired by the same heliosynchronous satellite.

In order to have a complete overview on the damaged sites, an older auxiliary image acquired over Palmyra is extracted from Google Earth. This has two positive aspects: firstly, it shows that expensive archive data could be replaced by more easily available data sources; secondly, it enables a multi-temporal representation of the evolution for damage extent over time.

In 2017, further destruction to Palmyra’s cultural sites has been reported (Danti et al. 2017). With the aid of two recent acquisitions, this additional damage has been assessed, and a more complete map reporting the chronological sequence of the attacks is derived.

The described methodology could be applied in such inaccessible areas affected by natural or anthropogenic hazards, until in situ investigations can be performed. The general planning related to the development of risk-preparedness strategies for CH sites could therefore benefit from the derived change maps, contributing to the effectiveness of rapid response strategies in case of disasters. Ideally, if World Heritage site VHR data for non-accessible sites would become easily available, an automatic change map could raise an alarm only minutes after the acquisition of a new image of the area. This should be later verified by experts—first, by visual analysis of the data and, subsequently, by information sources in situ. Projects aiming at integrating earth observation in cultural heritage monitoring processes in a solid framework could benefit from employing such a workflow (GEO 2016; CIP 2016).

Envisaging a possible frame for machine-assisted damage assessment in sensitive sites, the advantages for a user of being able to define areas with different priority are discussed. We analyse the case of civil unrest in Sirwah, Yemen, in which cultural sites have not been reported as damaged, but some surrounding buildings have been destroyed. In case of critical events, it may be relevant to expand the area of interest for the damage detection routine, as the destruction of surrounding buildings may indicate a threat to the cultural sites.

Future work should include an evaluation of the results for additional test sites in different time frames and geographical areas, while false alarms could be decreased by restricting the analysis to high priority areas comprising relevant CH sites only.

Acknowledgements The authors would like to thank Jiaojiao Tian (German Aerospace Center-DLR) and Vasiliki Lysandrou (Cyprus University of Technology-CUT) for their valuable inputs contained in the paper (Cerra et al. 2016), which was the starting point for the preparation of this book chapter.

References

- Agapiou A, Hadjimitsis DG, Alexakis DD (2013) Development of an image-based method for the detection of archaeological buried relics using multi-temporal satellite imagery. *Int J Remote Sens* 34:5979–5996
- Agapiou A, Lysandrou V, Themistocleous K, Hadjimitsis D (2016) Risk assessment of cultural heritage sites clusters using satellite imagery and GIS: the case study of Paphos District. *Cyprus Nat Hazards*:1–16. <https://doi.org/10.1007/s11069-016-2211-6>
- Aguilar M, del Mar Saldan˜a M, Aguilar FJ, Fern˜andez I (2013) Radiometric comparison between GeoEye-1 and WorldView-2 panchromatic and multispectral imagery. *INGEGRAF-ADM-AIP PRIMECA*. Ingegraf, Madrid, pp 1–9
- Al Masdar News Die Erforschung der sabischen Stadtanlage und Oase von Sirwah (Provinz Marib). Available online: <https://www.almasdarnews.com/article/yemeni-ceasefire-expires-clashes-erupt-across-ountry>. Accessed on 19 Oct 2017
- Bryce TR (2014) *Ancient Syria: a three thousand year history*. Oxford University Press
- Canteneau J (1934) *Inventaire des Inscriptions de Palmyre Fasc IX: le Sanctuaire de Bel*. Damascus Museum, Damascus, p 8
- Casana J, Panahipour M (2014) Satellite-based monitoring of looting and damage to archaeological sites in Syria. *J East Mediterr Archaeol Herit Stud* 2:128–151
- Cerra D, Plank S, Lysandrou V, Tian J (2016) Cultural heritage sites in danger - towards automatic damage detection from space. *Remote Sens* 8:9
- CIPA Heritage Documentation, 2016
- Contreras DA (2010) Huaqueros and remote sensing imagery: assessing looting damage in the Vir Valley, Peru. *Antiquity* 84:544–555
- Council of Europe. *European Landscape Convention; Report and Convention*; Council of Europe: Florence, Italy, 2000
- Cuneo A, Penacho S, Gordon LB (2015) Special report: update on the Situation in Palmyra, . Available online: <http://www.asor-syrianheritage.org/special-report-update-on-the-situation-in-palmyra>. Accessed on 19 Oct 2017
- Cunliffe E (2014) Remote assessments of site damage: a new ontology. *Int J Herit Digit Era* 3:453–473
- Danti M (2001) Palmyrene funerary sculptures at Penn. *Expedition* 43:33–40

- Danti M, Cuneo A, Gabriel M, Penacho S New Damage in Palmyra Uncovered by ASOR CHI. Available online: <http://www.asor-syrianheritage.org/new-damage-in-palmyra-uncovered-by-asor-chi>. Accessed on 19 Oct 2017
- Earth Observation in Cultural Heritage Documentation, 2016. Accessed on 19 Sept 2016
- Evans D (2016) Airborne laser scanning as a method for exploring long-term socio-ecological dynamics in Cambodia. *J Archaeol Sci*. <https://doi.org/10.1016/j.jas.2016.05.009>
- Gerlach I Die Erforschung der sabischen Stadtanlage und Oase von Sirwah (Provinz Marib). Available online (in German): <https://fallback.dainst.org/projekt/-/project-display/102061>. Accessed on 19 Oct 2017
- Grigorescu SE, Petkov N, Kruiizinga P (2002) Comparison of texture features based on Gabor filters. *IEEE Trans Image Process* 11:1160–1167
- Haghighat M, Zonouz S, Abdel-Mottaleb M (2015) CloudID: trustworthy cloud-based and cross-enterprise biometric identification. *Expert Syst Appl* 42:7905–7916
- Lasaponara R, Masini N (2007) Detection of archaeological crop marks by using satellite QuickBird multispectral imagery. *J Archaeol Sci* 34:214–221
- Lasaponara R, Masini N (2011) Satellite remote sensing in archaeology: past, present and future perspectives. *J Archaeol Sci* 38:1995–2002
- Lasaponara R, Masini N (2012) Remote sensing in archaeology: from visual data interpretation to digital data manipulation. *Satellite remote sensing: a new tool for archaeology*, vol 16. Springer, p 3
- Lowe DG (2004) Distinctive image features from scale-invariant Keypoints. *Int J Comput Vis* 60:91–110
- Manjunath BS, Ma WY (1996) Texture features for browsing and retrieval of image data. *IEEE Trans Pattern Anal Mach Intell* 18:837–842
- Plank S, Strunz G, van Ess M, Richardson P (October 2015) Monitoring of cultural heritage sites using VHR earth observation data. *Proceedings of the WorldView global Alliance—user conference*, Munich, Germany, 13–14
- Ramakrishnan AG, Raja SK, Ram HVR (6 September 2002) Neural network-based segmentation of textures using Gabor features. *Proceedings of the 12th IEEE Workshop on Neural Networks for Signal Processing*, Martigny, pp 365–374
- Schuetter J, Goel P, McCorrison J, Park J, Senn M, Harrower M (2013) Autodetection of ancient Arabian tombs in high-resolution satellite imagery. *Int J Remote Sens* 34:6611–6635
- Starcky J, Munajjed S (1960) Palmyra: the Bride of the desert. Directorate-General of Information (Syria), Damascus
- Tian J, Cui S, Reinartz P (2014) Building change detection based on satellite stereo imagery and digital surface models. *IEEE Trans Geosci Remote Sens* 52:406–417
- Trier ØD, Larsen SØ, Solberg R (2009) Automatic detection of circular structures in high-resolution satellite images of agricultural land. *Archaeol Prospect* 16:1–15
- Vijayaraj V, Bright EA, Bhaduri BL (2008) Rapid damage assessment from high resolution imagery. *Proceedings of the IEEE international geoscience and remote sensing symposium (IGARSS)*, vol 3, Boston, pp 499–502

The Use of UAVs for Cultural Heritage and Archaeology



Kyriacos Themistocleous

Abstract This chapter focuses on the uses of unmanned aerial vehicles (UAVs) for documenting and monitoring cultural heritage and archaeological sites. High-resolution aerial imagery from UAVs also allows the rapid generation of 3D digital surface models for documentation and model reconstruction in a variety of applications. This chapter provides various examples of cultural heritage and archaeological sites in Cyprus that have been documented with high-resolution cameras aboard UAVs. Photogrammetry is also used to create 3D models of the site, which can also be printed using a digital printer.

Keywords UAVs · Cultural heritage · Archaeology · Photogrammetry

Introduction

The documentation of architectural cultural heritage sites has traditionally been expensive and labor-intensive. Innovative technologies, such as unmanned aerial vehicles (UAVs), provide an affordable, reliable, and straightforward method of capturing cultural heritage sites, thereby providing a more efficient and sustainable approach to documentation of cultural heritage structures. UAVs have proven to be invaluable in the fields of archaeology and cultural heritage, as they provide a non-invasive, time- and cost-efficient way to document cultural heritage sites. Most importantly, they are able to include the cultural landscape in which ancient vestiges are located in the documentation process. UAVs are a low-cost, nonintrusive, non-contact, cost- and time-efficient alternative to traditional methods of archaeological documentation and monitoring as they are able to acquire high spatial resolution data with high temporal frequencies over large areas. Aerial imagery from UAVs also allows the rapid generation of 3D digital surface models for documentation and model reconstruction in a variety of applications.

K. Themistocleous (✉)

Department of Civil Engineering and Geomatics, Faculty of Engineering and Technology, Cyprus University of Technology, Limassol, Cyprus
e-mail: k.themistocleous@cut.ac.cy

© Springer Nature Switzerland AG 2020

D. G. Hadjimitsis et al. (eds.), *Remote Sensing for Archaeology and Cultural Landscapes*, Springer Remote Sensing/Photogrammetry,
https://doi.org/10.1007/978-3-030-10979-0_14

241

This chapter presents an overview of case studies conducted using UAVs to document and monitor archaeological and cultural heritage sites in Cyprus with high resolution. The case studies include the use of UAVs for the purposes of aerial photography and photogrammetry, which produces ortho-images and generates 3D models of the site.

UAVs

Although airborne and satellite sensors are the most widely used methods in remote sensing to date, UAVs are becoming an alternative remote sensing method, as they are easier to use and are accessible to a wider audience. Currently, unmanned aerial vehicles (UAVs) such as gliders and copters provide a low-cost, high-quality image comparable to airborne sensors. The use of UAVs for monitoring purposes provides a low-cost, non-invasive technique to acquire high spatial resolution data with high temporal frequencies, especially in areas that have limited coverage and are inaccessible to humans. Research indicates that aerial remote sensing and imaging can be conducted using large-scale low-altitude imaging and geospatial information (Colomina and Molina 2014; Cho et al. 2013; Mayr 2013; Petrie 2013). Recent developments in photogrammetry technology provide a simple and cost-effective method of generating relatively accurate 3D models from 2D images (Ioannides et al. 2013; Themistocleous et al. 2014b, 2015a, b, c). These techniques provide a set of new tools to capture, store, process, share, visualize, and annotate 3D models in the field (Themistocleous et al. 2014a, 2015b).

The use of cost-effective unmanned aerial vehicles (UAVs) are becoming common tools for researchers for numerous applications. According to Burkart (Burkhart et al. 2014), the emerging development of small versatile UAVs for use in remote sensing offers simple and affordable observation from the air. Since UAVs vary in size and payload capacity, various sensors can be installed onto the UAV platform (Fig. 1). The sensors that can be added to the UAV platform include visible spectrum cameras and multispectral, infrared, and thermal cameras (Themistocleous et al. 2014a), thereby creating an unmanned aerial system appropriate for remote sensing applications. Due to the decreasing size of the sensors, receivers, and antennas, it is now possible to create an integration of various sensors, as their low weight



Fig. 1 Left—Sony NEX 7 visible spectrum camera. Center—Tetracam multispectral camera. Right—FLIR thermal camera

and small size render them ideal for use on UAVs (Colomina and Molina 2014; Kostrzewa et al. 2003; Ruffino and Moccia 2005; Scholtz et al. 2011).

UAVs can be divided into two types: fixed-wing copter and glider. Each type of UAV has its own advantages and limitations, which are discussed in the sections below.

Fixed-Wing Copter

A copter system is a very powerful aerial platform with enhanced stability and maneuverability and powerful enough to lift a payload of several kilograms. For autonomous flight and improved maneuverability, the copter can be equipped with an internal GPS, gyros, compass, altitude control, telemetry, acceleration, and barometric sensors for altitude control. Copters are available with 4, 6, or 8 motorized propellers and can carry a payload of up to 2.5 kg on the mechanized viewing platform (Fig. 2). The main advantage of this configuration is that the copter can remain steady in the air and respond smoothly to flight commands from the operator, due to the five separate sensors and three gyroscopes that work together to maintain stable and controlled flight. The ground station transmitters allow the operator to easily control the copter system and the viewing angle of the camera. Using a video system, the live video of the camera is transmitted to a ground station. Flight times range from 8 to 25 minutes, depending on the payload and battery. To maximize flight time, two batteries can be connected in series to provide a flight time up to 40 minutes. The copter can be programmed to fly planned waypoint routes by using the GPS onboard navigation system and photographs can be triggered automatically. During the flight, the current position of the copter can be shown using a portable computer or a tablet.

Due to the internal GPS of the copter, the operator is able to take measurements of the same target at different heights by using the wireless PDA. The copter has a mech-



Fig. 2 Selected fixed-wing copters used in the case studies

anized camera mount that could be controlled remotely. The cameras and video recorders are attached to the camera mount and aerial photographs can be taken using the manual trigger through the ground control systems. The system can also be pre-programmed to take photographs at certain points and angles on a planned waypoint route. The camera mount is balanced horizontally and vertically by servomotors, which allows the camera to be vertical to the ground at all times. The copter had the capability to be raised up to 3 km in the air, thus providing data acquisition at higher elevations than the helium balloon platform. However, at high elevations, it was difficult for the operator to keep the copter within his line of sight and control the unit.

One of the main limitations of the fixed-wing copter is the battery capacity. Flight times are approximately 10 min when the payload was at maximum capacity and 20 min with normal payload, thereby minimizing the utilization of the copter for data collection. As well, the copter required calibration every time it was switched on in order to calibrate the internal GPS. The copter required that the operator have considerable experience in lift-off and landing copters to operate the copter and avoid damage to the instrument. The operator needs to be aware of the time limitations of the battery to avoid any crashes and possible damage to the copter. Special care is necessary in urban areas to avoid any collisions with electrical cables, buildings, etc. An additional problem of the copter is that it is quite large and bulky, which makes transport difficult.

Recently, there has been an influx of smaller copters with integrated cameras, such as the DJI Phantom series. These UAVs have an integrated 20 megapixel camera, which is extremely light and easy to manage. The unit has a built-in high-precision three-axis camera stabilization system that allows for smooth aerial photography. The integrated GPS autopilot system includes position holding, altitude lock, and stable hovering, thereby providing constant stability in flight. The UAV has a Wi-Fi wireless connection up to a distance of 300 meters, as well as real-time telemetry data and flight parameters. However, a main drawback of the copter is that the battery flight time is only 25 min. The unit has an intelligent operator control that displays the current position of the UAV in relation to the pilot as well as ground station support, thereby enabling extensive flight planning for automated flights.

Gliders

One of the benefits of the glider is that it has a flight duration of up to 90 min, which is four times the flight duration of other UAVs. The QuestUAV Q-POD is a glider UAV that can be used with different payload bays (Fig. 3). Q-Pods are designed to

Fig. 3 QuestUAV glider



be easily interchangeable. The modular design consists of one airframe and multiple sensor pods (Q-Pods). The A-frame carries the permanent equipment including the wings, motor, avionics, and autopilot. The Q-Pods slip easily into the A-frame and carry single or multiple sensors and the battery pack. The unit contains aircraft system status indicators, including current mode, critical sensor condition, GPS, onboard voltage monitoring, and communication link quality. As well, there is a real-time, auto-scaling moving map automatically linked with the planned waypoints and flight path. The UAV has a 100 km range and has an operational ceiling of 10,000 ft.

One of the biggest drawbacks of the Quest UAV system is that it required two to three people to operate it. As the glider is in constant motion, there are limitations on the types of sensors that can be used while the unit is in motion. The price point is more expensive than the previous systems examined. Also, extensive training and practice are required in order to operate the glider, due to safety requirements and flight regulations.

UAV Applications for Cultural Heritage

UAVs are being used for surveying cultural heritage sites due to their affordability, reliability, ease of use, and the quality of the processed measurements (Colomina and Molina 2014; Themistocleous et al. 2015a; Lo Brutto et al. 2014; Rinaudo et al. 2012). Research indicates that aerial remote sensing and imaging can be conducted using large-scale low-altitude imaging and geospatial information (Colomina and Molina 2014; Cho et al. 2013; Mayr 2013; Petrie 2013). Research indicates that UAV data provide more detailed surveys of the archaeological site (Hassani 2015; Remondino and Rizzi 2009; El-Hakim et al. 2004; Gruen et al. 2005; Rönholm et al. 2007; Guidi et al. 2009), which are used to document the site. UAVs are also useful to survey inaccessible and/or dangerous areas which cannot be accessed directly using other systems or piloted aerial systems (Everaerts 2008; Eisenbeiss 2009). Several cultural heritage researchers have used UAVs for archaeological sites in the Mediterranean (Rinaudo et al. 2012; Brumana et al. 2013; Remondino et al. 2011) as well as in Germany, Cambodia, and Hungary (Seitz and Altenbach 2011; Meszaros 2011). Also, researchers have used the combination of aerial imagery for 3D reconstruction of the cultural heritage site (Eisenbeiss 2009; Fiorillo et al. 2012).

Remote sensing technologies on a UAV platform are extremely useful for the detection and monitoring of cultural heritage features (Themistocleous et al. 2014a, b, c; Agapiou et al. 2013). UAVs can be an efficient, non-invasive, and low-cost resource to document cultural heritage sites (Themistocleous et al. 2014a, b, c; Agapiou et al. 2013) and can be fitted with sensors which are able to produce an unprecedented volume of high-resolution, geo-tagged image sets of cultural heritage sites from above (Themistocleous et al. 2014a, b; Kostrzewa et al. 2003; Ruffino and Moccia 2005; Scholtz et al. 2011). Researchers have used the combination of aerial imagery for 3D reconstruction of the cultural heritage site (Eisenbeiss 2009; Fiorillo et al. 2012) through the use of photogrammetry.

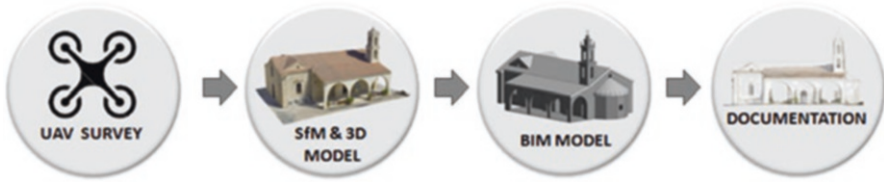


Fig. 4 Methodology

The methodology followed for the case studies presented in this chapter begins with a UAV survey where high-resolution aerial images are acquired. These images are then processed using Structure from Motion software, which creates a 3D digital model. The 3D model can then be exported into a BIM model, where the structure can be documented in terms of floor plans, elevations, and sections (Fig. 4).

Photogrammetry

Photogrammetry is a three-dimensional coordinate technique that uses computer analysis of photographic images for measurement. The fundamental principle of photogrammetry is aerial triangulation, where images from at least two different locations can be developed from each camera to point on the object and processed to produce the three-dimensional coordinates of the point of interest. Photogrammetry is used to conduct the image processing of the images acquired with the UAV, where the digital images are interpolated in order to create high-resolution, scaled, and geo-referenced 3D models from them. Photogrammetry generates the creation of 3D models by reconstructing a dense point cloud and generating polygonal mesh model based on the dense cloud data. In addition, the software has an automatic tool of texture projection, which makes automatic projection from the color directly on the surfaces possible (Meszaros 2011).

The first step in the program's procedure is called Structure from Motion (SfM) (Scopigno et al. 2015; Ingwer et al. 2015; Giuliano 2014). Structure from Motion is a photogrammetric method for creating three-dimensional models of a feature or topography from overlapping two-dimensional photographs taken from many locations and orientations to reconstruct the photographed scene. SfM analyses the dataset, detecting geometrical patterns in order to reconstruct the virtual positions of the cameras that were used in order to align the images, including building a sparse point cloud (tie points).

The second step involves the creation of a complete geometry of the scene using a multi-viewpoint stereo algorithms to build a dense point cloud. At this stage the dataset of images are employed to produce a high-resolution geometry of the surface. This step successfully creates a 3D model, also known as a digital surface model (DSM). The processing began with the orthomosaic production from these multiple images, which was used for digital terrain modeling (DTM) production from which

a contour map can be generated. All images derived from the UAV can be included in processing or it is possible to select a sub-set of images on key sites with the study area for more detailed analysis ensuring sufficient overlap and ground control points (GCPs) allow for this. Photogrammetry software allows generation of high-resolution geo-referenced orthomosaics, exceptionally detailed DTMs and textured polygonal models through the use of the image overlay (Eisenbeiss 2009).

Following, surfacing algorithms employ the dense cloud's 3D point positions and the look angles from the photos to the matched points to build the geometrical mesh. The coordinates from the GCPs are then applied in order to scale the model to the correct dimensions. The software automatically aligns images based on pairing of features and creates a "sparse cloud" of elevations based on these points. The completed alignment is then used to develop a dense point cloud which is used to create a surface which allows draping of the imagery over the model by creating and building a texture from the original images and overlays the imagery onto the model mesh (Themistocleous et al. 2014c). The photogrammetry software then builds a polygon mesh and calculates a texture for the mesh. The software generates the building of 3D models by reconstructing a dense point cloud and generating polygonal mesh model based on the dense cloud data. In addition, photogrammetry has an automatic tool of texture projection, which makes automatic projection from the color directly on the surfaces possible (Meszaros 2011).

Image Processing

When cameras used in acquiring images have a wide-angle lens, lens distortion removal is required by calibrating the camera and removing the distortion by estimating the camera calibration parameters of center principal point, square pixels, and distortion models using the Brown distortion model (Brown 1966). Camera calibration data can also be calculated by the Agisoft Lens software (and exported if needed) or imported from an external source.

In the examples presented in this chapter, Agisoft PhotoScan Pro photogrammetry software was used to conduct the image processing. Agisoft PhotoScan is capable of interpolating digital images in order to create high-resolution, scaled, and geo-referenced 3D models from them. All clear images with sufficient overlap were included in the processing in order to generate a dense point cloud of the church. Ground control points (GCP) were applied to correct the scale and geo-reference the model. To complete the geo-referencing task, the program requires either Global Positioning System (GPS) coordinates associated with cameras, provided in an EXIF/plain text file, or GCP coordinates that can be used to achieve higher accuracy (up to 1 cm). Based on the latest multi-view 3D reconstruction technology, the software operates with arbitrary images and is efficient in both controlled and uncontrolled conditions (Remondino et al. 2011). Photos can be taken from any position, providing that the object to be reconstructed is visible on at least two photos with sufficient overlay. Both image alignment and 3D model reconstruction are fully automated.

Building Information Modeling

After the 3D model generation, the point cloud model is converted to the .rcp indexed format and imported into Autodesk Revit software to generate a Building Information Model (BIM). BIM is an intelligent 3D model-based process that involves the generation and management of digital representations of physical and functional characteristics of places. It can also be defined as a BIM virtual information model. BIM design tools allow extraction of different views from a building model for drawing production and other uses. After the BIM model is constructed, drawings of the plans, elevations, and sections of the church can be generated directly from the BIM model for documentation purposes. Also, information such as material, color, height, thickness, etc. can be added to each component in the BIM database.

Case Studies

The below case studies feature a variety of examples of how UAVs were used in order to acquire aerial images and document different types of cultural heritage and archaeological sites. Different UAVs were utilized based on the survey area. Gliders were used for surveying an extensive area, whereas drones were used for smaller areas and structures. As previously mentioned, the methodology used was the same in all case studies. First, GCPs were established at each site and the high-resolution aerial images were acquired using UAVs with different sensors. Second, once the aerial imagery was obtained using the UAV, the images were processed using SfM software to create a 3D model and then produce an ortho-image and digital elevation model. In some of the structures, the 3D model was imported into BIM in order to produce drawings, floor plans, and elevations.

Curium Case Study

The study took place in the southwest of Cyprus, in the archaeological site of Curium, which is situated outside the modern city of Limassol, Cyprus. Curium is considered one of the most significant archaeological sites on the island. Although the Kingdom of Curium was established in the Cypro-Geometric period (1050–750 BC), the majority of the archaeological remains within the Curium archaeological area date to the Roman and Late Roman/Early Byzantine periods. The area is particularly noted for its magnificent Greco-Roman theater, which was initially constructed in the late second century BC, until being abandoned in the later fourth century AD, most likely following successive earthquakes in the area.

In the Curium study, the QuestUAV Q-Pod Surveyor was used (Themistocleous et al. 2014a) in order to cover the entire site with a 20MP high-resolution camera.

Quest UAV Q-Pods are small unmanned airborne vehicle (UAV) capable of carrying a payload in flight and flying a pre-programmed route that is created in its flight planning software. All the necessary flight permissions were acquired from the Cyprus Aviation Authority (CAA) and the Sovereign Bases Area Administration (SBAA). The selected UAV was flown at a low altitude of 125 meters to provide high-resolution data for survey. Single images were taken automatically with a 60% overlap in an x and y direction in order to build a large detailed ortho-image and create a 3D model for accurate survey work (Themistocleous et al. 2015b). A 20 minute flight was needed to survey a 1 square km area with a 3 cm resolution. The UAV included a GPS unit that geo-tagged all the aerial images with the latitude and longitude within the metadata file of every image (Themistocleous et al. 2014a). Fixed ground control points distributed throughout the site were used in order to geo-reference the image with an accuracy up to 2 cm. The result was a high-resolution ortho-rectified image of the Curium site, which included the ancient hill, amphitheater, and all the monuments (Figs. 5 and 6).

The aerial images were processed in Agisoft Photoscan in order to create a 3D textured model of the amphitheater, as well as a digital terrain model (DTM) (Themistocleous et al. 2014a) (Figs. 7 and 8). The survey of the Curium site was conducted in order to document the entire site and examine the capabilities of the SfM technique in large archaeological sites, such as the Curium site area.

The process used in this case study is very useful in documenting large archaeological landscapes as satellite imagery cannot provide the resolution that is available with UAV images. Ortho-images that are produced by UAV using photogrammetric methods are more accurate when used with GCPs and can provide more information since the resolution is very high, especially with cameras exceeding 20MP resolution. The capabilities of the state-of-the-art drones, UAVs, and multi-copters provide stable



Fig. 5 Ortho-image of the ancient Curium archaeological site

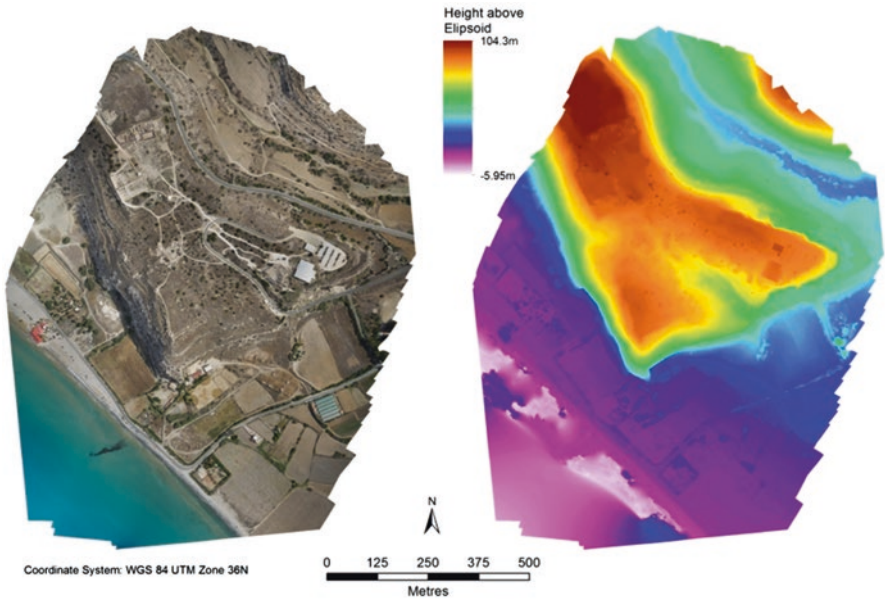


Fig. 6 Orthomosaic and reconstructed DTM of the ancient Curium archaeological site



Fig. 7 3D textured model of Curium in Agisoft PhotoScan Professional

aerial images using mechanisms to stabilize the camera, which are known as gimbles, thereby providing sharp and clear images that are geo-referenced due to the internal GPS of the UAV. This assists in the photogrammetry and modeling process, since the images are providing enough geo-referenced information in order to create an accurate and geometrically correct geo-referenced model.

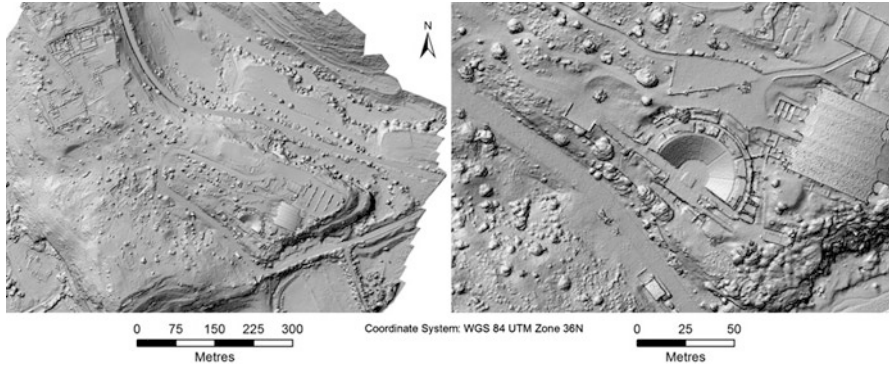


Fig. 8 DTM from Agisoft PhotoScan Professional



Fig. 9 3D model and 3D printed model of Curium amphitheater

The DTM of the amphitheater of the Curium archaeological site was used to print a 3D model (Fig. 9). The model was printed by “CU’Ting Edge” of Cyprus University of Technology, and it is now exhibited in the local museum of Curium. The model serves both for educational reasons as well as for visually impaired people (Themistocleous et al. 2016a).

Nea Paphos Mosaics and Archaeological Park Case Study

Nea Paphos was established at the end of the fourth century BC and was the capital city of Cyprus during the Roman period. The Nea Paphos archaeological park is a vast archaeological area, with remains of villas, palaces, theaters, fortresses, and tombs and is also a UNESCO World Heritage Site. Among the most significant remains discovered to date are four large and elaborate Roman villas (the House of Dionysos, the House of Aion, the House of Theseus, and the House of Orpheus), all with superb preserved mosaic floors. These mosaics constitute an illuminated album of ancient Greek mythology, with representations of Greek gods, goddesses, and heroes, as well as activities of everyday life. The mosaics of Nea Paphos are

extremely rare and are considered among the finest specimens in the world; they cover the Hellenistic period to the Byzantine period (UNESCO 2017).

Due to the size of the site, different UAVs were used to document archaeological sites in Nea Paphos, Cyprus (Themistocleous et al. 2014c, 2015a, b). Aerial images were taken with different UAV systems, including gliders and multi-rotors in order to survey the site. Archaeologists estimate that only 10% of Nea Paphos has been excavated. Therefore, researchers have been unable to reconstruct what Nea Paphos must have looked like at the time of its creation. Therefore, UAV surveys are important in assisting archaeologists and cultural heritage experts to manage the site and monitor environmental changes from erosion and pollution, since the site is located next to the sea and the modern city of Paphos.

In order to survey the entire site, 350 images were taken, and 56 GCPs were distributed over the site, generating a 3 cm per pixel resolution ortho-image and 13 cm per pixel DEM (Fig. 10). Contour lines were created to determine the topography of the area. Due to the high-resolution images derived from the UAVs, compared with satellite images, many crop marks are visible, which suggests possible underground archaeological features.

In order to document the famous mosaics in the archaeological park, multi-copters with a 20 MP high-resolution camera were flown at a low altitude of 50 meters and 80% overlap in both directions (forward and side overlap). This provided the ability to capture a higher-resolution model of 1 cm per pixel and create a more accurate 3D model of the site (Fig. 11).

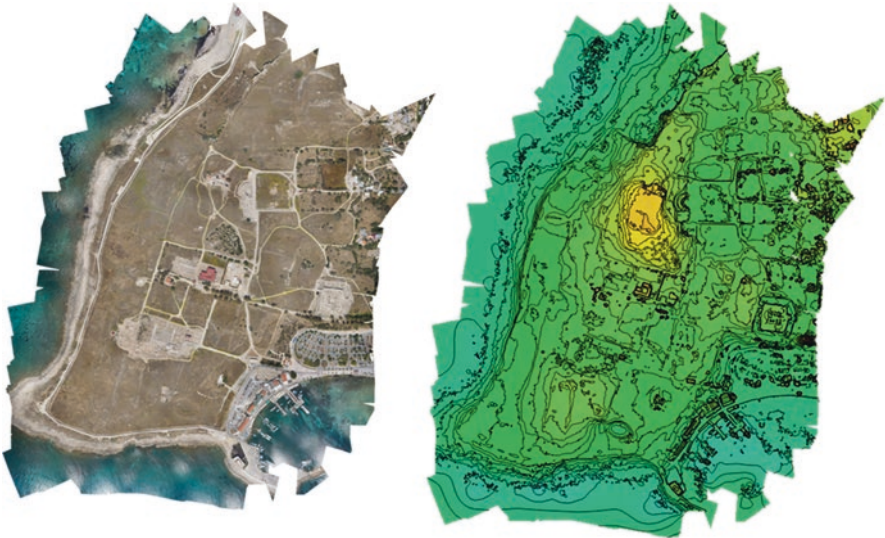


Fig. 10 Left: Ortho-image of Nea Paphos using a glider. Right: DEM with contour lines created from the 3D model

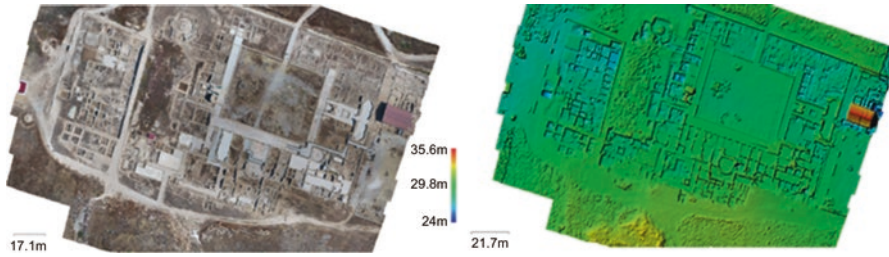


Fig. 11 Left: Ortho-image of the House of Aion, the House of Theseus, and the House of Orpheus. Right: DEM of the House of Aion, the House of Theseus, and the House of Orpheus created from the 3D model

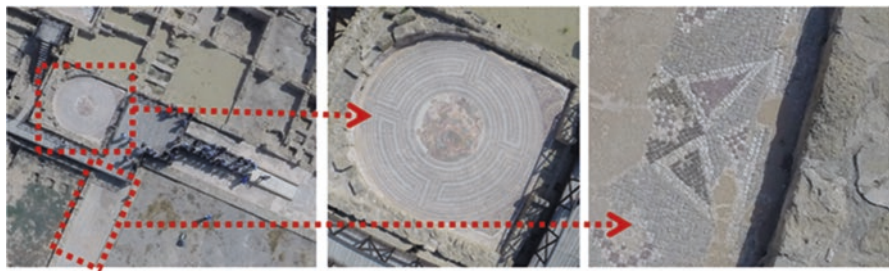


Fig. 12 Left—Aerial photograph of the archaeological park in Paphos, Cyprus. Center—Aerial photograph of the mosaic floor. Right—Aerial photograph of the mosaic corridor

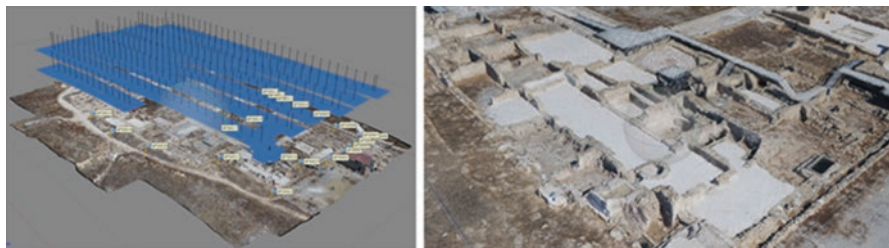


Fig. 13 3D model of archaeological park in Paphos using SfM

As a result, the images and the model generated from the high resolution images are extremely detailed to the point where the individual mosaics can be seen, as shown in Fig. 12.

Using all the images and GCPs acquired from the UAVs, a geo-referenced model and ortho-image were produced using the methodology described in this chapter and as shown in Fig. 13.

The geo-referenced ortho-images generated in this site will be compared with other images of the same study area at different times in order to identify any environmental changes in order for the relevant authorities to take the necessary actions to protect the site from further damage.

Fabrica Hill Case Study

Fabrica Hill is situated near Saint Paul's Pillar and the Ancient Theater Ruins in the city of Paphos. The Fabrica Hill most likely dates back to Hellenistic times and was used during Byzantine times as a quarry and storage area. The hill was named Fabrica because a textile mill existed at the site during the Middle Ages. The site includes some minor ancient mosaics that have been partially restored, as well as several ancient quarry caves from the Hellenistic period. The numerous underground caves are of sizeable proportions, and their coated walls may have been painted. The presence of these features makes Fabrica a very complex system and a challenging case study for accurate documentation (Themistocleous et al. 2014b). During the preparation for the "Paphos 2017- European Capital of Culture," the Municipality of Paphos requested that the site be documented in order to redesign the site and make it more accessible to tourists.

An aerial surveying of Fabrica Hill was conducted using a quadcopter equipped with a GoPro Hero 3 Camera (Themistocleous et al. 2014b, 2015b). In addition, the Leica laser scanner was used to support the UAV survey by providing an internal 3D model of the area. All images acquired by the copter were processed through the use of Agisoft Photoscan Profession software, while the point cloud data were processed in the Cyclone environment. Over 300 high-resolution images were taken above the Fabrica Hill and were post-processed using Agisoft Photoscan Professional software. The immediate outcome of the post-processing was the orthomosaic production deriving from the merging and layering of these multiple images (Fig. 14). The ortho-image was further exploited in order to produce the digital terrain model (DTM) of the area in order to generate a contour map. Further to the orthomosaic of the area, relative 3D models have been also retrieved. The most impressive models were those of the ancient amphitheater (Fig. 15).

All the 3D models and ortho-images were provided to the municipality and the architects in order to prepare a proposed plan for renovation of the area.

Asinou Church Case Study

The study area is the church of Panagia Phorbiotissa, better known as Asinou Church, which is located in the north foothills of the Troodos Mountains of Cyprus, which is a UNESCO World Heritage Site (Themistocleous et al. 2015c). A quadcopter with an added gimble, telemetry, and GoPro HERO3+ camera was used to acquire the aerial images of the church in order to create a 3D model. The small quadcopter was used due to its maneuverability, which was needed to take images above and around the church (Fig. 16).

The copter was flown in manual mode to ensure that all the images necessary for image processing are taken and to avoid any obstacles around the church, especially trees. During the flight, two operators were required for the aerial survey; one operator controlled the flight path of the UAV, while the other operator

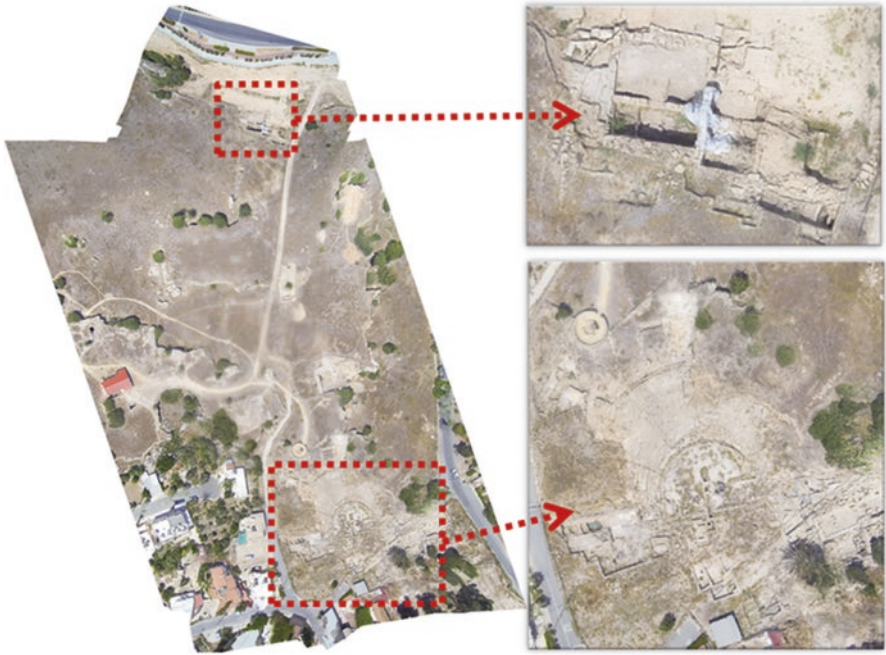


Fig. 14 Ortho-image of Fabrica Hills



Fig. 15 3D section of the amphitheater located at Fabrica Hill

monitored the UAV telemetry data. The telemetry information was transmitted to the operator on a monitor in order to verify the position, distance, height, and battery life of the quadcopter. This was necessary to guarantee the overlap and correct position of each image.



Fig. 16 Quadcopter with GoPro HERO3+ camera during flight



Fig. 17 Left, photographic image church; center, 3D model; right, 3D printed model

Over 1000 images were taken at Asinou Church, which were post-processed by removing the lens distortion and then processed using the Agisoft Photoscan Professional software. Since the GoPro HERO3+ camera used a wide-angle lens, lens distortion removal was required by calibrating the camera and removing the distortion using the appropriate distortion filter (Themistocleous et al. 2015c). Agisoft PhotoScan was used to conduct the image processing, thereby generating high-resolution geo-referenced orthomosaic, detailed DTMs, and textured polygonal models through the use of image overlay. Due to the manual flight parameters and low speed of the copter around the structure, the rolling shutter issue usually associated with the GoPro cameras were not an issue.

The processing began with the orthomosaic production from these multiple images, which was used for the 3D model (Fig. 17). Following the orthomosaic production, a high-resolution 3D mesh model of the church was generated and exported to a surface model (Themistocleous et al. 2015c). The surface model was imported into Autodesk 3DS Max in order to clean up, fix, and optimize the mesh. Any unnecessary noise or busy surroundings were cleaned up, and large mesh issues, such as particles, holes, spikes and tunnels, were fixed. The mesh was then

prepared for printing by exporting the corrected model into a .stl file, where a 3D printer was used to generate a 3D model. The model was printed using a Makerbot Replicator 3D printer with PLA filament and layer resolution of 100 microns, which provided an accurate representation of the church.

Foinikaria Church Case Study

The study focused on the Church of Panagia Chryseleousa in Foinikaria village, which is located in the Limassol District of Cyprus. The survey was done in cooperation with the Holy Bishopric of Lemesos in an effort to document the church in a short amount of time. In the study, the hexacopter with attached GoPro HERO+ 12MP camera was used to take aerial images of the church (Themistocleous et al. 2016b) (Fig. 18). The hexacopter was used due to its maneuverability to take images above and around the church. A gimbal was added to the camera to provide high-precision three-axis camera stabilization system that allows for smooth aerial photography. The integrated GPS included position holding, altitude lock, and stable hovering to provide constant stability in flight. The flying altitude was relatively low at 10 meters in order to produce higher-resolution images. The copter was flown in manual mode to ensure that all the images necessary for image processing are taken and to avoid any obstacles around the church, especially trees. During the flight, two operators were required for the aerial survey; one operator controlled the flight path of the UAV, while the other operator monitored the UAV telemetry data. The telemetry information was transmitted to the operator on a monitor in order to verify the position, distance, height, and battery life of the hexacopter.



Fig. 18 Foinikaria church, with UAV flyover and ground control point (GCP)

Over 1000 images were taken at the Foinikaria Church, which were post-processed by removing the lens distortion and then processed using the Agisoft Photoscan Professional software. The processing began with the orthomosaic production from these multiple images, which was used for the 3D model. Following the orthomosaic production, the model was exported from Agisoft into SketchFab for visualization purposes. The study found that particular areas were not well documented on the 3D model, due to an insufficient number of images in specific locations, such as the bell tower. This is evident below, where the bell tower is not clearly modeled.

Autodesk Revit software was used to generate a BIM 3D model of the church, including the bell tower (Fig. 19). The BIM model was overlaid with the point cloud (Themistocleous et al. 2016b).

The point cloud provided enough information so the structure of the building can be accurately modeled without the need of any in situ measurements. The point cloud information was especially necessary to model the roof, bell tower, arches, and openings. This provided a fast and accurate method for documenting the church. As well, the point cloud was able to capture the rough surface texture resulting of weathering (Fig. 20).

Sections of the 3D model overlaid with the point cloud. This provides detailed information regarding the exterior walls of the church and the structure of the narthex (Fig. 21).

Using the Revit software, drawings including floor plans, elevations, and sections of the church were generated (Fig. 22). A database was created to include information regarding the structure, including wall height, thickness, material, etc. This provided a valuable source of documentation of the church, for future restoration and maintenance works. Also, the documentation of the site was important to study possible expansion projects.

The elevations are also overlaid with the point cloud to provide additional information on the building, such as surface texture, color, and materials (Fig. 23).

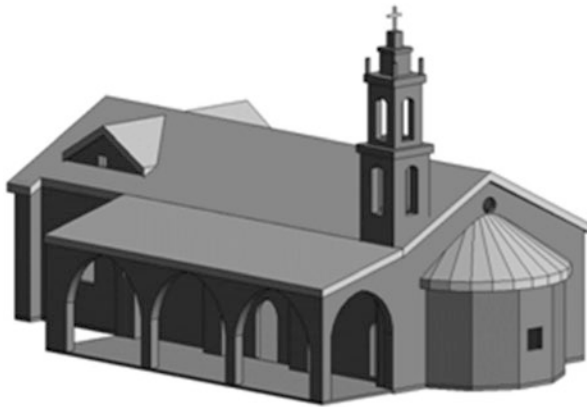


Fig. 19 BIM model of the church



Fig. 20 Left, 3D model of church; right, 3D point cloud model integrated with BIM model

Fig. 21 Point cloud section with BIM model

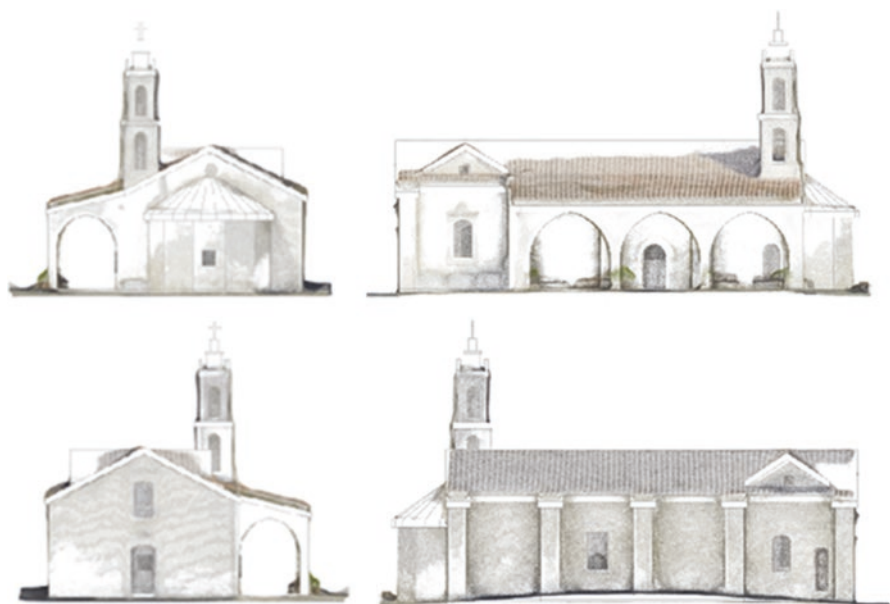
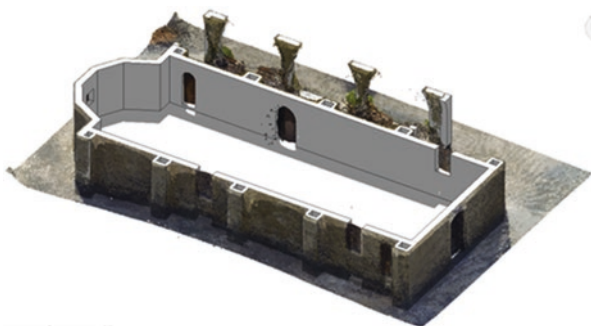


Fig. 22 Drawings of the Foinikaria church generated from BIM

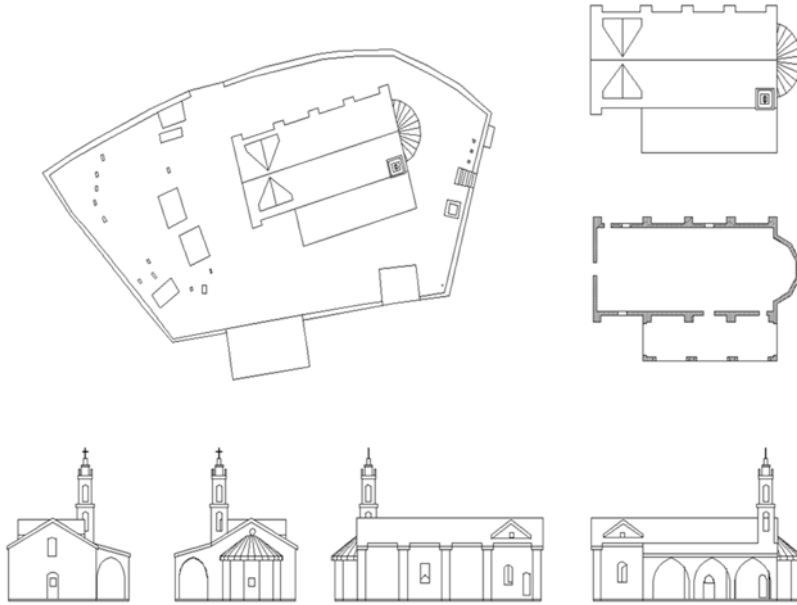


Fig. 23 Drawings of plans and elevations extracted from the BIM model

Choirokoitia Case Study

The Neolithic settlement of Choirokoitia is one of the most important prehistoric sites in the Eastern Mediterranean (UNESCO 2016). Included in the UNESCO World Cultural Heritage list since 1988, Choirokoitia is one of the best preserved Neolithic settlements in Cyprus and the Eastern Mediterranean. Occupied from the seventh to the fifth millennium BC, the site was officially abandoned in the fourth millennium BC for unknown reasons (UNESCO). Under the PROTHEGO project, which monitors and documents UNESCO cultural heritage sites vulnerable to geo-hazards, several UAV surveys have been done of the archaeological site of Choirokoitia, near Limassol Cyprus. Choirokoitia is a UNESCO World Heritage site that is vulnerable to ground deformations; therefore, UAVs were used to document the site (Themistocleous et al. 2016c). Surveying techniques, such as total station, leveling, and Global Navigation Satellite Systems (GNSS), were used to measure the positional changes of any point on the surface at millimeter level accuracy. In order to document the Choirokoitia sites, UAV images were used to create ortho-photos, dense clouds, 3D model, and digital elevation models (Themistocleous et al. 2017). Different multi-copter UAVs with a high-resolution 20MP camera were used to acquire images over the site with fixed ground control points for geo-referencing in order to produce a photogrammetric ortho-image



Fig. 24 Inspire 2 UAV with 20mp Zenmuse X5S camera and sensors



Fig. 25 Ortho-image of Choirokoitia site 29 October 2016

and point cloud 3D model of the demonstration site and also for comparison over temporal intervals (Fig. 24).

Aerial images were taken using UAVs on 29 October 2016 and 2 February 2017. Over 450 images were taken of the Choirokoitia site on 29 October 2016, and over 460 images were taken on 2 February 2017. Ground control points (GCP) were applied to correct the scale and geo-reference the model. The images were then pre-processed by removing the lens distortion and then processed using the Agisoft Photoscan Professional software (Fig. 25). The aerial imagery obtained from the UAVs was imported into SfM software to create rapid and automated generation of a point cloud model and 3D mesh model in order to document and monitor the Choirokoitia site for geo-hazards (Themistocleous et al. 2017).

All clear images with sufficient overlap were included in the processing in order to generate a dense point cloud of the Choirokoitia site. The images taken on 2 February 2017 were able to cover more of the mountain; therefore, the Choirokoitia site is outlined for clarification. In Fig. 26 and 27, the image on the left is from the

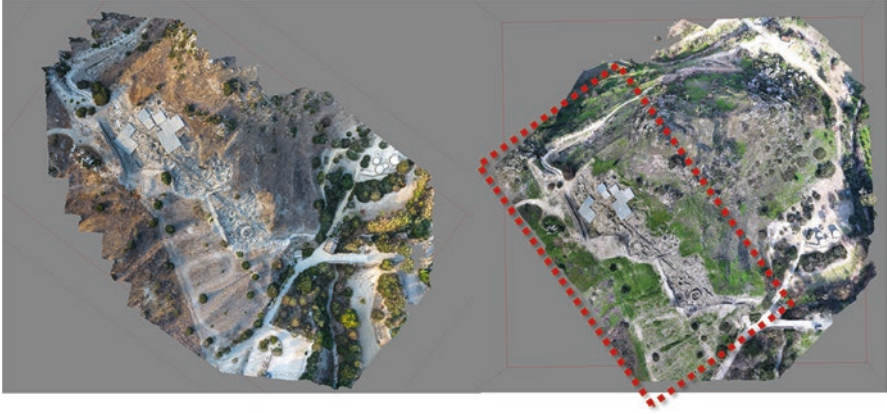


Fig. 26 Point cloud generation of Choirokoitia site

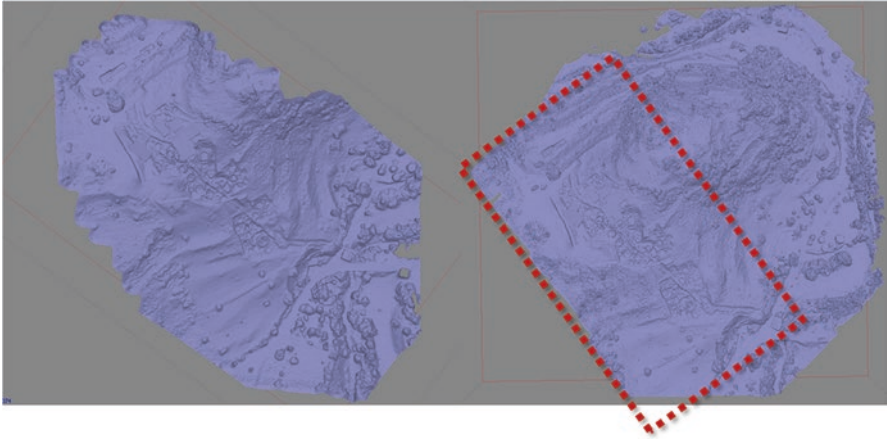


Fig. 27 3D surface model of Choirokoitia site

survey conducted on 29 October 2016, where the image on the right outlined in red is from the survey conducted on 2 February 2017.

As is evident, there was a dramatic difference in the level of vegetation present at the site on the dates that the images were acquired. The October 2016 images show sparse vegetation, while the images acquired in February 2017 show significantly more vegetation present at the site. As it was easier to identify vegetation in the images acquired in the winter campaign due to the color and morphology of the vegetation, masking was done in order to subtract the vegetation from the model in order to generate the DEM of the ground surface (Fig. 28). This was done by using interpolation of the areas where the vegetation was previously present. A contour

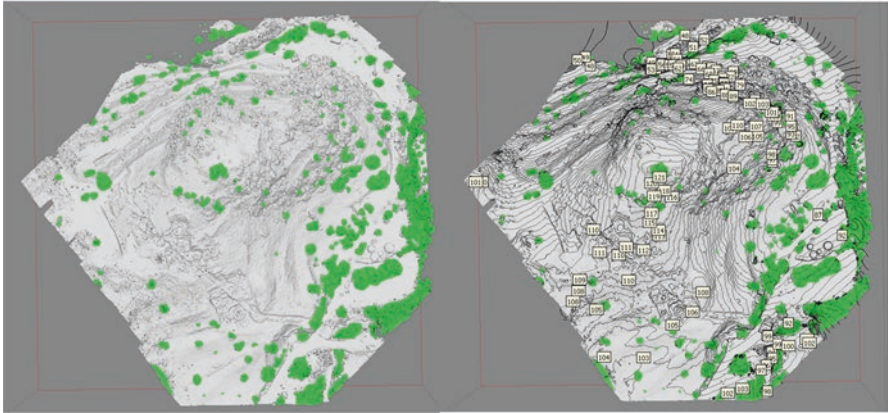


Fig. 28 Vegetation subtraction and contour generation

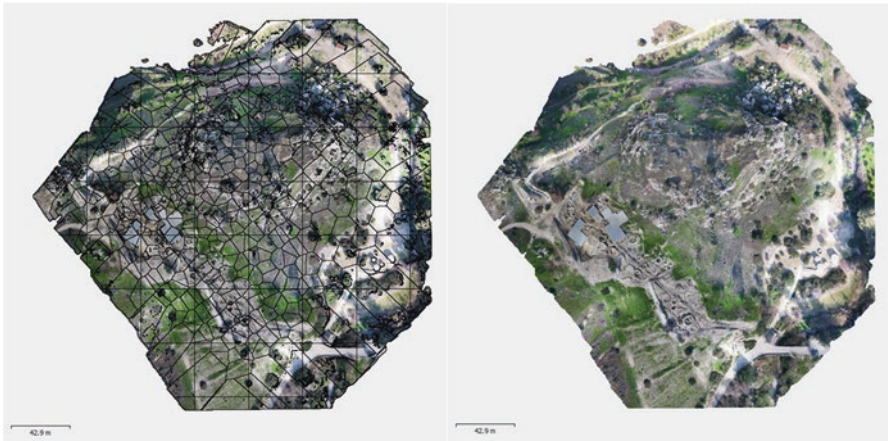


Fig. 29 Stitch imaging and ortho-generation

map of the area was then generated using stitch imaging using the DEM model without vegetation (Fig. 29).

The generated DEM model can assist in creating a simulation model to determine the rockfall patterns in the area (Fig. 30). In these types of simulations, it is important that vegetation be removed from the model in order to be more accurate using only the geological features of the landscape.

The ground-based geotechnical monitoring was also compared and validated with InSAR data to evaluate cultural heritage sites deformation trends and to understand its behavior over the last two decades.

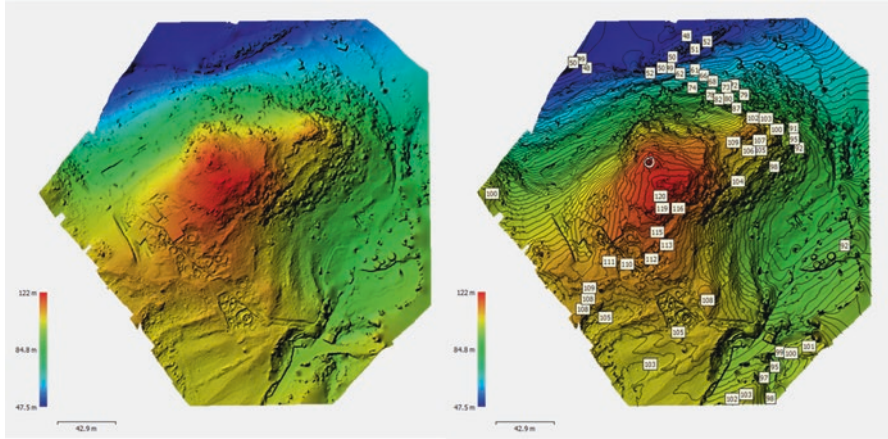


Fig. 30 Digital elevation model of Choirokoitia site

Amathus Necropolis Case Study

The ancient town of Amathus is situated on the south coast of Cyprus, about 7 km east of the town of Lemesos and dates to the Neolithic period. East and west of Amathus are two important necropolis with carved tombs which date from the Geometric to the Roman period. During the excavations of the tombs, rich archaeological material came to light, part of which is now exhibited in the Lemesos District Museum. The Department of Antiquities also focuses on the management, preservation and promotion of the archaeological site of Amathus, through the application of concrete strategies focused on securing its sustainability and development.

In cooperation with the Department of Antiquities, high-resolution digital cameras with VNIR sensors were used to document burial mounds in the Amathus archaeological site at varying elevations. The UAV survey was conducted as construction was scheduled to begin in the area; therefore, quick documentation of the archaeological site was necessary while the site was being excavated (Fig. 31). Since there was ongoing development in the area, the site was backfilled at the end of the archaeological excavation as a method of preservation and conservation. This example shows how UAVs can be important in documenting archaeological sites when documentation needs to be done in a limited time for a large area.

The aerial images in Fig. 32 were taken within a 1 month period, showing the excavations that took place on the site. Below, the image on the left shows the area at the beginning of the excavation, where the image on the right shows the area a month later, where different tombs were excavated.

At the site, there were various archaeological findings that were documented using the UAV while the site was being excavated. For example, the below image shows the documentation of a tomb that was located on the site. The UAV was able to enter into the burial chamber and document the entire structure. A 3D model was



Fig. 31 Ortho-image of the overall excavation site in Amathus, including detail of burial site



Fig. 32 Top, beginning of excavation; bottom, 1 month after the beginning of the excavation



Fig. 33 3D model of burial chamber at Amathus necropolis

created to show the capability of the UAV to provide detailed documentation of an archaeological dig, as shown in Fig. 33.

UAVs can be a valuable tool to document archaeological sites, especially when time is limited and high-resolution documentation is needed.

Conclusion

UAVs have become an extremely important tool for cultural heritage experts for the documentation and analysis of cultural heritage sites as they provide a cost-effective and efficient manner to acquire high spatial resolution data with high temporal frequencies, especially in areas that have limited coverage and are inaccessible to humans. The case studies presented in this chapter highlighted the ability of UAVs to provide high-resolution data of a cultural heritage site using a non-invasive technology and high accuracy with the use of ground control points.

The case studies examined various cultural heritage sites in Cyprus, where the high-resolution aerial imagery obtained from the UAVs was imported into Structure from Motion photogrammetry to create rapid and automated generation of a point cloud model and 3D mesh model. The high accuracy of the ortho-image and 3D model can be used to document and monitor changes of the cultural heritage sites over time. A printed 3D model can also be made of the structure. Also, the point cloud generated can be exported into BIM, in order to produce a BIM model and drawings of the structure. The high-accuracy documentation generated from the BIM model can be used for future renovation or expansion of the site.

Acknowledgment We would like to thank the ERATOSTHENES Research Centre and its staff for their invaluable assistance. Special thanks to the Department of Antiquities of Cyprus, the Cyprus Remote Sensing Society, the Cyprus Research Promotion Foundation, the Holy Bishopric

of Lemesos, QuestUAV, and the Southwestern Baptist Theological Seminary. Also, the author wishes to acknowledge the Cyprus Aviation Authority (CAA) and the Sovereign Bases Area Administration (SBAA) for their assistance in providing flight permission. Finally, additional thanks to the “ATHENA” project H2020-TWINN2015 of the European Commission, No. 691936, the “PROtection of European Cultural HERitage from Geo - hazards (PROTHEGO)” project JPICH HERITAGE PLUS/0314/36 and the Cultural Landscape risk Identification, Management and Assessment (CLIMA) project, JPICH HERITAGE PLUS/0314/07.

References

- Agapiou A, Cuca B, Themistocleous K, Alexakis DD, Hadjimitsis DG (2013) Integrated method for tracking changes in archeo-landscapes using remote and close-range technologies. Proceedings of the International Congress of Digital Heritage, 28 October–01 November, 2013, Marseille, France, 2013. Doi: <https://doi.org/10.1109/DigitalHeritage.2013.6743740>
- Brown DC (1966) Decentering distortion of lenses. *Photometr Eng* 32(3):444–462
- Brumana R, Oreni D, Van Hecke L, Barazzetti L, Previtali M, Roncoroni F, Valente R (2013) Combined geometric and thermal analysis from UAV platforms for archaeological heritage documentation. *ISPRS Annals of the Photogrammetry, Remote Sensing and Spatial Information Sciences*, Volume II-5/W1, XXIV Int. CIPA Symposium, Sept. 2–6, Strasbourg, France, pp. 49–54
- Burkhart A, Cogliati S, Schickling A, Rascher U (2014) A novel UAV-based ultra-light weight spectrometer for field spectroscopy. *Sensors J IEEE* 14(1):62–67
- Cho G, Hildebrand A, Claussen J, Cosyn P, Morris S (2013) Pilotless aerial vehicle systems: size, scale and functions. *Coordinates* 9:8–16
- Colomina I, Molina P (2014) Unmanned aerial systems for photogrammetry and remote sensing: a review. *ISPRS J Photogramm Remote Sens* 92:79–97
- Eisenbeiss H (2009) UAV Photogrammetry, Ph.D. Thesis. Institute für Geodesie und Photogrammetrie, ETH-Zürich. Zürich, Switzerland
- El-Hakim SF, Beraldin JA, Picard M, Godin G (2004) Detailed 3D reconstruction of large-scale heritage sites with integrated techniques. *IEEE Comput Graph Appl* 24(3):21–29
- Everaerts J (2008) The use of Unmanned Aerial Vehicles (UAVS) for remote sensing and mapping. *IAPRS SIS* 37:B11187–B11192
- Fiorillo F, Jimenez B, Remondino F, Barba S (2012) 3D surveying and modeling of the archaeological area of Paestum, Italy. *Virtual Archaeol Rev* 4:55–60
- Giuliano MG (2014) Cultural Heritage: an example of graphical documentation with automated photogrammetric systems. *International Archives of the Photogrammetry, Remote Sensing and Spatial Information Sciences* XL.5: 251–255. Gottingen: Copernicus GmbH. 2014
- Gruen A, Remondino F, Zhang L (2005) The Bamiyan project: multi-resolution image-based modeling. In: Baltasavias E, Gruen A, Van Gool L, Pateraki M (eds) *Recording, modeling and visualization of cultural heritage*. Taylor and Francis, Balkema. ISBN 0 415 39208 X, 45–54
- Guidi G, Remondino F, Russo M, Menna F, Rizzi A, Ercoli S (2009) A multi-resolution methodology for the 3D modeling of large and complex archaeological areas. *Int J Archit Comput* 7(1):40–55
- Hassani F (2015) Documentation of cultural heritage techniques, potentials and constraints. *International Archives of the Photogrammetry, Remote Sensing and Spatial Information Sciences*, Volume XL-5/W7, 25th Intl CIPA Symp. 2015, 31 August – 04 September 2015, Taipei, Taiwan
- Ingwer P, Gassen F, Püst S, Duhn M, Schällicke M, Müller K, Ruhm H, Rettig J, Hasche E, Fischer A, Creutzburg R (2015) Practical usefulness of structure from motion (SfM) point clouds obtained from different consumer cameras. *Proceedings of SPIE 9411, Mobile Devices and Multimedia: Enabling Technologies, Algorithms, and Applications 2015*, 941102

- Ioannides M, Hadjiprocopis A, Doulamis N, Doulamis A, Protopapadakis E, Makantasis K, Santos P, Fellner D, Stork A, Balet O, Julien M, Weinlinger G, Johnson PS, Klein M, Fritsch D (2013) Online 4D reconstruction using multi-images available under open access. *ISPRS Annals of Photogrammetry, Remote Sensing and Spatial Information Sciences II-5/W1*(2013):169–174
- Kostrzewa J, Meyer W, Laband S, Tere W, Petrovich P, Swanson K, Sundra C, Sener W, Wilmott J (2003) Infrared microsensory pay-load for miniature unmanned aerial vehicles. *Proceedings of the SPIE 5090, Unattended Ground Sensor Technologies and Applications*, v265
- Lo Brutto M, Garraffa A, Meli P (2014) UAV platforms for cultural heritage survey: first results. *ISPRS Annals Photogramm Remote Sens Spat Inf Sci II-5*(2014):227–234
- Mayr W (2013) Unmanned aerial systems -for the rest of us. *Proceedings of the 53rd Photogrammetric Week. Institute fur Photo-grammetrie, Universitat Stuttgart*, 125–134
- Meszaros J (2011) Aerial surveying UAV based on open-source hardware and software. *Proceedings of the International Archives of the Photogrammetry, Remote Sensing and Spatial Information Sciences, XXXVIII-1/C22*
- Petrie G (2013) Commercial operation of lightweight UAVs for aerial imaging and mapping. *GEOInformatics 16:28–39*
- Remondino F, Rizzi A (2009) Reality-based 3D documentation of world heritage sites: methodologies, problems and examples. *Proceedings of the 22nd CIPA symposium, October 11–15, 2009, Kyoto, Japan*
- Remondino F, Barazzetti L, Nex F, Caioni M, Sarazi D (2011) UAV photogrammetry for mapping and 3D modelling-current status and future perspectives. *Proceedings of the International Archives of the Photogrammetry, Remote Sensing and Spatial Information Sciences*, 25–31
- Rinaudo F, Chiabrando F, Lingua A, Span A (2012) Archaeological site monitoring: UAV photogrammetry can be an answer. *Proceedings of the International Archives of the Photogrammetry, Remote Sensing and Spatial Information Sciences Volume XXXIX-B5, 2012XXII ISPRS Congress, 25 August–01 September 2012, Melbourne, Australia.*, 583–588
- Rönholm P, Honkavaara E, Litkey P, Hyyppä H, Hyyppä J (2007) Integration of laser scanning and photogrammetry. *Int Arch Photogramm Remote Sens Spat Inf Sci 36(3/W52):355–362*
- Ruffino G, Moccia A (2005). *Integrated VIS_NIR Hyperspectral/thermal-IR Electro-optical Payload System for a Mini-UAV. American Institute of Aeronautics and Astronautics*, 647–664
- Scholtz A, Kaschwich C, Kruger A, Kufieta K, Schnetter P, Wilkens C, Kruger T, Vorsmann P (2011) Development of a new multipurpose UAS for scientific application. *Proceedings of the International Conference on Unmanned Aerial Vehicle in Geomatics (UAV-g), Zurich, Switzerland, September 14–16, 2011,ISSN 1682–1777 Vol XXXVIII-1/C22*
- Scopigno R, Cignoni P, Pietroni N, Callieri M, Dellepiane M (2015) Digital fabrication Technologies for Cultural Heritage (STAR). *EUROGRAPHICS Workshops on Graphics and Cultural Heritage*. doi:<https://doi.org/10.1117/12.2074892>
- Seitz C, Altenbach H (2011) Project ArchEye - the quadcopter as the archaeologist's eye. *Proceedings of the International Archives of the Photogrammetry, Remote Sensing and Spatial Information Sciences, XXXVIII-1/C22*, 297–302
- Themistocleous K, Agapiou A, King HM, King N, Hadjimitsis DG (2014a) More than a flight: the extensive contributions of UAV flights to archaeological research - the case study of curium site in Cyprus. *Proceedings of the Progress in Cultural Heritage: Documentation, Preservation, and Protection. 5th International Conference, EuroMed 2014, Limassol, Cyprus. Springer LNCS 8740, EuroMed2014 Conference*, 396–409
- Themistocleous K, Agapiou A, Cuca B, Hadjimitsis DG (2014b) 3D Documentation Of Cultural Heritage Sites. *Proceedings of the Progress in Cultural Heritage: Documentation, Preservation, and Protection. 5th International Conference, EuroMed 2014, Limassol, Cyprus, Springer LNCS 8740, EuroMed2014 Conference*
- Themistocleous K, Agapiou A, Alexakis D, Cuca B, Hadjimitsis DG (2014c) Lessons learnt from using UAVs in Cyprus: landscapes applications. *Proceedings of the Archland UAV Conference 2014, 23–25 May, Berlin, Germany, 2014*
- Themistocleous K, Agapiou A, Cuca B, Hadjimitsis DG (2015a) Unmanned aerial systems and spectroscopy for remote sensing applications in archaeology. *Proceedings of the 36th*

- International Symposium on Remote Sensing of Environment (ISRSE-36), 11–15 May, 2015, Berlin Germany
- Themistocleous K, Agapiou A, Lysandrou V, Hadjimitsis DG (2015b). The use of UAVs for remote sensing applications: case studies in Cyprus. Proceedings of the SPIE Remote Sensing Conference, 21–24 September, 2015, Toulouse, France
- Themistocleous K, Ioannides M, Agapiou A, Hadjimitsis DG (2015c). The methodology of documenting cultural heritage sites using photogrammetry, UAV and 3D printing techniques: the case study of Asinou church in Cyprus. Proceedings of the Third International Conference on Remote Sensing and Geoinformation of Environment, 2015, 16–19 March, 2015
- Themistocleous K, Agapiou A, Hadjimitsis DG (2016a) Experiencing cultural heritage sites using 3D modeling for the visually impaired. Proceedings of Euromed 2016: Digital Heritage, Progress in Cultural Heritage: Documentation, Preservation, and Protection, Lecture Notes in Computer Science, Vol. 10059, 171–177, 31 October – 4 November, 2016 Nicosia Cyprus
- Themistocleous K, Agapiou A, Hadjimitsis DG (2016b) 3D documentation and BIM modeling of cultural heritage structures using UAVS: the case of the Foinikaria church. Proceedings of the 3D Geoinfo Conference, International Archives of the Photogrammetry, Remote Sensing and Spatial Information Sciences, Volume XLII-2/W2, 2016 11th, 20–21 October 2016, Athens, Greece
- Themistocleous K, Agapiou A, Cuca B, Danezis C, Cigna F, Margottini C, Spizzichino D (2016c) Methodology for locale-scale monitoring for the PROTHEGO project: the Choirokoitia case study. Proceedings of SPIE 10005, Earth Resources and Environmental Remote Sensing/GIS Applications VII, 100050M, 26–29 September, 2016, Edinburgh, Scotland. doi:<https://doi.org/10.1117/12.2242047>
- Themistocleous K, Danezis C, Mendonidis E, Lympelopoulou E (2017) Monitoring ground deformation of cultural heritage sites using UAVs and geodetic techniques: the case study of Choirokoitia, JPI PROTHEGO project. SPIE Remote Sensing Conference, 11–14 September, 2017. Warsaw, Poland
- UNESCO World Heritage List “Choirokoitia”. <http://whc.unesco.org/en/list/848>. (1 March, 2016)
- UNESCO World Heritage List “Paphos”. <http://whc.unesco.org/en/list/79>. (20 August, 2017)

Part IV
Added Value of In-Situ Data

Remote Sensing Work in Palmyra/Syria



Andreas Schmidt-Colinet

Abstract The existence of a pre-Roman settlement of Palmyra is attested by literary sources. But, the location of this early settlement was unknown until recently. By several reasons its location was supposed to be located in the area outside the later Roman city. In 1997 and 1998, a geophysical prospection in the area south of the Wadi was carried out. A zone of about 2 ha was prospected by Caesium–Magnetometry. About 100 m² of this zone was measured also by electric resistivity. Result: Without excavation, a complete city plan can be recognized under the sand. Based on the magnetogram, small stratigraphic archaeological excavations proved a dating of these building structures between the third century BC and the third century AD. Thus, the location, date and part of the urban structure of ancient Palmyra were proved. Furthermore, the whole area can be protected now as antiquities zone by the Syrian authorities.

Keywords Palmyra · Syria · Hellenistic · Caesium–Magnetometry · Electric Resistivity · Satellite Pictures · Magnetogram

Introduction

All the antique ruins to be seen today at the ancient town of Palmyra in the Syrian desert are dated from the first century BC to the eighth century AD, that is, from the Roman imperial time up to the early mediaeval/early Islamic period (Figs. 1 and 2).

According to written antique sources, an important settlement – called POLIS (= city) in Greek texts – did exist at Palmyra in pre-Roman times already. As any traces of this ancient city were found never inside the Roman city wall even by deep sondages, the location of this early settlement was supposed to be located outside the later Roman city.

A. Schmidt-Colinet (✉)

Institute of Classical Archaeology, University of Vienna, Vienna, Austria

e-mail: Andreas.Schmidt-Colinet@univie.ac.at

© Springer Nature Switzerland AG 2020

D. G. Hadjimitsis et al. (eds.), *Remote Sensing for Archaeology and Cultural Landscapes*, Springer Remote Sensing/Photogrammetry,

https://doi.org/10.1007/978-3-030-10979-0_15

273

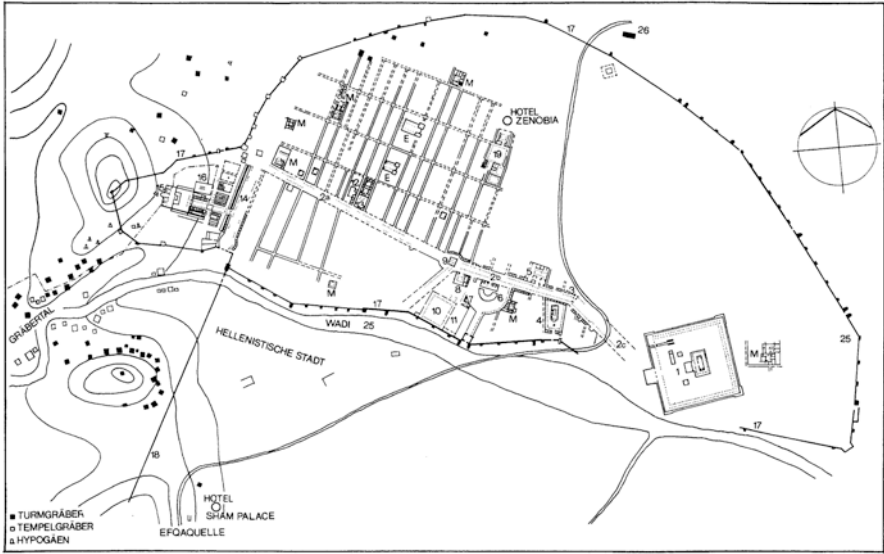


Fig. 1 Palmyra, General plan

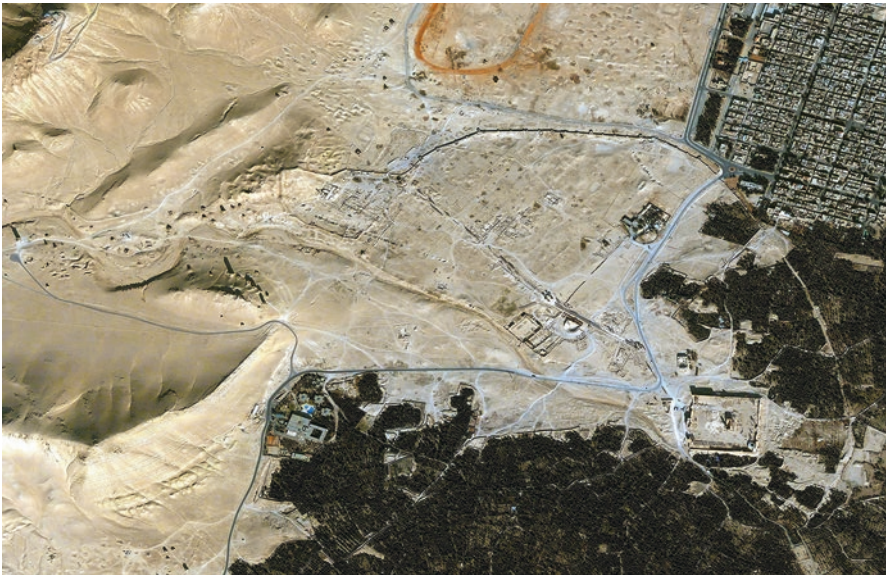


Fig. 2 Palmyra, Satellite picture. (Digital Globe, European Space Imaging, 2011)

Archaeological Excavation

In 1997, an international archaeological mission started a project on the location and research of this pre-Roman settlement of Palmyra. By several reasons, it was supposed to be located south of the roman town in the area between the Wadi al-Kubur and the oasis gardens. In this area, today only a few ruined walls can be made out above ground (Fig. 3).

In March 1997 and 1998, a geophysical prospection of this area was carried out combined with a digital ground modelling based on photogrammetry. A zone of about 20 ha was prospected by Caesium–Magnetometry within 40 × 40 m grids. Within this zone, a smaller area of about 100 m² was measured also by electric resistivity. With this method, archaeological building structures of different density hidden under the sand can be made visible without any excavation (Figs. 4, 5, 6 and 7).

The magnetogram shows a widespread city plan with street systems and adjacent buildings. Two main streets oriented NW–SE, resp., SW–NE join in a V-shaped conjunction in the East. The northern main street runs parallel to the Wadi at a distance of about 80–90 m. This road is the prolongation of the main route connecting Palmyra with Emesa/Homs in the West. Between the street and the Wadi, several large square house structures (perhaps peristyle houses) can be recognized.



Fig. 3 Palmyra, Area of the 'Hellenistic town' south of the Wadi, view from SW

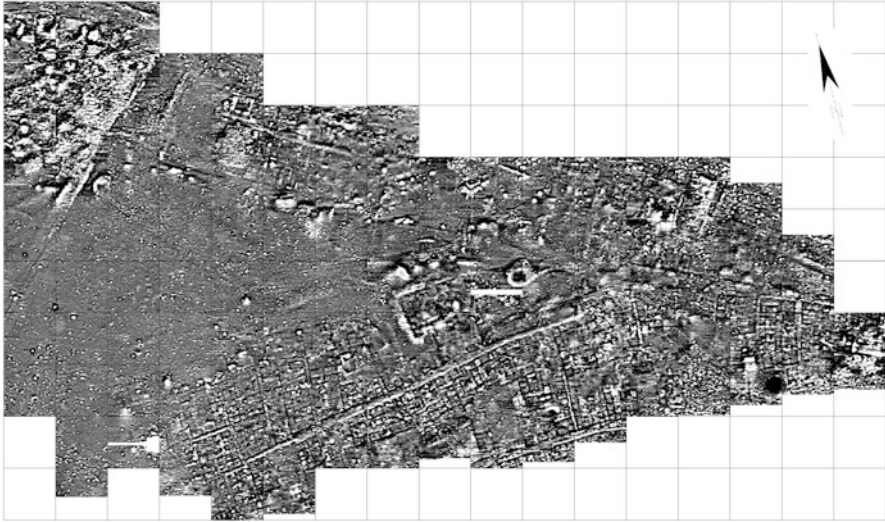


Fig. 4 Magnetogram of the area of the 'Hellenistic town'

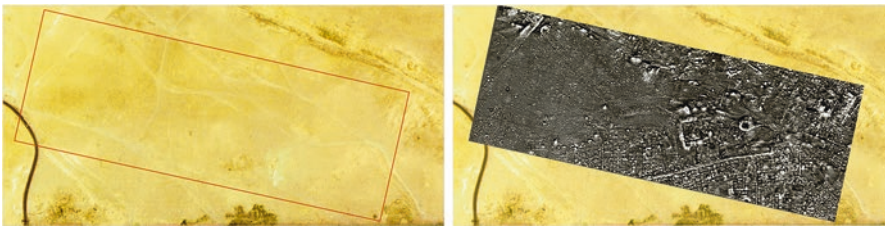


Fig. 5 Palmyra, Area of the 'Hellenistic town', satellite picture without and with the montage of the magnetogram

The southern main road is linked with another parallel road further in the south by several more-or-less rectangular smaller side roads. The main road is the prolongation of the main route connecting Palmyra with Damascus in the SW. A dense layout of smaller-scale houses can be recognized north and south of the main road down to the parallel road in the south and even further south.

In the very centre, within the angle between the two main roads, a large square building of about 40×40 m can be seen, the so-called Khan (see below). West of this monumental structure, there is an empty space without any building structures. Maybe it was used for camel caravans or for nomad's tents.

Finally, in the westernmost part, a city wall is visible. Outside the wall, many burned structures can be recognized, probably burned tombs.

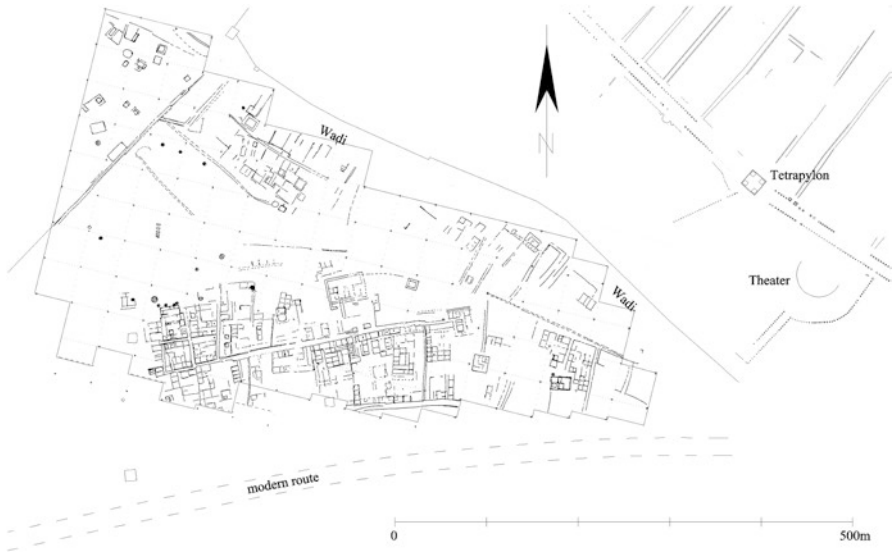


Fig. 6 Palmyra, interpretation of the magnetogram



Fig. 7 Palmyra, satellite picture with the interpretation of the magnetogram (in red)

Based on this first interpretation of the magnetogram, two small-scaled stratigraphic excavations were started (Fig. 8). The one (sondage I) had the aim to date the building structures visible on the magnetogram. The other (sondage II) should clear up the dating and the interpretation of the monumental building in the very centre.

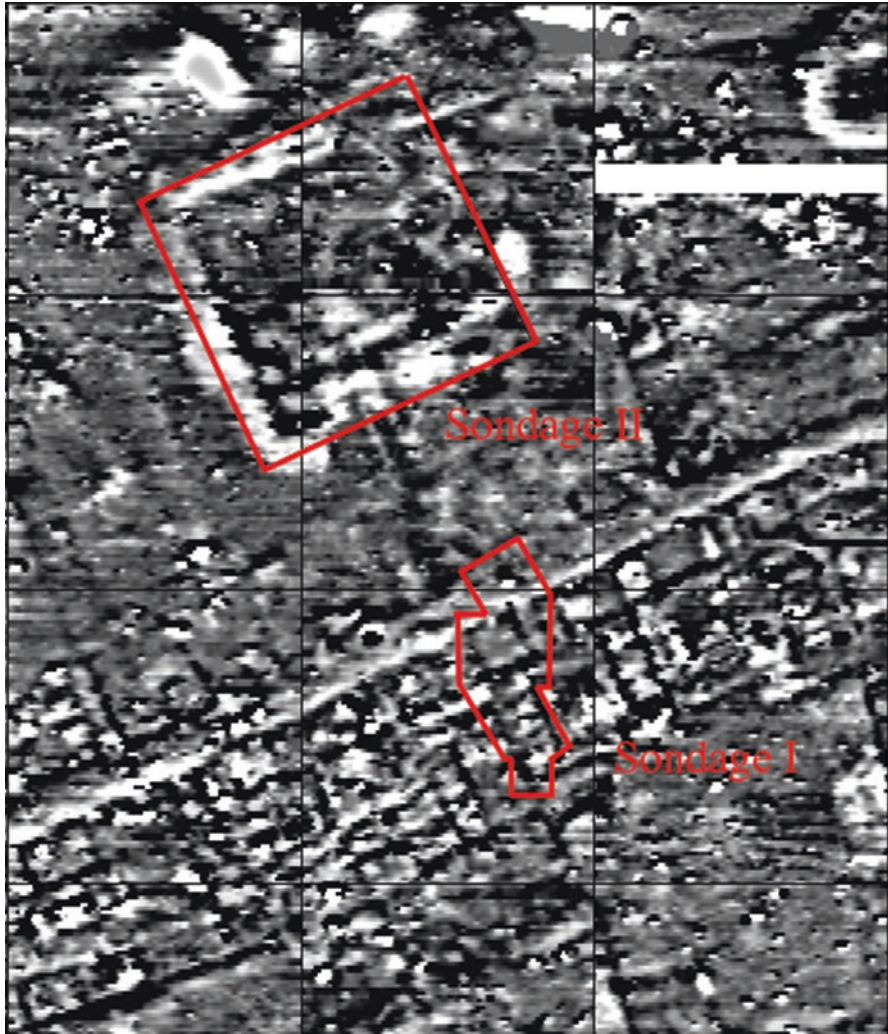


Fig. 8 Palmyra, Magnetogram with sondage I and II (in red)

With sondage I (Fig. 9) a section of the main road was excavated with adjacent dwellings. In the middle of the main road existed a water pipe line and a well. The latter as well as the earliest building structures south of the road can be dated to the second half of the third century BC by the small finds correlated with these structures. In general, the sounding proved a relative and absolute chronology of building activities from the third century BC up to the third century AD.

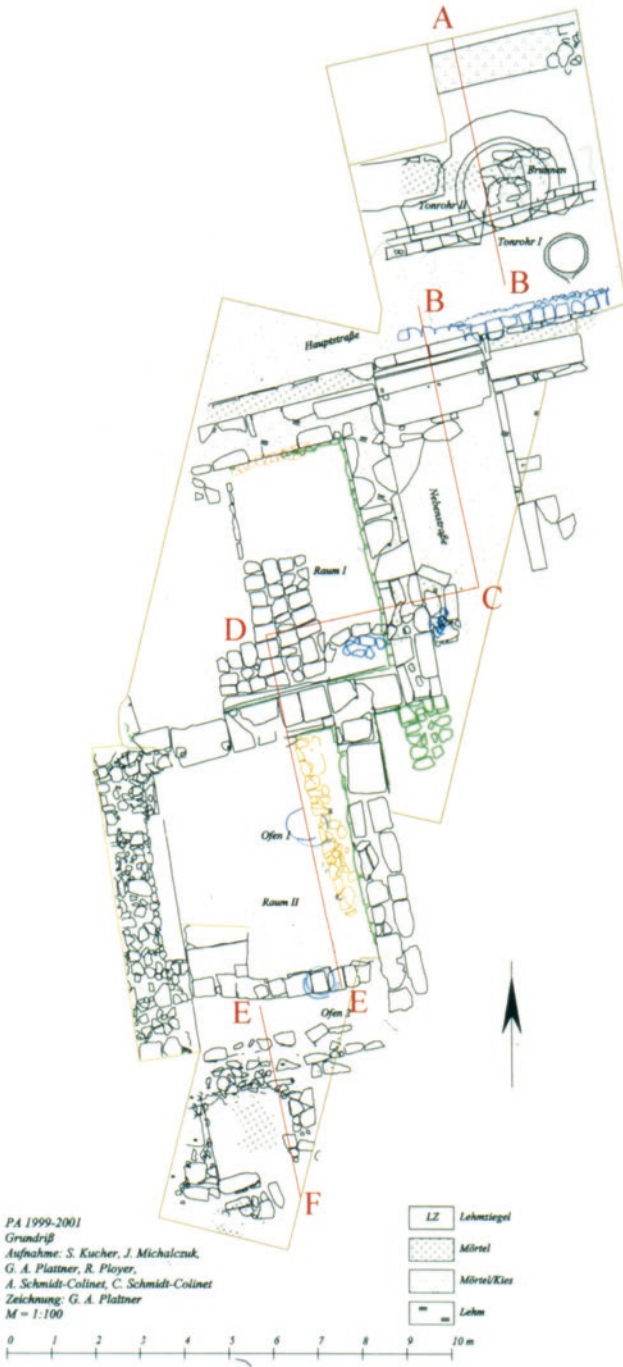


Fig. 9 Palmyra, Sondage I, ground plan



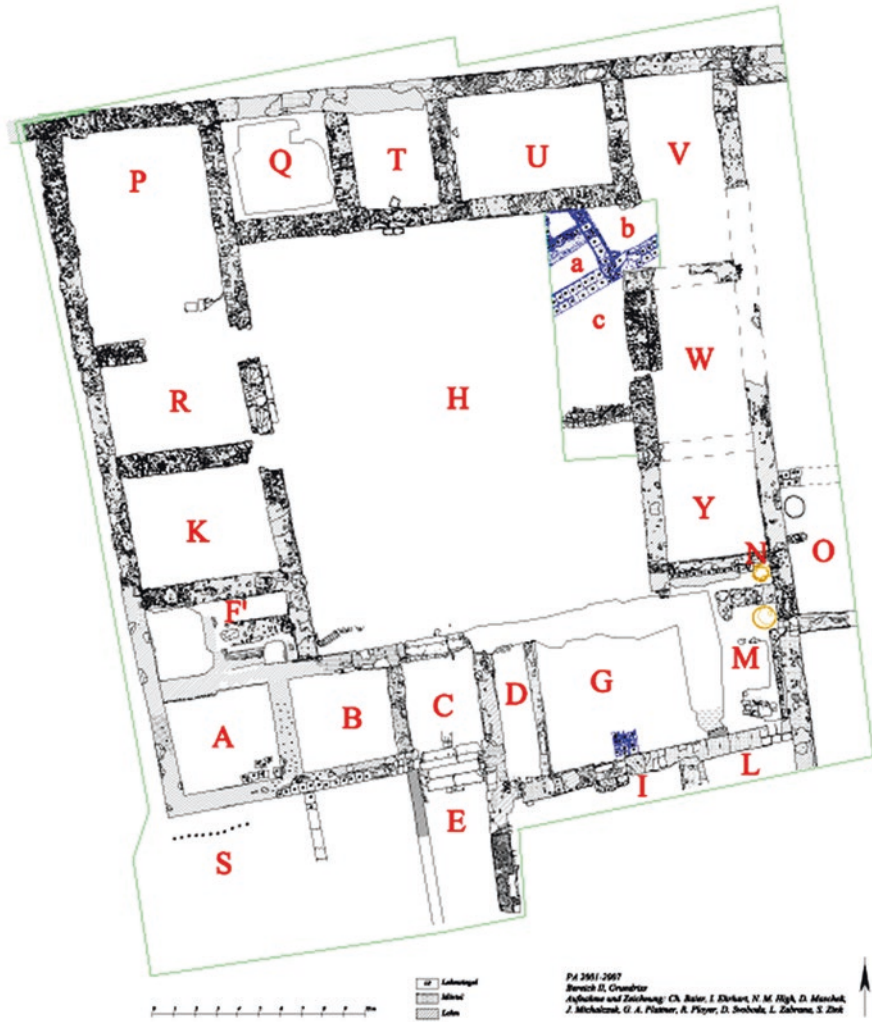


Fig. 10 Palmyra, Sondage II, Groundplan of the 'Khan'

With sondage II (Fig. 10) the residence of a noble family ('Khan') was excavated. The courtyard building with adjacent rooms existed from the middle of the first century BC up to the third century AD according to the small finds. The small finds also attest a worldwide international global trade of the owners of the house.

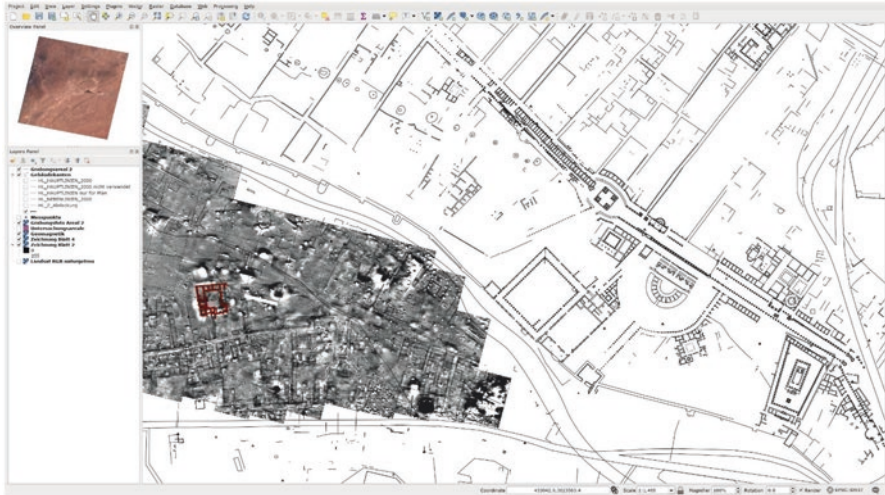


Fig. 12 Digital map of Palmyra, GIS Screenshot, work status spring 2017

References

- Becker H, Fassbinder JWE (1999) Combined Caesium Magnetometry and resistivity survey in Palmyra (Syria) 1997 and 1998. In: JWE F, Irlinger WE (eds) *Archaeological prospection. Third international conference on archaeological prospection Mu-nich, 9–11. September 1999*, Arbeitshefte des Bayerischen Landesamtes für Denkmalpflege 18 (Munich 1999), pp 156–160
- Browning I (1979) *Palmyra* (London 1979)
- Colledge MAR (1976) *The art of Palmyra* (London 1976)
- Ertel Ch, Ployer R (2013) *Sondage II: Ein späthellenistisch-römisches Hofhaus Baubefund, Architektur, Chronologie*, In: Schmidt-Colinet – al-As‘ad 2013, pp 118–169 (with English and Arabic summaries)
- Ertel Ch, Ployer R (2016) A Roman Residential house in the ‘Hellenis-tic’ Town of Palmyra: archaeology, function and urban aspects – vessel glass, in: J. Ch. Meyer – E. H. Seland – N. Anfinset (eds) *Palmyrena: City, Hinterland and Caravan trade between orient and occident. Proceedings of the conference held in Athens, December 1–3, 2012* (Oxford 93–106)
- Fassbinder JWE, Linck R (2013) *Geophysikalische Prospektion*. Schmidt-Colinet – al-As‘ad 2013, pp 79–88. (with English and Arabic summaries)
- General Organization of Remote Sensing (GORS) – Geospace (ed) *Syria. Archaeology from the space* (Damascus/Salzburg 2001)
- Hammad M (2010) *Palmyre. Transformations urbaines. Développement d’une ville antique de la marge aride syrienne* (Paris 2010)
- Linck R, Fassbinder JWE (2011) *Im Reich der Königin Zenobia. Satellitenradar- und Magnetometerprospektion in Palmyra, Syrien*, Bayerisches Landesamt für Denkmalpflege. *Denkmalpflege Informationen* 149(2011):74–77
- Linck R (2013) *Methodische Untersuchungen zur Weiterentwicklung der Boden- und Satellitenradarprospektion in der Archäologie*, Diss. Fakultät für Geowissenschaften der Ludwig-Maximilians-Universität (Munich 2013)
- Linck R (2016) *Geophysical prospection by ground- and space-based methods of the ancient town of Palmyra (Syria)*. In: JCh M, Seland EH, Anfinset N (eds) *Palmyrena: City, Hinterland and*

- Caravan trade between orient and occident. Proceedings of the conference held in Athens, December 1–3, 2012, Oxford, pp 77–86
- Plattner GA (2013) Sondage I: Eine hellenistisch-römische Straßenkreuzung und angrenzende Wohnbebauung Baubefund, Architektur, Chronologie. Schmidt-Colinet – al-As'ad 2013, pp 89–117. (with English and Arabic summaries)
- Schmidt-Colinet A (ed) (2015) Palmyra. Kulturbegegnung im Grenzbereich 3(Mainz 2015)
- Schmidt-Colinet A, al-As'ad Kh (2000) Zur Urbanistik des hellenistischen Palmyra. Ein Vorbericht, DaM 12, 2000, pp 61–93 pl. 7–16 (with contributions of H. Becker, Chr. Römer-Strehl and M. Stephani)
- Schmidt-Colinet A, al-As'ad Kh (2002) Archaeological news from Hellenistic Palmyra, Parthica 4, 2002, pp 157–166
- Schmidt-Colinet A, al-As'ad W (eds) (2013) Palmyras Reichtum durch weltweiten Handel. Archäologische Untersuchungen im Bereich der hellenistischen Stadt, 2 vols. (Vienna 2013, with English and Arabic summaries)
- Schmidt-Colinet A, al-As'ad Kh, al-As'ad W (2008) Zur Urbanistik des hellenistischen Palmyra. Zweiter Vorbericht, ZOrA 1, 2008, pp 452–478 (with contributions of R. Ployer and Chr. Römer-Strehl; with English and Arabic summaries)
- Schmidt-Colinet A, al-As'ad K, al-As'ad W (2013) Thirty years of Syro-German/Austrian archaeological research at Palmyra. In: Gawlikowski M, Majcherek G (eds) Fifty years of Polish Excavations in Palmyra 1959–2009. International Conference, Warsaw, 6–8 December 2010 (Warsaw 2013) = Studia Palmyreńskie 12, pp 299–318
- Schmidt-Colinet A, Plattner GA (2001) Geophysical survey and excavation in the, 'Hellenistic Town' of Palmyra. In: Doneus M, Eder-Hinterleitner A, Neubauer W (eds) Archaeological Prospec-tion. Fourth international conference on archaeological prospection Vienna, 19–23. September 2001, Vienna, pp 175–177
- Schnädelbach K (2010) Topographia Palmyrena 1. Topography, Docu-ments d'archéologie syrienne 18 (Damascus 2010)
- Starcky J Gawlikowski M (1985) Palmyre (Paris 1985)
- Wiegand Th (ed) (1932) Palmyra. Ergebnisse der Expeditionen von 1902 und 1917, 2 vols. (Berlin 1932)
- Will E (1992) Les Palmyréniens. La Venise des sables. (Ier siècle avant – IIIème siècle après J.-C.) (Paris 1982)

Monitoring Cultural Heritage Sites Affected by Geo-Hazards Using In Situ and SAR Data: The Choirokoitia Case Study



Kyriacos Themistocleous and Chris Danezis

Abstract This chapter focuses on the different methods for monitoring cultural heritage and archaeological sites affected by geo-hazards through the integrated method of using satellite imagery and field measurements. The Choirokoitia case study, which was one of the four UNESCO World Heritage list sites under the auspices of the PROTHEGO project, will be examined. PROTHEGO provides a new, low-cost methodological approach for the safe management of cultural heritage monuments and sites located in Europe, by integrating novel space technology based on interferometric synthetic aperture radar (InSAR), long-term low-impact monitoring systems and indirect analysis of environmental contexts to retrieve information on ground stability and motion in the 400+ UNESCO's World Heritage List monuments and sites of Europe.

Keywords Cultural heritage · Archaeology · Natural hazards · Remote sensing · UAV · Geodetic techniques · Photogrammetry

Introduction

Research indicates that archaeological and cultural heritage (ACH) sites are vulnerable to geological disasters, such as earthquakes, flooding, volcanoes, and catastrophic landslides, as well as slow-moving geo-hazards that take place over time, such as ground settlement, sinkholes, and slow-moving landslides (Themistocleous 2018; Agapiou et al. 2015, 2016; Margottini et al. 2016; Themistocleous et al. 2016a). However, the effects of geo-hazards on ACH sites have not been examined (Themistocleous et al. 2016b; Gutiérrez and Cooper 2002; Rohn et al. 2005; Canuti et al. 2009). The prevailing research tends to focus on the cultural heritage site in response to the geo-hazard and how to correct damage, instead of focusing on the

K. Themistocleous (✉) · C. Danezis
Department of Civil Engineering and Geomatics, Faculty of Engineering and Technology,
Cyprus University of Technology, Limassol, Cyprus
e-mail: k.themistocleous@cut.ac.cy

underlying geological and geotechnical context of the hazards in order to prevent damage to ACH sites by recognizing risks in order to establish effective conservation planning (Brimblecombe 2000; Fort et al. 2006; Tang et al. 2016).

The documentation of ACH sites has traditionally been expensive and labor-intensive since it involves field surveying, ground-based data collection, and periodical observations (Themistocleous et al. 2016a), which is especially difficult over large archaeolandscape and remote areas. The PROTHEGO (PROtection of European Cultural HERitage from GeO-hazards) provides a new, low-cost methodological approach for the safe management of cultural heritage monuments and sites located in Europe, by integrating novel space technology based on long-term low-impact monitoring systems, such as UAVs and geodetic techniques, interferometric synthetic aperture radar (InSAR) systems, and indirect analysis of environmental contexts to monitor and assess the risk of geo-hazards in the 400+ UNESCO's World Heritage List (WHL) of monuments and sites of Europe. The project includes the 395 monuments of UNESCO in Europe to monitor geo-hazards, with case studies conducted in 4 UNESCO sites in England, Spain, Italy, and Cyprus.

This paper will present an overview of the monitoring techniques using in situ and Earth observation for ACH sites affected by geo-hazards that are potentially unstable due to landslides, sinkholes, settlement, subsidence, active tectonics, as well as structural deformation. The Cyprus case study of Choirokoitia will be used as an example of how the PROTHEGO methodology can be utilized to identify geo-hazards.

Best Practices for Diagnosis, Monitoring, Mitigating, and Preserving Cultural Heritage Sites

The PROTHEGO project developed a methodology to identify cultural heritage sites that were at risk for geo-hazards. In order to identify the level of risk of the UNESCO WHL sites, a multi-criteria risk assessment is used to prioritize the severity of the geo-hazard, as well as to establish mitigation and conservation efforts (Silvestrou and Themistocleous 2018). To effectively assess the level of risk, the ACH sites must first be diagnosed through a condition assessment in order to identify damage and risks to estimate the physical condition of the site (Themistocleous et al. 2017a, 2018a, b). The condition assessment (which includes both qualitative and quantitative data) assesses the condition (level of damage) of the heritage place, level of risk and vulnerability, significance and value of the heritage place and prioritization of heritage and activities, and assessment of recovery needs. Best practices for the conservation of cultural heritage sites include diagnosis, monitoring, mitigation, and preservation of the site, as shown in Fig. 1.

Traditional methods of diagnosis include photographs, drawings, and topographical surveys. Currently, more innovative methods of diagnosing and documenting archaeological and cultural heritage sites include laser scanners, thermal cameras,

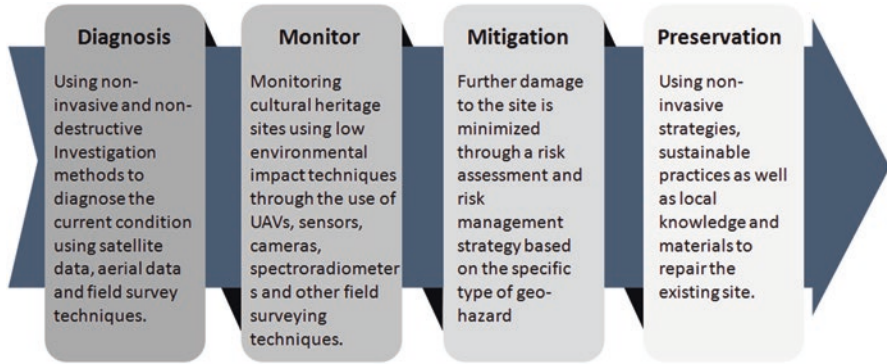


Fig. 1 Best practices for conservation of cultural heritage sites

Lidar, and digital images taken from an Unmanned Aerial Vehicle (UAV), which are used in conjunction with photogrammetry to create ortho-photos, 3D models, digital elevation models, and simulations (Themistocleous et al. 2017b, 2018a, b; Themistocleous 2017). Additional diagnostic techniques include ground-penetrating radar, laser scanning surveys, discontinuity mapping, infrared thermography, and kinematic analysis.

Monitoring focuses on the extent of the damage, deterioration, movement, humidity, precipitation, erosion, etc. of the ACH sites. Traditional methods of monitoring include in situ measurement campaigns, field measurements, and digital levels, which are time-consuming and labor-intensive. Low-impact monitoring includes techniques such as satellite radar interferometry, ground-based interferometry, total station, and traditional geotechnical network. Recent methods of monitoring are increasingly innovative and include satellite and aerial imagery, field surveying, wireless networks, GNSS control network, and 3D modeling and simulation. Sensors used to measure movement, slope, deformation, humidity, and precipitation include accelerometers, inclinometers, levelometer, crack-measuring devices, tiltmeters, piezometers, etc.

Once the ACH site has been diagnosed and monitored, further damage needs to be minimized. Mitigation strategies very much depend on the type of geo-hazard. Mitigation strategies include technical analysis of building materials, structural assessment of the site, condition assessment of the site, and simulation models. Multidisciplinary scientific approach is needed for a thorough risk assessment which should encompass multiple settings at a given site. Risk assessment procedures should be identified for determining more appropriate risk reduction strategies in the decision-making process. Mitigation requires a general description of the ACH site, the identification of the causative factors and triggering mechanism of the geo-hazard, and the use of traditional techniques to minimize risk as well as constant monitoring, stability management, and awareness. As well, an integral natural risk management for appropriate risk mitigation should be established for different priority levels of ACH sites by geo-hazards.

Preservation refers to the repair and replacement work necessary to prevent further damage to the site, preferably using the same, similar, or compatible materials. Preservation activities need to be aesthetically pleasing and complement the cultural heritage site. It is recommended that support structures and scaffolding be included, depending on the type of geo-hazard. The preservation techniques should reduce existing vulnerability to prevent the creation of new risks. Guidelines and intervention criteria should be established in order to preserve the site. Early warning, detection, and prevention actions should receive as much importance as post-disaster monitoring and remedial actions. Sustainable mitigation practices are necessary for preservation which include (a) effective solutions based on the best possible information available in order to solve the problem at hand, (b) environmental impact that is noninvasive and emphasizes the maximum preservation of the original aspect of the site, (c) sustainability by enhancing traditional knowledge and sustainable practices that have the maximum benefit of local experience, and (d) socioeconomic impact, by using local materials, workers, and artisans to maximize the reproducibility of conservation in case of future interventions.

Choirokoitia Study Area

The UNESCO World Heritage Site of Choirokoitia in Cyprus, which is one of the four case studies of the PROTHEGO project (see Fig. 2). The Neolithic settlement of Choirokoitia, occupied from the 7th to the 4th millennium BC, is one of the most important prehistoric sites in the eastern Mediterranean (UNESCO World Heritage List 2016). Choirokoitia is one of the best preserved settlements of this period in



Fig. 2 Choirokoitia site



Fig. 3 Reconstruction of the houses in Choirokoitia

Cyprus and the eastern Mediterranean. The site is located in the district of Larnaka, about 6 km from the southern coast of Cyprus, and lies on the slopes of a hill partly enclosed in a loop of the Maroni River. Occupied from the 7th to the 5th millennium BC, the village covers an area of approximately 3 ha at its maximum extent and is one of the most important prehistoric sites in the eastern Mediterranean. It represents the Aceramic Neolithic of Cyprus at its peak, which is the first human occupation of the island by farmers coming from the Near East mainland around the beginning of the 9th millennium. The site depicts how people lived in the Neolithic era which was mostly through agriculture and raising domestic animals.

Archaeological excavations at Choirokoitia consist of circular houses built from mudbrick and stone with flat roofs that were protected by successive walls (Fig. 3). On the top of the hill, a complex architectural system providing access to the village has been uncovered, which indicates that the settlement was built according to a preconceived plan. This indicates an important collective effort and suggests a structured social organization able to construct and maintain works of a large scale for the common good. The Choirokoitia site includes several circular buildings equipped with hearths and basins (assumed to be houses) arranged around a small courtyard where domestic activities took place.

To date, 20 houses have been excavated which were constructed with limestone, clay, and brick. According to UNESCO, the site was officially abandoned in the 4th millennium BC for unknown reasons.

Local-Scale Monitoring

Current research states that the integration of different survey techniques and ground-based radar interferometry are the most effective solution for monitoring and preserving ACH sites (Margottini et al. 2015). Satellite radar interferometry is capable of monitoring surface deformation with high accuracy using precise ground measurements. When ACH sites vulnerable to geo-hazards are identified, on-site

observations and modeling can be used to monitor the area over time. The local-scale monitoring methodology includes in situ observation and remote sensing techniques that are used to identify and measure the impact of the geo-hazard affecting the ACH site. The combination of topographic surveying, aerial images from UAVs, photogrammetry, and InSAR data can be used to map slow ground movements in the area of interest. This data is then compared and validated with ground-based geotechnical monitoring in order to evaluate the deformation trend at the ACH site. Also, advanced modeling is used to predict the effect of the geo-hazard in the area if preventive measures are not taken. As a result, ACH sites exposed to potential risks can be identified, and vital information can be provided to decision-makers in order to protect cultural and heritage sites from natural hazards.

Local-scale monitoring provides the opportunity to detect and analyze deformation phenomena for assessing the severity of geo-hazards by using integrated field monitoring techniques. Research indicates that the integration of InSAR data and conventional surveying offers the best solution for monitoring geo-hazards in cultural heritage sites, both in the short-term and the long-term (Margottini et al. 2015, 2018; Novellino et al. 2018). Geotechnical techniques are used to measure deformation over a relatively short measurement base, while in situ measurements using UAV, total station, laser scanning, and GPS are then used to measure such movements over extended time periods. In order to document the cultural heritage site affected by geo-hazards, UAV images and laser scanning are used (Themistocleous 2017; Themistocleous et al. 2017b).

To identify and assess geo-hazards at ACH sites, a methodology was developed for local-scale monitoring in order to assess risk from a geospatial perspective, as featured in Fig. 4. The methodology focused on long-term low-impact monitoring systems as well as indirect analysis of environmental contexts to investigate changes and decay of structure, material, and landscape (Themistocleous 2018; Themistocleous et al. 2016a). The first step of the methodology begins with using InSAR images to identify geo-hazards. Once InSAR ground motion data identify that a natural hazard has taken place at or near the ACH site, field monitoring is necessary to document and measure the severity of the change caused by the natural

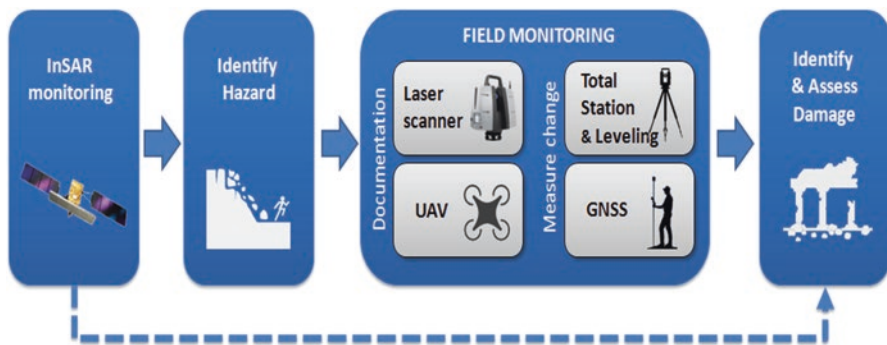


Fig. 4 Methodology for local-scale monitoring

hazard, if any. Documentation of the change can be performed either close range, using laser scanning, photogrammetry GNSS, and total stations, or by low-altitude sensors, using UAVs and drones. Once the changes are identified using field verification, InSAR images are again used to verify and assess the extent of the damage to the cultural heritage site (Themistocleous et al. 2018c).

Satellite Imagery

Synthetic Aperture Radar (SAR) imaging satellites, Interferometric SAR (InSAR), and Persistent Scatterers (PS) processing techniques (Rosen et al. 2000; Ferretti et al. 2011; Crosetto et al. 2010) are capable of measuring changes on Earth with millimeter precision. As a result, they can identify subtle and long-term changes that lead to damage to ACH sites.

Satellite Synthetic Aperture Radar (SAR) images are processed with multi-interferogram methods, such as the Persistent Scatterers (PS) technique, to identify ground displacement in the areas of interest, thereby providing an effective solution to measure large-scale surface deformations from space (Ferretti et al. 2011; Zhou et al. 2015; Hooper et al. 2012; Chen et al. 2012, 2013; Cigna et al. 2012, 2014). Differential Interferometric SAR (InSAR) methods integrate the radar returns from two or more radar scenes over the same area to detect changes occurred between acquisitions, thereby monitoring subtle ground movements across wide areas with millimeter accuracy (Chen et al. 2015; Tapete et al. 2013; Zhou 2013; Evans and Farr 2007; Polcari et al. 2015). Research indicates that SAR data can provide powerful information for archaeological and cultural heritage research, including archaeolandscapes, site detection, feature extraction (buried or emerging archaeological remains), change detection, and structural monitoring (Cigna et al. 2012, 2013; Lasaponara and Masini 2013; Tapete et al. 2012, 2016).

The Persistent Scatterer Interferometric Synthetic Aperture Radar (PSInSAR) technique is used for monitoring and measuring ground displacements with a millimetric resolution and to overcome the effects of natural decorrelation and atmosphere. The technique is also suitable for slope stability monitoring if movement is either creeping or moderate movement (on the order of <math><10\text{ cm/year}</math>). The PSInSAR technique uses a stack of SAR interferograms and determines the motion history for pixels that are identified to have temporal phase stability (i.e., pixels whose overall response is dominated by a strong back-scatterer). PS interferometry can be performed by relying on fixed targets, often called coherent scatterers or point scatterers (PS). In cases where few natural persistent scatterers exist in the area of interest, corner reflectors can be installed to provide artificial radar scatterers for use in PSI analyses. These devices installed in situ provide a strong response in the SAR images resulting in good interferometric phases to derive the deformation estimates. Corner reflectors are usually trihedral and vary in size depending upon the radar wavelength for which they are designed. In remote areas these interferometric outputs can be compared with in situ measurements (GPS, leveling, inclinometers) and used as initial input for any geotechnical modeling.

Unmanned Aerial Vehicles (UAVs)

In recent years, UAVs have become a common tool in cultural heritage and archaeological research since they provide higher resolution images compared with satellite imagery. They are used for surveying cultural heritage sites due to their affordability, reliability, and ease of use (Themistocleous et al. 2014a, b, c, 2015a, b, c; Agapiou et al. 2013; Lo Brutto et al. 2014; Burkhart et al. 2014; Colomina and Molina 2014). UAV data provides more detailed surveys of the archaeological site (Hassani 2015; Remondino and Rizzi 2009; El-Hakim et al. 2004; Gruen et al. 2005; Guidi et al. 2009; Rönholm et al. 2007), especially in areas that are inaccessible and/or dangerous which cannot be accessed directly using other systems or piloted aerial systems (Everaerts 2008; Eisenbeiß 2009). As well, UAVs can be used for low-altitude imaging and remote sensing of geospatial information (Themistocleous et al. 2014a, b, c; Colomina and Molina 2014). Remote sensing technologies on a UAV platform (see Fig. 5) are extremely useful for the detection and monitoring of ACH sites since they can be fitted with sensors which are able to produce an unprecedented volume of high-resolution, geo-tagged image sets of cultural heritage sites from above (Themistocleous et al. 2014a, b, c; Agapiou et al. 2013; Kostrzewa et al. 2003; Ruffino and Moccia 2005; Scholtz et al. 2011).

UAVs provide an affordable, reliable, and straightforward method of documenting ACH sites. Recent developments in photogrammetry technology provide a simple and cost-effective method of generating relatively accurate 3D models from 2D images (Themistocleous et al. 2014a, 2015a, b, c; Ioannides et al. 2013). To document ACH sites affected by the geo-hazards, aerial images taken from a UAV can be used to create ortho-photos, dense clouds, 3D model, and digital elevation models (Themistocleous 2017), as featured in Fig. 6. It is necessary for the UAV to be equipped with a high-resolution RGB camera to acquire images over the area of interest. The area should have fixed ground control points (GCPs) for georeferencing in order to produce a photogrammetric ortho-photo and point cloud 3D model of the area of interest and for comparison over temporal intervals.

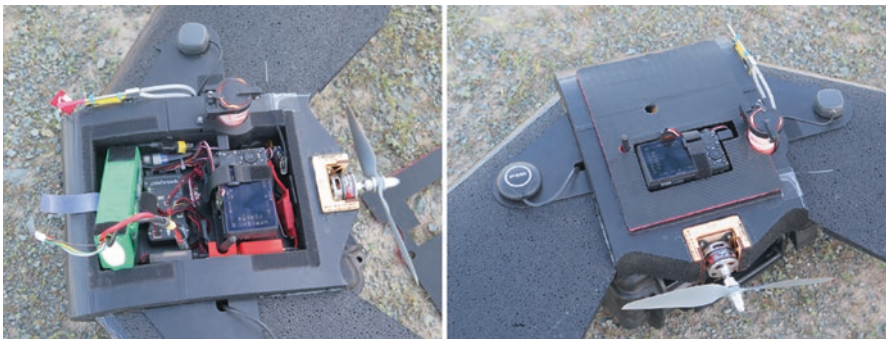


Fig. 5 UAVs fitted with sensors



Fig. 6 UAV flight over Chirokoitia UNESCO site

To process the aerial images taken from the UAV, it is necessary to position GCPs over the entire area prior to the flight to make the necessary corrections during the post-processing of the image to ensure the correct scale of the model. It is recommended that the GCPs be recorded with a double frequency GNSS system with estimated accuracy of less than 2 cm. The UAV with RGB camera will be flown over the area of interest using flight planning software to create a predetermined flight path, to ensure significant image coverage. The aerial images should have an 80% overlay within each image so that single images can be processed with photogrammetry in order to generate ortho-photos and create 3D models.

Laser Scanners

Laser scanners have become increasingly efficient in terms of point acquisition speed, portability, user-friendliness, and cost (Fassi et al. 2013). The technology allows user to produce a high-precision digital reference data that documents the condition of the ACH site so that comparisons over temporal intervals can be performed, provides a virtual model for replication, and makes possible easy mass distribution of digital data of the ACH site (Hassani 2015; Vilceanu et al. 2015). The laser scanner can be used for further 3D modeling of the area and to generate a digital surface model (DSM) of the site.

Surveying Techniques

Surveying techniques are used to determine the absolute positions and positional changes of any point on the surface, while geotechnical techniques are used to measure deformation over a relatively short measurement base. Surveying techniques, such as total station, leveling, and global navigation satellite systems (GNSS), measure the positional changes of any point on the surface at millimeter level accuracy and have successfully been used for measuring deformations in archaeological areas affected by hazards (Polcari et al. 2015; Fassi et al. 2013; Jiang et al. 2012). The GNSS provides location coordinates in global geographical system, which are highly useful in combination with other techniques for documenting mass targets and structural deformation (Hassani 2015). The total station is capable of acquiring large amounts of field data, together with the efficient and error-free transfer of the data to a computer (Haddad 2011).

Geodetic Techniques

A local geodetic network consists of a reference point and additional nodes, established at specific points of interest, such as points on peaks or ridges that may indicate/warn of a potential hazard (Themistocleous et al. 2017a; Themistocleous 2017). Network points are measured often using satellite (GNSS) and ground measurements (high-precision total stations and levels) to measure the potential relative motion with respect to the network reference point during the life-span of the monitoring activity, as shown in Fig. 7. The number of points in the network is largely a function of the geological vulnerability parameters of the area of interest. The network nodes (or control points) need to be incorporated into the site and placed in such way in order to ensure mutual visibility with the total station setup at the reference point (Themistocleous et al. 2017a; Themistocleous 2017).

Various GNSS units can be used to establish the geodetic network. In this case study, the Trimble Zephyr 2 GNSS and Leica GS15 Smart GNSS Receivers were used for establishing a GNSS control network, as shown in Fig. 8. The Trimble Zephyr 2 GNSS offers robust low-elevation tracking and submillimeter phase center repeatability, making it ideal for base station applications, as it can withstand shock and vibration. It is capable of multipath reduction and low-elevation satellite tracking. The Trimble Zephyr 2 GNSS supports submillimeter phase center accuracy and supports signals from GPS L2C/L5, GLONASS, Galileo, OmniSTAR, and SBAS. The Leica GS15 Smart GNSS Receivers are recommended as they adjust to any environment and deliver the most accurate results. They use multifrequency, consisting of GPS/GLONASS/Galileo/BeiDou. They are also static (phase) with long observations and have external data links for GSM/GPRS/UMTS/CDMA and UHF/VHF modem.



Fig. 7 Geodetic Network at Choirokoitia



Fig. 8 Trimble Zephyr 2 GNSS (left) and Leica GS15 Smart GNSS Receivers (right) for establishing a GNSS control network

Horizontal displacements can be measured using an industrial-grade total station, such as the Topcon MS05AXII, which has a 0.5" angular accuracy and 0.5 mm range accuracy, combined with specifically designed prisms and reflective targets to achieve maximum accuracy in validating potential displacements. Vertical motion can be measured using a high-precision digital level, such as the Leica DNA03. The leveling campaign will be carried out using Invar Barcode Staffs, achieving a vertical accuracy at the order of 0.3 mm/km (Themistocleous et al. 2017a; Themistocleous 2017).

Ground Sensors

Geotechnical and environmental ground sensors enable the correlation of geo-hazard events with their triggering mechanisms and assist in identifying the causal parameters for geo-hazard monitoring and simulation (Themistocleous et al. 2017b, 2018a, b). However, geotechnical instruments for subsurface movement monitoring, such as inclinometers and extensometers, are incapable of large-scale and long-distance monitoring (Zhu et al. 2017). Most sensors for measuring earth pressure, pore water pressure, ground temperature, and vibration are point (discrete) sensors.

GB-InSAR provide continuous monitoring of displacements from few millimeters per day up to 1 or more meters per day over unstable areas. GB-InSAR devices allow the assessment of ground deformations of faster landslides, by recording higher-frequency measurements (Corsini et al. 2006; Noferini et al. 2008). Fiber Bragg grating (FBG) sensors measure variations of temperatures, displacements, loads, earth pressures, pore water pressures, and soil moistures with high accuracy (Zhu et al. 2017). FBG sensors are still in their infancy and therefore are more suitable to be incorporated into geotechnical instrumentation to ensure accurate and real-time measurement. Capacitive sensors measure soil moisture levels by *capacitive sensing* instead of resistive *sensing* like other types of moisture sensor. Since they are resistant to corrosion, they are often used for long-term monitoring of a site. Piezometers measure pore water pressure. They can be buried or pushed into the ground to measure the groundwater pressure at the point of installation. Accelerometers measure acceleration force, such as tilt. They tend to be made up of multiple axes so that any acceleration caused due to movement in any of the axes is detected by the accelerometer. Crack meters measure the displacement between two points on the surface that are exhibiting signs of separation. A variety of other crack meters including Carlson and vibrating-wire sensors, dial gages, and mechanics feeler gages may be used to measure movement of cracks. Inclinometers monitor subsurface movements and deformations for long-term, precise monitoring horizontal displacements along various points on a borehole and also monitor the rate of movement. Tiltmeter stations monitor slope stability in highly active geological environment. They are commonly attached to a surface (internal or external) of a structure and measure vertical rotation of the surface. Extensometers measure

vertical movement. Due to their accuracy, they can be used for quick and accurate measurement of relative distances between pairs of reference points on the surfaces of structures.

Case Study Results

To support field monitoring, geometric documentation of the area was performed using a laser scanner, UAV systems, and photogrammetry. The data was geo-referenced using a geodetic network based on total station and level measurements. The focus of the documentation was the reconstruction of the cross sections over the identified areas of the demonstration site in order to investigate possible changes in the vertical and horizontal profiles of the study area. Under the framework of the PROTHEGO project, aerial images of the Choirokoitia site were taken using a UAV with an attached high-resolution 20MP RGB camera to acquire images over the site with fixed ground control points for geo-referencing in order to produce a photogrammetric ortho-photo of the site and for comparison over temporal intervals (see Fig. 9). The aerial images were processed using photogrammetry, where the digital images acquired from the UAV were interpolated in order to create high-resolution, scaled, and geo-referenced 3D models from them.

Aerial images of the Choirokoitia site using UAVs were taken on 29 October 2016, 2 February 2017, and 11 November and 8 March 2018, with approximately 450 images taken of the Choirokoitia site during each UAV flight. GCPs were used to correct the scale and geo-reference the model. The images were then preprocessed by removing the lens distortion and then processed using the Agisoft PhotoScan Professional software.



Fig. 9 Ortho-photo of the Choirokoitia site, with resolution of 2.26 cm/pix

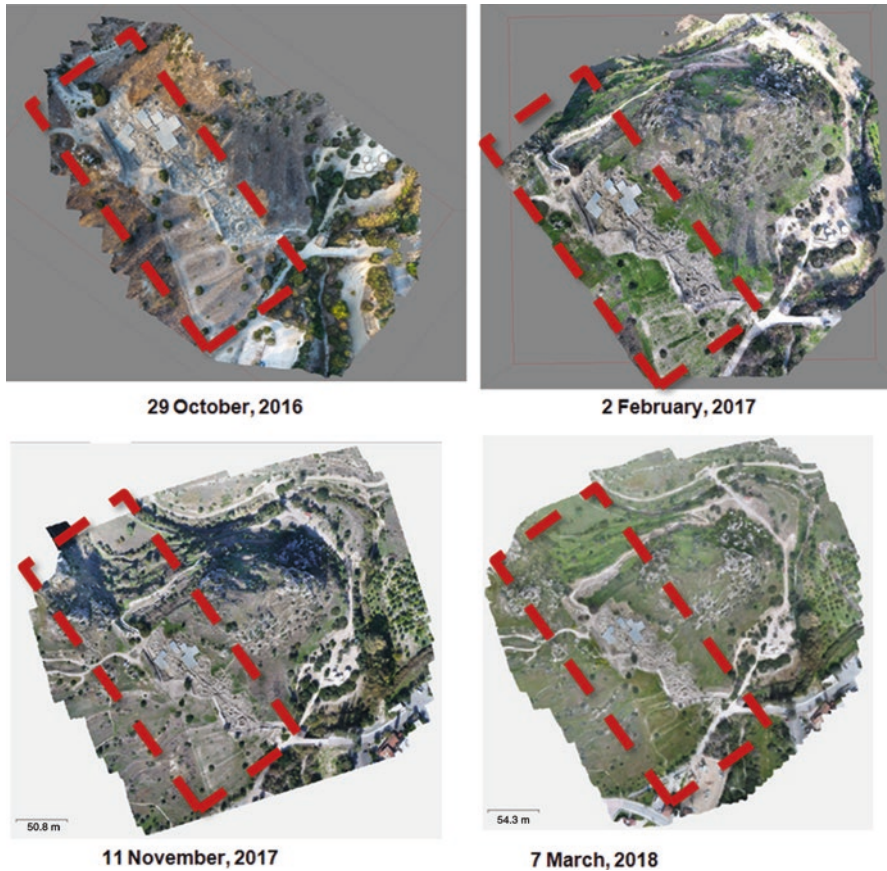


Fig. 10 Point cloud generations of Choirokoitia site (outlined in red)

All clear images with an overlap of 80% were included in the processing in order to generate a dense point cloud of the Choirokoitia site. The 3D point cloud generation for all four monitoring surveys is shown in Fig. 10.

There was a notable difference in the level of vegetation present at the Choirokoitia site on the dates that the images were acquired. The October 2016 and November 2017 images show sparse vegetation, while the images acquired in February 2017 and March 2018 show significantly more vegetation. Since it was easier to identify vegetation in the images acquired in the winter campaign due to the color and morphology of the vegetation, masking was done in order to subtract the vegetation from the model to generate the DEM of the ground surface. This was done by using interpolation of the areas with vegetation, using the images acquired in October 2016 and February 2017. Following, a contour map of the area was generated using stitch imaging using the DEM model without vegetation (Fig. 11).

Digital elevation models (DEMs) were generated to examine any possible changes in the case study area over time. The DEMs generated based on the images

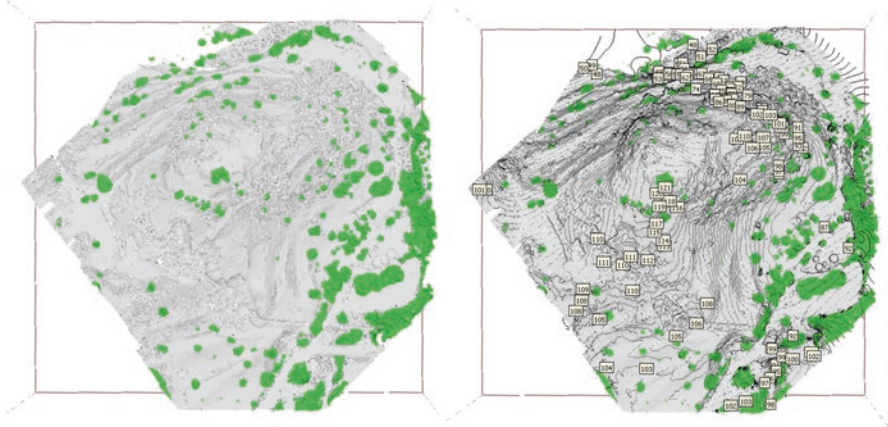


Fig. 11 Vegetation Subtraction and contour generation

from February 2017, November 2017 and March 2018 are shown in Fig. 12. As is evident, there is a slight shift at the top peak of the hill.

The final 3D model of the Choirokoitia site is presented in Fig. 13.

Table 1 features the results of the GNSS control network during the study time frame. There were four GPS sites which measured displacement east (DE), displacement north (DN), and displacement up (DU). The coordinates used are based on the Cyprus Local Transverse Mercator (LTM) projection system which is based on the Datum Cyprus Geodetic Reference System of 1993 (CGRS93) that uses the ellipsoid WGS84. The results of the GNSS control network found a change of 2 cm during the 24 months of the monitoring period of the site.

Rockfall Modeling

A rockfall simulation model was created through the collaboration of the Cyprus University of Technology with the University of Milano-Bicocca (Valagussa et al. 2018). The rockfall runout simulation was performed by using the 3D model HY-Stone (Agliardi and Crosta 2003; Crosta et al. 2004). Such 3D models have the ability to simulate block motion along a slope by including lateral dispersion of trajectories resulting from large- and small-scale morphological complexity (Agliardi and Crosta 2003; Crosta et al. 2004; Descoeurdes and Zimmermann 1987; Guzzetti et al. 2002; Dorren et al. 2006). The results were spatially distributed over the entire study area, without any interpolation of data computing along specific trajectories or imposing predetermined fall direction. The topography is by a raster DEM, which was converted in a vector topographic model (Triangulate Regular Network) (Guzzetti et al. 2002) for the modeling of impact and rolling. The stochastic nature of rockfall processes was introduced as a function of model spatial resolution and by random sampling most parameters from different PDF, such as uniform,

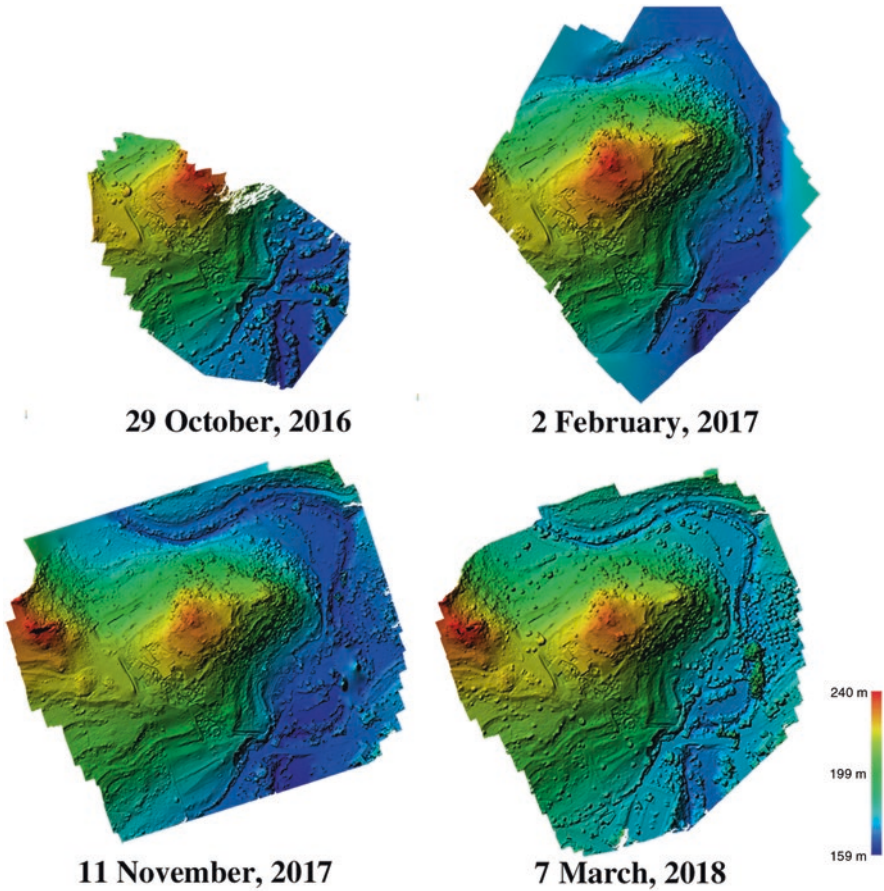


Fig. 12 DEM models of the Choirokoitia site

normal, lognormal, exponential, etc. The capability to simulate the effect of passive countermeasures, the dynamics of “flying rocks,” and the effect of vegetation were implemented and tested against actual events (Frattini et al. 2012). A special elasto-viscoplastic strain-hardening model for impact on soft ground was also implemented (Di Prisco and Vecchiotti 2006). The results of the rockfall model were provided in both raster and vector formats and included rockfall frequency, fly height, rotational and translational velocity, and kinetic energy, as well as information about motion type and impact locations.

A digital elevation model (DEM) was provided by the Cyprus University of Technology to the University of Milano-Bicocca and was regenerated with a cell size of 1 m. Following the creation of contour lines with 1 m spacing, the vegetation present inside the DEM was deleted. Rockfall sources refer to the cells from which rockfall occur. Each source cell was given a positive integer value, which specified



Fig. 13 3 D model of the Choirokoitia site generated with UAV images

Table 1 Results of GNSS Control network

GPS station	Coordinates (LTM) lat/long	DE meters	DN meters	DU meters
GPS1	231524.820/352001.675	+0.0023	-0.0025	-0.0027
GPS2	231314.725/351974.690	+0.0022	-0.0001	+0.0017
GPS3	231344.434/351922.148	+0.0000	+0.0000	+0.0000
GPS4	231453.791/351980.692	+0.0024	+0.0001	-0.0203

the number of the block that was simulated. For the study area, 100 blocks had been simulated from each cell. The source areas were mapped as a line beginning from a slope higher than 55 degrees, in accordance with the evidence of the ortho-photo with a resolution of 2 cm. All the simulated blocks are sphere with a density of

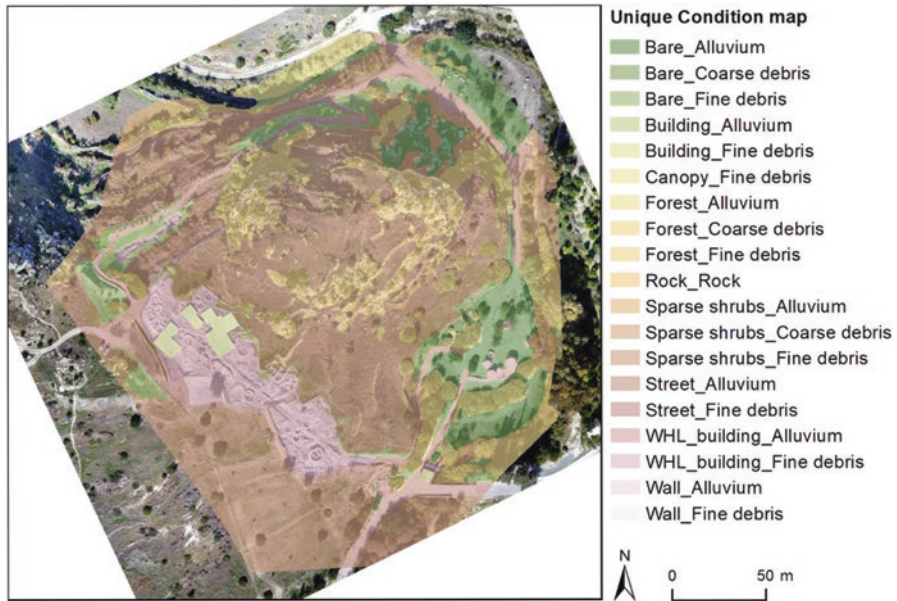


Fig. 14 Map of the land use and lithology for the Choirokoitia site

2700 kg/m³. The area has been divided in two homogenous zones in accordance with the evidence from the available data. Two datasets have been created for each area through the mapping of blocks from the ortho-photo with 2 cm resolution, and as consequence, two volumes have been defined. In the HY- Stone software, the volumes are randomly sampled from a negative exponential distribution.

For each cell, the normal (E_n) and tangential (E_t) restitution coefficients and rolling friction coefficient ($\tan r$) parameters control the amount of energy lost by blocks at impact in normal and tangential direction and by rolling over the slope surface, respectively. The coefficients ranged from 0 (no restitution) to 1 (total restitution). Raster datasets tend to be derived in GIS by reclassifying maps of “unique condition units,” which combined surface lithology and vegetation/land use derived through available data and photointerpretation (Fig. 14). In HY-Stone the variables are randomly sampled from a normal distribution, where the mean is corresponding to the parameter’s reference value.

The results of the HY-Stone focused on the cumulative count of rockfall trajectories passing through each cell of the DEM. This represents a proxy of the probability of rockfall propagation or runout to a given location in the space. The calculations included the number of transit for each cell of the DEM and arrested location of the blocks on the slope, the kinetic energy distribution along the simulated trajectories, and the maximum values of blocks kinetic energy (J) for each cell of the DEM (Fig. 15). As is evident, the rockfall would occur on the east side of the Choirokoitia site (Valagussa et al. 2018).

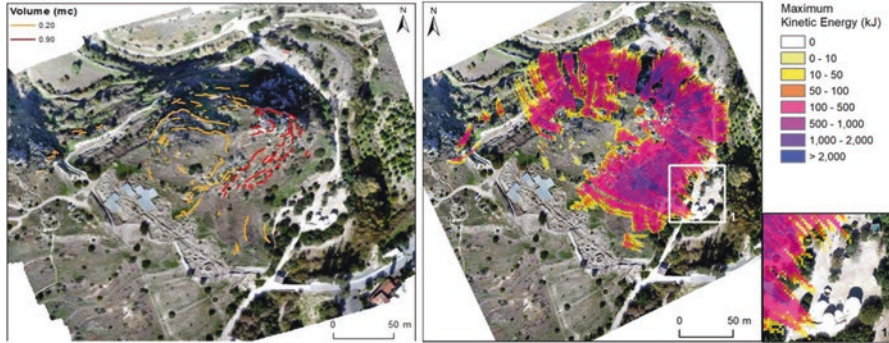


Fig. 15 Volume and values of kinetic energy (kJ) at the Choirokoitia site



Fig. 16 PSI Analysis of the Choirokoitia site (in white box) and the surrounding area

PSI Analysis

A PSI analysis was conducted at the Choirokoitia general area to determine any micro-movements in the area (Fig. 16). For the PSI analysis, 26 Cosmos Skymed SAR images from the years 2011–2017. For the dates defined, the points exhibit an average of 3.3 cm rate of movement per year (velocity). The archaeological site exhibits a rate of 0.24 mm and 0.11 mm for the two main targets identified within the site. Minor movement fluctuations (up to 4 mm) are also evident in the area for certain dates – these are often attributed to changes in temperature (expansion) or soil swelling due to the presence of water which also affects radar reflectivity (dielectric constant). The results of the PSI analysis found displacement at the same area as the GNSS control network. Longer-term monitoring of the site is required in order to diagnose the severity of the displacement.

Conclusions

The case study of Choirokoitia, Cyprus, provides an example of how to detect and analyze deformation phenomena for monitoring and predicting geo-hazards using InSAR ground motion data and field survey techniques to measure and document the extent of damage of the natural hazard on the cultural heritage site. The InSAR data, GNSS, and total station and level were used to measure the micro-movements, while the UAV and photogrammetry are used for documentation purposes and 3D modeling comparison. The PSI analysis and GNSS control network of the Choirokoitia site showed a small displacement, which indicates the need for longer-term monitoring of the site to diagnose the severity of the geo-hazards. The rockfall modeling indicated a potential rockfall situation near the Choirokoitia site, which may endanger visitors to the site. Local-scale monitoring data is the base for the development of geological and geotechnical modeling of the investigated sites, which will provide evolution models for the deformation processes affecting the heritage sites in order to recognize the best mitigation strategies and to evaluate the effectiveness of these actions for cultural heritage protection.

References

- Agapiou A, Hadjimitsis DG, Alexakis DD (2013) Development of an image-based method for the detection of archaeological buried relics using multi-temporal satellite imagery. *Int J Remote Sens* 34(16):5979–5996. <https://doi.org/10.1080/01431161.2013.803630>
- Agapiou A, Lysandrou V, Alexakis DD, Themistocleous K, Cucca B, Sarris A, Argyrou N, Hadjimitsis DG (2015) Cultural heritage management and monitoring using remote sensing data and GIS: the case study of Paphos area, Cyprus. *Comput Environ Urban Syst* 54:230–239. <https://doi.org/10.1016/j.compenvurbsys.2015.09.003>
- Agapiou A, Lysandrou V, Themistocleous K, Hadjimitsis DG (2016) Risk assessment of cultural Heritage sites clusters using satellite imagery and GIS: the case study of Paphos District, Cyprus. *J Int Soc Prev Mitigation Nat Hazards* 2:1–15. <https://doi.org/10.1007/s11069-016-2211-6>
- Agliardi F, Crosta G (2003) High resolution three-dimensional numerical modelling of rockfalls. *Int J Rock Mech Min Sci* 40(4):455–471
- Brimblecombe P (2000) Air pollution and architecture, past, present and future. *J Archit Conserv* 6:30–46
- Burkhardt A, Cogliati S, Schickling A, Rascher U (2014) A novel UAV-based ultra-light weight spectrometer for field spectroscopy. *Sens J IEEE* 14(1):62–67. <https://doi.org/10.1109/JSEN.2013.2279720>
- Canuti P, Margottini C, Fanti R, Bromhead EN (2009) Cultural heritage and landslides: research for risk prevention and conservation. *Landslides—disaster risk reduction*. Springer, Berlin/Heidelberg, pp 401–433
- Chen F, Lin H, Li Z, Chen Q, Zhou J (2012) Interaction between permafrost and infrastructure along the Qinghai–Tibet Railway detected via jointly analysis of C-band l-band small baseline SAR interferometry. *Remote Sens Environ* 123:532–540
- Chen F, Lin H, Zhou W, Hong T, Wang G (2013) Surface deformation detected by ALOS PALSAR small baseline SAR interferometry over permafrost environment of Beiluhe section, Tibet Plateau, China. *Remote Sens Environ* 138:10–18

- Chen B, Deng K, Fan H, Yu Y (2015) Combining SAR interferometric phase and intensity information for monitoring of large gradient deformation in coal mining area. *Eur J Remote Sens* 48:701–717. <https://doi.org/10.5721/EuJRS20154839>
- Cigna F, Del Ventisette C, Gigli G, Menna F, Agili F, Liguori V, Casagli N (2012) Ground instability in the old town of Agrigento (Italy) depicted by on site investigations and Persistent Scatterers data. *Nat Hazards Earth Syst Sci* 12:3589–3603
- Cigna F, Tapete D, Lasaponara R, Masini N (2013) Amplitude change detection with ENVISAT ASAR to image the cultural landscape of the Nasca region, Peru. *Archaeol Prospect* 20(2):117–131
- Cigna F, Lasaponara R, Masini N, Milillo P, Tapete D (2014) Persistent scatterer interferometry processing of COSMO-SkyMed StripMap HIMAGE time series to depict deformation of the historic centre of Rome, Italy. *Remote Sens* 6(12):12593–12618
- Colomina I, Molina P (2014) Unmanned aerial systems for photogrammetry and remote sensing: a review. *ISPRS J Photogramm Remote Sens* 92:79–97
- Corsini A, Farina P, Antonello G, Barbieri M, Casagli N, Coren F, Guerri L, Ronchetti F, Sterzai P, Tarchi D (2006) Space-borne and ground-based SAR interferometry as tools for landslide hazard management in civil protection. *Int J Remote Sens* 27(12):2351–2369. <https://doi.org/10.1080/01431160600554405>
- Crosetto M, Monserrat O, Iglesias R, Crippa B (2010) Persistent scatterer interferometry: potential, limits and initial C- and X-band comparison. *Photogramm Eng Remote Sens* 76:1061–1069
- Crosta GB, Agliardi F, Frattini P, Imposimato S (2004) A three-dimensional hybrid numerical model for rockfall simulation. *Geophys Res Abstr* 6:04502
- Descocudres F, Zimmermann T (1987) Three-dimensional dynamic calculation of rockfalls, In Herget G, Vongpaisal S (eds) *Proceedings of the sixth international congress on rock mechanics*. Montreal. Rotterdam, Balkema, pp 37–42
- Di Prisco C, Vecchiotti M (2006) A rheological model for the description of boulder impacts on granular strata. *Geotechnique* 56(7):469–482
- Dorren LKA, Berger F, Putters US (2006) Real-size experiments and 3D simulation of rockfall on forested and non-forested slopes. *Nat Hazards Earth Syst Sci* 6:145–153
- Eisenbeiß H (2009) UAV photogrammetry. Dissertation. ETH No. 18515, Institute of Geodesy and Photogrammetry, ETH Zurich, Switzerland, *Mitteilungen Nr.105*
- El-Hakim SF, Beraldin JA, Picard M, Godin G (2004) Detailed 3D reconstruction of large-scale heritage sites with integrated techniques. *IEEE Comput Graph Appl* 24(3):21–29
- Evans DL, Farr TG (2007) The use of interferometric synthetic aperture radar (InSAR) in archaeological investigations and cultural heritage preservation. In: Wiseman J, El-Baz F (eds) *Remote sensing in archaeology*. Springer, New York
- Everaerts J (2008) The use of unmanned aerial vehicles (UAVS) for remote sensing and mapping. B11187-1192. *The International Archives of the Photogrammetry, Remote Sensing and Spatial Information Sciences*, vol XXXVII. Part B1. Beijing 2008
- Fassi F, Fregonese L, Ackermann S, De Troia V (2013) Comparison between laser scanning and automated 3d modelling techniques to reconstruct complex and extensive cultural heritage areas. *The International Archives of the Photogrammetry, Remote Sensing and Spatial Information Sciences*, vol XL-5/W1, 2013 3D-ARCH 2013 – 3D virtual reconstruction and visualization of complex architectures, 25–26 February 2013, Trento, Italy
- Ferretti A, Fumagalli A, Novali F, Prati C, Rocca F, Rucci A (2011) A new algorithm for processing interferometric data-stacks: SqueeSAR. *IEEE Trans Geosci Remote Sens* 49(9):3460–3470. <https://doi.org/10.1109/TGRS.2011.2124465>
- Fort R, de Buergo MA, Gomez-Heras M, Vazquez-Calvo C (2006) Heritage, weathering and conservation. In: *Proceedings of the international conference on heritage, weathering and conservation (HWC-2006)*, 21–24 June 2006, Madrid, Spain
- Frattini P, Crosta GB, Agliardi F (2012) Rockfall characterization and modeling. In: Clague JJ, Stead D (eds) *Landslides types, mechanisms and modeling*. Cambridge University Press, Cambridge, pp 267–281. ISBN 978-1-107-00206-7

- Gruen A, Remondino F, Zhang L (2005) The Bamiyan project: multi-resolution image-based modeling. In: Baltasavias E, Gruen A, Van Gool L, Pateraki M (eds) *Recording, modeling and visualization of cultural heritage* Taylor & Francis, Balkema, ISBN 0 415 39208 X, pp 45–54
- Guidi G, Remondino F, Russo M, Menna F, Rizzi A, Ercoli S (2009) A multi-resolution methodology for the 3D modeling of large and complex archaeological areas. *Int J Archit Comput* 7(1):40–55
- Gutiérrez F, Cooper AH (2002) Evaporite dissolution subsidence in the historical city of Calatayud, Spain: damage appraisal and prevention. *Nat Hazards* 25(3):259–288
- Guzzetti F, Crosta G, Detti R, Agliardi F (2002) STONE: a computer program for the three-dimensional simulation of rock-falls. *Comput Geosci* 28(9):1079–1093
- Haddad NA (2011) From ground surveying to 3D laser scanner: a review of techniques used for spatial documentation of historic sites. *J King Saud Uni* 23(2):109–118
- Hassani F (2015) Documentation of cultural heritage techniques, potentials and constraints. *International Archives of the Photogrammetry, Remote Sensing and Spatial Information Sciences*, vol XL-5/W7, 25th Intl CIPA Symp. 2015, 31 August – 04 September 2015, Taipei, Taiwan
- Hooper A, Bekaert D, Spaans K, Arkan M (2012) Recent advances in SAR interferometry time series analysis for measuring crustal deformation. *Tectonophysics* 514–517:1–13. <https://doi.org/10.1016/j.tecto.2011.10.013>
- Ioannides M, Hadjiprocopis A, Doulamis N, Doulamis A, Protopapadakis E, Makantasis K, Santos P, Fellner D, Stork A, Balet O, Julien M, Weinlinger G, Johnson PS, Klein M, Fritsch D (2013) Online 4D reconstruction using multi-images available under Open Access. *ISPRS Ann Photogramm Remote Sens Spat Inf Sci II-5/W1*:169–174
- Jiang Y, Wdowinski S, Dixon TH, Hackl M, Protti M, Gonzalez V (2012) Slow slip events in Costa Rica detected by continuous GPS observations, 2002–2011. *Geochem Geophys Geosyst* 13:Q04006. <https://doi.org/10.1029/2012GC004058>
- Kostrzewa J, Meyer W, Laband S, Tere W, Petrovici P, Swanson K, Sundra C, Sener W, Wilmott J (2003) Infrared microsensory payload for miniature unmanned aerial vehicles. In: *Proceedings of SPIE 5090, unattended ground sensor technologies and applications*, p 265
- Lasaponara R, Masini N (2013) Satellite synthetic aperture radar in archaeology and cultural landscape: an overview. *Archaeol Prospect* 20:71–78
- Lo Brutto M, Garraffa A, Meli P (2014) UAV platforms for cultural heritage survey: first results. *ISPRS Ann Photogramm Remote Sens Spat Inf Sci II-5*:227–234
- Margottini C, Antidze N, Corominas J, Crosta GB, Frattini P, Gigli G, Giordan D, Iwasaky I, Lollino G, Manconi A, Marinos P, Scavia C, Sonnessa A, Spizzichino D, Vacheishvili N (2015) Landslide hazard, monitoring and conservation strategy for the safeguard of Vardzia Byzantine monastery complex. *Landslides* 12(1):193–204. <https://doi.org/10.1007/s10346-014-0548-z>
- Margottini C, Spizzichino D, Cigna F, Crosta GB, Frattini P, Themistocleous K, Fernandez Merodo JA (2016) European UNESCO cultural heritage and geo – hazards: the PROTHEGO project. In: *Proceedings of the fourth international conference on remote sensing and geo-information of environment*, 4–8 April, 2016, Paphos, Cyprus
- Margottini C, Spizzichino D, Leoni G, Bee EJ, Crosta GB, Frattini P, Themistocleous K, Fernandez Merodo JA (2018) Satellite monitoring applied to natural hazards and cultural heritage: the PROTHEGO project. In: *Sixth international conference on remote sensing and geo-information of environment*, 26–29 March, 2018, Paphos, Cyprus
- Noferini L, Takayama T, Pieraccini M, Mecatti D, Macaluso G, Luzi G, Atzeni C (2008) Analysis of ground-based SAR data with diverse temporal baselines. *IEEE Trans Geosci Remote Sens* 46(6):1614–1623
- Novellino A, Harrison A, Bee E, Wang L, Hobbs P, Margottini C, Themistocleous K, Crosta GB, Fernandez Merodo JA (2018) Characterising and modelling geohazard susceptibility in the UNESCO World Heritage Site of the Derwent Valley Mills (UK). *Geophysical Research Abstracts*, vol 20, EGU2018-13316-1, 2018, EGU General Assembly 2018, Vienna, 8–13 April 2018

- Polcari M, Fernández J, Palano M, Albano M, Samsonov S, Stramondo S, Zerbini S (2015) The 2014 Napa valley earthquake constrained by InSAR and GNSS observations. In: Proceedings of the EGU General Assembly 2015, 12–17 April, 2015, Vienna, Austria. id.6918
- Remondino F, Rizzi A (2009) Reality-based 3D documentation of world heritage sites: methodologies, problems and examples. In: Proceedings of the 22nd CIPA symposium, October 11–15, 2009, Kyoto, Japan
- Rohn J, Ehret D, Moser M, Czurda K (2005) Prehistoric and recent mass movements of the world cultural heritage site Hallstatt, Austria. *Environ Geol* 47(5):702–714
- Rönnholm P, Honkavaara E, Litkey P, Hyyppä H, Hyyppä J (2007) Integration of laser scanning and photogrammetry. *Int Arch Photogramm Remote Sens Spat Inf Sci* 36(3/W52):355–362
- Rosen PA, Hensley S, Joughin IR, Fuk KL, Madsen SN, Rodriguez E, Goldstein R (2000) Synthetic aperture radar interferometry. *Proc IEEE* 88(3):333–382
- Ruffino G, Moccia A (2005) Integrated VIS_NIR hyperspectral/thermal-IR electro-optical payload system for a mini-UAV. *American Institute of Aeronautics and Astronautics*, pp 647–664
- Scholtz A, Kaschwich C, Kruger A, Kufieta K, Schnetter P, Wilkens C, Kruger T, Vorsmann P (2011) Development of a new multi-purpose UAS for scientific application. *Int Arch Photogramm Remote Sens Spat Inf Sci* 38:149–154
- Silvestrou A, Themistocleous K (2018) Multi-criteria analysis of UNESCO sites in Cyprus: the case study of Choirokoitia. In: Sixth international conference on remote Sensing and geo-information of environment, 26–29 March, 2018, Paphos, Cyprus
- Tang P, Chen F, Zhu X, Zhou W (2016) Monitoring cultural heritage sites with advanced multi-temporal InSAR technique: the case study of the summer palace. *Remote Sens* 8:432. <https://doi.org/10.3390/rs8050432>
- Tapete D, Fanti R, Cecchi R, Petrangeli P, Casagli N (2012) Satellite radar interferometry for monitoring and early-stage warning of structural instability in archaeological sites. *J Geophys Eng* 9:S10–S25
- Tapete D, Casagli N, Fanti R (2013) Radar interferometry for early stage warning on monuments at risk. In: Margottini C, Canuti P, Sassa K (eds) *Landslide science and practice*. Berlin/Heidelberg, Springer, pp 619–625. <https://doi.org/10.1016/j.jksues.2011.03.001>
- Tapete D, Cigna F, Donoghue D (2016) Looting marks in space-borne SAR imagery: measuring rates of archaeological looting in Apamea (Syria) with TerraSAR-X staring spotlight. *Remote Sens Environ* 178:42–58
- Themistocleous K (2017) The use of UAVs to monitor archaeological sites: the case study of Choirokoitia within the PROTHEGO project. In: Fifth international conference on remote sensing and geo-information of environment, 20–23 March, 2017, Paphos, Cyprus
- Themistocleous K (2018) Local monitoring techniques for cultural heritage sites affected by geo-hazards. In: Sixth international conference on remote sensing and geo-information of environment, 26–29 March, 2018, Paphos, Cyprus
- Themistocleous K, Agapiou A, King HM, King N, Hadjimitsis DG (2014a) More than a flight: the extensive contributions of UAV flights to archaeological research – the case study of curium site in Cyprus. In: Proceedings of progress in cultural heritage: documentation, preservation, and protection. 5th international conference, EuroMed 2014, Limassol, Cyprus. Springer LNCS 8740, EuroMed2014 conference, pp 396–409
- Themistocleous K, Agapiou A, Cuca B, Hadjimitsis DG (2014b) 3D documentation of cultural heritage sites. In: Proceedings of progress in cultural heritage: documentation, preservation, and protection. 5th international conference, EuroMed 2014, Limassol, Cyprus. Springer LNCS 8740, EuroMed2014 conference
- Themistocleous K, Agapiou A, Alexakis D, Cuca B, Hadjimitsis DG (2014c) Lessons learnt from using UAVs in Cyprus: landscapes applications. In: Proceedings of the Archland UAV conference 2014, 23–25 May, Berlin, Germany
- Themistocleous K, Agapiou A, Cuca B, Hadjimitsis DG (2015a) Unmanned aerial systems and spectroscopy for remote sensing applications in archaeology. In: Proceedings of the 36th international symposium of remote sensing and environment. (ISRSE-36), 11–15 May, 2015, Berlin, Germany

- Themistocleous K, Ioannides M, Agapiou A, Hadjimitsis DG (2015b) The methodology of documenting cultural heritage sites using photogrammetry, UAV and 3D printing techniques: the case study of Asinou Church in Cyprus. In: Proceedings of the third international conference on remote sensing and geoinformation of environment, 16–19 March, 2015
- Themistocleous K, Agapiou A, deHoop M, Mayor AG, Rietkerk M, Dekker SC, Hadjimitsis DG (2015c) The use of UAV to document sloping landscapes to produce digital elevation models to examine environmental degradation. In: Proceedings of the third international conference on remote sensing and geo-information of environment, 16–19 March, 2015, Paphos, Cyprus
- Themistocleous K, Agapiou A, Hadjimitsis DG (2016a) Experiencing cultural heritage sites using 3D modeling for the visually impaired. In: Proceedings of Euromed 2016: digital heritage, progress in cultural heritage: documentation, preservation, and protection, lecture notes in computer science, vol 10059, 31 October – 4 November, 2016 Nicosia, Cyprus, pp 171–177
- Themistocleous K, Cuca B, Agapiou A, Lysandrou V, Tzouvaras M, Michaelides S, Hadjimitsis DG, Margottini C, Cigna F, Crosta G, Fernandez Merodo JA (2016b) The protection of cultural heritage sites from geo-hazards. In: Proceedings of the European Geosciences Union General Assembly 2016, 17–22 April, 2016, Vienna, Austria
- Themistocleous K, Danezis C, Mendonidis E (2017a) Best practices for monitoring, mitigation and preservation of cultural heritage sites affected by geo-hazards (in Greek). In: Euromed 2017 conference, 1–3 December, 2017, Volos, Greece
- Themistocleous K, Danezis C, Mendonidis E, Lympelopoulou E (2017b) Monitoring ground deformation of cultural heritage sites using UAVs and geodetic techniques: the case study of Choirokoitia, JPI PROTHEGO project. In: Proceedings of the SPIE remote sensing conference, vol 10428, 104280Q, Earth resources and environmental remote sensing/GIS applications VIII, 11–14 September, 2017, Warsaw, Poland. <https://doi.org/10.1117/12.2279478>
- Themistocleous K, Hadjimitsis DG, Michaelides S, Spizzichino DJ, Crosta GB, Fernandez Merodo JA, Bee E (2018a) Best practices for monitoring, mitigation and preservation of cultural heritage sites affected by geo-hazards. Geophysical Research Abstracts, vol 20, EGU2018-18220-1, 2018 EGU General Assembly 2018, Vienna, 8–13 April 2018
- Themistocleous K, Crosta GB, Frattini P, Valagussa A (2018b) Best practices for monitoring, mitigation and preservation of cultural heritage sites affected by geo-hazards: the results of the PROTHEGO project. In: Sixth International conference on remote sensing and geo-information of environment, 26–29 March, 2018, Paphos, Cyprus
- Themistocleous K, Michaelides S, Hadjimitsis DG (2018c) The integrated use of space TECHNOLOGIES, UAVs and field measurements intended for cultural heritage in Cyprus. Geophysical Research Abstracts, vol 20, EGU2018-5282-1, 2018 EGU General Assembly 2018, Vienna, 8–13 April 2018
- UNESCO World Heritage List, “Choirokoitia” <http://whc.unesco.org/en/list/848>. 1 March 2016
- Valagussa A, Frattini P, Crosta G, Themistocleous K, Margottini C, Spizzichino D, Bee E, Jose Antonio Fernandez-Merodo JA (2018) 3D rockfall modelling in the Choirokoitia UNESCO World Heritage Site. Geophysical Research Abstracts, vol 20, EGU2018-15358, 2018 EGU General Assembly 2018, Vienna, 8–13 April 2018
- Vilceanu C, Herban S, Alionescu A, Musat C (2015) Processing of environmental data using digital terrain models for the western part of Romania. In: 15th international multidisciplinary scientific geoconference SGEM 2015, Book 2, vol 2, No. SGEM2015 conference proceedings, ISBN 978-619-7105-35-3/ISSN 1314-2704. <https://doi.org/10.5593/SGEM2015/B22/S11.130>
- Zhou Z (2013) The applications of InSAR time series analysis for monitoring long-term surface change in peatlands. PhD thesis, University of Glasgow
- Zhou W, Chen F, Guo H (2015) Differential radar interferometry for structural and ground deformation monitoring: a new tool for the conservation and sustainability of cultural heritage sites. sustainability (Basel), ISSN 2071-1050, <https://doi.org/10.3390/su7021712>, pp 1712–1729
- Zhu H-H, Shi B, Zhang C-C (2017) FBG-based monitoring of geohazards: current status and trends. Sensors 17(3):452. <https://doi.org/10.3390/s17030452>

Correction to: Towards Early Warning for Damages to Cultural Heritage Sites: The Case of Palmyra



Daniele Cerra and Simon Plank

Correction to:
Chapter 13 in: D. G. Hadjimitsis et al. (eds.),
Remote Sensing for Archaeology and Cultural Landscapes,
Springer Remote Sensing/Photogrammetry,
https://doi.org/10.1007/978-3-030-10979-0_13

The chapter was originally published with low-quality figures (Figs. 1 to 15), which are now revised with high-quality figures.

The updated online version of this chapter can be found at
https://doi.org/10.1007/978-3-030-10979-0_13

© Springer Nature Switzerland AG 2020
D. G. Hadjimitsis et al. (eds.), *Remote Sensing for Archaeology and Cultural Landscapes*, Springer Remote Sensing/Photogrammetry,
https://doi.org/10.1007/978-3-030-10979-0_17

C1